# Investigating the mechanisms underlying *ATG7* related neurological disease

**James Lambton**

This thesis is submitted for the degree of Doctor of Philosophy

Translational and Clinical Research Institute

Faculty of Medical Sciences

Newcastle University

January 2025

# Abstract

The key catabolic process of autophagy relies on a set of core autophagy related (*ATG*) genes, of which very few have been directly associated with human disease. Genetic variants in *ATG4D, ATG5, ATG7* and *ATG9B* have been associated with developmental delay, intellectual disability, ataxia, cerebellar and corpus callosum abnormalities. Here the first *de novo* heterozygous missense *ATG7* subject is described, presenting similarly to the previously described *ATG7* cohort, with impairment of the LC3-conjugation system and accumulation of the autophagy adapter p62 (**PMID: 34161705**). Also described is the first foetal *ATG7* subject, harbouring segregating loss-of-function variants. Immunohistochemical and immunofluorescence analyses of subject brain tissue shows clusters of unmigrated neurons and p62 accumulation in neurons and cerebellar proliferative zone.

To investigate these findings further, I have developed and characterised an induced pluripotent stem cell derived neural model of ATG7 pathology. CRISPR/Cas9 genome editing was used to engineer *ATG7*$^{+/+}$, *ATG7*$^{+/-}$ and *ATG7*$^{-/-}$ iPSCs. Differentiation of these iPSCs into neuron-astrocyte co-cultures showed that *ATG7*$^{-/-}$ co-cultures recapitulated the biochemical phenotype of *ATG7* primary fibroblasts. *ATG7*$^{+/-}$ and *ATG7*$^{-/-}$ co-cultures also demonstrated altered proliferation and morphology. Astrocyte specific changes were observed, with differing astrocyte differentiation and cell death among the *ATG7*$^{+/-}$ and *ATG7*$^{-/-}$ cultures. Functional $Ca^{2+}$ live cell imaging showed increased intracellular $Ca^{2+}$ in *ATG7*$^{+/-}$ neurons, with both *ATG7*$^{+/-}$ and *ATG7*$^{-/-}$ neurons having impaired $Ca^{2+}$ recovery.

Finally, a cohort of 3 subjects from 2 unrelated families harbouring rare, damaging *ATG12* variants is also described, with affected individuals presenting with developmental delay, ataxia and cerebellar abnormalities. Biochemically they had mild impairment of either the ATG5-ATG12 or LC3-II conjugation pathway. The equivalent *atg12* variants were also unable to fully recover autophagy in *atg12*-null *Saccharomyces cerevisiae* models. Together these data expand the existing cohorts of *ATG* related congenital disorders, with the *ATG7* iPSC derived neural model elucidating disease mechanisms in addition to *ATG7*'s core role in autophagy.

# Acknowledgements

I would like to thank my supervisors Dr. Monika Winter, Professor Linda Lako and Professor Rob Taylor. Linda, thank you for your wealth of stem cell knowledge, and welcoming me into your lab so kindly. Rob, thank you for pushing me throughout the last three years and trying to get me to be the best scientist I can be. Monika, thank you not only for scientific help, but also for every other piece of advice, help and support you have given me over the last three years. I would not have been able to do this without all three of you. I would also like to thank Dr. Jack Collier for starting this project and helping to obtain the funding for my PhD.

I must also thank the many friends I've made over the last three years. I would not have made it through the last three years without the Mitochondrial Research Group, and the people who make it as exceptional as it is. I am especially grateful to everyone who has shared the office with me across my time here. A special thank you to Yasmin, Ben and everyone else who made Friday club what it is. You always know how to make the bad times feel not so bad after all.

I would also like to thank our many collaborators, especially Professor Michel Koenig, Dr. Aurélien Trimouille, Professor Eirik Frengen and Dr. Tom McWilliams. Alongside them I would also like to thank all the patients who consented to taking part in this work, as well their families, clinicians and all other staff involved. I must also thank my funders, the Pathological Society, for giving me the opportunity to undertake this work.

Most importantly, I would like to thank my parents. They have supported me in every way possible throughout my life, and my PhD it was no different. I could not have done any of this without the love and support you have always given me, and for that I will always be grateful.

# Table of Contents

# Figures

# Tables

# Abbreviations

| | |
|---|---|
| 19 kDa interacting protein-3 (NIP3)-like protein X | NIX |
| Adenosine monophosphate | AMP |
| Adenosine triphosphate | ATP |
| American College of Medical Genetics | ACMG |
| Artificial cerebral spinal fluid | ACSF |
| Autophagy Related | ATG |
| B27 supplement without Vitamin A | B27-RA |
| Bafilomycin A1 | BafA1 |
| Basic fibroblast growth factor | bFGF |
| Beta-III Tubulin | TUBIII |
| BNIP3-like | BNIP3L |
| Bone morphogenic protein | BMP |
| Bovine Serum Albumin | BSA |
| Brain derived neurotrophic factor | BDNF |
| Chaperone mediated autophagy (CMA) | CMA |
| Combined Annotation Dependent Depletion | CADD |
| Complimentary DNA | cDNA |
| CRISPR RNA | crRNA |
| Dibutyryl cAMP | dbcAMP |
| Double stranded DNA breaks | DSB |
| Doublecortin | DCX |
| Ectopic P-Granules autophagy protein 5 homolog | EPG5 |
| Electroencephalogram | EEG |
| Embryonic stem cells | ESC |
| Endoplasmic reticulum | ER |
| Excitatory amino acid transporters | EAAT |
| Glial derived neurotrophic factor | GDNF |
| Glial Fibrillary Acidic Protein | GFAP |
| Green fluorescent protein | GFP |
| Haematoxylin and eosin | H&E |
| Human embryonic stem cell | hESC |

| | |
|---|---|
| Huntingtin | HTT |
| Huntington’s disease | HD |
| Immunocytochemistry | ICC |
| Immunofluorescence | IF |
| Immunohistochemical | IHC |
| Induced pluripotent stem cells | iPSC |
| Inner autophagosomal membrane | IAM |
| Inner subventricular zone | ISVZ |
| Inositol-1,4,5-triphosphate receptors | $IP_3Rs$ |
| Intermediate zone | IZ |
| Intracellular calcium level | $[Ca^{2+}]i$ |
| LC3 interaction region | LIR |
| Lysosome associated membrane protein 2A | LAMP2A |
| Mammalian target of rapamycin | mTOR |
| Microtubule associated protein 1light chain beta 3 | MAP1LC3B |
| Suppressor Mothers Against Decapentaplegic homologs | SMAD |
| Neural stem cell | NSC |
| Neighbour of BRCA 1 | NBR1 |
| Neural stem cell | NSC |
| Non-homologous end joining | NHEJ |
| Oct3/4, Klf4, SOX2 and c-Myc | OKSM |
| Optineurin | OPTN |
| Outer autophagosome membrane | OAM |
| Outer mitochondrial membrane | OMM |
| Outer subventricular zone | OSVZ |
| Parkinson’s disease | PD |
| Phosphatidylethanolamine | PE |
| PIKC3C-complex 1 | PI3KC3-C1 |
| PIKC3C-complex 2 | PI3KC3-C2 |
| Pluripotent stem cells | PSC |
| Rhombic lip | RL |
| Rhombic Lip subventricular zone | $RV^{SVZ}$ |
| Rhombic lip ventricular zone | $RL^{VZ}$ |

| | |
|---|---|
| Single guide RNA | sgRNA |
| Soluble N-ethylmaleimide sensitive factor attachment protein receptor | SNARE |
| Translocase of the inner membrane | TIM |
| Translocase of the outer membrane | TOM |
| Transmission electron microscopy | TEM |
| Ubiquitin proteosome system | UPS |
| Unc-51-like kinase 1 | ULK1 |
| Ventricular zone | VZ |
| Western Blot | WB |

# 1 Introduction

## 1.1 Canonical Autophagy

Autophagy is a highly conserved catabolic process that is important for cellular homeostasis. The roles it plays in this process are varied, from starvation response to tumour suppression, and it is most often characterised as an intracellular quality control mechanism, degrading long lived proteins, protein aggregates, infectious agents, and damaged organelles. Autophagy was first characterised in 1962, where sections of cytoplasm in rat liver were described to be compartmentalised by membranes, for degradation purposes in response to glucagon perfusion (Ashford & Porter, 1962). However, these authors were not able to identify the origin of these membranes, nor the mechanism by which they were formed. It is now well-established that these membrane structures were formed during the latter stages of a process which would be named ‘autophagy’, by Christian de Duve a year later (Klionsky, 2008). Over the next 60 years, a variety of work using numerous model systems has elucidated many of the key processes underlying autophagy.

Autophagy has numerous functions in many organisms, being involved in differentiation, organelle quality control, protein turnover, immunity, starvation response and more (Harnett et al., 2017). As such, a number of distinct types of autophagy have been identified. Firstly, microautophagy refers to direct, non-specific, engulfment of small volumes of the cytosol by lysosomes for degradation (Li et al., 2012). Chaperone mediated autophagy (CMA) relies on direct delivery of proteins to lysosomes via a variety of chaperone proteins, delivering proteins to lysosome associated membrane protein type 2 A (LAMP2A), where they are unfolded and engulfed by the lysosome for degradation (Majeski & Fred Dice, 2004). Finally, macroautophagy, referred to hereafter as autophagy, is the most studied form. Autophagy relies on the formation of a double membrane vesicle, called an autophagosome, which encapsulates an area of the cytosol and its contents, or an organelle, ready for degradation. When fully formed, this autophagosome will fuse with a lysosome, producing an autolysosome, at which point the hydrolytic enzymes from the lysosomes can degrade the contents of the autolysosome (**Figure 1.1**) (Fleming et al., 2022).

### 1.1.1 Induction of autophagy

Mammalian target of rapamycin (mTOR) can be considered one of the main autophagy regulators. Forming two complexes implicated in autophagy initiation, mTORC1 and mTORC2, mTORC1 is the most studied form in relation to macroautophagy, while mTORC2 is implicated in initiation of CMA (Arias et al., 2015). The components of mTORC1 consist of mTOR, Raptor (Regulatory Associated Protein of mTOR), mLST8 (mammalian lethal with SEC13 protein 8), DEPTOR (DEP-domain-containing mTOR-interacting protein) and PRAS40 (40 kDa proline rich Akt substrate) (Hara et al., 2002; Kim et al., 2003; Sancak et al., 2007; Peterson et al., 2009). When active, mTORC1 holds a permanent state of inhibition over autophagy. Under nutrient rich conditions Rag GTPases, in combination with the Ragulator complex, mediate the localisation of mTORC1 to lysosomal membranes (Tsujimoto et al., 2023). This brings mTORC1 into proximity with Ras homolog enriched in brain (Rheb), its activator, which is responsible for relaying all upstream signals to mTORC1 (Sancak et al., 2010). In its active state, mTORC1 will function as a phosphatidylinositol 3-kinase (PI3K)-related kinase, allowing mTORC1 to perform its inhibitory function.

Firstly, at the transcriptional level, mTORC1 will phosphorylate transcription factor EB (TFEB), preventing its translocation to the nucleus. This results in suppression of TFEB target genes, including genes involved in lysosome biogenesis and autophagy machinery, such as WD repeat domain interacting protein 1 (*WIPI1*), microtubule associated protein 1light chain beta 3 (*MAP1LC3B*), sequestosome 1 (*SQSTM1*) and autophagy related 9B (*ATG9B*) (Settembre et al., 2012, 2011). In addition to transcriptional control, mTORC1 has direct control of the ULK1 complex comprised of Unc-51-like kinase 1 (ULK1), focal adhesion kinase family interacting protein of 200 kDa (FIP200), ATG13 and ATG101 (Jung et al., 2009). When active, mTORC1 phosphorylates ULK1 and ATG13 via Raptor, this leaves the ULK1 complex inactive, inhibiting autophagy initiation (Kim et al., 2011; Puente et al., 2016).

In times of energy depletion Liver Kinase B1 (LKB1), which is sensitive to the increasing adenosine monophosphate : adenosine triphosphate (AMP: ATP) levels, phosphorylates the AMP activated protein kinase (AMPK) (Gwinn et al., 2008a). Once

activated, AMPK recruits accessory proteins to inhibit the mTORC1 complex, as well as directly inhibiting mTOR in the mTORC1 complex (Gwinn et al., 2008b). This prevents mTORC1 from phosphorylating ULK1, resulting in subsequent phosphorylation of the Raptor unit of the mTORC1 complex by ULK1. This step prevents ATP loading to Raptor and therefore it's kinase activity (Dunlop et al., 2011). In addition, AMPK inhibition of mTORC1 can also be induced via p53's response to DNA damage resulting from oxidative stress. Two transcriptional targets of p53, Sestrin1 and Sestrin2, are able to activate AMPK and target it to phosphorylation of tuberous sclerosis complex 2 (TSC2), that is part of the TSC complex (Budanov & Karin, 2008). The TSC complex is a GTPase activating protein (GAP) for Rheb, converting it from active Rheb-guanidine triphosphate (GTP) to inactive Rheb-guanidine diphosphate (GDP) (Inoki et al., 2003). Phosphorylation by AMPK drives TSC2 activity in the TSC complex, inactivating Rheb and inhibiting mTORC1, thus releasing its inhibition on autophagy (Budanov & Karin, 2008). Under amino acid starvation, the Rag-GTPase/Ragulator pathway responsible for mTORC1 localisation to lysosomes is inhibited, which prevents its activation by Rheb (Sancak et al., 2008). Hypoxia is also able to activate autophagy, with hypoxia inducible factor 1 (*HIF-1*) upregulation in response to hypoxic stress, which is followed by induction of regulated in development and damage response 1 (*REDD1)* (Shoshani et al., 2002). REDD1 then relieves 14-3-3 mediated TSC complex inhibition, allowing Rheb inactivation and autophagy induction (DeYoung et al., 2008). Now free from mTORC1's inhibition, ULK1 can induce autophagy by initiating phagophore formation.

### 1.1.2 Phagophore nucleation

In mammals, autophagosome biogenesis starts with a phagophore, also known as an isolation membrane. These phagophores predominantly originate from the endoplasmic reticulum (ER) but can also have other origins like mitochondrial associated ER membranes (Axe et al., 2008). Phagophore production at these sites requires production of phosphatidylinositol-3-phosphate (PI3P), which is performed by phosphatidyl inositol 3-kinase catalytic subunit type 3 (PI3KC3), also known as VPS34 (Axe et al., 2008). PI3KC3 is able to form two distinct complexes, containing VPS15 and Beclin 1 scaffolding proteins respectively. PIKC3C-complex 1 (PI3KC3-C1) also contains ATG14L which targets the complex to the phagophore, while PI3KC3-complex 2 (PI3KC3-C2) contains UV radiation resistance associated gene protein

(UVRAG) for autophagosome maturation, which replaces ATG14L (Kihara et al., 2001; Itakura et al., 2008). ULK1 promotes this process by several means. Phosphorylation of AMBRA1 by ULK1 induces translocation of PI3KC3 and Beclin 1 from the cytoskeleton to the ER (Park et al., 2016). A direct interaction between ATG13 of the ULK1 complex and ATG14L stabilises the PI3KC3-C1 on the ER (Wold et al., 2016). Finally, ULK1 phosphorylation of PI3KC3, Beclin 1 and ATG14L increase the activity of PI3KC3-C1 (Mercer et al., 2018). These events result in areas of the ER enriched for PI3P known as omegasomes, to which downstream effectors can bind, including double FYVE-containing protein 1 (DFCP1) and Autophagy linked FYVE protein (ALFY) (Axe et al., 2008; Filimonenko et al., 2010). Omegasome development, and the related increase in PI3P, result in recruitment of WD-repeat domain phospoinositide-interacting proteins 1-4 (WIPI1-4), at differing timepoints through development. WIPI2 will then recruit the start of the microtubule associated protein light chain 3 (LC3) conjugation system to expand the forming lipid structure, called an elongation membrane (**Figure 1.1**) (Dooley et al., 2014a).

### 1.1.3 Phagophore elongation

Once WIPI2 is associated with the developing phagophore, it starts the recruitment of the ATG5-ATG12 conjugation system by directly interacting with ATG16L1 (**Figure 1.1**) (Dooley et al., 2014b). There are two main systems involved in expanding the elongation membrane into a phagophore. The first involves ATG12, which is conjugated to ATG5 by ATG7 and ATG10, that function similarly to E1, E2 ubiquitin activating enzymes, respectively (Mizushima et al., 1998). The ATG5-ATG12 complex then interacts with ATG16L1 dimers, and acts like an E3-like enzyme, producing a protein complex which sits in the expanding elongation membrane, termed a phagophore (Hanada et al., 2007). The next step involves the human homologues of the single yeast Atg8 protein. Human Atg8 homologues can be split into two families LC3 and gamma amino butyric acid receptor associated protein (GABARAP), with the former being the most well studied (Abdollahzadeh et al., 2017). Each family has three forms, with LC3 consisting of LC3A, LC3B and LC3C; and with GABARAP's consisting of GABARAP, GABARAP1 and GABARAP2 (Lee & Lee, 2016). Inactive LC3 is first cleaved at the C-terminus by ATG4, shortening it to 116 residues long, and exposing glycine as the terminal residue, to produce active LC3-I (Agrotis et al., 2019a). This active LC3-I is recognised by the extreme C-terminal domain of ATG7, an E1-like

enzyme, resulting in ATP dependant adenylation of LC3-I's exposed glycine residue by ATG7's C-terminal domain. (Yamaguchi et al., 2018; Noda et al., 2011). The adenylated LC3-I is then transferred to the N-terminal domain of the other protomer in ATG7's classical homodimer structure, which is bound to ATG3, an E2-like enzyme. Here ATG3 conjugates LC3-I to phosphatidylethanolamine (PE), generating LC3-II (Ichimura et al., 2000). The mechanisms underlying this pathway are further discussed later (**Chapter 1.6.1**). This provides LC3-II with the lipophilic properties required to insert itself into the expanding membrane structure (**Figure 1.1**). GABARAP undergoes a similar process, producing GABARAP-II, which colocalises with LC3-II (Kirkin et al., 2009a).

The insertion of the LC3-II into the membrane produces a slight disruption in the membrane, allowing space for the insertion of more material, expanding the phagophore (Maruyama et al., 2021a). Meanwhile, the asymmetric recruitment of LC3-II by the ATG5-ATG12-ATG16L1 promotes curvature of the phagophore (Glick et al., 2010a). Combined, these two processes produce two hemisphere phagophores, which eventually fuse to produce a sealed double membrane vesicle, called an autophagosome, encapsulating a portion of the cytoplasmic contents. Once the mature autophagosome is formed, the ATG5-ATG12-ATG16L1 complex dissociates from the membrane, but the LC3-II remains on the apical and luminal surfaces of the autophagosome (Barth et al., 2010).

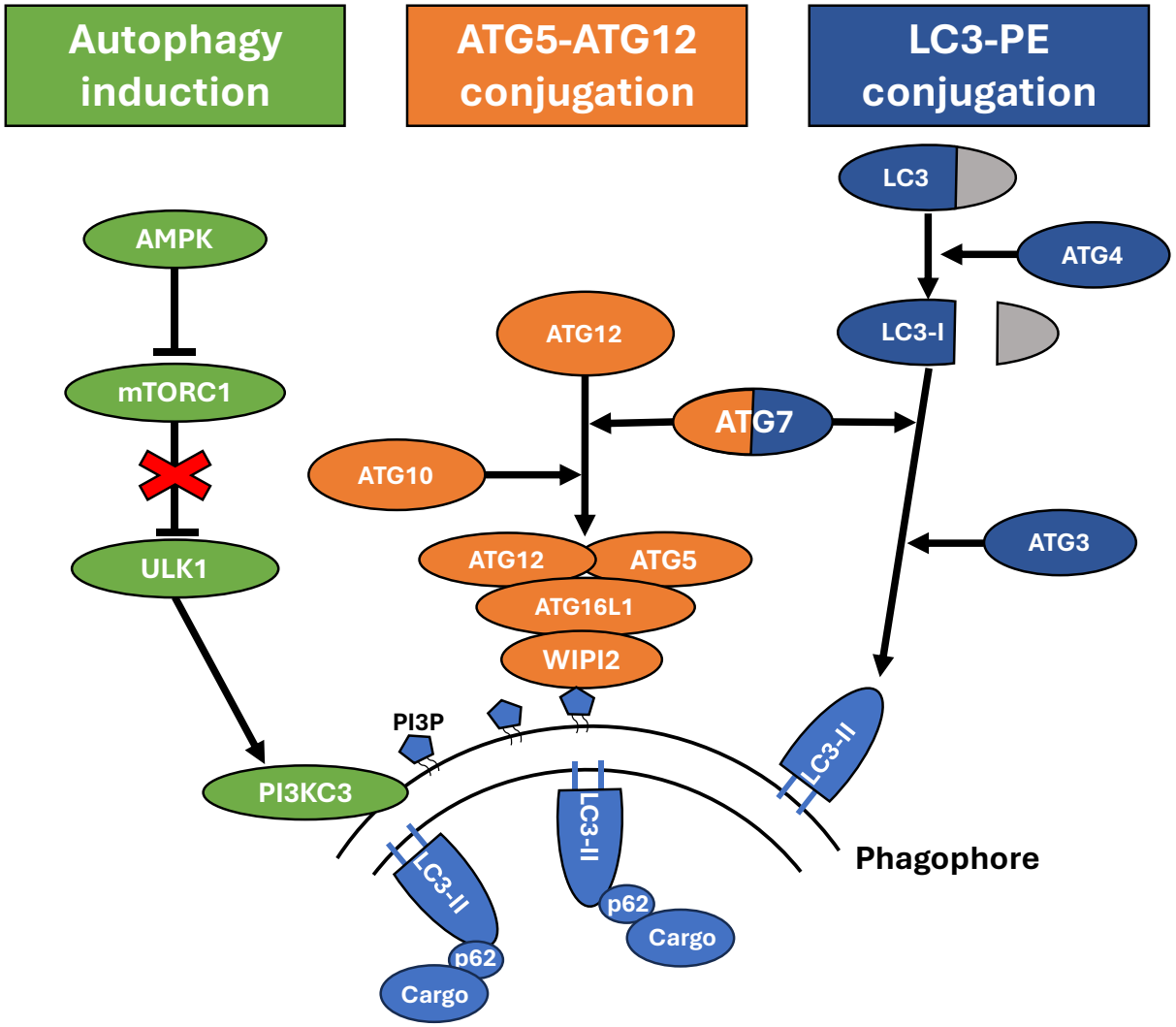


**Figure 1.1 Schematic of autophagy induction and the two core conjugation systems involved in autophagosome expansion**. Upon autophagy stimulus, such as increased AMP:ATP ratio, AMPK inhibits the mTORC1 complex by phosphorylation of mTORC1's Raptor subunit. This prevents phosphorylation of ULK1 complex's ATG13 and ATG101 components allowing the recruitment of PI3KC3 complexes to the phagophore, resulting in production of PI3P. PI3P serves as a base for WIPI2 recruitment, which in turns recruits the start of the conjugation machinery. Initially, ATG12 is conjugated to ATG5 by ATG7 and ATG10 The ATG5-ATG12 complex then interacts with ATG16L1 dimers which are recruited to the phagophore by WIPI2. Concurrently, ATG4 cleaves ATG8, depicted here as LC3, exposing its C-terminal glycine. The glycine is adenylated by ATG7, and transferred to ATG3 for conjugation to PE, producing LC3-II. LC3-II enables targeting of autophagy cargo to autophagosomes by autophagy adapters, such as p62.

### 1.1.4 Autophagosome-Lysosome fusion

Once an autophagosome has formed, it can be fused with a lysosome to deliver the degradative components required (Mauthe et al., 2018). To facilitate this process, the autophagosome and lysosome must be brought into proximity to allow membrane fusion, this is predominantly performed by soluble N-ethylmaleimide sensitive factor attachment protein receptors (SNAREs) (Yim & Mizushima, 2020). These SNARE proteins localise to opposing membranes on the autophagosome and lysosome and interact with one another, with specificity of which membranes being fused conveyed by the combination of SNARE proteins involved (**Figure 1.2**) (Parlati et al., 2000). One of the SNARE combinations involved in autophagosome-lysosome fusion is syntaxin 17 (STX17) and synaptosomal-associated protein 29 (SNAP29) on the outer autophagosome membrane (OAM) which interact with vesicle associated membrane protein 8 (VAMP8), or VAMP7, on lysosomes (**Figure 1.2**) (Fader et al., 2009; Itakura et al., 2012). These interactions are aided by tethering factors, recruited by Rab GTPases, amongst which is the homotypic fusion and protein sorting (HOPS) complex (Jiang et al., 2014). In the case of the HOPS complex, it is recruited to autophagosomes, late endosomes or lysosomes via Pleckstrin homology domain containing protein member 1 (PLEKHM1) under the control of the GTPase RAB7 (**Figure 1.2**) (McEwan et al., 2015). In this pathway, the GABARAP family of ATG8s have also been demonstrated to play a role in recruitment of PLEKHM1 to the autophagosome, aiding autophagosome-lysosome fusion (Nguyen et al., 2016). Additionally, ATG8-PE conjugation has been shown to play a key role in inner autophagosome membrane degradation in STX17 mediated fusion, with loss of ATG8 conjugation to PE resulting in impaired degradation of autolysosomes (Tsuboyama et al., 2016). Ectopic P-granules protein 5 (EPG5) has also been associated with tethering of autophagosomes and lysosomes. Binding Rab7 on late endosomes or lysosomes, and LC3 on autophagosomes, it then interacts with STX17/SNAP29 and VAMP7 and VAMP8 on autophagosomes and lysosomes respectively to promote tethering and fusion. (**Figure 1.2**) (Wang et al., 2016). Another important factor in autophagosome fusion is ATG14L. During expansion of the phagophore STX17 recruits PI3KC3 by using ATG14L as a targeting factor to curved regions of the membrane (Fan et al., 2011; Matsunaga et al., 2010). In addition to this, ATG14L is critical for fusion of the autophagosome with a lysosome. ATG14L stabilises the

STX17-SNAP29 complex, aiding tethering of the autophagosome and lysosome, promoting fusion (Diao et al., 2015).

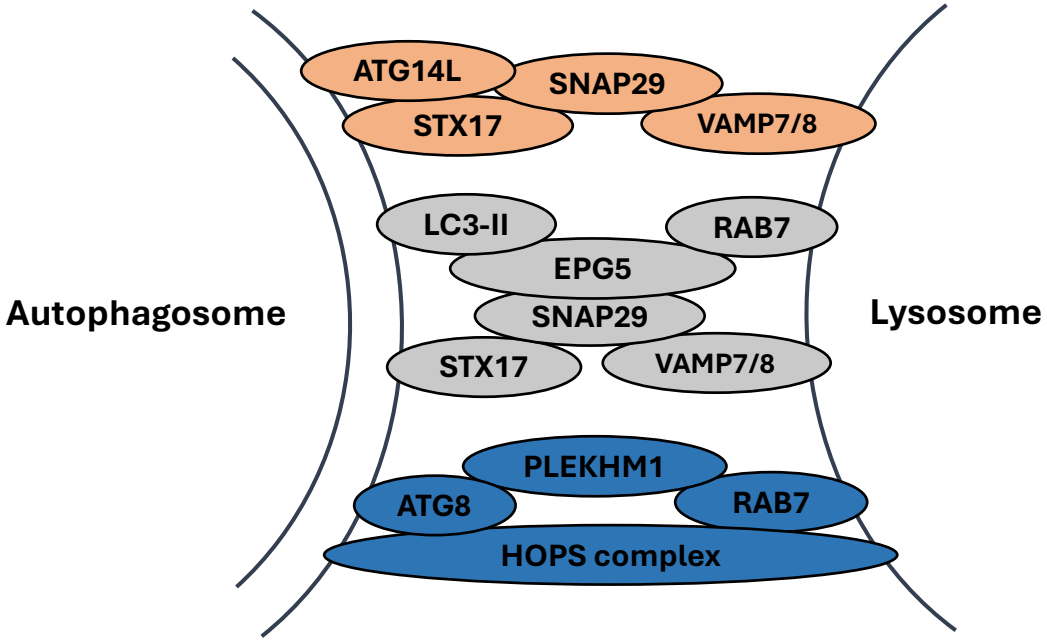


**Figure 1.2. Schematic of complexes mediating autophagosome-lysosome tethering to facilitate fusion**. One complex mediating autophagosome lysosome fusion involves STX17 and SNAP29 of the autophagosome interacting with VAMP7 or VAMP8 of the lysosome. The interaction between STX17 and SNAP29 is stabilised by ATG14L. A second complex also uses STX17, SNAP29 and VAMP7/8. Here EPG5 is recruited by LC3-II on the autophagosome and RAB7 on the lysosome to enhance tethering and promote fusion. ATG8s are also implicated in the recruitment of the HOPS complex via the recruitment of PLEKHM1 by RAB7 on late endosomes and lysosomes. Colours denote separate complexes involved in autophagosome-lysosome tethering.

## 1.2 Non-canonical autophagy

Initially, it was thought that *ATG5* and *ATG7* were essential genes, as loss of these genes will result in loss of functional autophagy, thus making them core autophagy genes (Mizushima et al., 1998; Hanada et al., 2007). However, it has been shown that removal of either of the *ATG7* or *ATG5* from cells does not prevent the formation of autophagosomes (Nishida et al., 2009; Tsuboyama et al., 2016). Additionally, patients with no detectable ATG7 are able to form autophagosomes in primary fibroblast cultures (Collier et al., 2021). This suggests that there is an alternative pathway capable of performing the same roles as these proteins.

In the first stages, canonical and alternative autophagy share select parts of their pathways. Alternative autophagy, like canonical autophagy, relies on activation of the ULK1 complex. Removal of ULK1 or FIP200 from *ATG5*$^{-/-}$ mouse embryonic fibroblasts results in a loss of the observed formation of autophagosomes, demonstrating the complex's requirement for initiation of the alternative autophagy pathway (Nishida et al., 2009). The following cascade of PIK3R4, PIK3C3 and Beclin 1 remains the same as described previously (**Chapter 1.1.2**). However, while this initiates phagophore formation, the process by which the phagophore is expanded is different.

For the expansion of the phagophore in alternative autophagy neither the ATG5-ATG12 complex, or the LC3 conjugation system are required, however, the exact process by which this is achieved is yet to be elucidated. It is thought that the *trans*-Golgi provides the majority of the material required to produce these phagophores as mannose-6-phophate receptors from the *trans*-Golgi co-localise with STX17 and LAMP2, both of which are commonly found on autolysosomes (Nishida et al., 2009). It has been also suggested that Rab9 plays a role in autophagosome production, co-localising on autolysosomes with LAMP2. This is supported by accumulation of elongation membranes when Rab9 is knocked down by siRNA, indicating that Rab9 is essential for phagophore elongation and maturation of autophagosomes, potentially acting as replacement for the LC3 conjugation system (Nishida et al., 2009).

However, while autophagosomes are able to form in the absence of specific core autophagy proteins, issues remain in the later stages of autophagosome development and eventual fusion to lysosomes. Knock out of *Atg3/ATG3* and *Atg5/ATG5* in mouse embryonic fibroblasts, and HeLa cells resulted in problems with autophagosome maturation and inner autophagosomal membrane (IAM) degradation (Tsuboyama et al., 2016). *Atg3* knock out results in elliptical autophagosomes, as opposed to spherical in the wild type, suggesting that Atg3 plays a role in the correct fusion of phagophores. In addition to this, knock out of *ATG3*, and to a lesser extent *ATG5*, results in a significantly increased duration between fusion with a lysosome, and the degradation of the IAM, a key step in the degradation process, and turnover of LC3-II (Tsuboyama et al., 2016). However, interestingly it was proposed that they were observing this phenomenon in residual canonical autophagy, despite the knockout of *ATG3* and *ATG5*, as opposed to alternative autophagy.

Alongside alternative methods of producing double membrane vesicles to degrade cytosolic components, non-canonical autophagy can also involve conjugation of ATG8 to single membranes (CASM) (Durgan et al., 2021). In CASM, cytosolic double stranded DNA, from bacteria or viruses, is bound by cyclic GMP-AMP synthase (cGAS), which produces cyclic guanidine monophosphate adenosine monophosphate (cGMP) (Sun et al., 2013). The cGAMP will bind to the effector protein stimulator of interferon genes (STING), results in translocation of STING from the endoplasmic reticulum to the Golgi (Gui et al., 2019). This redistribution of STING induces the localisation of the ATG16L1-ATG5-ATG12 complex to single membrane vesicles, where the WD40 domain of ATG16L1 induces the conjugation of PE or phosphatidylserine (PS) to LC3-I using the same machinery as canonical autophagy previously described (**Chapter 1.1.3**). The WD40 domain of ATG16L1 is dispensable for canonical autophagy, but required for CASM LC3 lipidation, marking a clear distinction between the two pathways (Fischer et al., 2020). This lipidation of LC3 is done without the canonical upstream machinery previously described (**Chapter 1.1.2**) (Sanjuan et al., 2007; Fischer et al., 2020; Durgan et al., 2021). The conjugation of ATG8 to single membranes marks these single membrane vesicles for degradation in response to potential infection, giving LC3 a role in intracellular pathogen defence (Fischer et al., 2020; Sun et al., 2013).

In addition to this viral response, CASM functions in lysosomal damage response via interaction with leucine-rich repeat kinase 2 (LRRK2). In response to lysosomal membrane damage or pH perturbations, LRRK2 is recruited along with LC3-II to the lysosome (Florey et al., 2015; Eguchi et al., 2024). This recruitment of LRRK2 to damaged lysosomes requires ATG16L1 WD40 domain mediated LC3-II localisation to these damaged lysosomes, indicating its reliance on CASM (Eguchi et al., 2024). Once recruited, LRRK2 recruits and phosphorylates the Rab GTPase Rab8A on the damaged lysosome which in turn recruits components of the endosomal sorting complex required for transport (ESCRT) machinery (Herbst et al., 2020). The ESCRT machinery enables repair of partially damaged lysosomes, saving them from degradation by autophagy, with loss of LRRK2 recruitment resulting in accumulation of damages vesicles (Herbst et al., 2020; Radulovic et al., 2018). This role in lysosomal repair marks an interesting role for ATG8s in circumventing autophagy, enabling repair of damaged vesicles.

## 1.3 Selective Autophagy

While bulk autophagy provides nutrients in times of starvation and cellular stress by degradation of discrete areas of the cytosol, selective autophagy conveys a more specific degradation of a variety of intracellular components (Vargas et al., 2022). The selective form of autophagy relies on recognition of polyubiquitinated structures, with selectivity being conveyed by the autophagy receptor proteins, which generally possess an LC3 interaction region (LIR) (Wirth et al., 2019). The LIR allows for recognition of LC3 via a four-residue motif, WXXL, which can directly interact with the LC3-PE family members on the expanding autophagosome, providing a targeting system for proteins, aggregates and organelles destined for degradation (Ichimura et al., 2008; Noda et al., 2008, 2010). A wide variety of selective autophagy substrates has been described, each with their own recognition mechanisms. and the three discussed in this thesis are the selective degradation of mitochondria (mitophagy), lipids (lipophagy) and protein aggregates (aggrephagy).

### 1.3.1 Mitophagy

Mitophagy is arguably the most well studied selective autophagy pathway. Mitochondria are highly dynamic organelles, and defects in function can lead to accumulation of damaging reactive oxygen species (ROS), which results in their clearance by mitophagy (Frank et al., 2012). While there are numerous potential triggers, mitophagy allows for the maintenance of a healthy mitochondrial network.

Under basal conditions, PTEN induced putative kinase 1 (PINK1) is imported to the mitochondria through the translocase of the outer membrane (TOM) and translocase of the inner membrane (TIM) complexes via its mitochondrial targeting sequence (Pfanner, 2021; Silvestri et al., 2005). Once inside the mitochondria, PINK1 is cleaved by presenilin associated rhomboid like (PARL) protease, resulting in its exit from the mitochondria and degradation by the proteosome system in the cytosol (Jin et al., 2010; Yamano & Youle, 2013). In times of mitochondrial stress, the mitochondrial membrane potential is reduced, leading to defective import of PINK1. This prevents PARL from cleaving the N-terminus of PINK1, resulting in its accumulation on the outer mitochondrial membrane (OMM) (Deas et al., 2011; Kondapalli et al., 2012). On the OMM PINK1 phosphorylates ubiquitin’s Serine65 on polyubiquitinated proteins on the OMM, this aids recruitment of Parkin to damaged mitochondria (Koyano et al., 2014).

Additionally, PINK1 is able to phosphorylate Parkin at Serine65 in its ubiquitin domain, activating it from its self-inhibited state (Sauvé et al., 2018; Gladkova et al., 2018).

Parkin is an E3 ubiquitin ligase which functions to ubiquitinate numerous OMM proteins. Parkin is phosphorylated at Serine65 by PINK1, resulting in greater Parkin recruitment, thus generating a feed forward mechanism (Kondapalli et al., 2012; Ordureau et al., 2014). The ubiquitination of proteins on the OMM of defective mitochondria recruits additional machinery for a variety of purposes. One such example is recruitment of p97, which mediates proteosome dependant degradation of mitofusins MFN1 and MFN2, and therefore preventing fusion of damaged mitochondria, which would interfere with mitophagy (Tanaka et al., 2010). RAB GTPases are also recruited, which aid mitophagy by facilitating the early stages of the autophagy pathway by aiding autophagosome formation as discussed (**Chapter 1.1.2**) (Yamano et al., 2018; Heo et al., 2018).

The result of the phospho-ubiquitin chains generated by PINK1/Parkin act as substrates for the recruitment of autophagy adapters. Optineurin (OPTN) and NDP52 have been identified as the two key receptors for mitophagy (Lazarou et al., 2015; Heo et al., 2015). Both interact with the phospho-ubiquitin chains, however this is an interaction aided by tank binding kinase 1 (TBK1). TBK1 acts to potentiate and stabilise the receptors' interaction with the phospho-ubiquitin chains (Lazarou et al., 2015; Heo et al., 2015). The LIRs of OPTN and NDP52 enable the targeting of mitochondria to pre-formed autophagosomes, however they are also able to interact with upstream autophagy machinery, including ULK1, DFCP1 and WIPI1 and ATG9 (Lazarou et al., 2015). Upstream autophagy machinery has also been shown to be recruited to the mitochondria in cells lacking LC3 conjugation machinery, suggesting that OPTN and NDP52 function to induce autophagy independently of their autophagy adapter functions (**Figure 1.3**) (Itakura et al., 2012).

Further complicating the role of autophagy adapters in mitophagy, is the discovery of ubiquitin independent mitophagy pathways, such as the 19 kDa interacting protein-3 (NIP3)-like protein X (NIX) and the BCL2/adenovirus E1B 19 kDa protein interacting protein 3 (BNIP3) pathway. Both NIX and BNIP3, a homologue of NIX, are localised to the mitochondria, and have been demonstrated to play central roles in mitochondrial clearance in erythroid cells initially, but now also other cell types, including neurons

(Novak et al., 2010; Hanna et al., 2012; Yuan et al., 2017). NIX, an outer mitochondrial membrane protein contains an LIR to allow LC3 interaction, but also contains a minimal essential region which binds WIPI2. This recruitment of WIPI2 to mitochondria allows for recruitment of the autophagy machinery for mitophagy (Bunker et al., 2023). Interestingly, BNIP3-like (BNIP3L) has been shown to require a minimal essential region, which does not include its LIR, in order to carry out mitochondrial clearance in erythroid cells, indicating roles outside of its interaction with LC3/GABARAP (**Figure 1.3**) (Zhang et al., 2012).

Both these ubiquitin independent mitophagy pathways can be regulated by F-box and leucine rich repeat protein 4 (FBXL4) (Nguyen-Dien et al., 2023; Cao et al., 2023; Elcocks et al., 2023). In cells not under stress conditions, the F-box protein is localised to the mitochondrial outer membrane. Here it recruits the rest of a ubiquitin ligase complex consisting of S-phase kinase associated protein 1, Cullin 1, a RING finger protein and an F-box protein, in this case FBXL4. This complex, known as SCF, is able to selectively ubiquitinylate both BNIP3 and NIX on the outer mitochondrial membrane, preventing their accumulation and therefore their mitophagy inducing activity (Nguyen-Dien et al., 2023; Cao et al., 2023; Elcocks et al., 2023).

### 1.3.2 Tissue specificity of mitophagy

While mitochondrial quality control is important in all tissues, the rate at which mitophagy occurs is spatially and temporally regulated amongst tissues. However, investigating the mitophagy has been historically difficult, with previous immunofluorescence, electron microscopy and biochemical approaches lacking sensitivity and specificity to targeted mitophagy (McWilliams et al., 2016). Despite these difficulties, the regulation of mitophagy in different tissues remained a subject of interest in the field, leading to the development of multiple reporter models.

The central mitophagy reporters are mt-Keima, and mito-QC. The mt-Keima mouse models consist of a coral derived fluorophore with a pH dependant excitation, with peak excitation at a neutral pH being at 458 nm, and at 561 nm at the more acidic pH found in lysosomes. This reporter is then targeted to the mitochondrial matrix using a cytochrome C oxidase subunit 8 (COX8) mitochondrial targeting sequence (**Figure 1.3**) (Katayama et al., 2011; Sun et al., 2015). However, while the reporter efficiently identifies mitochondrial delivery to acidified lysosomes, *in-vivo* and *in vitro*, it is limited

by its incompatibility with fixation, as the pH gradient across the lysosomal membrane is lost when fixing, limiting its use (Katayama et al., 2011; Sun et al., 2015). Mito-QC relies on a tandem reporter consisting of a mCherry-green fluorescent protein (GFP) targeted to the outer mitochondrial membrane using a fission protein 1 (FIS1) mitochondrial targeting sequence (**Figure 1.3**) (Allen et al., 2013). The tandem nature of the reporter circumvents the issue regarding fixation, as delivery to the lysosome quenches the GFP, but not mCherry signal. This results in tandem mCherry-GFP signal marking normal mitochondria, with mCherry alone marking mitochondria in lysosomes (**Figure 1.3**).

The mito-QC mouse has provided insights into the tissue specificity of mitophagy rates, particularly in relation to a tissue's development and metabolic demand. In the developing heart, one of the highest rates of mitophagy was determined to be in proliferating cells undergoing remodelling or differentiation, with mitophagy rates becoming more uniform in adult tissue (McWilliams et al., 2016). It was also established that Purkinje cells were the predominant site of mitophagy in the cerebellum. It was also noted the majority of mitolysosomes occurring in the cell body, consistent with the idea of retrograde transport of autophagosomes from dendrites to the cell body for lysosomal fusion and degradation (Ganesan & Cai, 2021; McWilliams et al., 2016).

The highest mitophagy rates occur in the highly metabolically active hepatic and renal tissues (McWilliams et al., 2016). Comparisons between mitophagy rates and mitochondrial content of cells in the proximal and distal convoluted tubules of the kidney has shown that mitophagy rate is not proportional to the mitochondrial load of a cell. Additional work has also established mitophagy rates in the developing kidneys are variable depending on gestational age, further hinting at mitophagy's role in differentiation and development of tissues (McWilliams et al., 2016).

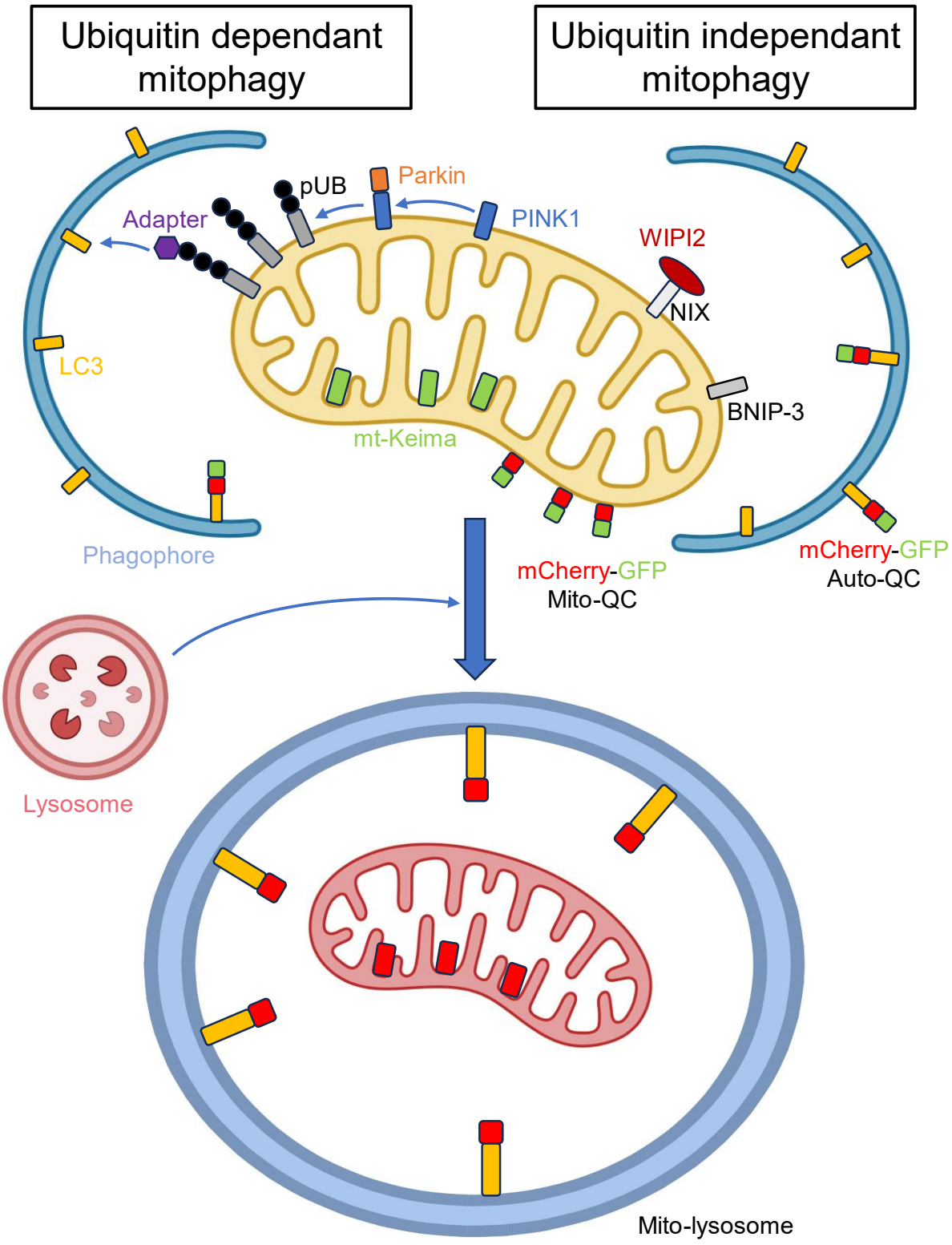


**Figure 1.3 Schematic of the ubiquitin dependant and ubiquitin independent pathways of mitophagy, and associated mitophagy and autophagy reporters**. In Ubiquitin dependant mitophagy, PINK1 accumulation on the OMM of depolarised mitochondria results in recruitment and phosphorylation of Parkin. Parkin will then phosphorylate outer mitochondrial membrane proteins, and the polyubiquitin chains will also become phosphorylated by PINK1 resulting in

phospho-ubiquitinylated (pUB) OMM proteins. Autophagy adapters such as OPTN will then interact with these pUB chains and mediate binding to LC3 on autophagosomes, resulting in encapsulation of mitochondria within mito-lysosomes. For ubiquitin independent mitophagy, OMM proteins NIX recruits the early autophagy protein WIPI2 to enhance formation of autophagosomes at the site of depolarised mitochondria, while also being able to interact with LC3 directly. BNIP3 also binds LC3 directly, targeting defective mitochondria to autophagosomes. Meanwhile the mito-QC reporter will be intact at neutral pH, with both GFP and mCherry fluorescing on the OMM. However, as mitophagy progresses, the acidified mito-lysosome results in the quenching of GFP, leaving only mCherry fluorescence detectable, marking mitochondrial degradation. The mt-Keima reporter on the inner mitochondrial membrane will be fluorescent at a 458 nm excitation under the neutral pH in healthy mitochondria. However, as mitochondria are delivered to lysosomes, the pH reduction associated with acidification results in mt-Keima's fluorescence shifting to an excitation wavelength of 561 nm, marking mitochondria in acidified lysosomes. The GFP-mCherry tag on LC3 in the auto-QC reporter will function similarly to mito-QC, however, is not specific to mitophagy. Autophagosome fusion with a lysosome, and the associated acidification, quenches the GFP signal, resulting in mCherry signal marking acidified auto-lysosomes, regardless of contents. Figure was made using Biorender.

In addition to disparity in mitophagy rates amongst tissues, a novel reporter termed auto-QC has demonstrated disparity between mitophagy and autophagy rates through ageing. Auto-QC utilises the same tandem mCherry-GFP reporter as mito-QC, however instead of mitochondrial targeting through its FIS1 mitochondrial targeting sequence, auto-QC is bound to LC3B, localising it to autophagosomes (**Figure 1.3**) (McWilliams et al., 2019). The auto-QC mouse generated revealed that in cerebellar Purkinje cells and external granule cells, mitophagy increases, while autophagy does not (Rappe et al., 2024). In addition, glial fibrillary acidic protein (GFAP) positive astrocytes were observed to have the same disparity between mitophagy and autophagy through age, however more so in cerebellar astrocytes than those of the dentate gyrus (Rappe et al., 2024). These data demonstrate that although intrinsically linked, there are marked differences between mitophagy dynamics and those of autophagy.

### 1.3.3 ER-phagy

The disruption of endoplasmic reticulum (ER) homeostasis from a variety of sources can result in the accumulation of unfolded proteins inside the ER, causing ER stress. This ER stress can result in upregulation of the unfolded protein response (UPR) and

ER associated degradation (Wilkinson, 2019). However, more recently autophagy has been evidenced to play a role in ER homeostasis.

FAM134B is an ER-phagy receptor which also plays a role in ER curvature through its reticulon homology domain (RHD), however it also possesses an LIR for LC3/GABARAP interaction (Bhaskara et al., 2019; Jiang et al., 2020). During ER stress, the ER protein CAMK2B, a calcium sensitive ER kinase, phosphorylates the RHD of FAM134B, to increase oligomerisation and scission of the ER (Jiang et al., 2020). The localisation and phosphorylation of FAM134B functions as the deciding factor in the localisation of FAM134B ER-phagy (Jiang et al., 2020). The LIR on FAM134B then allows interaction of the excised ER region with LC3/GABARAP positive autophagosomes for degradation (Forrester et al., 2019). Interestingly, CAMK2B has also been shown to upregulate bulk autophagy by phosphorylation of Beclin 1, potentially aiding in upregulation of ER-phagy (Li et al., 2017). Moreover, FAM134B has also been associated with starvation induced ER-phagy. Prolonged starvation was demonstrated to result in activation and translocation of the transcription factors TFEB and TFE to the nucleus. The targets of these transcription factors include *RETREG1,* the gene encoding FAM134B, and genes associated with lysosome biogenesis (Cinque et al., 2020).

### 1.3.4 Lipophagy

Autophagy has also been demonstrated to regulate cellular lipid stores (Singh et al., 2009). Cellular lipids are stored in lipid droplets (LDs) derived from the ER and are comprised of a core of neutral lipids, such as cholesterol and triglycerides, coated with a phospholipid monolayer (Choudhary et al., 2015; Tauchi-Sato et al., 2002). Lipid droplets act as a means of storing free fatty acids, an accumulation of which can be damaging to the ER and mitochondria (Velázquez et al., 2016; Fu et al., 2011; Nguyen et al., 2017). Lipophagy relies on a variety of autophagy machinery. It was initially found to be ATG7 dependant, demonstrating a requirement for the canonical autophagy conjugation systems (Singh et al., 2009).

In contrast to other selective autophagy pathways, bulk degradation of lipid droplets has been suggested to be initiated by CMA. Perilipin 2 and Perilipin 3 on the membrane of LD have been demonstrated to be substrates of CMA (Kaushik & Cuervo, 2015). Their CMA targeting motifs are recognised by heat shock cognate

protein of 70 kDa (hsc70) that chaperones them to the lysosome (Chiang et al., 1989; Cuervo & Dice, 1996). On the lysosome, the Perilipins are unfolded by a complex of lysosome associated membrane protein 2A (LAMP2A), hcs70 and heat shock protein 90 (hsp90) (Salvador et al., 2000; Bandyopadhyay et al., 2008). This complex allows the unfolded perilipins to pass through the membrane and into the lysosome for degradation (Agarraberes et al., 1997). CMA targeting of Perilipin 2 appears to be dependent on phosphorylation of Perilipin 2 by AMPK, a central autophagy regulator, as discussed (**Chapter 1.1.1**)(Kaushik & Cuervo, 2016).

Removal of perilipins from the membrane of LDs results in the recruitment of cytosolic lipases, such as adipose triglyceride lipase (ATGL) and hormone-sensitive lipase (HSL) (Kaushik & Cuervo, 2015). Recruitment of these lipases to the LD result in preferential lipolysis of larger LDs, generating smaller LDs (Schott et al., 2019; Paar et al., 2012). As both ATGL and HSL contain LIRs, they are able to interact with LC3/GABARAP, recruiting these smaller LDs for degradation in autophagosomes (Martinez-Lopez et al., 2016).

There are other mechanisms proposed to be involved in lipophagy. Rab7 has been suggested to directly recruit lysosomes to LDs under autophagy inducing conditions, where the LD is internalised and degraded. It is also demonstrated that lipophagy is negatively affected by the silencing of Rab7 (Schroeder et al., 2015; Lizaso et al., 2013). These pathways however do not account for the localisation of p62 with LDs during lipophagy (Wang et al., 2017). Perilipin 1 has also been suggested to undergo ubiquitination in response to ethanol induced autophagy, recruiting p62 in the process. The LIR of p62 allows recruitment of the LDs associated with ubiquitinated Perilipin 3 and degradation, in a p62 dependant manner (Lizaso et al., 2013; Wang et al., 2017).

### 1.3.5 Aggrephagy

Unfolded proteins pose a danger to cellular homeostasis, with unfolded proteins being prone to aggregation due to being highly unstructured. These aggregates can result in stress to the ubiquitin proteosome system (UPS), dysregulation of which can cause cell death due to amino acid starvation (Suraweera et al., 2012). While smaller, soluble aggregates may be degraded by the UPS, larger insoluble aggregates require selective autophagy for degradation, known as aggrephagy (Scotter et al., 2014; Vargas et al., 2022).

Protein aggregates are often polyubiquitinated, allowing p62 to interact with the protein aggregate and LC3/GABARAP containing autophagosomes, resulting in degradation of the aggregate (Bjørkøy et al., 2005). However, in the case of aggrephagy, p62 plays a more complex role. For aggrephagy, the recognition of ubiquitinated proteins by p62 is aided by direct interaction with WD repeat domain 81 (WD81) (Liu et al., 2017). WD81 contains 2 separate LIRs, also allowing interaction with LC3, preferentially LC3C. This interaction with LC3C is required for aggrephagy, as in its absence, p62 is still able to localise with insoluble protein aggregates, however they are unable to be degraded (Liu et al., 2017).

Additionally, p62 is able to recruit components of the upstream autophagy machinery. Localisation of p62 to protein aggregates results in the recruitment of the ULK1 complex via a direct interaction between p62 and FIP200 (Turco et al., 2019). This interaction occurs upstream of LC3 binding, suggesting it is involved in directly recruiting the autophagy machinery at the site of the protein aggregate, with it being displaced in the presence of LC3 in p62's LIR (Turco et al., 2019).

Another important event for aggrephagy is the oligomerisation of p62. In order for p62 to function as an autophagy adapter it is required to oligomerise once in contact with the ubiquitin chains (Wurzer et al., 2015; Zaffagnini et al., 2018). This p62 oligomerisation results in a phase separation effect of the p62-ubiquitin-protein aggregate which is thought to drive segregation of the aggrephagy cargo (Sun et al., 2018).

## 1.4 Autophagy in neurodegeneration

While autophagy plays numerous roles in homeostasis, as discussed (**Chapter 1.1**), one of the conserved phenotypes observed across autophagy disorders is neurological impairment, as discussed (**Chapter 1.5/Table 1.1**). This poses the question as to why neural tissues are so susceptible to autophagy disruption. In order to better understand this, autophagy's role in other neurological diseases can be studied.

Autophagy plays a central role in homeostasis and quality control, disruption of which can be damaging in many tissue types. This is especially important in tissues with high energy demands, such as the brain (Harris et al., 2012). The majority of the energy

demand of the brain is attributed to neurons, and more specifically neuron synapses (Lennie, 2003). Maintenance of synaptic function requires continuous turnover of proteins, above that of less active cells, and local generation of ATP, both processes rely on functional autophagy (Rangaraju et al., 2014; Ziv, 2018). This reliance on autophagy has led to its implication in neurological disease, in particular age-related neurodegeneration (Palmer et al., 2024). A number of age-related neurodegeneration disorders have been associated with the accumulation of protein aggregates, including Parkinson's disease (PD), Alzheimer's disease (AD), amyotrophic lateral sclerosis (ALS) and Huntington's disease (HD) (Fujikake et al., 2018).

### 1.4.1 Parkinson's disease

PD is hallmarked by the specific degeneration of dopaminergic neurons in the substantia nigra of the pars compacta and the accumulation of protein aggregates. (Spillantini et al., 1997). These protein aggregates are known as Lewy bodies and contain the pre-synaptic protein α-synuclein (Spillantini et al., 1997). This was followed by identification of number of genes associated with familial PD. These include, but are not limited to, α-synuclein's gene (*SNCA*), leucine rich repeat kinase 2 (*LRRK2*), *PINK1* and *PARKIN* (Singleton et al., 2003; Polymeropoulos et al., 1997; Zimprich et al., 2004; Valente et al., 2004; Kitada et al., 1998). Despite the identification of numerous genes associated with PD, its pathology is relatively uniform. Aggregated α-synuclein in the presynaptic terminal is often found in PD and associated with loss of synapse function, an event that precedes neuronal cell death (Braak et al., 1999; Tanji et al., 2010). Interestingly, it has been suggested that the reason for dopaminergic neurons of the substantia nigra being so specifically degraded is due to their increased axonal complexity and metabolic demand over other dopaminergic neurons (Pacelli et al., 2015).

The accumulation of α-synuclein has been demonstrated to interfere with autophagy. Accumulation of wild type α-synuclein results in an impairment of autophagosome-lysosome fusion due to a decrease in SNAP29, a key component of the SNARE complex required for fusion, as discussed (**Chapter 1.1.4**) (Tang et al., 2021). In addition, overexpression of α-synuclein results in the mis-localisation of ATG9, resulting in impairment of omegasome formation and therefore reduction in autophagy initiation (Winslow et al., 2010). Variant α-synuclein is also able to modulate

autophagy, however in the opposing fashion. Variant α-synuclein has been demonstrated to upregulate autophagy and mitophagy in neurons, reducing healthy mitochondrial volume in the cell, leading to cell death (Choubey et al., 2011)

The association of *PINK1* and *Parkin* to PD provides a direct link between PD and mitophagy, their roles in which are described above (**Chapter 1.3.1**). Both *PINK1* and *Parkin* models have demonstrated that patient variants in these genes result in loss of mitophagy in dopaminergic neurons, with Parkin models also resulting in mitochondria associated aggregate formation (Lee et al., 2010; Suzuki et al., 2017). However, *in-vivo* knockout of *PINK1* in mice demonstrates that mitophagy is unaffected by the loss of PINK1 in tissues of high metabolic demand, including dopaminergic neurons (McWilliams et al., 2018). This is potentially due to PINK1/Parkin independent forms of mitophagy as discussed previously (**Chapter 1.3.1**). Parkin's non-mitophagic functions may move its role in PD away from mitophagy. Mouse and fly models have demonstrated Parkin interacting substrate accumulates in Pink1 and Parkin models, resulting in dopaminergic neuron loss (Shin et al., 2011; Pirooznia et al., 2020).

The most common *LRRK2* variants are gain of function variants (Li et al., 2014). One of these gain in function variants, R1441C, resulted in accumulation of enlarged autophagosomes, while knockdown of *LRRK2* was demonstrated to increase autophagic activity (Alegre-Abarrategui et al., 2009). This is potentially due to LRRK2's ability to modulate Rab GTPases. LRRK2's ability to phosphorylate Rabs and prevent their correct turnover from GTP and GDP bound states, and thus potentially interfering with autophagosome lysosome fusion (Pfeffer, 2023).

### 1.4.2 Alzheimer's disease

Alzheimer's disease is one of the most common causes of dementia, predominantly being diagnosed after the age of 65 (Alzheimer's Association, 2019). It is characterised by extracellular β-amyloid deposition, neurofibrillary tangles and aggregated hyperphosphorylated Tau protein (Duyckaerts et al., 2009). To generate β-amyloid, its precursor amyloid precursor protein (APP) is cleaved by presenilin 1 (PSEN1) and presenilin 2 (PSEN2). Incidentally the genes of these three proteins, *APP*, *PSEN1*, *PSEN2* respectively, are the three genes associated with autosomal dominant AD (LaFerla et al., 2007).

In relation to increasing protein aggregates, the upstream autophagy machinery is impaired in AD. Hyperphosphorylation of Tau, which leads to its Tau aggregate formation, is increased by acetylation of Tau, that can be mediated by the acetyltransferase p300 (Min et al., 2015). A parallel role of p300 is its acetylation of Raptor, activating it and the mTORC1 complex with which its associated, leading to inhibition of autophagy if p300 is active (Son et al., 2020). These processes would increase the accumulation of hyperphosphorylated tau aggregation, enhancing pathology. In contrast to autophagy inhibition, the extracellular plaques observed in AD have been shown to require autophagy machinery to form. *Atg7* knockout mice were found to have reduced extracellular β-amyloid plaques, with an increase in intracellular β-amyloid accumulation. While this intracellular accumulation results in neurodegeneration, the model demonstrates that autophagy machinery is required for export of β-amyloid (Nilsson et al., 2013).

Human studies have demonstrated accumulation of autophagosomes in synaptic terminals and neurites of patients with AD. These autophagosomes were also more abundant in neurons with tau pathology and were proposed to be impeded from lysosomal autophagosome fusion, suggesting a more complex modulation of autophagy in AD (Nixon et al., 2005). Additionally, AD models have demonstrated that lysosome acidification is compromised in AD, resulting in accumulation of β-amyloid in autolysosomes, which precedes extracellular plaque formation (Lee et al., 2022).

### 1.4.3 Amyotrophic lateral sclerosis

The underlying pathology of ALS involves the loss of motor neuron cell bodies, degeneration of the corticobulbar and corticospinal tracts and loss of lower motor neurons axons, resulting in muscle denervation (Hardiman et al., 2017). Its pathology is associated with protein aggregates and can be caused by a number of genes including TAR DNA-binding protein 43 *(TDP-43*), fused in sarcoma (*FUS*), Cu-Zn superoxide dismutase (*SOD1*) and *C9orf72*, however the composition of the protein aggregates is dependent on the causative gene of that case (Mackenzie et al., 2007; Vance et al., 2009; Kato et al., 2001; Ramos-Campoy et al., 2018).

The majority of ALS cases arise from variants in *TDP-43*, which produces TDP-43, an RNA processing protein (Mead et al., 2023). Cytoplasmic aggregates can be found in spinal cord neurons of ALS patients harbouring TDP-43 variants, which contain TDP-

43, p62 and LC3 implicating autophagy in disease pathology (Sasaki, 2011). TDP-43 has a dual role on autophagy in AD. Firstly, loss of TDP-43 results in upregulation of autophagy at the transcriptional level. This is conveyed by TDP-43's RNA binding role, where it directly interacts with and stabilises Raptor mRNA. Loss of TDP-43 results in a decrease of Raptor mRNA, subsequently reducing mTORC1's inhibition of autophagy. This results in translocation of the transcription factor TFEB to the nucleus for translation of autophagy and lysosomal related proteins, as discussed (**Chapter 1.1.1**) (Xia et al., 2016). This induction increases the number of autophagosomes produced, however loss of TDP-43 also leads to a reduction in Dynactin 1 production. Dynactin 1 plays a key role in lysosomal transport, a process which is essential for autophagosome lysosome fusion, as a result of this Dynactin 1 reduction, late-stage autophagy impairment has also been observed (Xia et al., 2016; Korolchuk et al., 2011).

A variety of *C9orf72* variants have also been shown to modulate autophagy in relation to AD. C9orf72 functions as an effector for Rab1A, mediating translocation of ULK1 during autophagosome biogenesis, functioning as a positive regulator of autophagy (Webster et al., 2016). Downstream, C9orf72 associates with Smith-Magenis syndrome chromosome region, candidate 8 (SMCR8) and WD repeat domain 41 (WDR41) which interacts with Rabs on the lysosomal surface during times of nutrient deprivation, aiding in recruitment of the HOPS complex, enabling autophagosome-lysosome fusion (Amick et al., 2020; Zhang et al., 2023). In line with these autophagic roles, depletion of C9orf72 results in reduced autophagy flux in a variety of neurons and cell types and resulted in aggregate accumulation (Ho et al., 2019; Almeida et al., 2013).

More directly, autophagy adapters have been implicated in ALS. Variants in p62, OPTN and TBK1 have been implicated in autophagy disruption, resulting in motor neuron cell death (Sundaramoorthy et al., 2015; Teyssou et al., 2013; Brenner et al., 2024). Variants surrounding p62's LIR, along with its variants disrupting its oligomerisation result in protein aggregates, and motor dysfunctions in models (Lattante et al., 2015; Carroll et al., 2018). ALS associated OPTN variant p.E478G results in reduced recruitment of LC3 to depolarised mitochondria in HeLa cells (Wong & Holzbaur, 2014a). The same OPTN variant has also been shown to impair autophagosome lysosome fusion due to dysfunction myosin VI mediated intracellular

trafficking (Sundaramoorthy et al., 2017). Additionally, variants in the OPTN modulator TBK1 have been shown to result in motor neuron death associated with accumulation of dysfunctional mitochondria and damaged lysosome in neural models (Moore & Holzbaur, 2016; Brenner et al., 2024).

### 1.4.4 Huntington's disease

Huntington's disease is associated with both motor and cognitive degeneration with age (Walker, 2007). This age-associated decline results from an expansion of a CAG repeat in the disease gene Huntingtin (*HTT*), giving polyglutamine tract expansion in the N-terminal of the protein, with the number of repeats being directly correlated to disease (Macdonald, 1993; Duyao et al., 1993). These polyglutamine tracts result in aggregation of Huntingtin into structures resembling the β-amyloid aggregates of AD, in the nucleus and cytoplasm (Scherzinger et al., 1997; DiFiglia et al., 1997). Huntingtin and mutant Huntingtin are both degraded by autophagy, particularly in the stages prior to aggregate formation, meaning autophagy modulation will have an effect on mutant Huntingtin aggregation, (Ravikumar, 2002; Zhao et al., 2024).

To this end, a single variant in *ATG7* has been associated with an earlier onset of HD (Metzger et al., 2013, 2010). The HD patients harbouring the p.V417A variant in a core autophagy protein *ATG7*, results in an onset four to six years earlier than those without (Metzger et al., 2013, 2010). Additionally, Huntingtin aggregates have been demonstrated to interfere with autophagy. Aggregates have been shown to interfere with autophagy induction due to starvation by preventing Beclin 1 activation by Ataxin-3 (Ashkenazi et al., 2017). They have also been proposed to interfere with cargo recognition, with HD models being able to produce and turnover autophagosomes, however sequestration of cytosolic cargo into these autophagosomes was impaired (Martinez-Vicente et al., 2010). Finally, HD mouse model primary neurons have shown a disruption of autophagosomal retrograde transport from the axon tip to the cell body, resulting in impaired autophagosome turnover (Wong & Holzbaur, 2014b).

## 1.5 Congenital disorders of ATG genes

Recent advances in sequencing technologies allowed for the identification of a growing number of genetic disorders associated with autophagy related genes. The dynamic nature of autophagy results in these monogenetic disorders effecting different

stages of autophagy, with tissue specific expression profiles and the differing metabolic requirements of tissues result in specific tissues being more susceptible than others (Teinert et al., 2020). The genes associated with congenital autophagy disorders are outlined below (**Table 1.1**). While these disorders result in a variety of presentations, the majority have neurological involvement which can be characterised by neurodevelopmental defects. Many of these patients have clear MRI changes, including atrophy of the corpus callosum, cerebellar and cerebral atrophy and ventricular abnormalities. They also commonly present with developmental delay and ataxic phenotypes (Teinert et al., 2020).

While there are a multitude of genetic disorders associated with genes involved in autophagy, there are very few associated with core *ATG* genes. However, a number of core autophagy genes have been defined as risk factors for a range of other diseases. For example, an *ATG16L1* variant, resulting in p.T300A, has been identified as a risk factor in Crohn's disease with minimal effect on canonical autophagy (Hampe et al., 2007; Rioux et al., 2007; Fujita et al., 2009). Aside from their association with other genetic diseases, like *ATG7* in HD as discussed (**Chapter 1.4.4**), only four core *ATG* genes have been described to cause disease: *ATG4*, *ATG5*, *ATG7* and *ATG9*.

### 1.5.1 Congenital disorder of ATG4D

As discussed, (**Chapter 1.1.3**), ATG4 is a protease which cleaves the C-terminus of LC3/GABARAP proteins to expose the C-terminal glycine required for conjugation to PE by ATG7 and ATG3 (Ichimura et al., 2000). The same LC3/GABARAP proteins are delipidated by ATG4 also (Kauffman et al., 2018). In humans there are four ATG4 homologs, ATG4A, ATG4B, ATG4C and ATG4D, each with different activities and specificities to LC3/GABARAPs (Li et al., 2011).

So far, three individuals from two unrelated families have been described harbouring bi-allelic *ATG4D* variants (Morimoto et al., 2023). All three individuals had global developmental delay, speech impairment and abnormal facial features, with two unrelated individuals having motor dysfunction and seizures. One individual also had non-progressive atrophy of the cerebellum. Transmission electron microscopy of *ATG4D* subject derived and control primary fibroblasts and lymphoblastoid cells showed autophagosomes were able to form when induced with Torin 1, with late-stage autophagy blocked by Bafilomycin A1 as part of an autophagy flux assay. Western

blotting showed no increase in autophagy adapter p62, indicating correct turnover of autophagic substrates. *In-vitro* analysis of GABARAPL1 cleavage by ATG4D demonstrated that all but one of the variant ATG4D isoforms was detrimental to GABARAPL1 cleavage and therefore priming. Additionally, these three variants failed to fully recover GABARAPL1 priming in a tetra knockout model lacking all 4 *ATG4* isoforms (Morimoto et al., 2023). These patients demonstrate that while the four different *ATG4* isoforms are thought to be redundant, loss of one of the isoforms is sufficient to produce human disease, even if there is only minimal effect on autophagy.

**Table 1.1. Outline of autophagy related congenital diseases and their associated genetic cause.**

| Disorder (OMIM ID) | Gene | Inheritance Pattern | Stage involvement | Reference |
|---|---|---|---|---|
| ***SQSTM1/p62*-associated childhood-onset neurodegeneration (OMIM #617145)** | *Sequestosome 1 (SQSTM1/p62)* | Autosomal recessive | Cargo detection | (Muto et al., 2018; Haack et al., 2016) |
| ***TBCK*-encephaloneuropathy (OMIM #616900)** | *TBC1 domain-containing kinase (TBCK)* | Autosomal recessive | Autophagy induction | (Chong et al., 2016; Bhoj et al., 2016) |
| **Beta-propeller protein-associated neurodegeneration (OMIM #300894)** | *WD repeat-containing protein 45 (WDR45)* | X-linked | Autophagosome formation | (Saitsu et al., 2013) |
| **SPG49 (OMIM #615031)** | *Tectonin beta-propellor-repeat containing protein 2* | Autosomal recessive | Autophagosome formation | (Covone et al., 2016; |

| | | | | |
|---|---|---|---|---|
| | *TECPR2* | | | Heimer et al., 2016) |
| **AP-4-HSP (SPG47, SPG50, SPG51, SPG52) (OMIM #614066; #612936; #613744; #614067)** | *Adapter related complex 4 beta-1 subunit (AP4B1)* *Adapter related complex 4Mu-1 subunit (AP4M1)* *Adapter related complex 4 epsilon 1 subunit (AP4E1)* *Adapter related complex 4 sigma-1 subunit (AP4S1)* | Autosomal recessive | Autophagosome formation | (Abdollahpour et al., 2015; Hardies et al., 2015; Moreno-De-Luca et al., 2011; Verkerk et al., 2009) |
| **SPG15 (OMIM #270700)** | *Zinc finger five domain-containing protein 26 (ZFYVE26)* | Autosomal recessive | Autophagosome maturation<br>Lysosome reformation | (Elleuch et al., 2007; Goizet et al., 2009; Boukhris et al., 2009) |
| **Vici syndrome (OMIM #242840)** | *Ectopic P-Granules autophagy protein 5 homolog (EPG5)* | Autosomal recessive | Autophagosome-lysosome fusion | (Dionisi Vici et al., 1988; Cullup et al., 2013; Maillard et al., 2017) |
| **Autosomal-recessive spinocerebellar ataxia 20 (OMIM #616354)** | *Sorting nexin 14 (SNX14)* | Autosomal recessive | Autophagosome-lysosome fusion | (Sousa et al., 2014; Thomas et al., 2014) |

| | | | | |
|---|---|---|---|---|
| **SPG11 (OMIM #604360)** | *Spatacsin (SPG11)* | Autosomal recessive | Lysosome reformation | (Nakamura et al., 1995; Casali et al., 2004; Ueda et al., 1998) |

### 1.5.2 Congenital disorder of ATG5

ATG5 covalently binds to ATG12 to form the ATG5-ATG12 complex, interacting with ATG16L1 to recruit autophagy machinery at the expanding autophagosome as described (**Chapter 1.1.3**) (Hanada et al., 2007). Individuals carrying *ATG5* variants were initially described as having a non-progressive ataxia with cerebellar hypoplasia as part of a wider cohort (Yapici & Eraksoy, 2005). Later investigations resulted in the identification of homozygous missense variants in *ATG5*, resulting in a p.E122D change in *ATG5* in two sibling from one family of the cohort (Kim et al., 2016). The two affected individuals were described as having developmental delay, cerebellar abnormalities, speech impairment and ataxia.

The p.E122D variant lies in a region close to ATG5's interface with ATG12, with subject derived lymphoblastoid cells showing a loss of the ATG5-ATG12 conjugate, and LC3-II conjugation impairment in response Torin 1/Bafilomycin A1 autophagy flux assay. The p.E122D variant however was stable and able to non-covalently bind to ATG16L1. In an *atg5* yeast model, the p.E122D variant was unable to fully rescue the autophagy flux deficit of *atg5* null *Saccharomyces cerevisiae*, and unable to recover the ataxic phenotype of *Atg5*-null *Drosophila melanogaster* (Kim et al., 2016). These *ATG5* patients, were the first *ATG* patients described, demonstrating that loss of core *ATG* genes is compatible with human life.

### 1.5.3 Congenital disorder of ATG7

ATG7 functions as an E1-like enzyme, playing a role in ATG5-ATG12 conjugation and LC3 conjugation to PE, as discussed (**Chapter 1.1.3**) (Mizushima et al., 1998; Ichimura et al., 2000). Twelve patients from five unrelated families were identified

harbouring biallelic loss of function variants in *ATG7*, with 5 patients from one family harbouring a homozygous loss of function variant (Collier et al., 2021). All subjects presented with ataxia, intellectual disability and delayed development, with brain MRIs all showing cerebellar hypoplasia and atrophy of the corpus callosum.

Primary subject derived fibroblast investigations showed that Subject 1 had no detectable ATG7, and accumulated p62 under basal conditions. An impairment in ATG5-ATG12 conjugation was also identified, along with a reduction in ULK1. Autophagy flux assays using AZD8055 to induce autophagy and chloroquine to block end stage autophagy also showed no detectable LC3-II in Subject 1 fibroblasts. TEM analysis of subject 1 fibroblasts showed abundant autophagosomes, with some also containing mitochondria. The remaining 5 subject samples, from the 4 remaining families, all showed decreased ATG7, and p62 accumulation, aside from subjects 3 and 4 from Family 2. Primary patient fibroblasts also all showed reduction in LC3-II production in response to an autophagy flux assay. Complementation studies using *Atg7*-null mouse embryonic fibroblasts and *S. cerevisiae* also showed the *ATG7* variants found in the subjects were unable to recover LC3 lipidation. This cohort represents the largest group of *ATG* subjects, also the first subjects with a complete loss of LC3-II production.

Cultured myoblasts from one individual (Subject 2, Family1) showed no detectable ATG7, accumulation of p62 and minimal LC3-II under basal conditions. Immunohistochemical (IHC) analysis of skeletal muscle biopsy from the same subject again showed p62 accumulation, impaired mitochondrial function, and accumulation of neutral lipids. Transmission electron microscopy (TEM) of the same subject's biopsy also showed accumulation of lipid containing granules. These studies demonstrated the clinical significance of impaired autophagy flux in humans while expanding the clinical spectrum of *ATG* related congenital disorders of autophagy.

### 1.5.4 Congenital disorder of ATG9B

Lipid scramblases allow for translocation of lipids between two lipid layers, in a bidirectional manner, independent of ATP. Autophagy related 9 (ATG9), mediates the transfer of lipids delivered by ATG2 from the outer phospholipid layer to the inner layer. ATG9 is the only lipid scramblase involved in autophagosome biogenesis, and has two isoforms, ATG9A and ATG9B, with ATG9B being able to compensate for ATG9A

(Matoba et al., 2020; Chiduza et al., 2024; Guardia et al., 2020). ATG9 localises to the phagophore in the early stages of autophagosome biogenesis and mediates the transfer of lipids to the expanding autophagosome (Matoba et al., 2020). ATG9B is specifically expressed in the placenta and pituitary gland (Chiduza et al., 2024). Two siblings have been reported to have recessively inherited a homozygous deletion of eleven nucleotide in ATG9B, resulting in a nonsense change (Kılıç et al., 2024). *In-vitro* models show that variant ATG9B localises as wild type ATG9B, however, the Golgi derived vesicles on which it localises are misformed. In addition, the variant ATG9B was shown to be less stable than the wild type. A knock in mouse model of the ATG9B truncation was found to have no phenotype. Histological analysis of *ATG9B* variant mouse placentas showed no change when compared to wild type. Various behaviour models also showed no change between the *ATG9B* variant mice and wild type (Kılıç et al., 2024). The *ATG9B* patients, and accompanying models, demonstrate the tissue specific nature of *ATG* diseases. However, there were no assessments of autophagy related proteins, other than *ATG9B*, or autophagy flux, so relating disorders of *ATG9B* to the other described *ATG* disorders is difficult.

## 1.6 ATG7

The core autophagy gene *ATG7* encodes the human homologue of the yeast and mouse *atg7* and *Atg7,* respectively (Galluzzi et al., 2017). The resulting protein ATG7 functions in both the key conjugation systems required for autophagy, the ATG5-ATG12 and LC3 conjugation systems, as described (**Figure 1.1**) (Tanida et al., 1999; Mizushima et al., 1998; Ichimura et al., 2000). Variants identified in *ATG7* also forms the largest cohort of *ATG* patients to date. Subjects harbouring *ATG7* variants present with developmental delay, intellectual disability, ataxia, cerebellar hypoplasia and posterior atrophy of the corpus callosum. Additional phenotypes include sensorineural hearing loss, optic atrophy and seizures, as discussed (**Chapter 1.5.3)** (Collier et al., 2021).

### 1.6.1 ATG7 structure and function

ATG7 functions as a homodimer, with LC3 binding to the extreme C-terminal domain (ECTD) of an ATG7 molecule (**Figure 1.4**) (Komatsu et al., 2001; Yamaguchi et al., 2018). LC3 is then transferred to the adenylation domain of ATG7 resulting in a conformational change to ATG7's crossover loop, a relatively unstructured region

containing the catalytic cysteine in the adenylation domain. This conformational change brings the C-terminal glycine into close proximity of the α-phosphate group of the bound adenosine triphosphate (ATP), leading to the adenylation reaction and formation of a thioester bond (M. Yamaguchi et al., 2018; Noda et al., 2011).

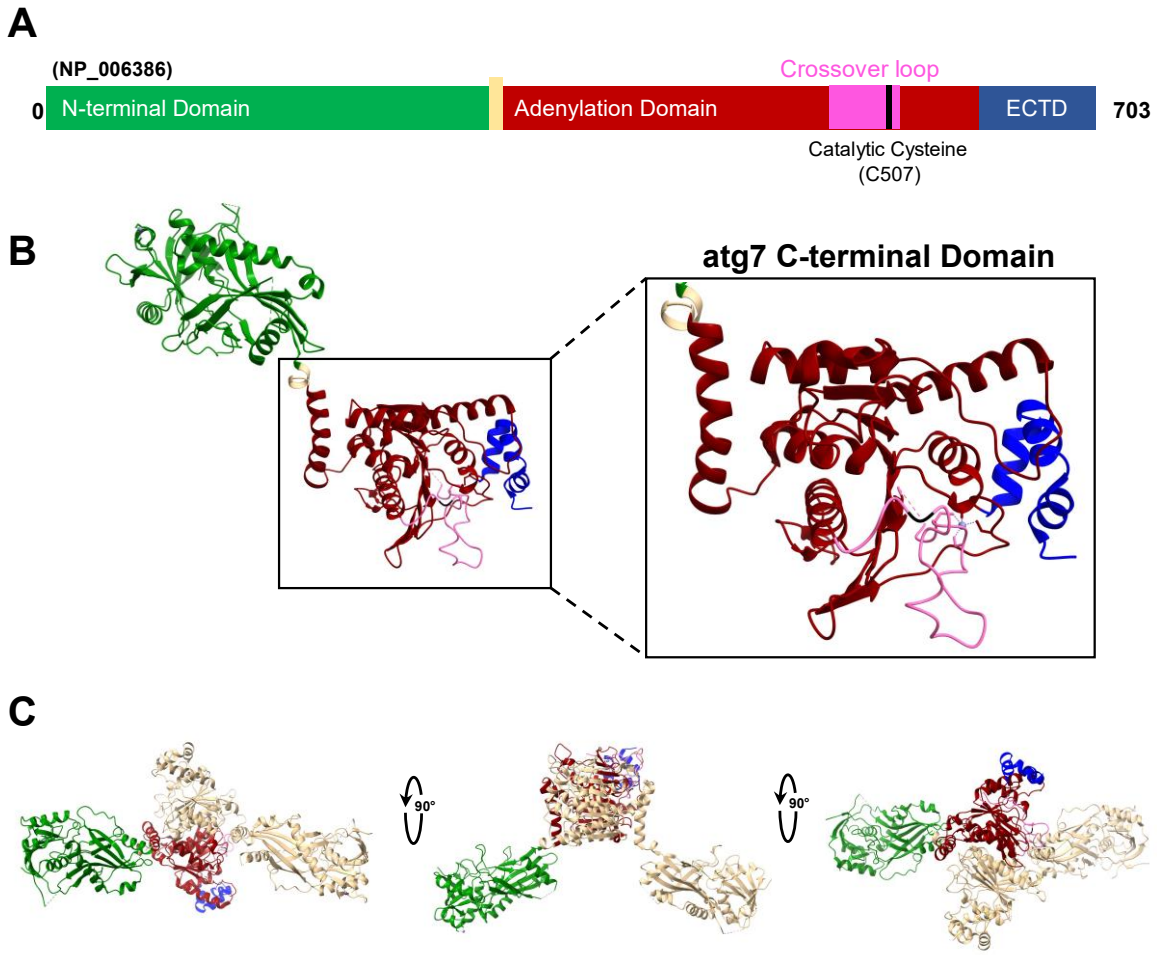


**Figure 1.4. Domains and structural features of ATG7. A**. Schematic of human ATG7. A 703 amino protein consisting of an N-terminal region (green), a C-terminal region containing the adenylation domain (red). Contained in the adenylation domain is the cross over loop (pink), a relatively unstructured region containing the catalytic cysteine at amino acid 507 (black). The C-terminal domain also contains the extreme C-terminal domain (ECTD) (blue), responsible for LC3-I recruitment. Protein Data Bank accession number 3VH2. **B**. Crystal structure of S. cerevisiae atg7 monomer (Noda et al., 2011). Domains are coloured as in A. **C**. Crystal structure of atg7 homodimers. One protomer is coloured as in A, the second is tan. Protein Data Bank accession number 3VH2 (Noda et al., 2011).

ATG3 has a flexible region which is negatively charged, this allows it to bind to the positively charged N-terminal domain of ATG7 (Noda et al., 2011). The orientation of the ATG7 dimer places the N-terminal domain of one protomer alongside the C-terminal domain of the other. This allows LC3-I bound to the C-terminal domain of one protomer to be transferred to the ATG3 bound to the opposing protomer's N-terminal, in a *trans* manner. This transfer then allows ATG3 to efficiently lipidate LC3-I (Noda et al., 2011).

This lipidation of LC3 is enhanced by the product of the second key conjugation system, ATG5-ATG12 (Hanada et al., 2007). To generate this dimer, ATG12 is first activated by ATG7, before being transferred to ATG10 for conjugation to ATG5. This reaction requires ATG7 and ATG10, with the ATG5-ATG12 conjugate interacting with ATG16L1 to form a trimeric complex, as discussed (**Chapter 1.1.3**) (Shintani, 1999; Mizushima et al., 1998; Tanida et al., 1999).

### 1.6.2 ATG7 isoforms

There are three distinct isoforms of ATG7 in humans, with ATG7(1) being the most common, followed by ATG7(2) and then ATG7(3) being the least expressed (**Figure 1.5A**)(Ogmundsdottir et al., 2018). ATG7(1) is the full-length protein, consisting of 703 amino acids, ATG7(2) lacks 26 residues in the C-terminus domain, and ATG7(3) lacks a 38 residue N-terminal region and a 40 residue C-terminal region, which does not overlap with the residues missing from ATG7(2). While the function of ATG7(2) is unknown, it is highly expressed in blood, however it is unable to facilitate LC3 lipidation (**Figure 1.5B**) (Ogmundsdottir et al., 2018).

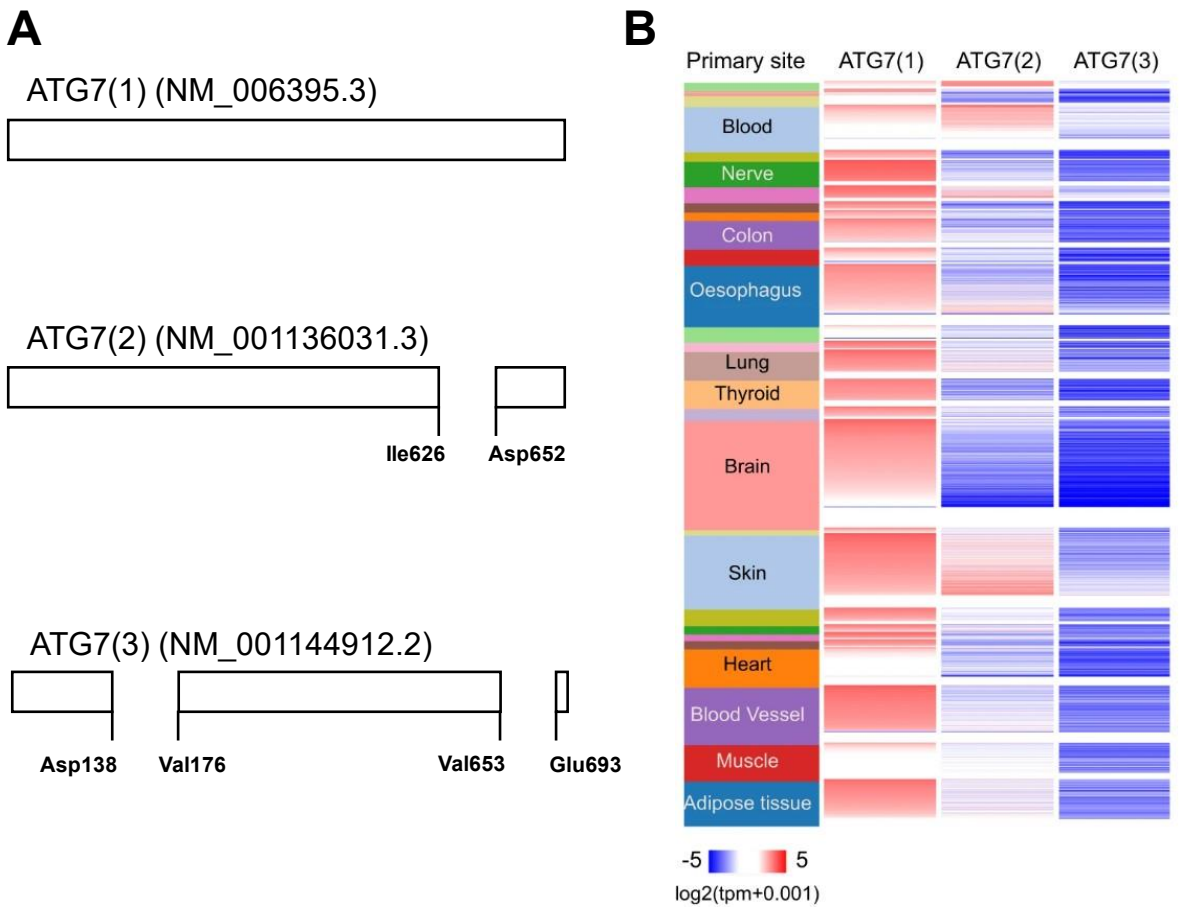


**Figure 1.5 Differences in splicing and expression of the ATG7 isoforms**. **A.** Schematic of the three ATG7 isoforms, and the regions omitted. NCBI RefSeq numbers are indicated. **B.** RNA sequencing data obtained from GTEx (https://www.gtexportal.org/home/) showing expression levels of the three ATG7 isoforms across tissues. From top to bottom tissues are: bone marrow, cervix uteri, bladder, fallopian tube, kidney, liver, blood, pituitary, nerve, testis, prostate, small intestine, colon, stomach, oesophagus, pancreas, spleen, lung, thyroid, adrenal gland, brain, salivary gland, skin, breast, vagina, uterus, ovary, heart, blood vessel, muscle, adipose tissue. Figure adapted from Ogmundsdottir et al., 2018

### 1.6.3 Non-Autophagic roles of ATG7

Parallel to ATG7's role in degradation of cytosolic components, ATG7 functions in LC3 associated phagocytosis (LAP), a form of CASM, previously discussed (**Chapter 1.2**). Here, recognition of extracellular material, such as dead cell fragments and pathogens, are recognised by cell surface ligands and endocytosed into phagosome. Upon entry to the cell, RUN domain Beclin-1 interacting and cysteine rich domain containing protein (Rubicon) on the phagophore interacts with the PI3KC3-C2 complex via its UVRAG subunit to target it to the phagophore. This is followed by LC3 recruitment and autophagy machinery dependant lipidation on the phagosome,

promoting lysosomal fusion and degradation. The defining factor of LAP over autophagy is the localisation of LC3-II to single membrane vesicles (Peña-Martinez et al., 2022). LAP has been associated with clearance of bacteria, immune responses and the vision cycle (Kim et al., 2013; Cunha et al., 2018; Sarkar et al., 2017; Fadok et al., 1998).

Aside from its E1-like role in canonical autophagy and LAP, ATG7 also plays a role in the cell cycle. Under basal conditions ATG7 binds to the tumour suppressor p53, preventing phosphorylation of p53, however this interaction is increased in times of starvation. The target of p53, p21, is a cell cycle regulator which prevents cell cycle progression from G1 to S phase under stress. ATG7 inactivation of p53 eliminates transcription of *p21,* preventing cell cycle arrest. Loss of ATG7 also results in increased expression of proapoptotic genes *phorbol-12-mysristate-13-acetate-induced protein 1 (Noxa),* resulting in increased activation of Bcl-2 associated X protein X (Bax) and Bcl-2 homologous antagonist killer (Bak) resulting in apoptosis induction. This is in addition to upregulation of p53 upregulated modulator of apoptosis (*Puma*) in the absence of ATG7 (Lee et al., 2012).

### 1.6.4 Animal models of ATG7

The majority of ATG7 research has been carried out using an array of mouse models, elucidating the global and tissue specific effects of ATG7 deficiency. Systemic knockout of genes involved in the two core conjugation systems results in a neonatal lethal phenotype, this includes Atg3, Atg5, Atg12, Atg16l1 and Atg7 (Kuma et al., 2004; Sou et al., 2008; Malhotra et al., 2015; Saitoh et al., 2008; Komatsu et al., 2005). *Atg7* null mice develop normally, however die within 24 hours of birth (Komatsu et al., 2005). These knockout (KO) mice had no detectable Atg5-Atg12 conjugate or LC3-II, demonstrating loss of both conjugation systems. Atg7 KO mice were only able to form few autophagosomes which were smaller than those found in wild type mice. There was accumulation of defective mitochondria and protein aggregates, denoted by ubiquitin positive inclusions. However, the neonatal lethal phenotype of these mice makes further investigations difficult, resulting in the development of a variety of conditional knockout models. These models have allowed for the investigation of *Atg7*'s role in a variety of mouse tissues (Kuma et al., 2017).

### 1.6.5 Conditional models of ATG7

To study the effect of *Atg7* ablation in adult mice, a tamoxifen inducible systemic knockout model has been created. These mice can survive between two and three months after *Atg7* ablation (Karsli-Uzunbas et al., 2014). Mice also suffered from impaired glucose metabolism, muscle wasting, neurodegeneration and a fatal loss of starvation response.

Conditional knockout of *Atg7* in the central nervous system also results in premature death within 28 weeks of birth (Komatsu et al., 2006). Mice suffered from neuronal loss in the cerebrum and cerebellum, particularly Purkinje cells of the cerebellum, resulting in an ataxic phenotype and behavioural abnormalities. Purkinje cell specific *Atg7* KO resulted in axonal swelling, loss of axon terminals, and Purkinje cell death (Komatsu, Wang, et al., 2007). Dopaminergic midbrain neuron specific deletion resulted in dysregulation of presynaptic transmission (Hernandez et al., 2012). Forebrain *Atg7* deletion resulted in age-related neurodegeneration with accumulation of ubiquitin/p62 and phosphorylated Tau inclusions (Inoue et al., 2012). Microglia specific deletion of *Atg7* resulted in aberrant dendritic spine pruning, altered synaptic behaviour, demonstrating how the cross talk between neurons and other cells of the brain can affect neuronal health (Kim et al., 2017). Hippocampal neural stem cell (NSC) specific deletion showed that adult mice are able to maintain their NSC pool and differentiate adult born neurons correctly during adulthood (Jung et al., 2020).

One of the findings from systemic *Atg7* KO mice was enlarged livers (Komatsu et al., 2005). Liver specific deletion of *Atg7* resulted in p62 accumulation and aggregate formation along with liver injury (Komatsu, et al., 2007). However, liver injury was recovered by dual KO of p62 along with *Atg7*, suggesting p62 accumulation itself may play a role in the *Atg7* associated tissue injury.

As observed with the deletion of *Atg7* in adult mice, skeletal muscle specific deletion of *Atg7* results in muscle atrophy and an age dependant decrease in strength (Masiero et al., 2009). Tissues showed accumulation of mitochondria and an aberrant cell ultrastructure. *Atg7* was also demonstrated to be protective of mitochondria during exercise induced muscle damage, particularly in females (Lo Verso et al., 2014).

Cardiac muscle deletion of *Atg7* results in lipid accumulation and systolic dysfunction in response to a high fat diet, exacerbating a cardiomyopathy phenotype (Tong et al.,

2019). Loss of *Atg7* in smooth muscle results in dysregulation of calcium homeostasis (Michiels et al., 2015). Smooth muscle cells had an enlarged sarcoplasmic reticulum, altered $Ca^{2+}$ homeostasis, impaired calcium handling and increased susceptibility for depolarisation. Endothelial deletion of *Atg7* resulted in reduced release of secretory granules, impaired fatty acid storage and metabolism and enhanced endothelial to mesenchymal transition (Torisu et al., 2013; Singh et al., 2015; Altamimi et al., 2019).

In the pancreas, *Atg7* deletion results in necroptosis, inflammation, fibrosis and premature death due to impaired exocrine and endocrine signalling (Zhou et al., 2017). *Atg7* is required for islet alpha and beta cell function and architecture, with loss of *Atg7* reducing beta cell mass and calcium dynamics as well as alpha cell architecture, resulting in a loss of adaptability to a high fat diet (Jung et al., 2008; Himuro et al., 2019; Ebato et al., 2008).

In the haematopoietic system, it has been established *ATG7* is required for clearance of mitochondria during the differentiation process (Zhang et al., 2009; Cao et al., 2016). As a result of this, *Atg7* KO in the haematopoietic system results in severe anaemia and T lymphocyte apoptosis, interestingly loss of *Atg7* only appeared to effect specific subsets of blood cells (Mortensen et al., 2010). T lymphocytes lacking *Atg7* had expanded ER and impaired calcium influx in response to T cell receptor stimulation (Jia et al., 2011). This calcium handling impairment was due to impairment of intracellular calcium store release from the ER. Haematopoietic stem cell KO of *Atg7* resulted in accumulation of mitochondria, ROS and DNA damage. This was accompanied by increased proliferation and loss of function, with *Atg7* KO immune cells unable to recover immune compromised mice (Mortensen et al., 2011).

Chondrocyte specific deletion of *Atg7* resulted in accumulation of type II procollagen in the ER, resulting in abnormal extracellular matrix formation (Cinque et al., 2015). This led to a decrease in tibial and femoral lengths. Osteoblast KO of *Atg7* was found to also cause decreased cell proliferation and mineralisation of the extracellular matrix. These cells were also found to be under ER stress in an *Atg7*-null dependant manner, with the ER stress found to be driving the disease phenotype observed (Li et al., 2018).

In the intestine, removal of *Atg7* from the epithelium results in little histological change to the small intestine, aside from increased inflammatory response (Inoue et al., 2012; Cadwell et al., 2009; Fujishima et al., 2011). They were also more susceptible to

bacterial infection (Inoue et al., 2012). Deletion in intestinal stem cells results in increased oxidative stress and impaired DNA damage response, along with altered gut-microbiome interactions (Trentesaux et al., 2020).

Deletion of *Atg7* in the outer hair cells of mouse ears results in early onset hearing loss, accompanied by accumulation of dysfunctional mitochondria (Zhou et al., 2020). *Atg7* deletion in the retinal pigmented epithelium of the eye resulted in retinal degeneration similar to that observed in age related macular degeneration (Zhang et al., 2017). This was associated with p62 accumulation, oxidative stress and DNA damage.

Together these models demonstrate the tissue specific nature of phenotypes associated with *ATG7* deletion. Not only does phenotype severity vary, but also the underlying mechanism associated with the observed pathologies across models.

### 1.6.6 Non-mammalian models of autophagy

Yeast forms the basis of our genetic understanding of autophagy. The first genetic screens for autophagy mutants were carried out in *S. cerevisiae* in 1993, followed by the identification of the first autophagy related gene, *Atg*1 in 1997 (Tsukada & Ohsumi, 1993; Matsuura et al., 1997). Following the subsequent discovery of other *Atg* genes, first confirmation of conservation between the mammalian and yeast systems proved pivotal. This came when the first mammalian *ATGs* were identified, ATG5 and ATG12 and it was demonstrated that the yeast Atg5-Atg12 conjugation system was conserved.

In addition to the initial discovery and characterisation of autophagy in *S. cerevisiae,* the highly conserved nature of autophagy, *S. cerevisiae* can be utilised to demonstrate pathogenicity of novel variants. In the first report of congenital bi-allelic loss of function *ATG7* variants, *atg7* knockout *S. cerevisiae* complemented with an *atg7* variant homologous to the subject variants demonstrated the variability associated with *ATG7* variants. Some variants were unable to recover autophagy in a Pho8Δ60 assay, while other variants saw minimal reductions (Collier et al., 2021). The yeast Pho8Δ60 assay quantifies the autophagic delivery of a modified alkaline phosphatase Pho8 in the yeast vacuole (Noda & Klionsky, 2008). Similar experiments using a *S. cerevisiae* model expressing a GFP-atg8 demonstrated that atg8 degradation is not recovered by *ATG7* variants, but with smaller changes in others (Guimaraes et al., 2015).

During metamorphosis of *D. melanogaster* larva, there is a large increase in autophagy to account for the significant reorganisation of tissue occurring. Although, *Atg7* null *D. melanogaster* larvae are viable, they suffer from a variety of conditions (Juhász et al., 2007). Atg7 was shown to be required for developmental autophagy in the midgut of the developing larvae, as well as starvation induced autophagy in larval fat bodies. As a result of this, the *ATG7* null mutants suffer from delayed development of the midgut, but do not show any major developmental defects. The null mutants were however hypersensitive to nutrient and oxidative stress, resulting in reduced life span, as well as progressive neuronal degeneration.

In order to investigate the role of autophagy in *Danio rerio* embryogenesis, *ATG7* knockdowns have previously been produced (Lee et al., 2014). It was confirmed that autophagy was occurring in wild type *D. rerio* embryos, and that knockdown of *Atg7* inhibits autophagy in developing embryos. As a result of this, embryos displayed a number of developmental defects, with 31% of *Atg7* knockdowns having cardiac defects, such as pericardial oedema, defective blood flow through the heart and numerous structural defects. Of the autophagy knockdowns generated (*Atg5, Atg7* and *Beclin 1)*, the *Atg7* knockdown produced the most profound effect on the developing heart's gene expression pattern, resulting in the most severe developmental defects.

## 1.7 Project Aims

The main aim of this project was to increase our understanding of disease pathology associated with loss of function variants in core *ATG* genes. This was to be performed using two approaches outlined below.

The first was a disease model approach. To date the majority of research directly associated with core autophagy disorders has been performed using animal models or systems. While these may provide valuable insight into the potential autophagy impairment associated with these disorders, they do not recapitulate the wider patient phenotypes associated congenital autophagy disorders. To fill this gap, the aim was to generate a clinically relevant disease model for these predominantly neurological presenting disorders. For this purpose, induced pluripotent stem cells harbouring both full and heterozygous *ATG7* knockout would be generated alongside isogenic controls. Subsequent differentiation into neuron-astrocyte co-culture would provide novel

insight into the neural specificity associated with *ATG7* related neurological disease. The aim was to characterise the biochemical phenotype associated with ATG7 impairment and the resulting developmental and morphological changes in ATG7 deficient neural co-cultures. Finally, the aim was to characterise any functional impairment in the neurons of these co-cultures using calcium imaging analysis.

Secondly, a patient-based approach was employed, identifying new patients harbouring variants in *ATG7*, and also identify novel congenital disorders of autophagy. These new patients would be identified through existing collaborations and the GeneMatcher platform. Addition to the existing *ATG7* patient cohort would allow the expansion of the range of pathologies associated with *ATG7* disorders, providing further insight into the genetic inheritance patterns associated with *ATG7* related neurological disease. It will also provide a wider perspective of the range of phenotypes associated with congenital autophagy defects, allowing for better patient diagnosis. Identification and characterisation of novel core autophagy disease genes would not only provide greater clinical understanding of congenital disorders of autophagy, but also provide a deeper understanding of autophagy in human development and disease.

# 2 Materials and Methods

## 2.1 Equipment

| | |
|---|---|
| Analogue Tube Roller | Thermo Fisher Scientific |
| Aspiration System Vacusafe | Integra |
| Cell Culture Incubator with CO2, MCO-18AIC | PHCBI |
| Panasonic | |
| Cellometer Auto 1000 Automated Cell Counter | Nexcelom |
| Centrifuge 5417R | Eppendorf |
| Centrifuge 5418 | Eppendorf |
| Centrifuge Universal 32 | Hettich |
| Ceramic Plate Stirrer, U151 | Stuart |
| ChemiDoc MP Imaging System | Bio-Rad |
| Class II Microbiological Safety Cabinet (NH-EN-2004) | Faster |
| CoolCell Freezing Container | Biocision |
| Electrophoresis Unit, HU10 Mini-Plus Horizontal Unit | Scie-Plas |
| Genetic Analyser, ABI 3130xl | Applied Biosystems |
| Incucyte S3 Live-cell Analysis System | Essen Bioscience |
| Leica DM 500 light microscope | Leica |
| Microcentrifuge, Techinico | Griffin Education |
| Mini-Protean Tetra Cell system | Bio-Rad |
| NanoDrop Spectrophotometer, ND-1000 | ThermoScientific |
| Orbital Shaker SSL1 | Stuart |
| pH Meter 3510 | Jenway |
| SpectraMax M5e Multimode Plate Reader | Molecular Devices |
| Thermal Cycler, Veriti 96 Well | Applied Biosystems |

## 2.2 Consumables

| | |
|---|---|
| 96 Well PCR Plate, Semi-skirted, Clear | StarLab |
| Aspiration Pipette | Greiner |
| Cell Star Disposable Tubes (15 ml) | Greiner Bio-One |
| Cell Star Falcon Tubes (50 ml) | Greiner Bio-One |
| Flat Bottom 6 Well Plates | Greiner Bio-One |

| | |
|---|---|
| Flat Bottom 12 Well Plates | Greiner Bio-One |
| Flat Bottom 24 Well Plates | Greiner Bio-One |
| Flat Bottom 96 Well Plates | Greiner Bio-One |
| Immobilon-P PVDF membrane (0.45 µm) | Merck |
| Millex-GS Syringe Filter Unit | Merck |
| Nunc Cryotube Vials | Thermo Fisher Scientific |
| PCR Tubes (200 µl) | StarLab |
| Sarogold Pro Food Wrap | Sarogold |
| Serological Pipettes (5 ml, 10 ml, 25 ml) | Greiner |
| Stericup-GP, 0.22 µm, Polyethersulfone, 500 mL | Merck |
| T25 cm Tissue Culture Flask | Sarstedt |
| T75 cm Tissue Culture Flask | Satstedt |
| Universal Tubes (30 ml) | Sarstedt |

## 2.3 Reagents

### 2.3.1 Tissue Culture

| | |
|---|---|
| DMEM, High Glucose, With Pyruvate | Thermo Fisher Scientific |
| mTeSR Basal medium | StemCell Technologies |
| DMEM/F12 | Gibco |
| Neurobasal | Gibco |
| PSC Neural Induction Medium | Gibco |
| N2 | Gibco |
| B27 minus Vitamin A | Gibco |
| Laminin | Gibco |
| Basic fibroblast growth factor (bFGF) | Gibco |
| Brain derived neurotrophic factor (BDNF) | StemCell Technologies |
| Glial derived neurotrophic factor (GDNF) | StemCell Technologies |
| Ascorbic acid | Sigma-Aldrich |
| Dibutyryl cAMP (dbcAMP) | Sigma-Aldrich |
| Poly-L-ornithine | Sigma-Aldrich |
| Matrigel | Corning |
| Rock inhibitor (Y27632) | Tocris |

| | |
|---|---|
| DMSO | Sigma-Aldrich |
| DPBS, No Calcium or Magnesium | Thermo Fisher Scientific |
| HBSS, No Calcium or Magnesium | Thermo Fisher Scientific |
| Fetal Bovine Serum (FBS) | Sigma-Aldrich |
| MEM Non-Essential Amino Acids (x100) | Thermo Fisher Scientific |
| Penicillin-Streptomycin (10,000 U/mL) | Thermo Fisher Scientific |
| TrypLE Thermo | Fisher Scientific |
| Versene | Gibco |
| Uridine | Sigma-Aldrich |

### 2.3.2 SDS-PAGE/Immunoblotting

| | |
|---|---|
| Acrylamide/Bis-acrylamide, 30%, 29:1 | Bio-Rad |
| SuperSignal West Pico PLUS Chemiluminescent Substrate | Thermo Scientific |
| Ammonium Persulphate | Sigma-Aldrich |
| Blue Wide Range Protein Ladder | Cleaver Scientific |
| Dried Skimmed Milk Powder | Marvel |
| Glycerol | Sigma-Aldrich |
| Glycine | Sigma-Aldrich |
| Hydrochloric Acid | Sigma-Aldrich |
| Methanol | Sigma-Aldrich |
| Magnesium Chloride | Sigma-Aldrich |
| N, N, N’, N’- Tetramethylethylenediamine (TEMED) | Sigma-Aldrich |
| Sodium chloride | Sigma-Aldrich |
| Nonidet P-40 | Sigma-Aldrich |
| Phenylmethylsulphonyl Fluoride | Sigma-Aldrich |
| Pierce Protease Inhibitor Cocktail Tablet | Thermo Fisher Scientific |
| Protein Assay Dye Reagent Concentrate | Bio-Rad |
| Tris-Buffered Saline | Sigma-Aldrich |
| Tween-20 | Sigma |
| Sodium Dodecyl Sulphate (SDS) Pellets | Sigma-Aldrich |
| Trizma Base | Sigma-Aldrich |

### 2.3.3 Polymerase chain reaction

| | |
|---|---|
| DreamTaq DNA polymerase | Thermo Fisher Scientific |
| DreamTaq Green Buffer | Thermo Fisher Scientific |

### 2.3.4 Agaraose gel electrophoresis

| | |
|---|---|
| GeneRuler 1 kb plus DNA ladder | Thermo Fisher Scientific |
| GeneRuler 100 Plus DNA ladder | Thermo Fisher Scientific |
| Molecular grade agarose | Bioloine |
| Ethidium bromide | Invitrogen |
| Tris-Acetate-EDTA (TAE) buffer | Formedium |

### 2.3.5 Sanger sequencing

| | |
|---|---|
| Big Dye Terminator v.31 Cycle Sequencing Kit | Applied Biosystems |
| Exonuclease I, 20U $\mu L^{-1}$ | Thermo Fisher Scientific |
| Fast AP, thermosensitive alkaline phosphatase, 1U $\mu L^{-1}$ | Thermo Fisher Scientific |

## 2.4 Solutions

### 2.4.1 SDS-Polyacrylamide Resolving Gel

| **Reagent** | **Final Concentration** |
|---|---|
| Tris-HCL pH 8.5 | 380 mM |
| Bis-acrylamide 30% | X |
| Sodium dodecyl sulphate (SDS) | 0.1% |
| Ammonium Persulfate (APS) | 0.1% |
| Tetramethylethylendiamine (TEMED) | 0.1% |

### 2.4.2 3.75% SDS-Polyacrylamide stacking gel

| **Reagent** | **Final Concentration** |
|---|---|
| Tris-HCL pH 6.8 | 380 mM |

| | |
|---|---|
| Bis-acrylamide 30% | 3.75 |
| Sodium dodecyl sulphate (SDS) | 0.1% |
| Ammonium Persulfate (APS) | 0.1% |
| Tetramethylethylendiamine (TEMED) | 0.1% |

### 2.4.3 1X SDS-PAGE Running Buffer

| **Reagent** | **Final Concentration** |
|---|---|
| Trizma Base | 25 mM |
| Glycine | 192 mM |
| SDS | 0.1% |

### 2.4.4 1X SDS-PAGE Transfer Buffer

| **Reagent** | **Final Concentration** |
|---|---|
| Trizma Base | 25 mM |
| Glycine | 192 mM |
| SDS | 0.02% |
| Methanol | 15% |

### 2.4.5 Tris-Buffered Saline (0.1% Tween-20)

| **Reagent** | **Final Concentration** |
|---|---|
| Tris-Buffered saline | 1X |
| Tween-20 | 0.1% |

### 2.4.6 Artificial cerebrospinal fluid (ACSF)

| **Reagent** | **Final concentration** |
|---|---|
| NaCl | 125 mM |
| KCl | 5 mM |
| $CaCl_2 \cdot 2H_2O$ | 2 mM |
| $MgCl_2 \cdot 6H_2O$ | 1 mM |
| HEPES | 10 mM |
| D-Glucose | 25 mM |
| Deionised water | |

## 2.5 Antibodies

**Table 2.1. Table of primary and secondary antibody used in this work.**

| Primary Antibodies | **Antibody** | **Dilution** | **Origin** | **Manufacturer** |
|---|---|---|---|---|
| Western Blotting (WB) | ATG7 | "1:1000" | Rabbit | Cell Signaling (#8558) |
| | ATG7 | "1:1000" | Rabbit | Abcam (ab52472) |
| | ATG3 | "1:500" | Rabbit | Cell Signaling (#3415) |
| | ATG5 | "1:500" | Rabbit | Cell Signaling (#2630) |
| | ATG12 | "1:1000" | Rabbit | Abcam (ab303488) |
| | p62 | "1:1000" | Rabbit | Abcam (ab109012) |
| | LC3B | "1:1000" | Rabbit | Cell Signaling (#2775) |
| | GAPDH | "1:10000" | Mouse | Proteintech (60004-1-Ig) |
| Immunofluorescence (IF) - Immunocytochemistry (ICC) | GFAP | "1:500" | Mouse | Cell Signaling (#3670) |
| | TUBIII | "1:1000" | Rabbit | Abcam (ab18207) |
| | MAP2 | "1:5000" | Chicken | Abcam (ab5392) |
| | Caspase 3 | "1:400" | Rabbit | Cell Signalling (#9661) |
| | Sox2 | "1:500" | Rat | eBioscience (14-9811-82) |
| | Nestin | "1:1000" | Mouse | Cell Signaling (#22475) |
| IHC-Formalin Fixed Paraffin Embedded (FFPE) | p62 | "1:2000" | Rabbit | Abcam (ab207305) |
| IF-FFPE | Calbindin D-28K | "1:500" | Mouse | Swant (300) |
| | NeuN | "1:500" | Mouse | Abcam (ab104224) |

| | | | | |
|---|---|---|---|---|
| | MAP2 | "1:500" | Rabbit | Abcam (ab300645) |
| | GFAP | "1:200" | Mouse | Cell Signaling (#3670) |
| | Olig2 | "1:20" | Mouse | Sigma-Aldrich (MABN50) |
| | Doublecortin | "1:1000" | Mouse | Invitrogen (MA5-17066) |
| | p62 | "1:100" | Mouse | BD Transduction Labratories (610833) |
| | p62 | "1:100" | Rabbit | Abcam (ab207306) |
| **Secondary Antibodies** | **Antibody** | **Dilution** | **Origin** | **Manufacturer** |
| WB | Anti-rabbit | "1:3000" | Pig | DAKO (P0399) |
| | Anti-mouse | "1:2000" | Rabbit | DAKO (P0260) |
| IF-ICC | Alexa Fluor 488 anti-chicken | "1:2000" | Donkey | Invitrogen (A78948) |
| | Alexa Fluor 546 anti-mouse | "1:2000" | Goat | Invitrogen (A21143) |
| | Alexa Fluor 546 anti-mouse | "1:2000" | Goat | Invitrogen (A21123) |
| | Alexa Fluor 546 anti-rabbit | "1:2000" | Goat | Inivtrogen (A11010) |
| | Alexa Fluor 647 anti-mouse | "1:2000" | Goat | Invitrogen (A21241) |
| | Alexa Fluor 647 anti-mouse | "1:2000" | Goat | Invitrogen (A21242) |
| | Alexa Fluor 647 anti-chicken | "1:2000" | Donkey | Invitrogen (A78952) |
| IF-FFPE | Alexa Fluor 546 anti-rabbit | "1:100" | Goat | Invitrogen (A48254) |
| | Alexa Fluor 488 anti-mouse IgG2b | "1:100" | Goat | Invitrogen (A21141) |
| | Alexa Fluor 546 anti-mouse IgG2a | "1:100" | Goat | Invitrogen (A21133) |

| | | | | |
|---|---|---|---|---|
| | Alexa Fluor 405 anti-rabbit | "1:100" | Goat | Invitrogen (A31553) |

## 2.6 Cell Lines

### 2.6.1 Mammalian cell lines

Primary human skin fibroblasts have been obtained from patients with appropriate, informed consent and are stored within The Newcastle Mitochondrial Research Biobank (REC Reference: 16/NE/0267) with ethical approval from the North East - Newcastle & North Tyneside 1 Research Ethics Committee. All work undertaken was compliant with the governance arrangements under the local Research Ethics Committee and with the ethical principles of the Declaration of Helsinki.

### 2.6.2 Cell maintenance

Primary fibroblasts were cultured in Gibco® DMEM (4.5 g/L glucose, 2 mM L-glutamine, 1 mM sodium pyruvate) with 10% fetal calf serum (FCS), 50 µg/mL uridine (Sigma), 1x non-essential amino acids (Gibco), 1x penicillin/streptomycin (Sigma Aldrich) and incubated at 37°C in 5% $CO_2$. Cells were passaged at approximately 80% confluency. Cells were washed with 1x phosphate buffered saline (PBS) and dissociated with 3 ml TrypLE Express (Gibco®) for 5 minutes at 37°C in 5% $CO_2$ before being centrifuged for 5 minutes at 160 xg. Cells were reseeded at a 1:3 ratio.

### 2.6.3 Cell counting

Cells were dissociated as described according to cell type. Cells were resuspended in 1 mL appropriate media and 10 µL cell suspension was mixed with 10 µL Trypan Blue (Sigma) and counted using a Cellometer Auto 1000 Bright Field Cell Counter (Nexelcom).

### 2.6.4 Cell Storage

Primary fibroblasts were dissociated and pelleted as described (**Chapter 2.6.2**). The resulting pellet was then resuspended in 500 µL of FCS and added to a cryotube containing 500 µL FCS with 20% DMSO (Sigma) (10% final concentration). The cryotube was then stored in a CoolCell™ (Sigma Aldrich) at -80°C for 48 hours before being moved into permanent liquid nitrogen storage.

To revive frozen primary fibroblasts, cells were thawed at 37°C and immediately transferred to 5 mL of pre-warmed DMEM and centrifuged at 160 xg for 5 minutes. The supernatant was removed, and the pellet resuspended in 10 mL DMEM to be seeded for expansion.

## 2.7 Protein Studies

### 2.7.1 Total protein cell lysis

Cells were harvested at ~80% confluency as described (**Chapter 2.6.2**). Pellets were then washed in 1x PBS before being lysed in ice cold lysis buffer (50mM Tris/HCl pH 7.4, 130 mM NaCl, 2 mM $MgCl_2$, 1mM PMSF, 1% Nonidet P-40, one cOmplete™ EDTA-free protease inhibitor tablet (Roche)), vortexed and incubated on ice for 20 minutes. Samples were centrifuged at 2350 x*g* for 5 minutes, with the supernatant being stored in pre-cooled Eppendorf tubes at -80°C for future use.

### 2.7.2 Bradford Assay

To determine protein concentration of cell lysates a standard curve was generated using Bovine Serum Albumin (BSA) at final concentrations of 0, 2, 5, 10, 15 and 20 μg/mL in $dH_2O$ with 200 μL Total Protein Concentration Reagent (Bio-Rad) to give a final volume of 1 mL, before being vortexed and incubated at room temperature for 5 minutes. For samples, 3 μL and 5 μL of lysates were mixed with $dH_2O$ to make up to 800 μL, followed by 200 μL Total Protein Concentration Reagent (Bio-Rad) before being vortexed and incubated at room temperature for 5 minutes. Samples and standards were vortexed after incubation, with 200 μL being added to a well of 96 well plate in duplicate. Absorbance was measured at 595 nm on an ELx800 microplate reader (Bio-Tek). A standard curve was generated, and protein concentration of samples was calculated using the linear regression of the standard curve.

### 2.7.3 SDS-PAGE

The protein concentration of each sample was determined via Bradford assay using the Protein Assay Dye Reagent Concentrate (Bio-Rad) as per manufacturer's instructions and as described (**Chapter 2.7.2**). Following this, samples of equal protein quantity were incubated with sample dissociation buffer (6.25 mM Tris/HCl pH 6.8, 10% glycerol, 2% SDS, 0.01% bromophenol and 100 mM dithiothritol) at 95°C for 5

minutes. For non-reducing gels, the sample dissociation buffer did not contain DTT. Protein samples were separated on 8%, 12% or 15% SDS polyacrylamide gels at 150 volts using the Mini-Protean® Tetra Cell System (Bio-Rad) in running buffer as described (**Chapter 2.4.3**).

### 2.7.4 Immunoblotting

Resolved proteins were transferred onto Immobilon-P PVDF membrane (Merck Millipore) with the Mini-Protean® Tetra Cell System (Bio-Rad) system at 100 V for one hour at 4°C in transfer buffer, described (**Chapter 2.4.4**). Membranes were blocked for one hour on a rocker at room temperature in 5% skimmed milk power (Marvel) dissolved in tris buffered saline (Santa Cruz) with 0.1% Tween-20 (Sigma) (TBS-T). Immunoblotting was performed either overnight or for one hour at room temperature with primary antibodies diluted as described (**Chapter 2.5**), in 5% skimmed milk in TBS-T. Membranes were then washed three times for 10 minutes each in TBS-T and incubated in HRP-conjugated secondary antibody for 1 hour at room temperature in 5% milk in TBS-T. Membranes were again washed 3 times for 10 minutes each in TBS-T before visualisation using SuperSignal West Pico PLUS Chemiluminescent Substrate (Thermo Scientific) and imaged with a ChemiDoc XRS+ Imaging system using Image Lab Software (BioRad).

### 2.7.5 Autophagy flux assays

Primary patient and age-matched control fibroblasts were cultured as described (**Chapter 2.6**). When 80% confluent, cells were harvested and counted using a 1:1 ratio of cell suspension to trypan blue solution (Gibco) in a Cellometer Auto 1000 cell counter (Nexcelcom). 100,000 cells were seeded into 60 mm dish and cultured for 2 to 3 days to reach ~ 60% confluency. Subsequently, cells were treated with either 1 µM DMSO, 100 µM chloroquine (Sigma), 1 µM AZD8055, or both 100 µM chloroquine and 1 µM AZD8055 (final concentrations) at 37°C. Cells were harvested after the indicated hours of treatment for immunoblotting analysis.

### 2.7.6 Structural modelling

Canonical amino acid sequences were obtained from UniProt. AlphaFold Colab2 was used under standard setting, with existing crystal structures used as a custom

template where available, to generate 5 models (Jumper et al., 2021). The first ranked model as denoted by AlphaFold Colab2 was then used for analysis. Models were viewed using ChimeraX version 18.0, and amino acid changes were modelled using ChimeraX's SwappAA function.

## 2.8 Microscopy

### 2.8.1 Immunocytochemistry

Cells were dissociated and counted according to cell type as previously described and seeded onto appropriately coated sterile 13 mm cover slips (VWR) in 24 well plates. Cells were grown for the required length of time before the media being removed and immediately fixed with warm 4% paraformaldehyde (PFA) (Thermo Scientific) for 15 minutes at 37°C. Cells were then washed 3 times with sterile phosphate buffered saline (PBS) (Sigma-Aldrich). PFA was then quenched with 50 mM $NH_4Cl$ for 10 minutes at room temperature before washing 3 times with PBS. Cells were permeabilised using 0.1% Triton X-100 (Sigma-Aldrich) for 10 minutes at room temperature before washing 3 times with PBS. Cells were blocked for 10 minutes in 5% FBS (Gibco) in PBS before being stained with primary antibodies described (**Chapter 2.5**) in 5% FBS in PBS for 1 hour at room temperature. Cells were washed 3 times for 10 minutes each with PBS and stained for 1 hour at room temperature with secondary antibodies described (**Chapter 2.5**) in 5% FBS in PBS with Hoechst (Thermo Scientific) at 2 μg/mL. Cells were washed 2 times with PBS for 10 minutes each and then twice for 10 minutes with $dH_2O$. Cover slips were mounted using Prolong Golf antifade mounting mountant (Invitrogen) and imaged using Zeiss Axioimager 2 using a Colibri 1-LED lightsource and a Flash 4 camera and viewed using the Zen Blue Software package.

## 2.9 Software and online tools

| **Program** | **Source** |
|---|---|
| FIJI v1.0 | FIJI v1.0 Open Source |
| ImageLab v6.1 | Bio-Rad |

| | |
|---|---|
| NIS-Elements Advanced Research v4.50 | Nikon |
| Zen v2.5 Blue Edition | Zen |
| QuPath-0.5.0 | QuPath |
| Leica Application Suite v3.4.2.18368 | Leica |
| ChimeraX v1.8 | University of California, San Francisco |

| **Tool** | **URL** |
|---|---|
| Blast Local Alignment Search Tool | https://blast.ncbi.nlm.nih.gov/Blast.cgi |
| Combined Annotation Dependent Depletion | https://cadd.gs.washington.edu/snv |
| Genome Aggregation Database (gnomAD) | https://gnomad.broadinstitute.org |
| Genotype-Tissue Expression (GTEx) | https://gtexportal.org/home/ |
| Benchling | https://benchling.com |
| Synthego ICE analysis | https://ice.synthego.com |
| Primer Blast | https://www.ncbi.nlm.nih.gov/tools/primerblast/ |

# 3 Developing an iPSC derived neural model of *ATG7* related neurological disease

## 3.1 Introduction

### 3.1.1 Induced pluripotent stem cells

Pluripotent stem cells (PSCs) are a form of cells which can divide indefinitely and differentiate into any somatic cell in the adult body (Boya et al., 2018). Historically, embryonic stem cells (ESCs), from the inner cell mass of blastocysts, have been research's main source of PSCs, however availability and ethical issues are key drawbacks of this PSC source (Evans & Kaufman, 1981; De Wert & Mummery, 2003). In recent years research has benefitted from induced pluripotent stem cells (iPSCs). In 2006, iPSCs were reportedly produced from adult mouse fibroblasts, and subsequently from human adult fibroblasts in 2007, by expressing a defined set of transcription factors (Takahashi & Yamanaka, 2006; Takahashi et al., 2007). Ectopic expression of Oct3/4, Klf4, SOX2 and c-Myc (OKSM factors) was found to generate cells with similar morphology, proliferation, surface antigens and gene expression as ESCs (Takahashi et al., 2007). Initial efforts utilised fibroblasts but now peripheral blood mononuclear cells (PBMCs) are also routinely used (Staerk et al., 2010). This provides a pool of PSCs more accessible than ESCs, permitting their wider use in research.

Autophagy plays a key role in the maintenance and differentiation of stem cells. The process by which the OKSM factors revert somatic cells back to a pluripotent state relies on transient inhibition and activation of the major autophagy regulator mTOR (Wang et al., 2013). In the early stages of somatic cell reprogramming, mTOR signalling is inhibited, releasing mTOR's inhibition of autophagy, corresponding an upregulation of autophagy (Wang et al., 2013). This is supported by evidence suggesting mTOR inhibitors can aid reprogramming in the early stages, while at the latter stages of reprogramming they hinder the process (Chen et al., 2011; He et al., 2012). In addition to this, SOX2, one of the OKSM factors, has been shown to supress mTOR expression by recruiting the Nucleosome Remodelling and Deacetylase (NuRD) complex to the mTOR promoter region, inhibiting expression for the first 2

days of reprogramming (Wang et al., 2013). After these first 2 days, the inhibition is released, further supporting the importance of transient autophagy modulation in iPSC reprogramming.

The ability of iPSCs to differentiate into any adult cell type provides the opportunity to investigate previously hard to access cells and tissues. Given the inaccessibility and high risk involved when obtaining neural tissue, an iPSC derived neural model would circumvent issues associated with obtaining tissue from living patients. To this end considerable work has been undertaken to generate cells of neural lineage from ESCs initially, but subsequently from iPSCs as well.

### 3.1.2 Neural differentiation

To generate neurons and astrocytes, one current method involves the generation of multipotent neural stem cells (NSCs) before terminally differentiating them into the cell type of interest (Wang et al., 2022). At present, one of the most efficient methods for the production of neural stem cells is via small molecule manipulation of intracellular signalling pathways, generally resulting in inhibition of Mothers Against Decapentaplegic homologs (SMADs) transcription factors (Chambers et al., 2009). SMAD signalling acts as the effector of a family of signalling peptides active throughout life, known as the transforming growth factor-β (TGFβ) family. The TGFβ family can be further split into sub-families, such as nodals, activins, bone morphogenic protein (BMPs), anti-Muellerian hormone and more (Hata & Chen, 2016). The transcriptional effectors of these TGFβ peptides are SMAD1, SMAD2, SMAD3, SMAD5 and SMAD8, each with their own specificity. For example, BMPs are primarily served by SMAD1, SMAD5 and SMAD8, with activins and nodals being served by SMAD2 and SMAD3 (Senft et al., 2018; Zanotti et al., 2008). The intermediaries of these interactions are TGFβ receptor complexes, also known as activin-like kinase (Alk) receptors, which have specificities for upstream TGFβ sub-families, and downstream SMAD effectors. BMP signals are recognised by ALK1, ALK2, ALK3, and ALK6 which activates SMAD1 and SMAD5, while nodal and activin signals are recognised by ALK4, ALK5, ALK7 which in turn phosphorylate SMAD2 and SMAD3 (Derynck & Zhang, 2003; Zanotti et al., 2008; J. Li et al., 2011). Once phosphorylated, the receptor specific Smad is bound by Smad4, the common Smad, forming the active heteromer complex, which results in translocation to the nucleus and transcriptional activation of non-neural gene

targets, and repression of neural related gene targets (Xu et al., 2002; Inman et al., 2002). Combined, this transcriptional control allows maintenance of pluripotency and restricts differentiation. Inhibition of BMP and TGFβ signalling using Noggin and SB431542 respectively, releases the restriction on differentiation and induces neural patterning (Chambers et al., 2009).

An additional significant pathway in the generation of neural stem cells is Wnt/β-catenin signalling. Wnt proteins, similar to TGFβ ligands, are peptides secreted during development generating a concentration gradient determining organisation and orientation of the neural crest, a NSC rich structure in developing brains (Sutton et al., 2021). Under this concentration gradient, Wnt1, Wnt3a and Wnt8a activate Wnt signalling by stabilising β-catenin, a transcription factor, allowing its translocation to the nucleus. However, when the Wnt ligands are not present, Axin, adenomatous polyposis coli (APC), casein kinase 1α (CK1) and glycogen synthase kinase 3β (Gsk3β) form a complex to phosphorylate β-catenin, marking it for degradation, preventing its transcriptional function (Saint-Jeannet, 2013). This pathway is also a candidate for chemical manipulation to produce NSCs, as demonstrated by the small molecule inhibition of Gsk3β using CHIR99021, to artificially induce Wnt signalling in vitro, being able to efficiently generate NSCs similar to those of a neural crest lineage (Leung et al., 2016).

Once NSCs have been generated, neuronal/astrocyte differentiation can be undertaken in a variety of ways depending on the brain region of interest. A large number of differentiation protocols focus on producing pure cultures of neurons; however, a co-culture of neurons and astrocytes has been shown to increase the quality of the neuronal networks produced (Sultan et al., 2015; Chung et al., 2015; Clarke & Barres, 2013a). To generate these co-cultures, the neurons and astrocytes can be grown separately and then combined, allowing control over the neuron-astrocyte ratio, or differentiated *in-vivo* from a common precursor (Shi et al., 2012). One such protocol describes the production of electrophysiologically active neurons and astrocytes with a frontal cortex identity (Gunhanlar et al., 2018). The protocol relies on well-established supplements N2 and B27 to maintain neural cells, and using the B27 supplement without Vitamin A (B27-RA) to prevent caudalisation (Price & Brewer, 2001; Tao & Zhang, 2016) The protocol also uses brain derived neurotrophic factor

(BDNF) to increase the number of neurons generated and neuronal branching, and GDNF to promote neuronal survival (Labelle & Leclerc, 2000; Pansri et al., 2021; C. C. Wu et al., 2016; Airaksinen & Saarma, 2002). Additionally, ascorbic acid and dibutyryl cyclic adenosine monophosphate (dbcAMP) are utilised to enhance neuronal differentiation via Wnt activation and neuronal survival respectively (Rharass et al., 2017; Kim et al., 2011).

### 3.1.3 CRISPR/Cas9 genome editing

CRISPR/Cas9 genome editing technology allows for the targetable and specific editing of a model system's genome (Ran et al., 2013). Current CRISPR targeting relies on a single chimeric ribonucleotide sequence comprised of a 20-nucleotide CRISPR RNA (crRNA) and an additional transactivating RNA (tracrRNA), known as a single guide RNA (sgRNA). The crRNA traditionally contains a ribonucleotide sequence complementary to the target sequence, with the tracrRNA being partially complementary to the crRNA, functioning as a binding point for the required endonuclease (Jinek et al., 2012). The complementary sequence of the sgRNA to the target loci, allows for the specificity of the technique. To enable DNA cutting, the sgRNA is bound to the endonuclease Cas9 to form a ribonucleoprotein. As the sgRNA recognises its complementary genomic sequence it binds the DNA, and upon a recognition of an additional trinucleotide motif known as a protospacer adjacent motif (PAM), Cas9 cleaves the DNA, producing double stranded breaks (DSBs) (Jinek et al., 2012).

The non-homologous end joining (NHEJ) pathway is the cell's non-specific method of repairing DSBs. For this the DNA repair machinery generates short overhangs on each end of the DSB, generating homology regions, which can be reconnected by the cell's repair machinery. However, this is a highly error-prone process and can generate small insertions or deletions (indels). This can be exploited to produce frameshift mutations resulting in premature stop codons, leading to knock out of a gene of interest in human cells (Jinek et al., 2013). Alternatively, homology directed repair (HDR) is a more specific DNA repair process. Once a DSB is recognised by the cell's repair machinery, larger overhangs adjacent to the DSB are generated by nucleases. Subsequently, a repair template is introduced in a form of a single stranded oligodeoxynucleotide (ssODN). This ssODN is comprised of a DNA sequence complementary to the 75 base

pairs flanking the cut site in each direction, known as homology arms, which allows complementary binding to the overhangs adjacent to the DSB. HDR can be exploited by including edits in the ssODN sequence, whereby ligation of the ssODN into the DSB and adjacent overhangs results in these edits being incorporated into the genome (Ran et al., 2013). This method allows for insertion of specific edits, which can be used to CRISPR correct any potentially pathogenic variants in patient lines, and thus generating isogenic control lines with restored gene function, with the same nuclear genetic background as the patient line.

## 3.2 Methods

### 3.2.1 iPSC maintenance

Wild type (WT2) induced pluripotent stem cells (iPSCs) were obtained from Prof. Majlinda Lako (Melguizo-Sanchis et al., 2018). These iPSCs were cultured in mTeSR1 basal medium (Stemcell Technologies) with mTeSR 5X supplement (Stemcell Technologies) with 5 mg/mL Penicillin/Streptomycin (Gibco) on plates coated with 100 μg/mL growth factor reduced Matrigel (Corning) in DMEM/F12 (Gibco). iPSCs were cultured under humidified conditions at 37°C and 5% $CO_2$. Media was changed daily.

### 3.2.2 Passaging of iPSC cultures

When iPSCs were 75-80% confluency cells were dissociated with Versene (Gibco) for 3-5 minutes at 37°C. Versene was then removed, and cells were collected in 2 mL of mTeSR1 media and split in a 1:3 ratio as cell clumps.

### 3.2.3 iPSC cell storage and recovery

For cryopreservation cells were dissociated and collected as described (**Chapter 3.2.2**) and then centrifuged for 5 minutes at 300 x *g* at room temperature. Cells were then resuspended in freezing media consisting of Foetal Bovine Serum (FBS) (Gibco), 10% dimethyl sulfoxide (DMSO) (Sigma) and 10 μm ROCK inhibitor (Y-27632 dihydrochloride) final concentration. iPSCs were stored at -80°C in a Mr. Frosty freezing container (Thermo Scientific) for at least 24 hours before being moved into long term liquid nitrogen storage.

For recovery, cells were thawed and added to 5 mL mTeSR1 containing 10μM ROCK inhibitor and centrifuged at 300 x*g* for 5 minutes at room temperature. The supernatant was aspirated, and the remaining pellet resuspended in mTeSR with 10μM ROCK inhibitor and plated onto Matrigel coated dishes. Media was changed the following day to remove the ROCK inhibitor.

### 3.2.4 Nucleofection of iPSCs with Cas9/sgRNA RNP

To generate the Cas9/sgRNA ribonucleoprotein, 100 pmol of Alt-R S. p. HiFi Cas9 Nuclease V3 (IDT) was incubated with 200 pmol sgRNA (IDT) for 10 minutes at 25°C. Wild type iPSCs were cultured as described (**Chapter 3.2.1**) to 60% confluency before dissociation with StemPro Accutase (Gibco) and centrifuged at 300 x *g* for 5 minutes, and resuspended with 100 μL of P3 Primary Cell 4D-Nucleofector X Kit L nucleofection solution (Lonza). Cell suspension was subsequently electroporated using the kit's electro-cuvettes in the 4D-Nucleofector using program CB150 and following manufacturers instructions. After nucleofection, 500 μL of mTeSR1 (Stemcell Technologies) with 10μM ROCK inhibitor (Tocris) was added. Nucleofected cell suspension was spread over 5 Matrigel (Corning) coated 10 cm plates in 4 mL of mTeSR1 (Stemcell Technologies) with 10μM ROCK inhibitor (Tocris). Media was replaced (without ROCK inhibitor) two days after seeding and then every other day thereafter.

### 3.2.5 iPSC colony isolation and screening

Approximately 7-10 days after seeding, colonies arising from single cells were manually picked and placed into one well of a 24 well plate coated with Matrigel (Corning). Colonies were allowed to expand for approximately 7 days before dissociation with Versene (Gibco). Cells were collected in 500 μL of mTeSR1 media and two drops of this cell suspension were added to 50 μL DirectPCR Lysis Mouse Tail (Viagen) with 2 μL Proteinase K (800 units/mL) (Sigma), with the rest being re-plated for sub-culturing. Genomic DNA was extracted by incubation of the cell suspension at 56°C for 16 hours, and then at 95°C for 15 minutes. DNA concentrations were determined using a NanoDrop One (Thermo Scientific).

### 3.2.6 Polymerase chain reaction.

PCR amplification of DNA was performed using 50 ng of DNA. PCR was performed using the mixture in **Table 3.1**. Reaction conditions are described in **Table 3.2**.

**Table 3.1 Reagents for PCR amplification of 50 ng DNA.**

| Reagent | Volume (μL) |
|---|---|
| 10x DreamTaq buffer | 2.5 |
| 2 nM dNTPs | 2.5 |
| DreamTaq | 0.125 |
| 10 μM Forward primer | 1.0 |
| 10 μM Reverse Primer | 1.0 |
| DNA | 1.0 |
| Nuclease free water | 16.875 |

**Table 3.2 Reaction conditions for PCR**

| Temperature | Time | Number of cycles |
|---|---|---|
| 95°C | 3 minutes | 1 cycle |
| 95°C | 30 seconds | 30 cycles |
| 56°C | 30 seconds | |
| 72°C | 30 seconds | |
| 72°C | 10 minutes | 1 cycle |
| 4 | Hold | |

### 3.2.7 T7E1 endonuclease assay

After 7 days of growth, one full 10 cm plate of nucleofected iPSCs were dissociated with StemPro Accutase at 37°C for 3-5 minutes and collected in mTeSR1 media before centrifugation at 300 x *g* for 5 minutes. The supernatant was aspirated, and the pellet resuspended in 100 μL of DirectPCR Lysis Mouse Tail (Viagen) with 4 μL Proteinase K (800 units/mL) (Sigma), incubated and the DNA concentration quantified (**Chapter 3.2.5**). Genomic DNA was used for PCR to amplify the region of interest as described (**Chapter 3.2.6**), and to estimate the efficacy of genome editing the Alt-R Genome Editing Detection Kit (IDT) was used as per manufacturer's instructions. The products

of the T7E1 reactions were visualised on 2% agarose gel with a ChemiDoc XRS+ Imaging system (BioRad) with the Image Lab Software (Biorad).

### 3.2.8 Sanger sequencing

Region of interest surrounding target site was amplified using PCR, and products were run on 3% agarose gel with a ChemiDoc XRS+ Imaging system (BioRad) with the Image Lab Software (Biorad). Clones found to have amplicons differing in size to the wild type control due to indels were cleaned using 0.5 μL Exonuclease I (200units/μL) (ThermoFisher) with 1 μL FastAP (ThermoFisher) per 5 μL of PCR product. Sanger sequencing was performed using BigDye Terminator v.3.1 Cycle Sequencing Kit (ThermoFisher) on ABI130xl Genetic analyser (ThermoFisher). Analysis of resulting sequences was analysed for insertion or deletions using Inference of CRISPR Edit (ICE) analysis (Synthego; https://www.synthego.com/products/bioinformatics/crispr-analysis).

### 3.2.9 SDS-PAGE

SDS-PAGE and immunoblotting analysis of candidate CRISPR/Cas9 clones was performed as described (**Chapter 2.7**).

### 3.2.10 iPSC characterisation and karyotyping

Knockout clones identified by Sanger sequencing and immunoblotting were dissociated using Versene (Gibco) at 37°C for 5 minutes, collected in mTeSR1 media and centrifuged at 300 xg for 5 minutes. Cell pellets (>2x$10^6$ cells/test) were sent to the Pluritest Assay Service (Thermo Scientific) for pluripotency testing and the Karyostat+ Genetic Stability Assay Service (Thermo Scientific) to check karyotype of the clones.

### 3.2.11 Neural induction and neural precursor cell maintenance

For neural induction iPSCs were allowed to become 75-80% confluent before splitting 1:3 and plated onto Matrigel coated plates, as described (**Chapter 3.2.2**). The iPSCs were allowed to recover overnight. The following day (day 0) mTeSR1 media was replaced with PSN Neural Induction Medium (Gibco) supplemented with 50X Neural Induction Supplement (Gibco). Media was then replaced as per manufacturer's instructions until day 7. At day 7 cultures were 100% confluent and considered pre-

neural precursor cells (pre-NPCs) at Passage 0. At this point cells were dissociated using StemPro Accutase for 3-5 minutes at 37°C after which cell suspension was collected and centrifuged at 1000 xg for 5 minutes. Supernatant was aspirated, and cells resuspended in neural expansion medium (NEM) (DMEM/F12 (Gibco), 1% N2 (Gibco), 2% B27-RA (Gibco), 1 μg/mL laminin (Gibco), 20 ng/mL basic fibroblast growth factor (b-FGF) (Gibco) and 1% penicillin/streptomycin (Gibco)) with 10 μM ROCK inhibitor and plated onto Matrigel coated plates. Media was changed after 36 hours to NEM without ROCK inhibitor and changed every 2-3 days thereafter. At 90% confluency cells were split using StemPro Accutase as described (**Chapter 3.2.10**), with ROCK inhibitor being removed 48 hours after splitting by media change. Once cells had reached Passage 5, they were considered ready for neural differentiation.

### 3.2.12 Cryopreservation of NPCs

Passage 1, and above, NPCs were dissociated with StemPro Accutase at 37°C and centrifuged as described (**Chapter 3.2.10**). Once pelleted, cells were resuspended in NEM containing 10% DMSO and 10 μM ROCK Inhibitor before being placed into a Mr. Frosty freezing container at -80°C for at least 24 hours before being moved into long term liquid nitrogen storage.

For recovery, cells are thawed and added to 5 mL NEM with 10μM ROCK inhibitor and centrifuged at 300 xg for 5 minutes at room temperature. The supernatant was aspirated, and the remaining pellet resuspended in NEM with 10μM ROCK inhibitor and plated onto Matrigel coated dishes. Media was then changed the following day to remove ROCK inhibitor.

### 3.2.13 Neural differentiation

NPCs (Passage 5-10 only) were dissociated and pelleted as described in 6.2.5. The NPC pellet was resuspended in NEM into a single cell suspension and 10 μL of cell suspension was mixed with 10 μL of trypan blue (Sigma) to determine cell numbers using Cellometer Auto 1000 Bright Field Cell Counter (Nexelcom). NPCs were seeded at 50,000 cells per $cm^2$ on plates coated with 0.01% poly-L-ornithine (Sigma) and 20 μg/mL laminin in DMEM/F12 in NEM media. Cells were allowed to recover overnight before being changed to neural differentiation medium (NDM) (Neurobasal media (Gibco), 1% N2 supplement, 2% B27 without retinoic acid, 1% non-essential amino

acids (Gibco), 20 ng/mL brain-derived neurotrophic factor (Stemcell Technologies), 20 ng/mL glial cell-derived neurotrophic factor (Stemcell Technologies), 1 uM dibutyryl cAMP (Sigma), 100 uM ascorbic acid (Sigma), 2 μg/mL laminin, 1% penicillin/streptomycin). Media was changed three times a week for the first four weeks of differentiation, with only half the media being changed three times a week for the following four weeks. After eight weeks of differentiation, cultures were used for experiments.

## 3.3 Results

### 3.3.1 Design of *ATG7* targeted sgRNA and primers for amplification

To generate a knockout model of *ATG7*-related neurological disease, 20bp sgRNA sequences were generated to produce double stranded DNA breaks (DSB) at specific loci in the *ATG7* gene. Non-homologous end joining of these DSBs should then produce insertion/deletion mutations (indels), resulting in a frame shift, thus knocking out *ATG7* gene expression and mimicking the biochemical phenotype of S1 (Collier et al., 2021).

To generate the sgRNA sequence, three tools were used; CRISPR sgRNA Design Tool (Benchling; https://www.benchling.com/), True Design Genome Editor (Invitrogen; https://apps.thermofisher.com/apps/genome-editing-portal/) and the Alt-R CRISPR HDR Design Tool (IDT; https://eu.idtdna.com/pages/tools/alt-r-crispr-hdr-design-tool). The key considerations during design were:

i. High on-target activity
ii. Minimal off target effects
iii. Cut site is less than 15 bp away from mutation site
iv. The sgRNA sequence is recommended by at least two of the three CRISPR sgRNA design tools

The target for the sgRNA was chosen to be exon 2 of *ATG7* in order to minimise the likelihood of truncated protein being produced. The final sgRNA sequence targeted the start of exon 2 of *ATG7* (RefSeq; ATG7-001; ENST00000354449) (**Table 3.3**).

To assess editing, primer pairs were designed using the Primer Wizard Tool (Benchling; https://benchling.com/), which runs using Primer3 (**Table 3.3**). These primers produced a 300 bp product. The cut site was 184 bases into the product.

**Table 3.3. Sequences designed for CRISPR and amplification of region surrounding cut site.**

| Purpose | Sequence |
|---|---|
| sgRNA | 5'-AGAAGAAGCTGAACGAGTAT-3' |
| Forward Primer | 5' TCTTTCTCACCAGGTTTTGCA 3' |
| Reverse Primer | 5' GCCTTGGGCTCAACAAAGAG 3' |

### 3.3.2 T7E1 endonuclease assay confirms CRISPR/Cas9 cutting

To assess efficiency CRISPR/Cas9 cutting at the population level, a 60% confluent 10cm plate of nucleofected iPSCs were dissociated and taken for DNA extraction. After NHEJ, the indels created should differ throughout the population. Amplification of wild type *ATG7* exon 2 should generate a 300 bp amplicon, with any indels either lengthening or shortening the sequence. For the T7 endonuclease assay, the DNA extracted from the nucleofected iPSC population was amplified to generate a pool of *ATG7* exon 2 amplicons of varying lengths, if effective cutting had occurred. This pool of exon 2 amplicons was melted to produce single stranded DNA molecules, which were then re-annealed with other ssDNA fragments. Any indels in the reannealed DNA resulted in mismatches occurring, producing heteroduplexes. The resulting mismatches can be recognised by a T7 endonuclease, which will cut the DNA into two fragments of different lengths, which can be detected by separating the products by agarose gel electrophoresis. Post nucleofection, the T7 endonuclease assay resulted in cutting observed in the population at the expected position in the amplicon, producing fragments at 180 bp and 120 bp (**Figure 3.1A**). This suggested effective Cas9 mediated cutting of the DNA had occurred, allowing screening to continue.

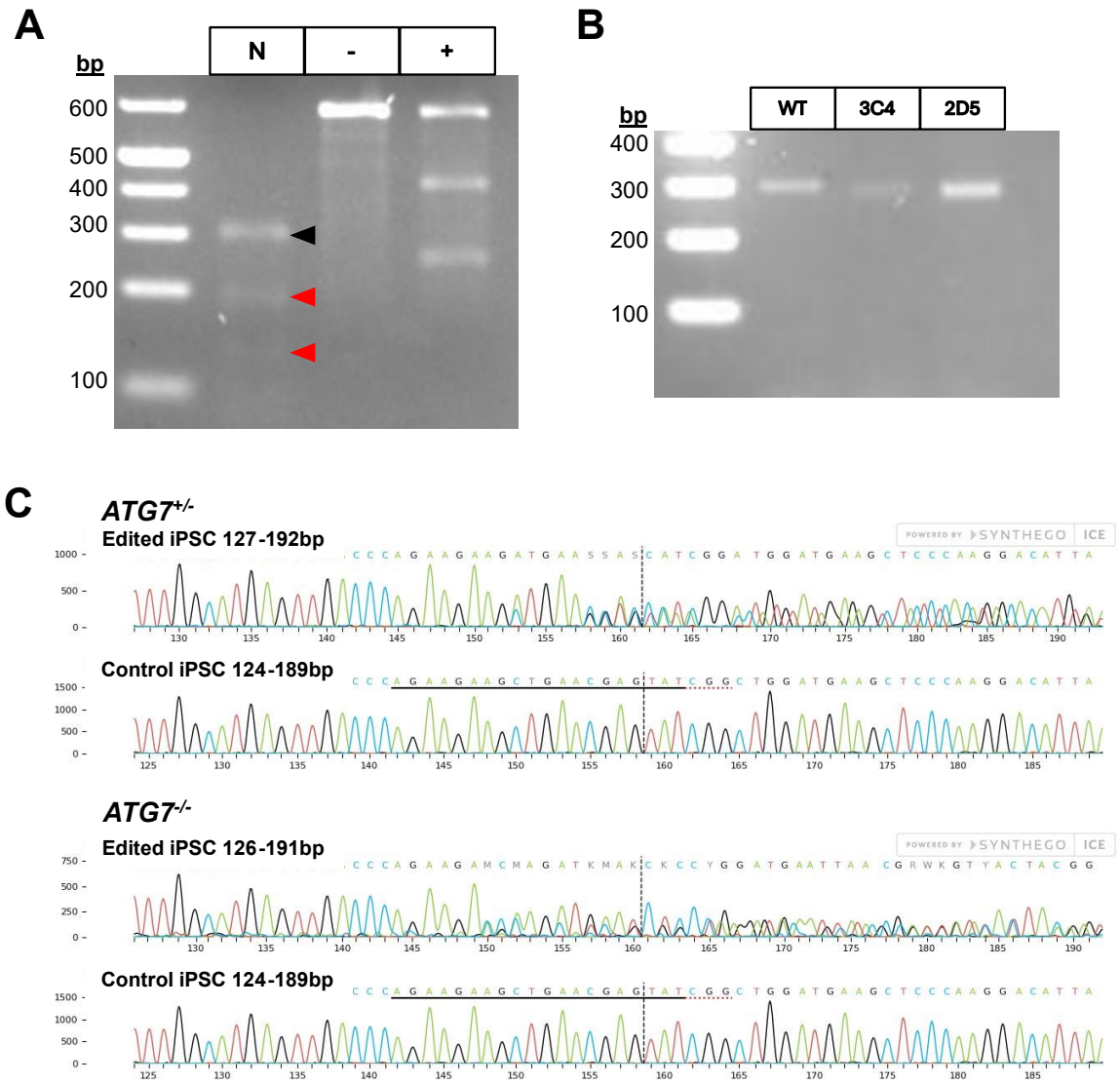


**Figure 3.1 Identification of ATG7 knockout clones from CRISPR/Cas9 mediated gene editing**. **A.** Agarose gel electrophoresis of T7E1 endonuclease assay to confirm Cas9 mediated DNA cleavage. Nucleofected iPSC sample (N) shows three bands. The 300 bp band is wild type amplicons which did not form heteroduplexes (black arrow), the 180 and 120 bp bands are from mutated colonies whose amplicons formed heteroduplexes to be digested by T7E1 nuclease. Positive (+) and negative (-) controls provided with the kit were also run to ensure correct T7E1 function. **B.** Agarose gel electrophoresis (3% agarose gel) of colonies derived from a single cell to identify clones with differing amplicon length to the wild type (WT). Here, both clone 3C4 and 2D5 were found to have deletions, resulting in the smaller amplicon observed when compared to the wild type. Clone 3C4 was taken forward for Sanger sequencing. **C.** Identification of CRISPR edits (ICE) analysis (Synthego) performed on clones suspected to be ATG7$^{+/-}$ and ATG7$^{-/-}$ compared to a wild type control. The ATG7$^{+/-}$ and ATG7$^{-/-}$ clones were found to be harbouring monoallelic and biallelic mutations in ATG7 respectively.

### 3.3.3 Identification of *ATG7*$^{+/-}$ and *ATG7*$^{-/-}$ iPSC clones

After confirmation of effective CRISPR/Cas9 mediated genome editing, 74 single cell colonies were manually picked and sub-cultured. PCR and gel electrophoresis identified eleven potential clones with amplicons of a size different to that of the wild type (**Figure 3.1B**). Sanger sequencing of these eleven clones identified four clones with monoallelic *ATG7* mutations, and one clone with biallelic *ATG7* mutations with ICE analysis (Synthego) confirming ATG7$^{+/-}$ and ATG7$^{-/-}$ clones (**Figure 3.1C**). The selected *ATG7*$^{+/-}$ and *ATG7*$^{-/-}$ clones were then taken for whole cell protein extraction for SDS-PAGE and immunoblotting analysis. *ATG7*$^{+/-}$ iPSCs showed a decrease in ATG7 compared to wild type iPSCs, and the *ATG7*$^{-/-}$ clone had no detectable ATG7 (**Figure 3.2A**).

The *ATG7*$^{+/-}$ clone also showed no increase in autophagy adapter protein p62 compared to the wild type, however the *ATG7*$^{-/-}$ clone did have an increase in p62 compared to the wild type (**Figure 3.2A**). This reflects what was observed in S1 of the original *ATG7* patient cohort (Collier et al., 2021). S1 had no detectable ATG7 in primary fibroblasts, and an accumulation of p62, similar to *ATG7*$^{-/-}$ clone described here. These data suggest that the isolated *ATG7*$^{+/-}$ and *ATG7*$^{-/-}$ clones are monoallelic and biallelic knockouts of *ATG7* respectively, at both the genetic and protein level, with *ATG7*$^{-/-}$ clones reflecting the biochemical ATG7 and p62 phenotype of S1.

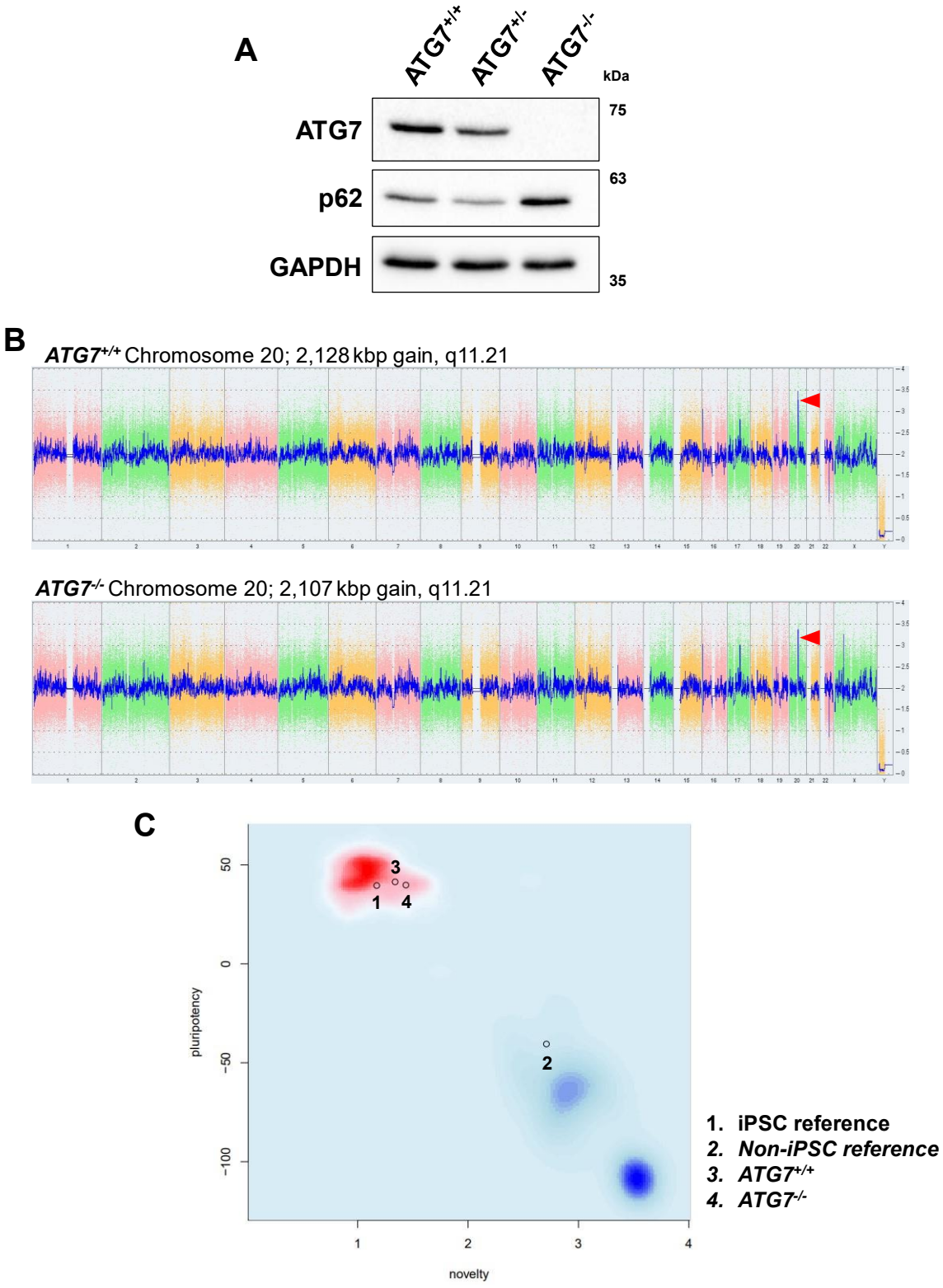


**Figure 3.2 Confirmation of ATG7 knockout and iPSC characterisation confirming karyotype and pluripotency. A.** SDS-PAGE and immunoblot analysis of ATG7$^{+/+}$, ATG7$^{+/-}$ and ATG7$^{-/-}$ clones confirm a reduction in ATG7 for the ATG7$^{+/-}$ clone and no detectable ATG7 in the ATG7$^{-/-}$ clone. Immunoblot analysis also demonstrated that only the ATG7$^{-/-}$ clone had an observable increase in the autophagy adapter protein p62. **B.** Karyotype analysis (Karyostat+; Thermo

Scientific) shows both the ATG7$^{+/+}$ and ATG7$^{-/-}$ clones have a gain in chromosome 20, starting at the same location in both clones, cytoband q11.21. ATG7$^{+/+}$ has a gain of 2,128 kbp, while ATG7$^{-/-}$ has a gain of 2,107 kbp. This locus is well characterised for genomic instability during gene editing and is not predicted to effect downstream experiments. **C.** Pluripotency testing of iPSCs (Pluritest; Thermo Scientific) analysing pluripotency markers (pluripotency) and how well the tested samples fit the reference iPSC model. Both clones cluster with the distribution of pluripotent reference set (red), with only the non-iPSC reference clustering close to the distribution of non-pluripotent reference (blue).

### 3.3.4 Quality control of ATG7 knockout iPSCs

To ensure the quality of the generated iPSCs lines, wild type *ATG7*$^{+/+}$ and *ATG7*$^{-/-}$ lines were sent for pluripotency testing and karyotyping (Karyostat+, Pluritest; Thermo Fisher Scientific). Karyotyping analysis (Karyostat+; Thermo Fisher Scientific) identified a chromosomal gain in each of the tested lines at the q11.21 cytoband, a common finding in genetically manipulated iPSCs. The most relevant gene in this duplicated region was *BCL2L1*. However, given the similarity of the chromosomal gain in the tested lines, it was not predicted to interfere with downstream experiments (**Figure 3.2B**). Pluripotency analysis (Pluritest; Thermo Fisher Scientific) showed that both lines were pluripotent as they clustered with well characterised iPSC lines upon analysis (**Figure 3.2C**). Together this suggested the isolated lines can be taken forward for neural differentiation.

### 3.3.5 Neuronal-astrocyte co culture of ATG7 knockout iPSCs

To ensure the selected *ATG7*$^{+/-}$ and *ATG7*$^{-/-}$ clones were able to differentiate into neurons and astrocytes they were taken forward to differentiation. First neural induction had to be undertaken to differentiate iPSCs into multipotent neural stem cells (NSCs), which have committed to an ectodermal fate. After 7 days of neural induction and at least one passage, cells were plated for immunofluorescence to characterise expression of NSC markers. NSCs should express both SOX2, a transcription factor associated with neural precursor cells, and Nestin, an intermediate filament associated with cells of a neural lineage. All three cell lines showed robust expression of SOX2 and Nestin suggesting they had all been successfully differentiated into NSCs, with any visible differences likely a result of seeding density (**Figure 3.3A**).

Once NSCs were over Passage 5, they were dissociated and plated at 50,000 cells/cm$^2$ on poly-L-ornithine and laminin coated plates. Cultures underwent eight

weeks of differentiation in neural differentiation media (NDM) to produce a neuronal astrocyte co-culture. To assess the ability of the lines to differentiate, immunofluorescence was undertaken at the end of the 8 weeks to investigate neuronal differentiation with Beta-III Tubulin (TUBIII) and astrocyte differentiation using Glial Fibrillary Acidic Protein (GFAP). After 8 weeks of differentiation all 3 lines robustly expressed both TUBIII and GFAP, with TUBIII showing the expected neurite outgrowths, and GFAP highlighting astrocytes with the expected star-like morphology (**Figure 3.3B**). Together, the immunofluorescence data show that the engineered *ATG7*$^{+/-}$ and *ATG7*$^{-/-}$ iPSC lines can differentiate into neurons as astrocytes, expressing classical NSC markers and following neural differentiation specific neuronal and astrocytic markers.

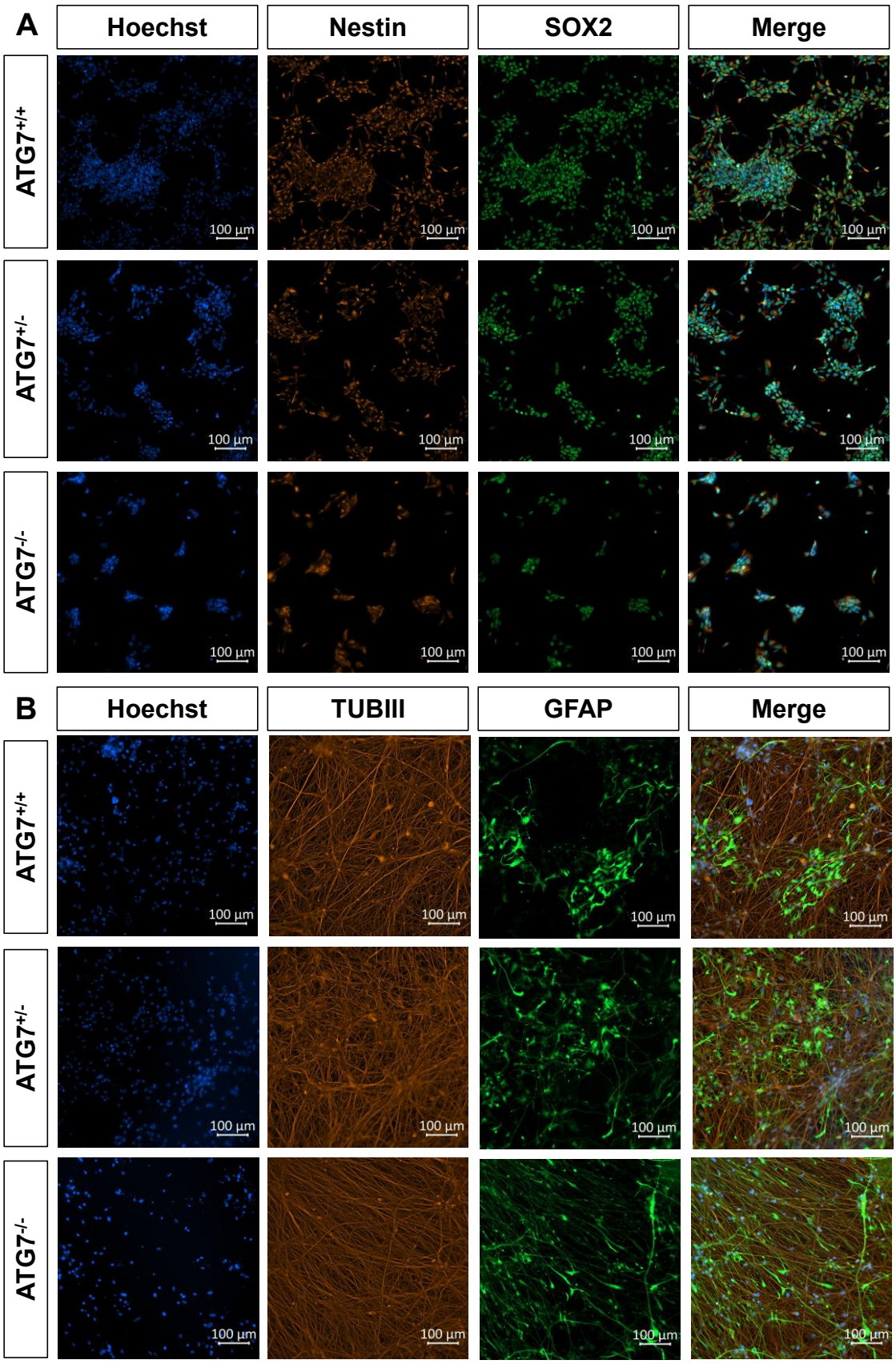


**Figure 3.3 Immunocytochemical immunofluorescence analysis of differentiated neural stem cells and neural culture from ATG7 knockout and control lines. A.** Representative

immunofluorescence images of neural stem cells after 7 days of neural induction. Hoechst used as a nuclear stain with SOX2 and Nestin acting as neural stem cell nuclear and intermediate filament markers respectively. All three lines tested showed robust expression of both Nestin and SOX2, suggesting successful neural induction in all lines. **B.** Representative immunofluorescence images of neuronal-astrocyte co-cultures after 8 weeks differentiation from Passage >5 NSCs. Beta -3-Tubulin (TUBIII) is used as a microtubule marker for neuronal cells, and glial fibrillary acidic protein (GFAP) is used as an intermediate filament marker for astrocytes. All three cell lines showed robust expression of both TUBIII and GFAP, indicating all three lines were able to differentiate into neurons and astrocytes using the differentiation protocol described (**Chapter 3.2.13**).

## 3.4 Discussion

This chapter has demonstrated the utility of CRISPR/Cas9 gene editing to generate a physiologically relevant cell model to investigate the neurological phenotypes observed in the *ATG7* patient cohort. The use of sgRNA targeted to exon 2 of *ATG7* was combined with Cas9 to form a ribonucleoprotein and delivered to the nucleus of WT iPSCs via nucleofection. This generated a pool of iPSCs harbouring DSBs which had undergone NHEJ, which was confirmed with the T7E1 endonuclease assay. Further culture of these cells to generate colonies arising from single cells allowed for the isolation of 74 CRISPR clones for genetic screening with PCR amplification of a 300 bp region surrounding the sgRNA target. Agarose gel electrophoresis allowed for the identification of clones with PCR products of differing size from the wild type *ATG7* amplicon, indicating the presence of indels in eleven out of the 74 clones. Sanger sequencing of the eleven clones identified four clones with single allele indels, and 1 with biallelic indels, confirmed with ICE analysis (Synthego). Given the stresses from nucleofection, genome editing, and multiple passages required to generate CRISPR clones, pluripotency testing and karyotyping was undertaken. Pluripotency testing confirmed the resulting *ATG7*$^{+/-}$ and *ATG7*$^{-/-}$ iPSC lines were pluripotent. Karyotyping identified an approximately 2,100 kb gain in chromosome 20, starting at the q11.21 cytoband, in both the tested *ATG7*$^{+/-}$ and *ATG7*$^{-/-}$ iPSC lines. This was not predicted to affect downstream experiments given the similarity in the chromosomal gain in both the *ATG7*$^{+/-}$ and *ATG7*$^{-/-}$ iPSCs. A 7-day neural induction was undertaken to differentiate the iPSC lines into neural stem cells (NSCs). Following this 7-day induction, the differentiated cells were passaged and analysed with immunofluorescence to confirm the identity of the resulting cells. All three lines induced

(*ATG*$^{+/+}$, *ATG7*$^{+/-}$ and *ATG7*$^{-/-}$) were found to have robust expression of NSC markers nestin and SOX2, suggesting the neural induction had successfully differentiated the iPSC lines to NSCs. Once NSCs were at passage 5, they were used for neural differentiation. Following 8 weeks of neural differentiation, immunofluorescence showed that the cultures had neurons, signified by TUBIII staining, and astrocytes, signified by GFAP staining. Together the data presented in this chapter suggest that when *ATG7* is knocked-out in WT iPSCs, they not only retain their pluripotency, but are able to successfully differentiate into neurons and astrocytes.

Chromosomal gain at 20q11.21 is a consistent finding when working with pluripotent stem cells (Amps et al., 2011). A recent review has suggested that 20% of the PSC lines reported in literature worldwide had either trisomy or partial gains in chromosome 20, with 53 lines harbouring gains that start at q11.21 (Krivec et al., 2024). These copy number variants are predominantly a single duplication, resulting in a copy number of 3 for a 0.6-4 mbp section of chromosome 20 (Amps et al., 2011). It has been proposed that the proximity to the centromere of chromosome 21 at the proximal end, and the GGAAT motif found at the distal end of this loci provides the susceptibility for the chromosomal gain via microhomology mediated break-induced replication, giving reason for its widespread occurrence (Merkle et al., 2022; Halliwell et al., 2021). While the chromosomal gain includes a number of genes with varying functions, all lines with 20q11.21 gains include a gain in *BCL2L1* (Krivec et al., 2024). Bcl-xL, one isoform of *BCL2L1*'s product, has been noted to have upregulated expression in ESCs harbouring the 20q11.21 CNV (Nguyen et al., 2014). As a result of this they were found to have decreased apoptosis as single cells, and increased colony forming compared to those without the gain, which was rescued via knockdown of *BCL2L1* (Nguyen et al., 2014). The increased survival and colony forming ability is attributed by reduction in mitochondrial mediated apoptosis via the BAX pathway (Avery et al., 2013; Edlich et al., 2011). The significance of improved survival and colony formation is particularly relevant in the context of the presented data due to the single cell nature of the CRISPR/Cas9 mediated genome editing. As described (**Chapter 3.2.4)**, after nucleofection, cells are seeded as single cells to allow isogenic colonies to form for cloning and expansions. This requires Rock inhibitors to prevent cell death via inhibiting myosin contraction, which in turn increases survival when dissociating and cloning PSCs (Chen et al., 2010; Watanabe et al., 2007). Despite the addition of Rock

inhibitor, when iPSCs were seeded as single cells, widespread cell death was observed 48 hours after nucleofection. A 20q11.21 chromosomal gain may have made the lines which were eventually isolated and expanded more resistant to apoptosis, increasing the likelihood of survival and expansion, explaining the common occurrence across the lines established in this chapter.

The ability of the *ATG7*$^{-/-}$ iPSCs to form NSCs and subsequently neurons and astrocytes also raises questions about the role of autophagy in cell fate and differentiation. This was first highlighted in ESCs using a GFP tagged LC3 model, which demonstrated differentiation induced by SB431542, the TGFβ receptor inhibitor, led to increased LC3-GFP puncta (Tra et al., 2011). This was not seen when undifferentiated cells were treated with SB431542, indicating the autophagy increase denoted by the increased LC3-GFP puncta are likely due to the differentiation process, suggesting a role of autophagy in differentiation itself (Tra et al., 2011). The direct effect of SB431542 on autophagy during differentiation does bring into question how the mechanisms underlying the differentiation protocol used here are effected in *ATG7*$^{-/-}$ iPSCs and then NSCs. However, as has been demonstrated, the *ATG7*$^{-/-}$ iPSCs can be differentiated into NSCs, suggesting SB431542 effect on autophagy during differentiation is not vital for generating cells with an endodermal fate *in-vitro*.

In addition to TGFβ signalling, Wnt signalling has also been implicated in autophagy regulation. It has been demonstrated that Wnt signalling is negatively regulated by autophagy (Gao et al., 2010). Wnt ligand recognition results in activation of Dishevelled (Dvl) which inhibits GSK3β, releasing its inhibitory effect on β-catenin, allowing nuclear translocation and translation of target genes, some of which are involved in neural patterning. Autophagy however degrades Dvl, allowing GSK3β to continue degrading β-catenin, thus inhibiting it (Gao et al., 2010). As a result, it appears that the loss of autophagy in the *ATG7*$^{-/-}$ iPSCs produces an endogenous effect similar to the small molecule inhibition of GSK3β, CHIR99021 treatment, potentially giving them an increased potential for ectodermal fate under a non-directed differentiation.

# 4 Characterisation of the *ATG7* neuron-astrocyte co-culture model

## 4.1 Introduction

### 4.1.1 Autophagy in neural development

Autophagy plays a central role in neurogenesis. During embryonic development, neural stem cells (NSCs) divide symmetrically, generating two cells of the same potency, thus expanding the stem cell niche of the ventricular zone (Molnár et al., 2019). Autophagy plays an important role in the maintenance of NSC populations in the developing brain (Stavoe & Holzbaur, 2019). ATG7 and ATG16L1 modulation has previously been shown to influence cell surface membrane levels of Notch1 (Wu et al., 2016). Notch1 is a central regulator of neural stem cells and their downstream fate by transducing external signals, usually cell surface ligands in close proximity. When activated, Notch1 is cleaved from the cell surface membrane and its intracellular domain is translocated to the nucleus to interact with CBF1/RBPjκ/Su(H)/Lag1 (CSL). This interaction releases CSL's repressor function and allows Mastermind to bind to the dimer and activate transcription of its target genes (Kopan & Ilagan, 2009). Notch1 is primarily turned over by endocytosis, followed by degradation in an autophagy dependant manner via amphisomes or early autophagic structures (Wu et al., 2016). ATG7 knockdown experiments, alongside *ATG16L1* hypomorphic mice experiments, have demonstrated an increase in Notch1 signalling via the increased expression of *Hes1,* which plays a role in maintaining NSCs (Wu et al., 2016). This demonstrates autophagy's role in Notch1 signalling, with *ATG16L1* hypomorphic mice primary cultures showing an impairment of normal neural differentiation, with primary neurons demonstrating increased levels stem cell markers nestin and Pax6, with decreased levels of neuronal markers Tbr1 and β-3 Tubulin (Wu et al., 2016).

In addition to direct autophagy impairment altering the proliferation and maintenance of NSCs, upstream regulation of autophagy has the capability to be detrimental to neurogenesis. Epithelial v-like antigen 1 (EVA1A*)* is a transmembrane protein which inhibits mTOR, allowing autophagy activation (Wang et al., 2007). *Eva1a* knockout mice showed a clear autophagy deficit, accompanied by an increase in p62 expression

(Li et al., 2016). Alongside the observed autophagy phenotype, there was a decrease in NSC proliferation and differentiation, without a concomitant increase in TUNEL positive cells, indicating the deficits were not due to cell death. Both phenotypes were recovered by EVA1A overexpression and chemical autophagy induction *in-vitro* (Li et al., 2016).

As NSCs mature and start to migrate towards what will become the cortical surface of the brain, into the subventricular zone, they begin to divide asymmetrically, generating more differentiated cells, known as neural precursor cells (NPCs) (Liénard et al., 2024). The change of cell divisions from symmetrical to asymmetrical is an important process in neurogenesis, and again one that has been shown to be affected by autophagy modulation. Dominant negative mutations in the autophagy adapter protein ALFY have been shown to result in microcephaly (Kadir et al., 2016). Microcephaly is associated with a reduced brain size, and related reduction in head size caused by dysregulation of the switch from symmetrical division in the neural stem cell niches to asymmetrical, resulting in depletion of NSC pools in the developing brain (Paridaen & Huttner, 2014). *Drosophila* models overexpressing mutant ALFY also showed reduced brain size, with ALFY shown to regulate Wnt signalling, which is an important factor in regulating cell fate, as discussed (**Chapter 3.1.2**) (Kadir et al., 2016).

Autophagy also plays a role as differentiation continues to progress. Autophagy related genes, including *ATG7 and Becn1*, show increased expression profiles in mouse olfactory bulb during neuronal differentiation in response to an increased metabolic demand of differentiation (Vázquez et al., 2012). Loss of Beclin-1 mediated autophagy was shown to reduced levels of neuronal markers *in-vivo,* and *in-vitro* three dimensional cultures, known as neurospheres, were shown to produce fewer neurons. Additionally, *ATG5* null olfactory bulb progenitors produced cultures with reduced neuronal marker TUJ1 and fewer cells capable of generating neurites (Vázquez et al., 2012). Further to this, knockdown of *Atg5* in mouse cortex demonstrated an increase in the number of NPCs in the ventricular and subventricular zones, accompanied by a reduction in the number of cortical neurons (Lv et al., 2014). Additionally, the resulting cortical neurons had significantly fewer neurites and neurite branches, suggesting a role for *Atg5* in neuronal morphological development (Lv et al., 2014).

### 4.1.2 Role of astrocytes in neuron development

During development neurons and astrocytes constantly interact, with astrocytes affecting numerous aspects of neuronal development. For instance, retinal ganglion cells of the CNS cultured with astrocytes were found to generate more mature synapses, and in greater numbers, with increased synaptic activity compared to those cultured without, demonstrating the important role of astrocytes in neuronal development (Ullian et al., 2001; Pfrieger & Barres, 1997). Following this, astrocytes have been widely shown to excrete numerous factors aiding synapse formation and maturation (Clarke & Barres, 2013b). These factors can be neuron sub-type specific, inducing enhanced axonal length and branching as well as the number of active GABAergic and glutamatergic synapses via secretion of soluble molecules, such as BDNF, cholesterol and transforming growth factor β1 (TGFβ1) (Hughes et al., 2010; Mauch et al., 2001; Gómez-Casati et al., 2010; Diniz et al., 2012).

Furthermore, in ESC derived forebrain neuronal cultures supplemented with exogenous astrocytes, the differentiation and maturation of the neurons was correlated to that of the astrocytes (Johnson et al., 2007). Synaptic maturation and activity were accelerated in culture with astrocytes, however astrocyte conditioned media was only able to increase synaptic maturation, suggesting an important role of direct neuron-astrocyte contacts (Johnson et al., 2007). Additionally, the timeline of neuron and astrocyte development has been correlated. Synaptic formation and the start of action potentials occurred at the same time point as astrocytic projection outgrowth, at 7 weeks in culture, demonstrating the close relationship between neuron and astrocyte development *in-vitro* (Johnson et al., 2007).

### 4.1.3 Calcium Handling

The role of calcium signalling in the CNS is broad and complex. Calcium signalling plays roles in long term potentiation, long term depression, gene expression, neuronal development and more (Kawamoto et al., 2012; Grover & Teyler, 1990; Bolshakov & Siegelbaum, 1994; Lohmann & Wong, 2005). At rest, neurons maintain an intracellular calcium level ($[Ca^{2+}]i$) of 0.1-0.5 μM, relatively low compared to the extracellular concentration of approximately 1 mM (Kawamoto et al., 2012). Upon activation of voltage dependant calcium channels or ligand gated ion channels an influx of calcium

enters the cell, increasing $[Ca^{2+}]i$. The $[Ca^{2+}]i$ can then be further increased by calcium release from the endoplasmic reticulum via ryanodine receptors and inositol-1,4,5-triphosphate receptors ($IP_3Rs$), along with calcium exported from mitochondria via a sodium/calcium exchanger (Chavis et al., 1996; Tu et al., 1998; DeLuca & Engstrom, 1961). At the end of the calcium signal, $[Ca^{2+}]i$ is decreased by the reverse mechanisms, calcium is exported via plasma membrane transporters and sequestered back into the endoplasmic reticulum or mitochondria, with the addition of calcium buffering proteins aiding in the reduction of free calcium ions (Zaidi et al., 2003; Pivovarova & Andrews, 2010).

### 4.1.4 Glutamate Signalling

Glutamate is the most common excitatory neurotransmitter found in the human brain. There are two main types of glutamate receptors: ionotropic glutamate receptors and metabotropic glutamate receptors (Willard & Koochekpour, 2013). Ionotropic glutamate receptors result in influx of positively charged ions, including calcium, upon activation. Ionotropic glutamate receptors comprise of four domains -intracellular, extracellular, transmembrane and ligand binding domain. The binding of glutamate to the ligand binding domain results in a conformational change to the transmembrane domain allowing influx of cations (Traynelis et al., 2010). Activation of a sufficient number of ionotropic glutamate receptors results in an action potential. Following the action potential, sodium dependant excitatory amino acid transporters (EAATs) on the post synaptic membrane and surrounding glia remove the glutamate stimulus, allowing intracellular ion levels to return to a resting state (Magi et al., 2019). Five separate EAATs have been isolated so far, EAAT1 - EAAT5. Each isotype has specific cell type and nervous system localisation. For example, EAAT2 is primarily associated with astrocytes in the brain and spinal cord, while EAAT3 is primarily associated with neurons in the hippocampus and cerebellum (Mennerick et al., 1998; Kugler & Schmitt, 1999).

### 4.1.5 Aims

This chapter aims to analyse the biochemical phenotype associated with *ATG7* loss of function in a tissue specific model system by investigating the effect on the two key conjugation systems of which ATG7 is an important part. It will also analyse the differences in development as cultures differentiate using time point analysis

throughout differentiation. Additionally, this chapter will investigate cell type specificity of the observed detrimental effects. Finally, this chapter will also investigate the resulting effect of *ATG7* dysfunction on neurons using calcium imaging.

## 4.2 Methods

### 4.2.1 Cell culture

Neuron-astrocyte co-cultures were cultured as described (**Chapter 3.2**).

### 4.2.2 SDS-PAGE and Immunoblotting

SDS-PAGE and immunoblotting was performed as described (**Chapter 2.7**).

### 4.2.3 Autophagy flux analysis

NPCs were seeded at a density of 30,000 cells per $cm^2$, in 12-well plates as described (**Chapter 3.2.13**). Cultures were differentiated for eight to ten weeks before being used for autophagy flux analysis as described (**Chapter 2.7.5**).

### 4.2.4 Immunofluorescence

Immunofluorescence imaging using eight to ten week differentiated neurons and astrocytes was performed as described (**Chapter 2.8.1**)

### 4.2.5 Calcium imaging

NPCs were differentiated for eight to ten weeks in 24 well plates at a density of 30,000 cells per $cm^2$. For calcium imaging, cells were loaded with 5 μM Fluo-4 AM-ester (Invitrogen) in neural differentiation media supplemented with 0.01% Pluronic acid F127 (Thermo Scientific) for 30 minutes at 37°C. After loading, cells were washed three times with warmed artificial cerebral spinal fluid (ACSF) (**Chapter 2.4.6**). Cells were then left to incubate at room temperature in the dark in fresh ACSF for 20 minutes. Cover slips were placed onto a continuously perfused microscope stage. Images were acquired at a rate of 2 per second using a 16x Fluor objective (Nikon) with a 470±30 nm LED in a PE-1 system (CoolLED) and a Prime BSI Express Camera (Teledyne Photometrics). Images were exported as TIFFs and stabilised using the Image Stabiliser FIJI plug in. Stabilised images were used to measure fluorescence of neuron cell bodies, with at least 10 ROIs per image and background fluorescence was subtracted. Changes to intracellular calcium concentration ($[Ca^{2+}]i$) in response to

glutamate stimulus were calculated as a fluorescence ratio using the formula below where $F_1$ = Fluorescence at given timepoint and $F_0$ = Fluorescence before glutamate stimulus.

$$\frac{F1-F0}{F0}$$

For analysis of $[Ca^{2+}]i$ recovery, fluorescence ratio values at minute intervals after peak fluorescence are expressed as a ratio of the peak fluorescence ratio, giving the ratio of recovery at the given time point.

## 4.3 Results

### 4.3.1 ATG7$^{-/-}$ neural co-cultures have impaired autophagic conjugation pathways

To determine the effect of *ATG7* loss on the core autophagy conjugations systems in neuron-astrocyte co-cultures, wild type (*ATG7*$^{+/+}$), heterozygous knockout (*ATG7*$^{+/-}$) and biallelic knockout (*ATG7*$^{-/-}$) NSCs were differentiated for 8 weeks, as described (**Chapter 3.2.13**). Firstly, the impact of different ATG7 deficiencies on the steady state level of autophagy-related proteins was investigated. SDS-PAGE and immunoblot analysis revealed that, *ATG7*$^{-/-}$ co-cultures showed undetectable levels of ATG7, while *ATG7*$^{+/-}$ co-cultures showed a reduction, but not complete loss of ATG7 when compared to *ATG7*$^{+/+}$ (**Figure 4.1A**). Interestingly, only *ATG7*$^{-/-}$ co-cultures showed an increase in the autophagy adapter protein p62. In addition to this, using antibodies specific for ATG5, immunoblotting demonstrated that the *ATG7*$^{-/-}$ co-cultures had a reduction, but not complete loss of covalently bonded ATG5-ATG12 complex. This reduction in ATG5-ATG12 complex was accompanied by the appearance of a band at a molecular weight which corresponds to that of unbound ATG5 monomer. Unbound ATG5 monomer is not observed in *ATG7*$^{+/-}$ co-cultures. This would suggest that complete loss of ATG7 results in impairment of the ATG5-ATG12 conjugation pathway, demonstrated by the decrease of ATG5-ATG12 conjugate and increase in unbound ATG5 (**Figure 4.1A**). This may hinder autophagic degradation, resulting in the observed increase in p62 expression. However, the data would also suggest the remaining ATG7 present in *ATG7*$^{+/-}$ co-cultures is adequate for ATG5-ATG12 conjugation, given its heterodimer levels being comparable to that seen in *ATG7*$^{+/+}$ co-

cultures. The lack of increase in p62 in *ATG7*$^{+/-}$ supports the hypothesis that reduced level of ATG7 observed in *ATG7*$^{+/-}$ is sufficient for autophagic degradation.

Having established alterations to the ATG5-ATG12 conjugation system in *ATG7*$^{-/-}$ co-cultures, autophagy flux assays were undertaken to determine the effect on the LC3 conjugation system. To do this, differentiated cultures of neurons and astrocytes were treated with AZD8055 to induce autophagy, and then Chloroquine to block late-stage autophagy, as described (**Chapter 1.5.3**). This allows the visualisation of the rate at which autophagosomes can be produced by using LC3-I lipidation to LC3-II as a marker of autophagosome formation. Lipidation of LC3-I is a conjugation pathway which requires ATG7 function. ATG7 adenylates the C-terminus of LC3-I, priming it for conjugation to phosphatidylethanolamine by ATG3. Analysis of LC3 by immunoblot analysis demonstrated that *ATG7*$^{-/-}$ *neural* co-cultures showed undetectable levels of LC3-II, while *ATG7*$^{+/-}$ co-cultures showed a reduction in LC3-II production relative to *ATG7*$^{+/+}$ co-cultures **(Figure 4.1B)**. This data shows that complete loss of ATG7 results in an impairment of LC3-I conjugation to PE to produce LC3-II. It also suggests that the reduction of ATG7 seen in *ATG7*$^{+/-}$ co-cultures does have a damaging impact on LC3-II production. However, given the normal steady state p62 levels observed in *ATG7*$^{+/-}$ co-cultures, the reduced levels of LC3-II in *ATG7*$^{+/-}$ appear sufficient to maintain degradative autophagy at a level which prevents p62 accumulation.

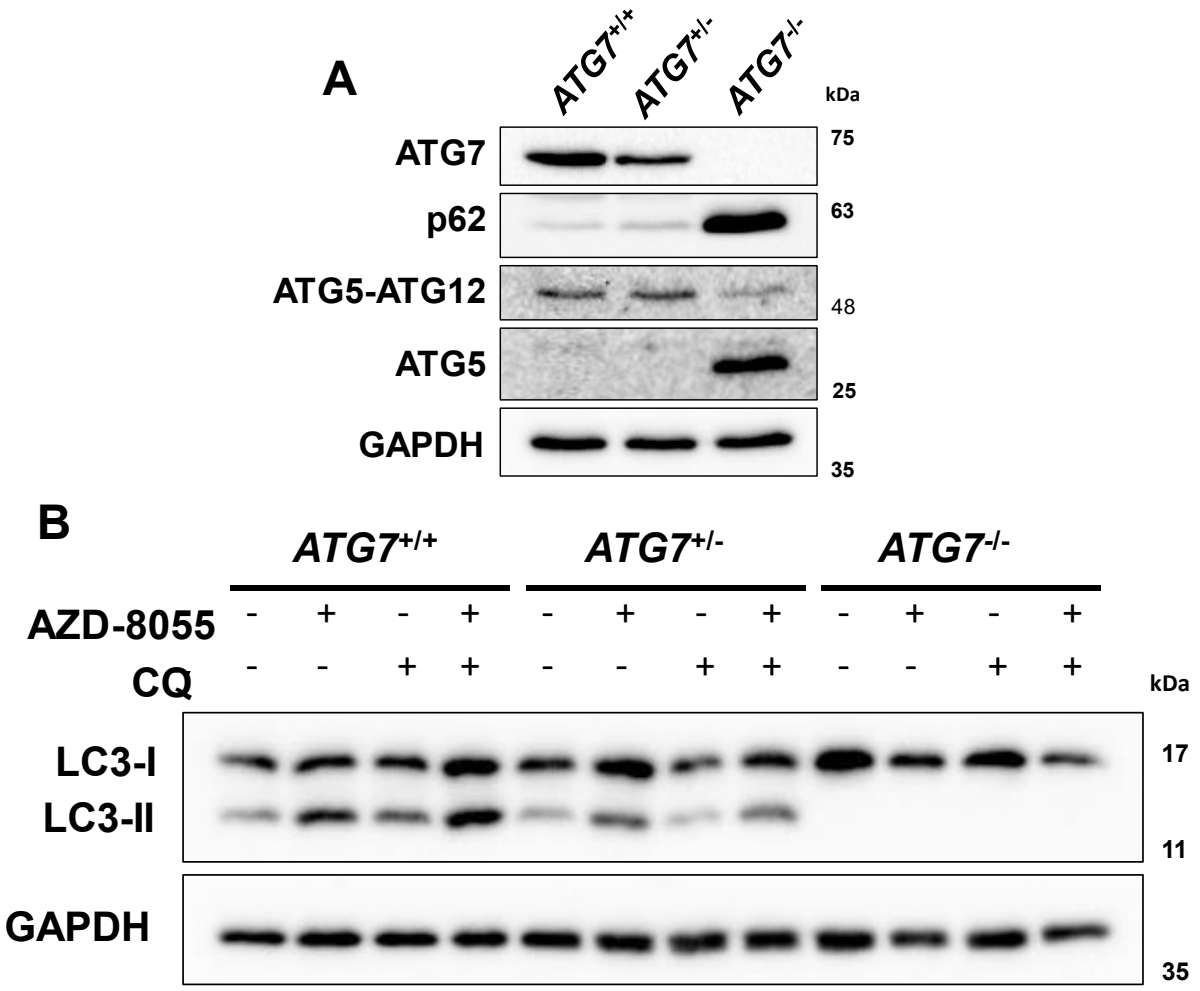


**Figure 4.1. Immunoblot analysis of autophagy related proteins and autophagy flux assays in neuron-astrocyte co-culture**. **A.** Immunoblot analysis of autophagy related proteins in ATG7$^{+/+}$, ATG7$^{+/-}$ and ATG7$^{-/-}$ neuron-astrocyte co-cultures after 8 weeks of differentiation. (n=3). **B**. Immunoblot analysis of autophagy flux assay treating 8-week differentiated cultures with 1 mM AZD-8055 to induce autophagy and 100 mM chloroquine to block late-stage autophagy for 2 hours. (n=3). In A. and B. GAPDH was used as a loading control.

### 4.3.2 ATG7$^{-/-}$ neural co-cultures show morphological changes

Given the modulation of steady state autophagy related protein levels and autophagy flux observed across the models, a morphological analysis was undertaken across the 8 weeks of differentiation of all three lines to determine their effect on neural development. Morphological analysis was performed using phase contrast images quantified using the Incucyte NeuroTrack software **(Figure 4.2A)**. Cell body properties were analysed by quantifying the number of cell clusters, in combination with cell cluster area. This showed that all three lines formed a similar number of cell clusters,

a common phenotype of neuronal differentiation, however, both the *ATG7*$^{+/-}$ and *ATG7*$^{-/-}$ lines ended the differentiation with fewer cell clusters than *ATG7*$^{+/+}$ however only *ATG7*$^{+/-}$ and *ATG7*$^{+/+}$ cultures were significantly different (**Figure 4.2B**).

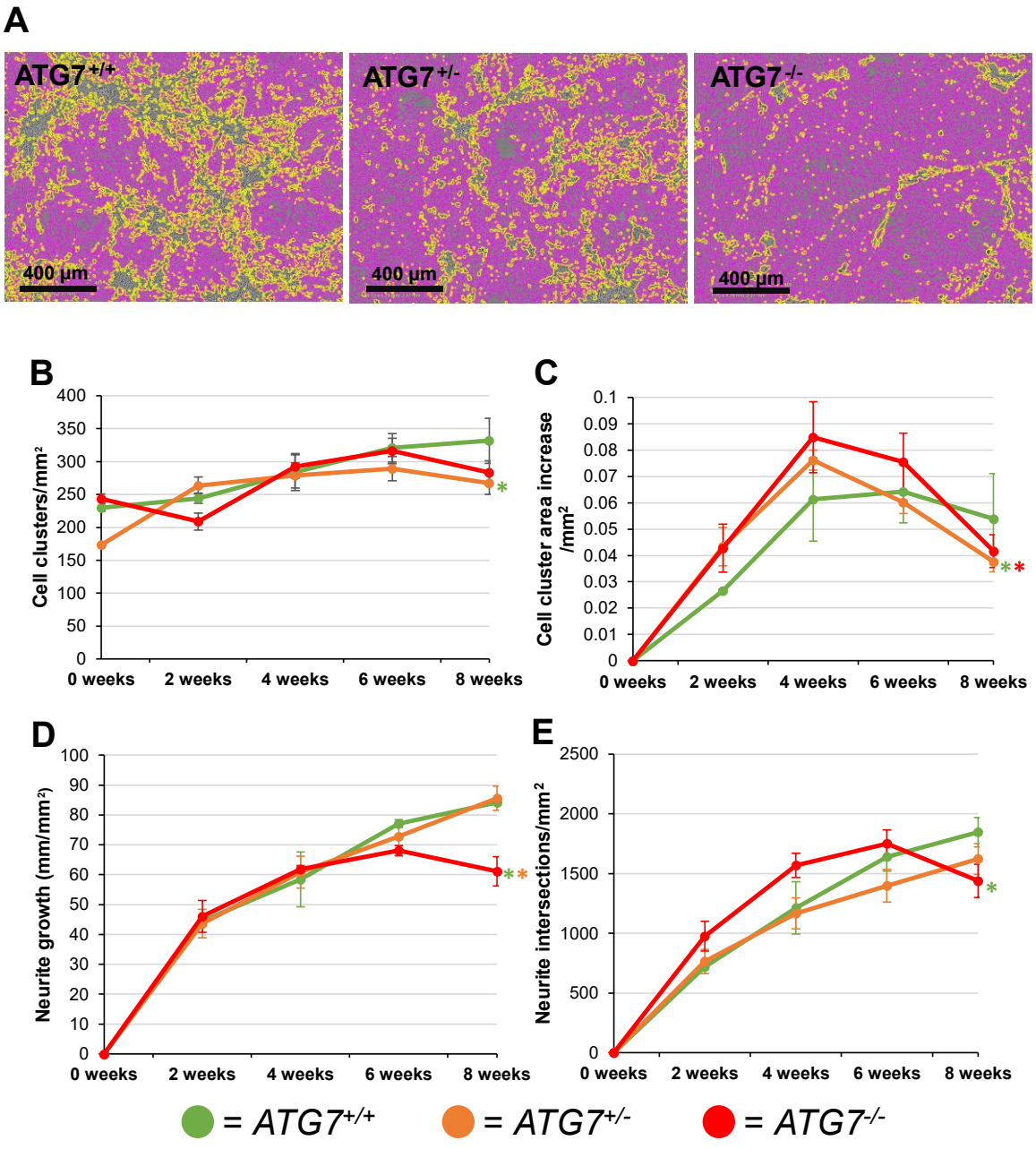


**Figure 4.2. Morphological timepoint analysis of developing neuronal-astrocyte co-cultures.** **A.** Representative images of ATG7$^{+/+}$, ATG7$^{+/-}$ and ATG7$^{-/-}$ co-cultures with Neurotrack software overlay after 8 weeks differentiation. Purple indicates neurites, yellow outlines indicate cell body clusters. **B.** Growth of cell clusters through development in each co-culture, expressed as cell body cluster area per mm$^2$. (n=4) (*$p < 0.05$ ANOVA and Tukey's *post-hoc* test, colour denotes genotype of comparison).**C.** Time point analysis of cell body clusters over time across each co-culture per

$mm^2$. (n=4) (*p < 0.05 ANOVA and Tukey's *post-hoc* test, colour denotes genotype of comparison). **D.** Neurite outgrowth over time across $ATG7^{+/+}$, $ATG7^{+/-}$ and $ATG7^{-/-}$ co-cultures quantified as mm per $mm^2$. (n=4) (*p < 0.05 ANOVA and Tukey's *post-hoc* test, colour denotes genotype of comparison). **E.** Number of new neurite intersections through development, characterised by the number of overlapping neurite branches per $mm^2$. (n=4). (*p < 0.05 ANOVA and Tukey's *post-hoc* test, colour denotes genotype of comparison). Error bars denote standard error.

As for the area of the cell clusters, $ATG7^{+/-}$ and $ATG7^{-/-}$ lines grew at a faster rate than the $ATG7^{+/+}$ line, likely due to increased cell division in the early differentiation stages before becoming post mitotic (**Figure 4.2C**). However, this was contrasted with sharp decline in cell cluster area after week four of differentiation, while the $ATG7^{+/+}$ plateaued, potentially indicating increased cell death when $ATG7^{+/-}$ and $ATG7^{-/-}$ lines transition to a post mitotic state. The changes observed in $ATG7^{+/-}$ cultures were found to be significant when compared to $ATG7^{+/+}$ and $ATG7^{-/-}$ cultures, however despite following a similar pattern, the changes observed in $ATG7^{-/-}$ cultures did not reach significance, likely due to the standard error associated with this assay.

In addition to cell bodies, neurite length was analysed. This demonstrated that both the $ATG7^{+/-}$ and $ATG7^{-/-}$ lines were able to generate neurites of similar length to $ATG7^{+/+}$ co-cultures (**Figure 4.2D**). While neurite growth plateaued for the $ATG7^{-/-}$ co-cultures after week six $ATG7^{+/+}$ and $ATG7^{+/-}$ neurites continued to grow up until week 8. The differences in neurite growth between $ATG7^{-/-}$ cultures and $ATG7^{+/-}$ and $ATG7^{+/+}$ cultures were significant.

In addition to this, the network complexity was quantified by the number of neurite intersections per $mm^2$. This demonstrated that over the 8 weeks, $ATG7^{-/-}$ neurite complexity developed at a rate above that of the $ATG7^{+/-}$ and the $ATG7^{+/+}$ lines over the first 6 weeks (**Figure 4.2E**). However, between weeks 6 and 8 there was a decrease in the number of intersecting neurites observed in the $ATG7^{-/-}$ cultures, which was not observed in $ATG7^{+/-}$ and the $ATG7^{+/+}$ cultures. Over the eight weeks, only the differences observed between $ATG7^{+/-}$ and the $ATG7^{-/-}$ cultures were found to be significant. However, the reduction in network complexity, but not the average neurite length in $ATG7^{-/-}$ cultures, supports the hypothesis that decrease in cell cluster areas across the same time period is due to neuronal cell death. Neuronal cell death would result in a reduction in overall neurites, reducing the likelihood of intersections without reducing the average neurite length.

### 4.3.3 Astrocytes are the predominantly affected cell type after 8 weeks of neural differentiation in the absence of ATG7

As there were clear morphological changes observed across the differentiation immunofluorescence analysis was undertaken to determine if there were observable changes to the distinct cell-types of the co-cultures. Given the morphological changes observed were most prominent in the *ATG7*$^{-/-}$ cultures, cultures were stained with p62, as *ATG7*$^{-/-}$ co-cultures showed a large increase in p62 when immunoblotted (**Figure 4.1A)**. This immunofluorescence was performed alongside MAP2 in light of the neuron cluster area and neurite differences seen in both the *ATG7*$^{+/-}$ and *ATG7*$^{-/-}$ co-cultures, indicating neurons are being negatively affected. Analysis of the cultures however demonstrated that while robust p62 staining was observed in both the *ATG7*$^{+/-}$ and *ATG7*$^{-/-}$, it did not co-localise with the neuronal MAP2 marker (**Figure 4.3**). The indication that neurons are not accumulating p62 at the end of the 8-week differentiation could suggest that the p62 positive cells are astrocytic in nature.

To investigate if the potentially p62 positive astrocytes were being disproportionately negatively affected, cleaved caspase 3 was used as a cell death marker, alongside MAP2 and GFAP, to investigate cell death in the neuron and astrocyte populations. This demonstrated that after 8 weeks differentiation, across all three genotypes, astrocytes were the most common cleaved caspase-3 positive cells (**Figure 4.4A and B**). However, the *ATG7*$^{+/-}$ and *ATG7*$^{-/-}$ co-cultures had an 8-fold and 16-fold increase respectively in the number of caspase 3 positive astrocytes per mm$^2$, when compared to that the *ATG7*$^{+/+}$ co-cultures. In addition, there were no caspase-3 positive neurons observed in either the *ATG7*$^{+/+}$ or the *ATG7*$^{+/-}$ co-cultures and there were 20 times fewer cleaved caspase-3 positive neurons observed in the *ATG7*$^{-/-}$ co-cultures when compared to the number of positive astrocytes per mm$^2$ in the same cultures (**Figure 4.4B**).

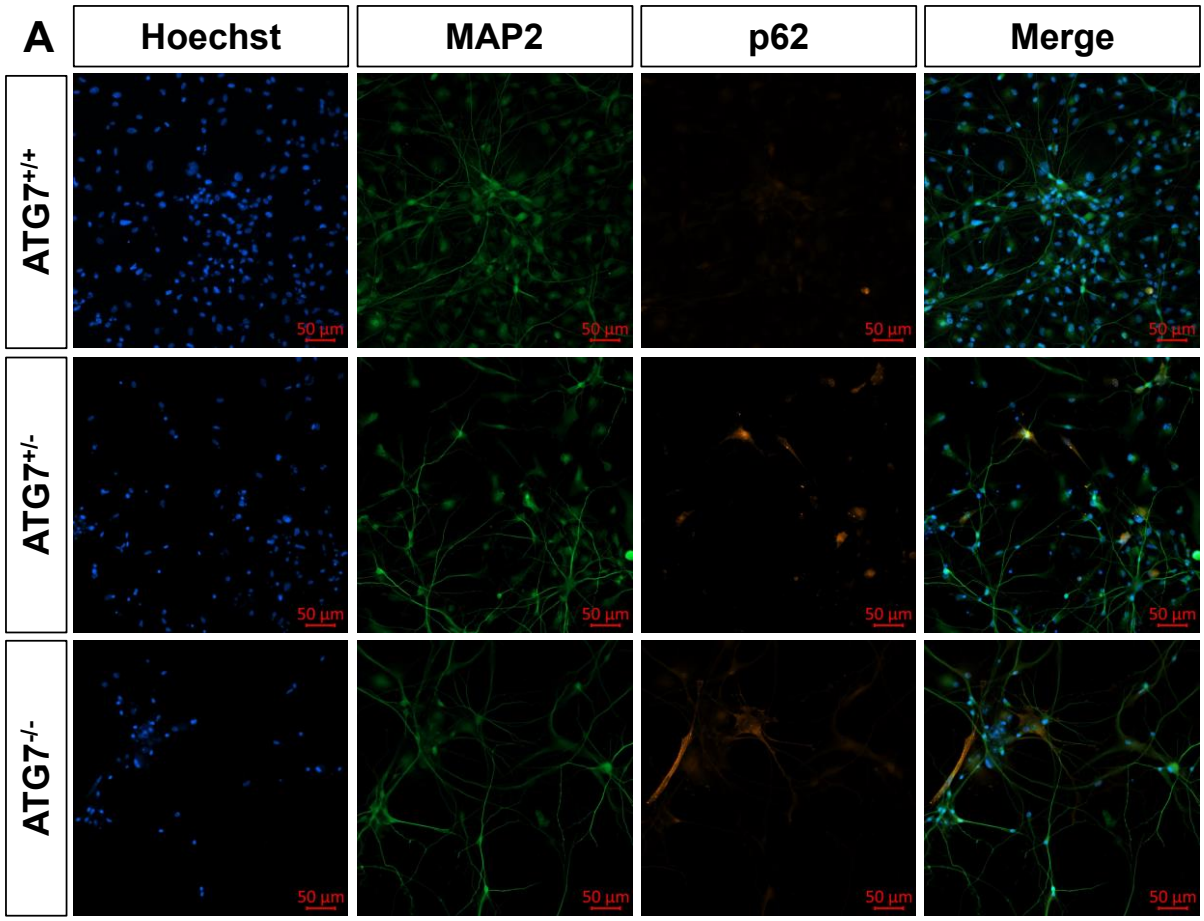


**Figure 4.3. Immunofluorescence staining of p62 does not co-localise with neurons in ATG7$^{+/+}$, ATG7$^{+/-}$ and ATG7$^{-/-}$ co-cultures after 8 weeks differentiation. A.** Representative immunofluorescence images of eight week differentiated co-cultures stained for autophagy adapter p62 and neuronal marker MAP2. Images taken using a 20x objective. (n=2)

As astrocytes were undergoing caspase-3 mediated cell death at differing rates between the genotypes, we also assessed the number of GFAP positive astrocytes at the end of the 8-week differentiation protocol. Here, *ATG7*$^{+/-}$ cultures were found to increased number of astrocytes when compared to the wild type *ATG7*$^{+/+}$ co-cultures, however this increase did not reach significance (**Figure 4.4C**). In contrast, *ATG7*$^{-/-}$ co-cultures were significantly decreased when compared to both the *ATG7*$^{+/+}$ and *ATG7*$^{+/-}$ co-cultures. This in combination with the increased cell death observed in *ATG7*$^{-/-}$ suggests that astrocytes may be more susceptible to cell death, which in turn results in fewer astrocytes at the end of the differentiation protocol.

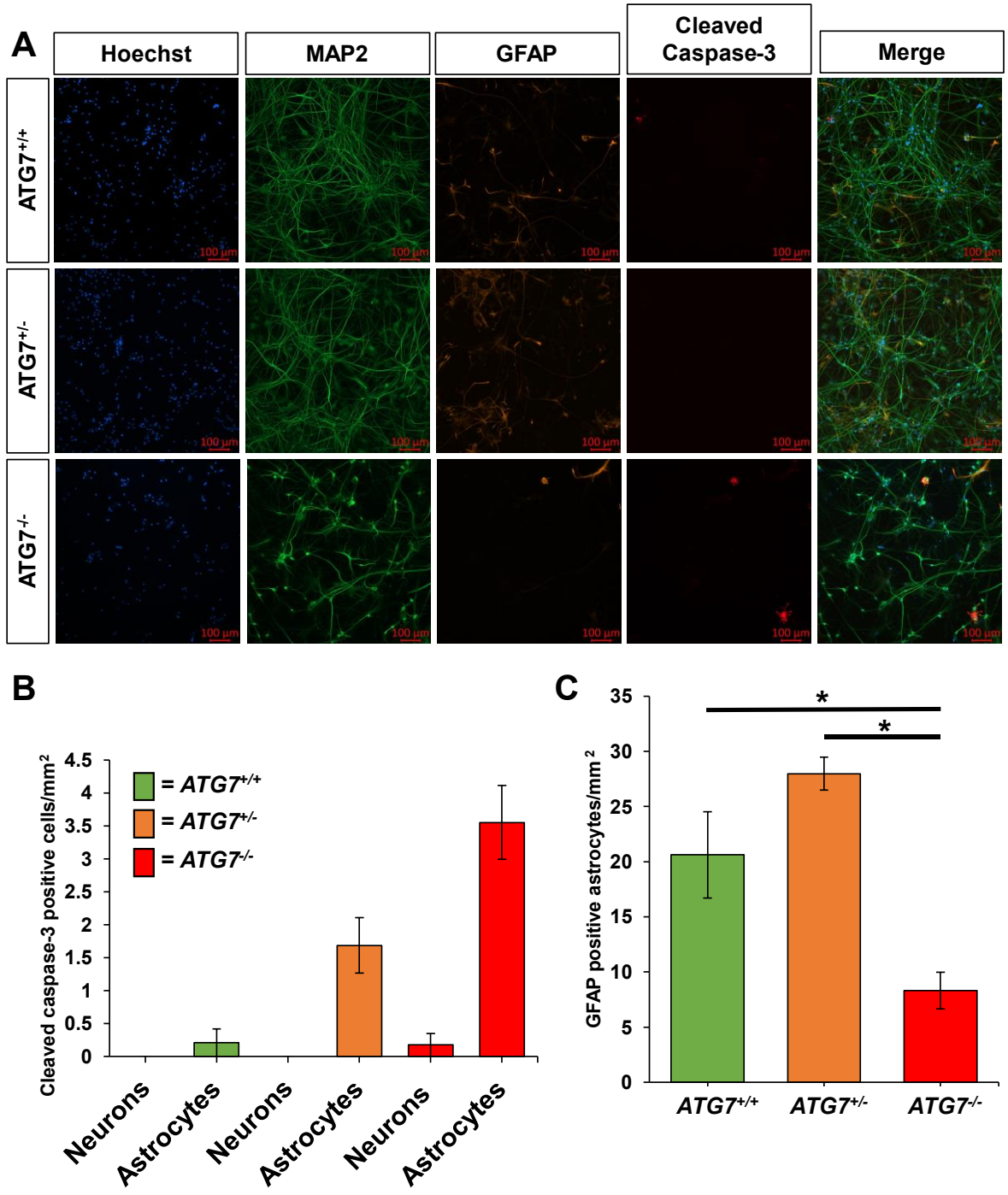


**Figure 4.4. Analysis of caspase-3 mediated cell death in neurons and astrocytes across ATG7$^{+/+}$, ATG7$^{+/-}$ and ATG7$^{-/-}$ co-cultures after 8 weeks differentiation. A.** Representative images of cleaved caspase 3 positive neurons and astrocytes across ATG7$^{+/+}$, ATG7$^{+/-}$ and ATG7$^{-/-}$ co-cultures, using MAP2 as a neuronal marker, and GFAP as an astrocytic marker. Images taken using a 10X objective. **B.** Quantification of the number of caspase 3 positive neurons and astrocytes per mm$^2$ in ATG7$^{+/+}$, ATG7$^{+/-}$ and ATG7$^{-/-}$ co-cultures. (n=2). **C.** Quantification of the number of GFAP positive astrocytes per mm$^2$ in ATG7$^{+/+}$, ATG7$^{+/-}$ and ATG7$^{-/-}$ co-cultures (n=3) (*$p < 0.05$ ANOVA and Tukey's *post-hoc* test).

### *4.3.4 ATG7* impairment hinders calcium handling in neurons

As described (**Chapter 4.1.3**), the intracellular calcium concentrations ($[Ca^{2+}]i$) of neurons and astrocytes are highly dynamic and interrelated. Astrocytes play a role in potentiation and recovery of glutamate mediated neural signalling as discussed (**Chapter 4.1.4**). As there have been clear differences between the astrocyte-*ATG7* lines, quantification of intracellular calcium flux in neurons was performed using the ratiometric calcium dye Fluo-4 under, in combination with a 1 mM glutamate stimulus. Interestingly, both the $ATG7^{+/+}$ and $ATG7^{-/-}$ co-cultured neurons generated $[Ca^{2+}]i$ peaks of comparable values, with fluorescence ratios of 0.94 and 1.05 respectively (**Figure 4.5A and B**). Meanwhile, the heterozygous knockout line, $[Ca^{2+}]i$ generated a significantly higher $[Ca^{2+}]i$ peak than both the $ATG7^{+/+}$ and $ATG7^{-/-}$ cultures, with a fluorescence ratio of 1.48 in response to the glutamate stimulus. There was no significant difference between the $ATG7^{+/+}$ and $ATG7^{-/-}$ cultures (**Figure 4.5A and B**).

As calcium signalling relies on influx and then subsequent efflux of calcium, in order to prevent cytotoxicity, the recovery of $[Ca^{2+}]i$ was quantified. This was taken as a ratio of the fluorescence signal over time after the peak fluorescence, compared to peak fluorescence value. As expected, $ATG7^{+/+}$ neurons recovered their $[Ca^{2+}]i$ throughout the four minute recovery period (**Figure 4.5A and C**). Both the $ATG7^{+/-}$ and $ATG7^{-/-}$ neuronal cell bodies did not share the same recovery characteristics, unable to recover to the same extent as the $ATG7^{+/+}$ neurons. As a result, the $ATG7^{+/-}$ and $ATG7^{-/-}$ cultures had significantly higher recovery ratios 4 minutes after their peak fluorescence, suggesting that they both had calcium handling impairments after glutamate stimulation. There was no significant difference in the final recovery ratio between the $ATG7^{+/-}$ and $ATG7^{-/-}$ neurons.

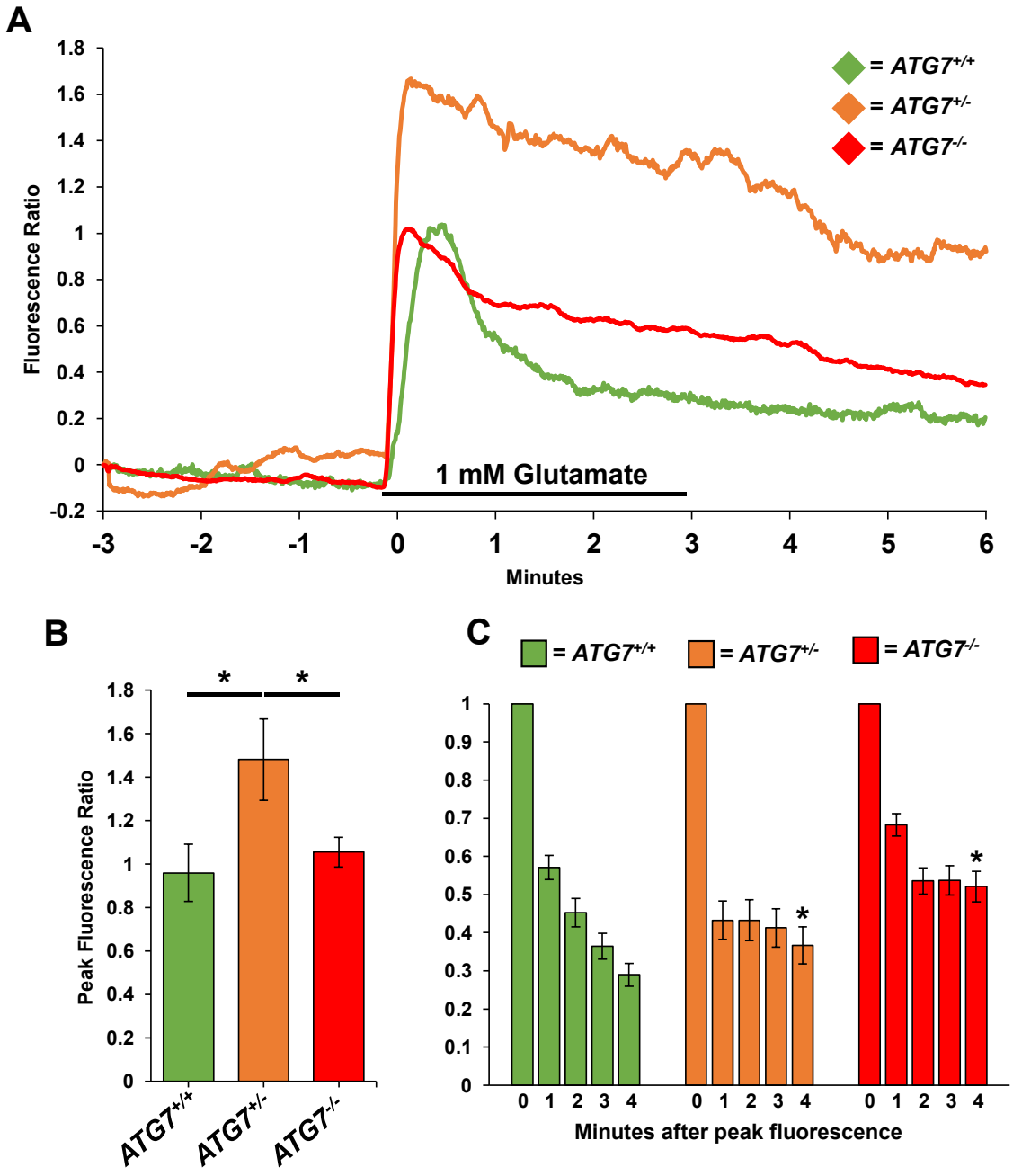


**Figure 4.5. Calcium imaging analysis of neural co-cultures showed dysregulation of calcium handling in ATG7$^{+/-}$ and ATG7$^{-/-}$ neurons. A.** Representative curves of fluorescence ratio of Fluo-4 calcium sensitive fluorescent dye, indicating changing intracellular calcium levels in response to 1 mM glutamate stimulus. **B.** Quantification of peak fluorescence in response to 1 mM Glutamate stimulus (n=4) (*p < 0.05 ANOVA and Tukey's *post-hoc* test). **C.** Quantification of the recovery in fluorescence ratio at minute intervals after the peak fluorescence, with fluorescence expressed as a ratio of peak fluorescence. Significance calculated compared to 4 minute recovery of *ATG7*$^{+/+}$ neurons, no statistical significance between *ATG7*$^{+/-}$ and *ATG7*$^{-/-}$ neurons (n=4) (*p < 0.05 ANOVA and Tukey's *post-hoc* test).

## 4.4 Discussion

In this chapter, the biochemical effects of loss of ATG7 in an iPSC derived neural model have been characterised. Immunoblot analysis demonstrated loss of the ATG5-ATG12 conjugation system in *ATG7*$^{-/-}$ cultures, but not in *ATG7*$^{+/-}$ cultures, after 8 weeks of neural differentiation. The LC3 conjugation system was also affected, with no detectable LC3-II in *ATG7*$^{-/-}$ cultures, and reduced levels in *ATG7*$^{+/-}$ cultures when compared to *ATG7*$^{+/+}$ cultures. Interestingly, only *ATG7*$^{-/-}$ cultures had an increase in p62 protein levels. Time point analysis over eight weeks demonstrated that both *ATG7*$^{-/-}$ and *ATG7*$^{+/-}$ had hindered development through differentiation, characterised by reduced neurite growth or cell cluster areas, indicating early cell death. Immunofluorescence analysis demonstrated that p62 staining does not colocalise with the neuronal marker MAP2, and that the majority of cells undergoing caspase-3 mediated cell death are GFAP positive astrocytes. Additionally, there are significant differences in the number of astrocytes between wild type and *ATG7* deficient co-cultures. Finally, calcium imaging demonstrated impaired recovery from calcium signalling in response to glutamate stimulus in both the *ATG7*$^{+/-}$ and *ATG7*$^{-/-}$ lines, with *ATG7*$^{+/-}$ neurons also showing significantly greater calcium influx in response to the stimulus compared to *ATG7*$^{+/+}$ and *ATG7*$^{+/-}$ neurons.

The loss of both key conjugation systems in *ATG7*$^{-/-}$ is expected given ATG7's role in both, as discussed (**Chapter 1.1.3**). While the loss of the LC3 conjugation is not surprising, the retention of some detectable ATG5-ATG12 conjugate in the *ATG7*$^{-/-}$ is. When initially described in yeast, loss of *atg7* (then *Apg7*) was found to result in complete loss of atg5-atg12 conjugate in the yeast knockout system, this contrasts with the observations in this *ATG7*$^{-/-}$ model (Mizushima et al., 1998). However, there have been two previously described affected siblings harbouring biallelic loss of function variants in *ATG7* which also have no detectable ATG7 using both N and C-terminal targeted antibodies (Collier et al., 2021). Subject derived fibroblasts, from one of the siblings (Subject 1) has also shown low levels of detectable ATG5-ATG12 conjugate. This may be a technical phenomenon associated with improved antibodies with increased sensitivity, or potentially an organism specific observation where human cells are able to generate a small amount of ATG5-ATG12 conjugate even in the absence of ATG7 given its more complicated machinery compared to that of yeast.

While the number of cell clusters formed through differentiation was comparable between all three lines, likely due to the same seeding density being used, the change in cluster area growth over time is different. This may be the result of autophagy impairment on Notch1 signalling, as discussed (**Chapter 4.1.1**). As autophagy is one of the main degradation routes for Notch1, the loss of autophagy may be resulting in the NSCs retaining their proliferative phenotype for longer than the *ATG7*$^{+/+}$ NSCs in the early stages of differentiation (Wu et al., 2016). While this could be confirmed via Western blot analysis at various timepoints through differentiation, it seems more likely the increased cell cluster area is due to ATG7's role in the cell cycle, as discussed (**Chapter 1.6.3**). Given all three lines plateaued or decreased after 4 weeks it is more likely that they were differentiating at the same rate and the *ATG7*$^{+/-}$ and *ATG7*$^{-/-}$ cells were dividing more rapidly due to impaired ATG7 function.

Surprisingly, the *ATG7*$^{-/-}$ neurons are able to generate neurite outgrowth comparable to the *ATG7*$^{+/+}$ neurons for the first four to six weeks. Firstly, autophagy impairment has been shown to be detrimental to axonal outgrowth in ATG7 and ATG9 knockout mouse models (Coupé et al., 2012; Yamaguchi et al., 2018). These findings are consistent with reduced neurite growth and branching of cultured dorsal root ganglion cells in response to nutrient chemical autophagy inhibition. Despite this, reduced autophagy has also been proposed to increase neuronal outgrowth (Ban et al., 2013; Yang et al., 2017). Interference with ATG7 or ATG12 has been demonstrated to increase axonal growth, particularly at the early stages in mouse primary neurons (Ban et al., 2013; Yang et al., 2017). In the case of ATG12, this was associated with an increase in mitochondria in the neurons, potentially increasing the ATP generating capacity and by the extension of the metabolically demanding process of axonal growth (Yang et al., 2017; Courchet et al., 2013). The retention of mitochondria may also explain the increased rate of neurite intersections observed in *ATG7*$^{-/-}$ neurons over the first 6 weeks of differentiation, with no corresponding increase in neurite growth. Mitochondria have been shown to play a key role in maturation of dendrites from their precursor structures, becoming stationary at the site of branching and providing the required ATP and cytoskeletal remodelling, allowing branching (Spillane et al., 2013; Courchet et al., 2013). If the *ATG7*$^{-/-}$ neurons had a similar increase in mitochondria as the ATG12 impaired neurons, this increase in mitochondrial abundance could result in increased branching. However, it should be noted the ATG7

impaired neurons had no report of increased mitochondria, therefore needing further investigation (Ban et al., 2013).

The cell type specific differences between the three lines are one of the more unexpected findings. The decrease in astrocytes observed at the end of 8 weeks differentiation between *ATG7*$^{+/+}$ and *ATG7*$^{-/-}$ is most likely a result of increased cell death. This is supported by the cleaved caspase-3 positive astrocytes being more prevalent in the *ATG7*$^{-/-}$ cultures. While the minimal number of cleaved caspase-3 positive neurons in *ATG7*$^{-/-}$ cultures is unexpected, the time point data (**Figure 4.2B**) suggests that neuronal cell death may be occurring before 8 weeks. The decrease in cell cluster area between weeks 4 and 8 of differentiation is likely when neurons are undergoing cell death, and also likely explains the decrease in neurite growth and branching observed in *ATG7*$^{-/-}$ neurons at the same timepoints. This earlier point of cell death in neurons is also an explanation for p62 not co-localising with neurons. Neurons accumulating p62 would be the most susceptible to cell death, resulting in a negative selection against p62 positive neurons, leaving few remaining after eight weeks differentiation.

The increase in astrocytes in the *ATG7*$^{+/-}$ cultures is interesting, especially when paired with the observed increased astrocytic cell death. While the increase in cell death will be due to the increase in astrocytes, however, the reason for increased astrocytic differentiation is less clear. The simplest explanation is again the increased proliferation rate observed (**Figure 4.2C**). Increased rate of proliferation during the symmetrical division stage of differentiation will produce an increased number of cells, which would be supported if the ratio of neurons to astrocytes were conserved, however more quantitative methods, like qRT-PCR, would be required to assess the cell ratios. The time point analysis indicates similar growth rates for both the *ATG7*$^{+/-}$ and *ATG7*$^{-/-}$ models, however, it is interesting that *ATG7*$^{+/-}$ line shared the reduction in cell body cluster growth of that observed in *ATG7*$^{-/-}$ line (**Figure 4.2C**). This would suggest both co-cultures underwent neuronal cell death after four weeks differentiation, making the retention of astrocytes in the *ATG7*$^{+/-}$ cultures curious. It would imply the astrocytes of the *ATG7*$^{+/-}$ cultures have greater resistance to cellular stress associated with autophagy disruption, compared to the neurons, a phenotype not shared by the *ATG7*$^{-/-}$ model. This however, and most other questions posed by these data, would be answered by an immunofluorescence analysis of neuron and

astrocyte markers alongside p62 and cleaved caspase 3 at the two, four, six and eight week timepoints.

The increase in astrocyte number is also a potential reason for the increase in intracellular calcium concentration. Previous studies have demonstrated that astrocytes are able to modulate synaptic transmission via exocytic glutamate release (Bezzi et al., 2004; Zhang et al., 2004; Jourdain et al., 2007). Glutamate release from the post synaptic cleft is detected by astrocytic metabotropic and ionotropic glutamate receptors, resulting in additional glutamate release from astrocytes in a calcium dependant exocytic manner (Porter & McCarthy, 1996; Bezzi et al., 1998). This then acts to increase intracellular calcium levels in neurons (Jourdain et al., 2007; Bezzi et al., 1998; Porter & McCarthy, 1996). This would suggest the additional astrocytes observed in *ATG7*$^{+/-}$ allows this potentiation to occur to a greater extent than in *ATG7*$^{+/+}$. However, it could be argued that *ATG7*$^{+/-}$ is increased as there is no observed astrocytic potentiation in *ATG7*$^{+/+}$ neurons. The comparable calcium peaks between *ATG7*$^{+/+}$ and *ATG7*$^{-/-}$, in addition to the significantly different astrocyte numbers per $mm^2$, would suggest there is no effect from the astrocytes in these two genotypes. This is likely due to the experimental protocol, with the ACSF supplemented with 1 mM glutamate used, which is sufficient to allow *ATG7*$^{-/-}$ neurons to respond in line with the *ATG7*$^{+/+}$ and the additional astrocytes in *ATG7*$^{+/-}$ cultures allowing potentiation above this. It should be noted that 1 mM glutamate is comparable to glutamate concentration in the post synapse of cultured hippocampal neurons, however, post-synaptic glutamate concentrations in rat hippocampal brain slices are reportedly slightly higher, at 1.4 mM glutamate (Clements et al., 1992; Budisantoso et al., 2013).

While the *ATG7*$^{+/-}$ and *ATG7*$^{-/-}$ neurons have significantly different peaks, their recovery rates are comparable, suggesting that both co-cultures have impaired calcium recovery mechanisms. The decrease in recovery observed in both the *ATG7*$^{+/-}$ and *ATG7*$^{-/-}$ lines is likely due to calcium handling, as opposed to impaired glutamate handling due to the experimental design. ACSF containing 1 mM glutamate is continuously perfused throughout the majority of the recovery period, up to three minutes after addition. In the same time frame, *ATG7*$^{+/+}$ neurons were able to significantly recover at each consecutive timepoint, without the plateau observed in the other lines. It is also unlikely to be astrocyte mediated given the disparity between astrocyte populations between the two cultures. This implies that neuronal calcium

handling itself is compromised. As discussed (**Chapter 4.1.3**), there are three main calcium recovery mechanisms, efflux via plasma membrane transporter, sequestering by calcium buffering proteins, and organelle uptake. Mitochondria are one of the central calcium buffering organelles maintaining intracellular calcium concentrations. Under normal circumstances, the proton gradient generated during normal oxidative phosphorylation results in import of calcium via the calcium uniporter (Gleichmann & Mattson, 2011). Import of calcium is increased in response to an increase in cytosolic calcium concentration, ATP/ADP ratio and mitochondrial membrane potential, all playing a role in the recovery of calcium influx (Brini et al., 2014). However, *ATG5*$^{-/-}$ iPSC derived neurons have previously been shown to have a reduction in ATP and ADP levels, along with a reduction in mitochondrial membrane potential (Sun et al., 2023). If this was the case in the neuron-astrocyte co-cultures described here, these impairments could potentially lead to disruption of the mitochondrial calcium uniporter, hindering calcium recovery following stimulus. While loss of mitochondrial membrane potential would usually result in mitophagy and subsequent mitochondrial turnover, as expected, *ATG5*$^{-/-}$ neurons have an increased mitochondrial load due to loss of core autophagy machinery (Sun et al., 2023). Investigations into mitochondrial load and mitochondrial membrane potential in the *ATG7*$^{+/-}$ and *ATG7*$^{-/-}$ neurons compared to *ATG7*$^{+/+}$ would strengthen this hypothesis. However, no electrophysiology was performed using *ATG5*$^{-/-}$ neurons, and they were not cultured with astrocytes, which, as discussed, are necessary for full beneficial effect to neuronal development (Sun et al., 2023).

Biochemical, morphological and electrophysiological analysis has demonstrated a range of detrimental effects associated with ATG7 impairment on neuron-astrocyte co-cultures, suggesting astrocytes may be more susceptible to ATG7 impairment than first thought.

# 5 Segregating *ATG7* variants can be incompatible with life.

## 5.1 Introduction

### 5.1.1 Neuron production in the developing brain

In the developing brain, neurons are produced in the ventricular zone, which lies on the wall of the lateral ventricle, and then latterly the subventricular zone, which lies deeper into the brain (**Figure 5.1A**) (Subramanian et al., 2017). At the start of neural development, in the embryonic stage, the ventricular zone is a single layer of cells known as neuroepithelial cells, however these develop into radial glial cells (RGCs), which expand and become the central proliferative cell (Homem et al., 2015). Following asymmetrical division, they will migrate away from the ventricle, into the expanding brain, which forms from the inside moving outwards (Noctor et al., 2008). As RGCs migrate outwards and continue to proliferate, they form the subventricular zone (**Figure 5.1A**) (Subramanian et al., 2017). Once the RGCs are a part of the subventricular zone, they are termed basal radial glia. In addition to their role in proliferation and neuron generation, RGCs also have long processes, connecting the ventricular zone to the cortical plate (Levitt & Rakic, 1980). The cortical plate is the structure preceding the cortex, in which the six layers of the cortex are formed through development (Terashima et al., 2021). These long processes connecting the ventricular zone to the cortical plate act as a scaffold along which the newly generated neurons can migrate (**Figure 5.1A**) (Rakic, 1972). Migration of neurons through the intermediate zone, which will eventually become white matter between the ventricular zone and the cortex, is an important step in the establishment of their proper positioning in the cortex (Rakic, 1972).

### 5.1.2 The human brain at 24 weeks post conception

Around 24 weeks post conception, the developing foetal brain bears some of its major landmarks with the formation of the prominent gyri and sulci, however the majority of more complex folding does not commence until after 24 weeks post conception (Dubois et al., 2008; Dubois et al., 2008). At this time point, neuronal differentiation has started to slow in the ventricular zone, and neuron generation is performed mostly

by the basal RGCs of the subventricular zone, with neuronal migration along radial glia from the ventricle to the cortex well underway (Nowakowski et al., 2016; Bystron et al., 2008). The innermost cortical layers are well formed, and axonal growth is extending deep into the brain (Kostović & Judaš, 2002). Pre- and post-synaptic neurons are starting to form, with the cortical projections to the thalamus being among the first functional synaptic inputs to arise around this time point (Kostovic & Goldman-Rakic, 1983). Commencing at 24 post conception weeks, permanent cortex circuitry starts to form, which is a critical stage in brain development (Molliver et al., 1973).

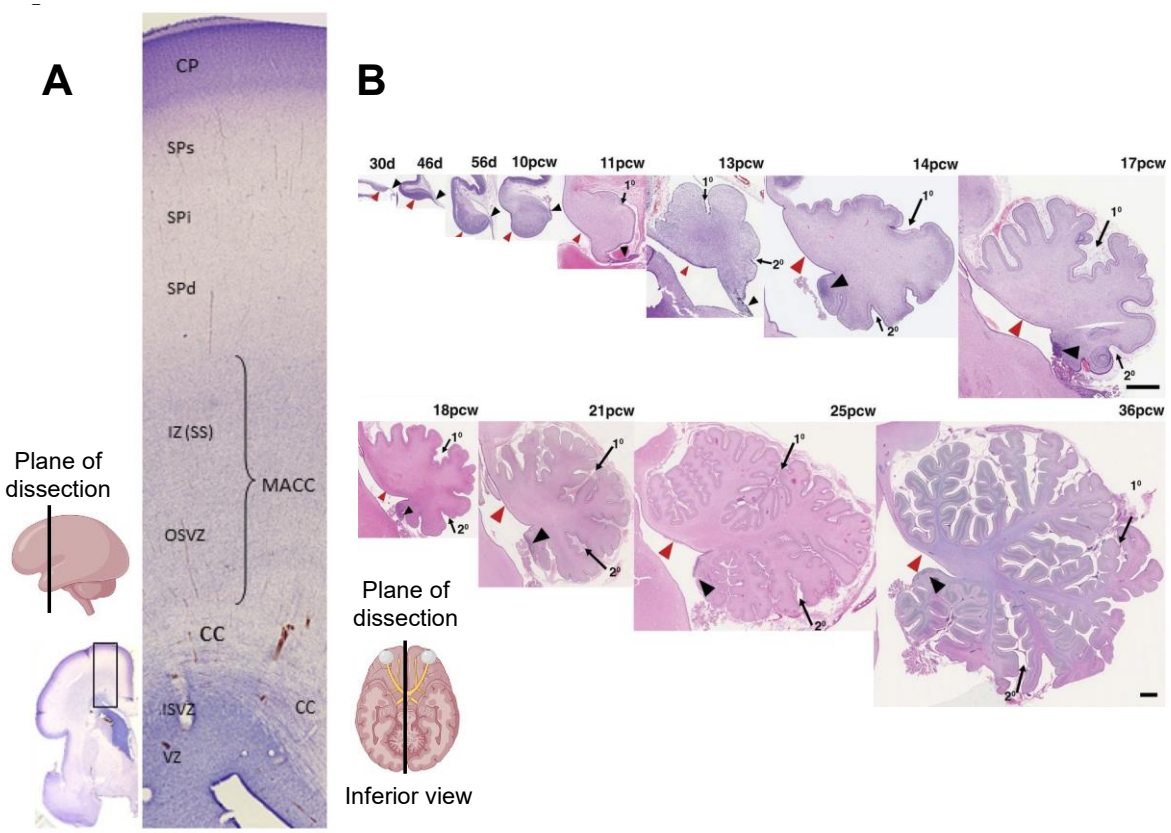


**Figure 5.1 Organisation of the developing cerebrum at 22-25 post conception weeks and development of the human cerebellum. A.** Nissl-stained sections of the neocortex demonstrating the cellular organisation of the developing cortex, coronal plane of dissection indicated (left). Layers from top to bottom; cortical plate (CP), subplate (SP), intermediate zone (IZ), outer subventricular zone (OSVZ), corpus callosum (CC), inner subventricular zone (ISVZ) and ventricular zone (VZ). The subplate is comprised of multiple layers (SPs, Spi and SPd) and the sagittal strata (SS) of the IZ and the OSVZ form the multilaminar axonal cellular compartment (MACC). The OSVZ and ISVZ are separated by fibers of the forming corpus callosum (CC). **B.** Development of the cerebellum through development with H&E-stained sections, midsagittal plane of dissection indicated (bottom left). Red arrow indicates the cerebellar ventricular zone from which Purkinje neurons arise in early development, with black arrow showing the rhombic lip from which

proliferation occurs after 20 post conception weeks. Additionally, the primary fissures ($1^0$) and secondary fissures ($2^0$) are noted with arrows. Scale bars: 100 μm. Figures are adapted using Biorender from Kostović et al., 2021 and Haldipur et al., 2019.

### 5.1.3 Corpus callosum development

The corpus callosum is the major connection between the two hemispheres of the brain, playing a key role in the higher functions of the cerebral cortex, particularly in functions which are more dependent on one hemisphere than the other, like speech (De León Reyes et al., 2020; Paul et al., 2003). The corpus callosum appears at week 11 post conception, stemming from the wall of the thalamus, at the midline of the developing brain (Rakic & Yakovlev, 1968). By 24 weeks, the corpus callosum has separated from the thalamus, sitting above, with connections from callosal neurons from the opposite hemisphere well developed (Rakic & Yakovlev, 1968). While the majority of connections are still yet to form, only the brain stem-afferent neurons and some forebrain afferents are connected via the corpus callosum (Jovanov-Milošević et al., 2010). The corpus callosum will continue to expand through the foetal period, however in early infancy, this is mirrored by a decrease in cross sectional area, indicative of neuronal pruning (LaMantia & Rakic, 1990). While most corpus callosum studies focus on histological examination, corpus callosum changes are also visible using MRI scans, with corpus callosum malformations being readily observed and used as disease indicators (Nosarti et al., 2008).

### 5.1.4 Cerebellum development

Formation of the cerebellum starts at 30 days post conception and continues until 2 years after birth (Rakic & Sidman, 1970; Haldipur et al., 2011). The cerebellum has two progenitor zones, the ventricular zone giving rise to GABAergic neurons, including Purkinje neurons, and the rhombic lip, giving rise to glutamatergic neurons (**Figure 5.1B**) (Leto et al., 2016). As with the rest of the brain, the cerebellum is formed from the inside moving outwards, this results in the neurons of the cerebellar nuclei, like the dentate nucleus, to be formed first, followed by more superficial neurons of the cerebellar cortex (Leto et al., 2016). In the first 10 weeks post conception, the ventricular zone contains radial glial cells, and produces a subventricular zone containing basal progenitors, similar to that seen in the cerebrum. After 10 weeks post conception, the ventricular zone shrinks, and the rhombic lip (RL) expands (**Figure**

**5.1B**) (Haldipur et al., 2019). Again, the rhombic lip can be separated into a ventricular zone ($RL^{VZ}$), and a subventricular zone ($RV^{SVZ}$), with RGCs and basal progenitors respectively (Haldipur et al., 2019). The cerebellum increases to 5 times its starting volume between 22 post conception weeks and birth, and 24 weeks, which also marks the start of an increase in folding, required to generate the highly foliated cerebellum (**Figure 5.1B**) (Volpe, 2009; Limperopoulos et al., 2005). At 24 weeks post conception, Purkinje cells are observable in the Purkinje layer, however they are poorly differentiated until 36 weeks post conception (Rakic & Sidman, 1970).

This chapter aims to investigate the pathology of a foetal subject harbouring recessively inherited *ATG7* variants. Frozen liver tissue was used to establish steady state levels of ATG7 and p62. Meanwhile, formalin fixed paraffin embedded brain tissue was used to investigate the underlying neuropathology associated with this developmental disorder.

## 5.2 Methods

### 5.2.1 Frozen liver tissue total protein extraction

Frozen liver tissue was obtained from Dr. Aurélien Trimouille (CHU Bordeaux-Pellegrin, France). RIPA buffer (1% IGEPAL, 0.5% Sodium deoxycholate, 0.1% SDS, 1 mM PMSF, 1.5% Triton X-100, 10 mM β-mercaptoethanol) was added to frozen liver tissue and homogenised with an Ultra-Turrax high speed homogeniser. Samples were incubated on ice for 30 minutes before being centrifuged at 4,000 x *g,* the lipid layer was discarded, and the supernatant was retained for further experiments.

### 5.2.2 Immunoblot analysis of steady state proteins

Protein concentration of liver lysates was estimated as described (**Chapter 2.7.2**). Proteins were separated and immunoblotted as described (**Chapter 2.7**).

### 5.2.3 Immunohistochemistry

Formalin fixed paraffin embedded (FFPE) post-mortem tissue was obtained from Dr. Aurélien Trimouille (CHU Bordeaux-Pellegrin, France). Sections were dewaxed by two washes with Histoclear (National Diagnostics), for 20 and 15 minutes respectively. Sections were rehydrated through a series of ethanol solutions (100%, 100%, 95%, 70%) for 5 minutes each before two final five minute washes with distilled water.

Sections then underwent heat mediated antigen retrieval, were submersed in boiling citrate buffer (pH 6) for 10 minutes before being left to cool for 20 minutes. Sections were thoroughly washed in distilled water and subsequently quenched for endogenous peroxidase activity by immersion in 3% hydrogen peroxide for 20 minutes at room temperature. Sections were washed in phosphate buffered saline with 0.5% Triton X-100 (Sigma-Aldrich) (PBST). The required antibody was then diluted as described (**Chapter 2.5**) in PBST and incubated for 1 hour at room temperature. MenaPath Universal Probe (Menarini) was added for 30 minutes at room temperature. Sections were then incubated with MenaPath Polymer HRP reagent (Menarini) for 30 minutes at room temperature. Menarini diaminobenzidine (DAB) is then added for 3 minutes before washing, and counter staining with haematoxylin. Once counterstained, sections were dehydrated, cleared and mounted with distyrene plasticiser xylene (DPX) (CellPath). Sections were imaged using a Nikon E800 microscope with a Leica DFC430 colour camera or a Zeiss Axioscan 7 using a X-Cite® XYLIS LED light source and an Axiocam 705 colour camera.

### 5.2.4 Immunofluorescence

Sections underwent rehydration and antigen retrieval as described (**Chapter 5.2.3**) and then blocked using 10% normal goat serum (NGS) (Thermo Fisher Scientific) in PBST for 1 hour at room temperature. Antibodies were then diluted as described (**Chapter 2.5)** in 10% NGS in PBST and incubated overnight at 4°C. After washing with PBST 3 times, secondary antibodies were diluted 1:100 and incubated for 1 hour at room temperature before washing 3 times with PBST. Sections were then counter stained with Sudan Black B before being left to dry at room temperature and mounted using Prolong Gold antifade mountant (Invitrogen). Sections were imaged using a Leica SP8 confocal microscope using 2 Hybrid Detectors and 2 photomultiplier tubes, with solid state 488 nm, 552 nm and 638 nm lasers.

## 5.3 Results

### 5.3.1 *ATG7* subject identified with polymalformative syndrome

A foetus harbouring recessively inherited bi-allelic loss of function *ATG7* variants has been identified using trio whole exome sequencing by Dr. Aurélien Trimouille (CHU Bordeaux-Pellegrin). The subject was found to have a paternally inherited c.1775dupT,

p.Ser593Ilefs*17 variant and a maternally inherited c.1711C>T, p.Gln571* variant in the *ATG7* gene (RefSeq; NM_006395.2) (**Figure 5.2A**). The subject was found to have polymalformative syndrome, comprising corpus callosum anomalies, cleft palate, hyperechogenic kidneys and a ventricular septal defect, leading to termination at 24 gestational weeks.

### 5.3.2 Undetectable ATG7 protein levels in frozen liver tissue.

To determine the biochemical result of the biallelic *ATG7* variants identified by WGS, frozen liver tissue was obtained from the foetus, along with two age matched control samples. Immunoblotting of liver lysates showed a complete loss of ATG7 protein in the subject, with ATG7 being present in both the unaffected control livers (**Figure 5.2B**). In addition, the subject was found to have an increased level of autophagy adapter p62 when compared to Control 1 which had no detectable p62, and Control 2 which had only minimal p62 protein levels present. This suggests that the lack of ATG7 in the liver tissue was sufficient to disrupt autophagy and result in an accumulation of material marked for degradation. Functional autophagy assays were not carried out due to a lack of living cells available from the subject.

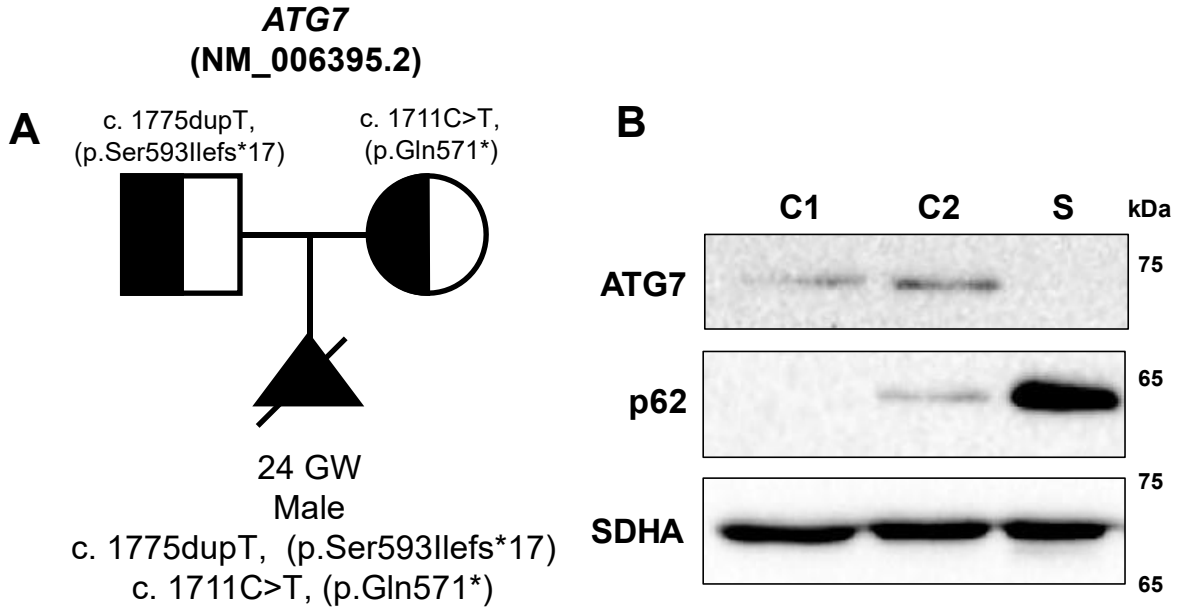


**Figure 5.2 Pedigree and biochemical characterisation of foetal subject. A.** Pedigree demonstrating recessive inheritance of ATG7 variants in the subject, a male of 24 gestational weeks. **B.** Western blot analysis of ATG7 and p62 in foetal frozen liver samples from age-matched controls (C1, C2) and ATG7 subject (S) shows loss of detectable ATG7 and an accumulation of p62 in the subject. SDHA is used as loading control (n = 3).

### 5.3.3 Subject cerebellum shows altered structural development.

In addition to frozen liver samples, FFPE post-mortem brain tissue was provided for investigations by Dr. Aurélien Trimouille (Bordeaux University, France). In collaboration with Dr. Daniel Erskine (Newcastle University), haematoxylin and eosin (H&E) staining of formalin fixed paraffin embedded sections was performed alongside immunohistochemical (IHC) and immunofluorescence staining of subject and control brain tissue.

Given cerebellar hypoplasia and ataxia are common phenotypes across all the previously reported *ATG7* patients, the cerebellum of the subject and controls was examined. Adjacent sections showed that there were p62 foci in distinct folia of subject's cerebellum (**Figure 5.3A**). These distinct p62 puncta were not observed in either of the control samples. Immunofluorescence staining for the Purkinje cell marker calbindin showed that the p62 positive cells were not Purkinje cells (**Figure 5.3B**). Inspection of the Purkinje cell layer using calbindin demonstrated a single, intermittent layer of Purkinje cells, in contrast to the multiple layers of Purkinje cells seen in the control. In addition, there appeared to be clusters of non-migrated cells in the cerebellum of the subject, which were not present in either of the controls (**Figure 5.4A**). Immunofluorescence analysis of adjacent sections showed that these clusters of non-migrated cells were calbindin positive Purkinje cells (**Figure 5.4B**). Interestingly, there were also cells positive for Sudan Black B staining, which was used as a counter stain, indicating an accumulation of neutral lipids, which was not observed in the controls. H&E staining of the subject cerebellum also showed malformation of the dentate nucleus, while both controls had morphologically normal dentate nuclei (**Figure 5.5A**). While the control case's dentate nucleus had the classical serrated appearance, the subject's dentate nucleus appeared segmented and dense.

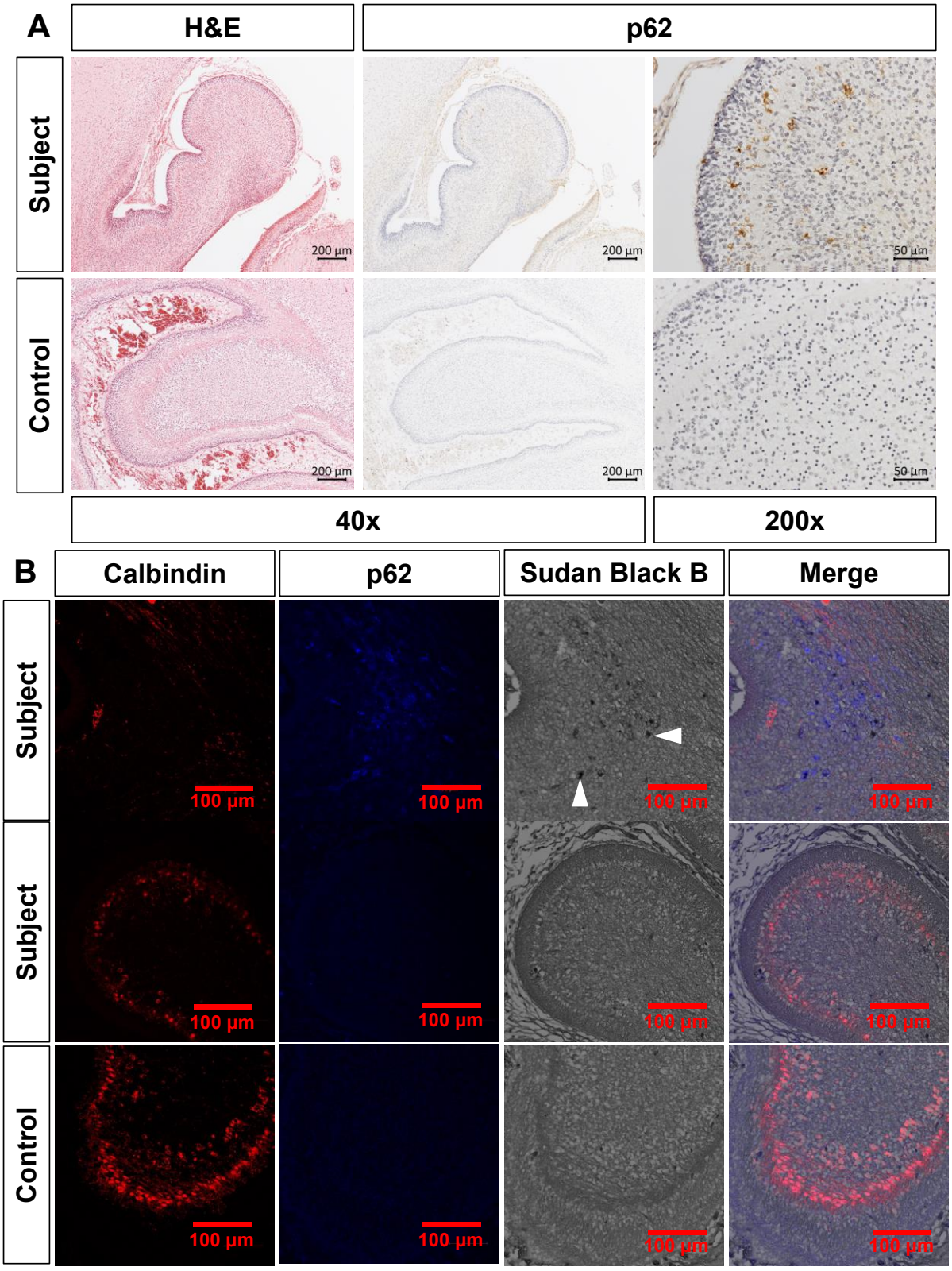


**Figure 5.3 Immunohistochemical and immunofluorescence analysis of ATG7 subject cerebellum.A.** H&E-stained sections of subject and control cerebellar folia (left) and p62 stained sections (centre and right) showing distinct p62 positive puncta in the subject. **B.** Immunofluorescence images of subject and control cerebellum showing the p62 positive puncta

are not calbindin positive Purkinje cells. In addition to the p62 puncta, there are also cells accumulating neutral lipids, indicated by the Sudan Black staining in the subject folia, examples denoted by white arrows.

Subject cerebellum also had observable p62 staining in the rhombic lip (**Figure 5.5B**). Staining was strongest in the ventricular zone of the rhombic lip, however there is also clear staining in the rhombic lip subventricular zone also. In contrast, there was no observable p62 staining in the ventricular zone, or subventricular zones of the cerebrum.

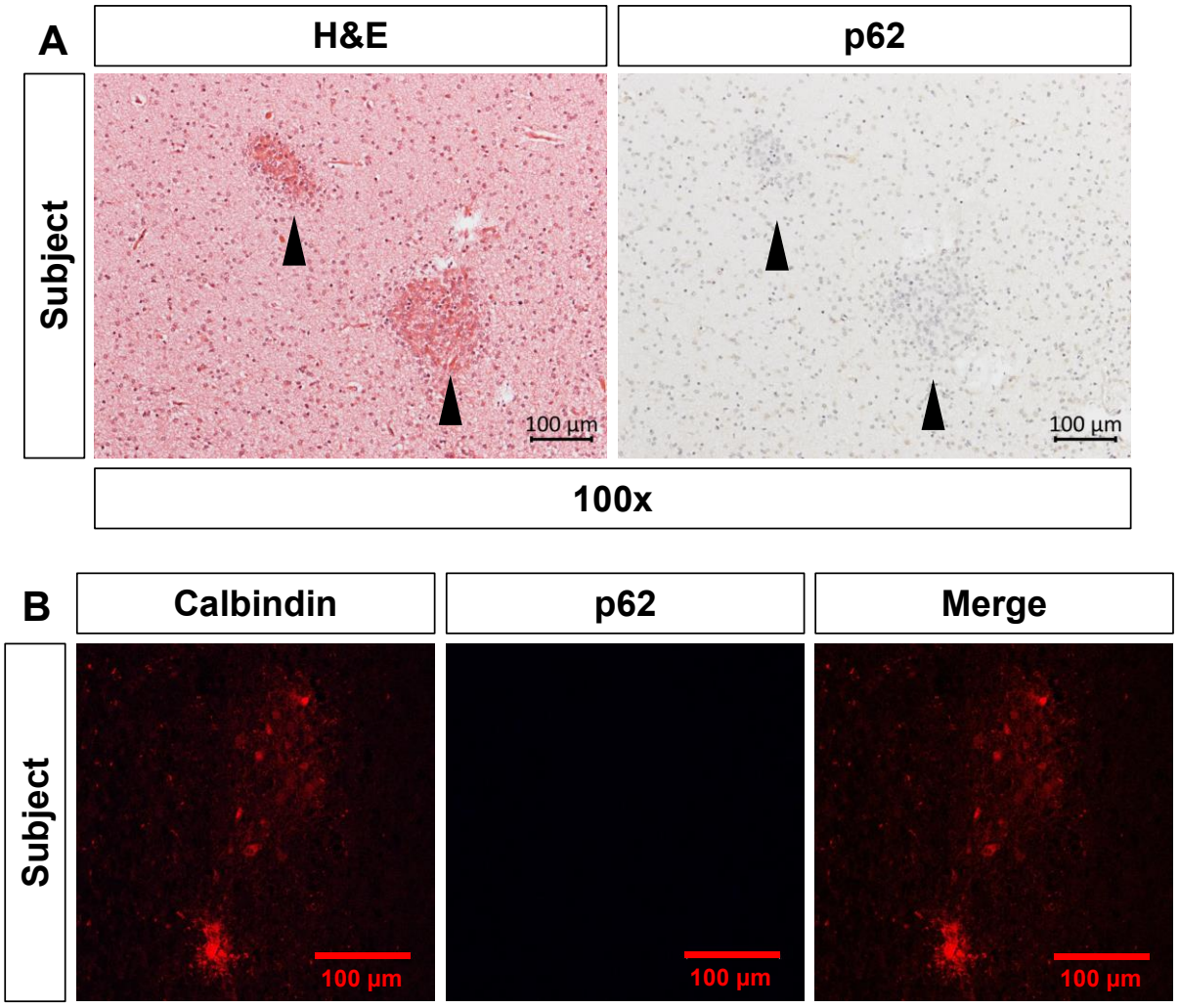


**Figure 5.4 Identification of non-migrated cells in the ATG7 subject cerebellum. A**. H&E staining of non-migrated neurons in the subject cerebellum, indicated by arrowheads, alongside p62 staining of the non-migrated cells. **B.** Immunofluorescence images of the non-migrated cells seen in A. Cells are calbindin positive suggesting they're calbindin positive Purkinje cells.

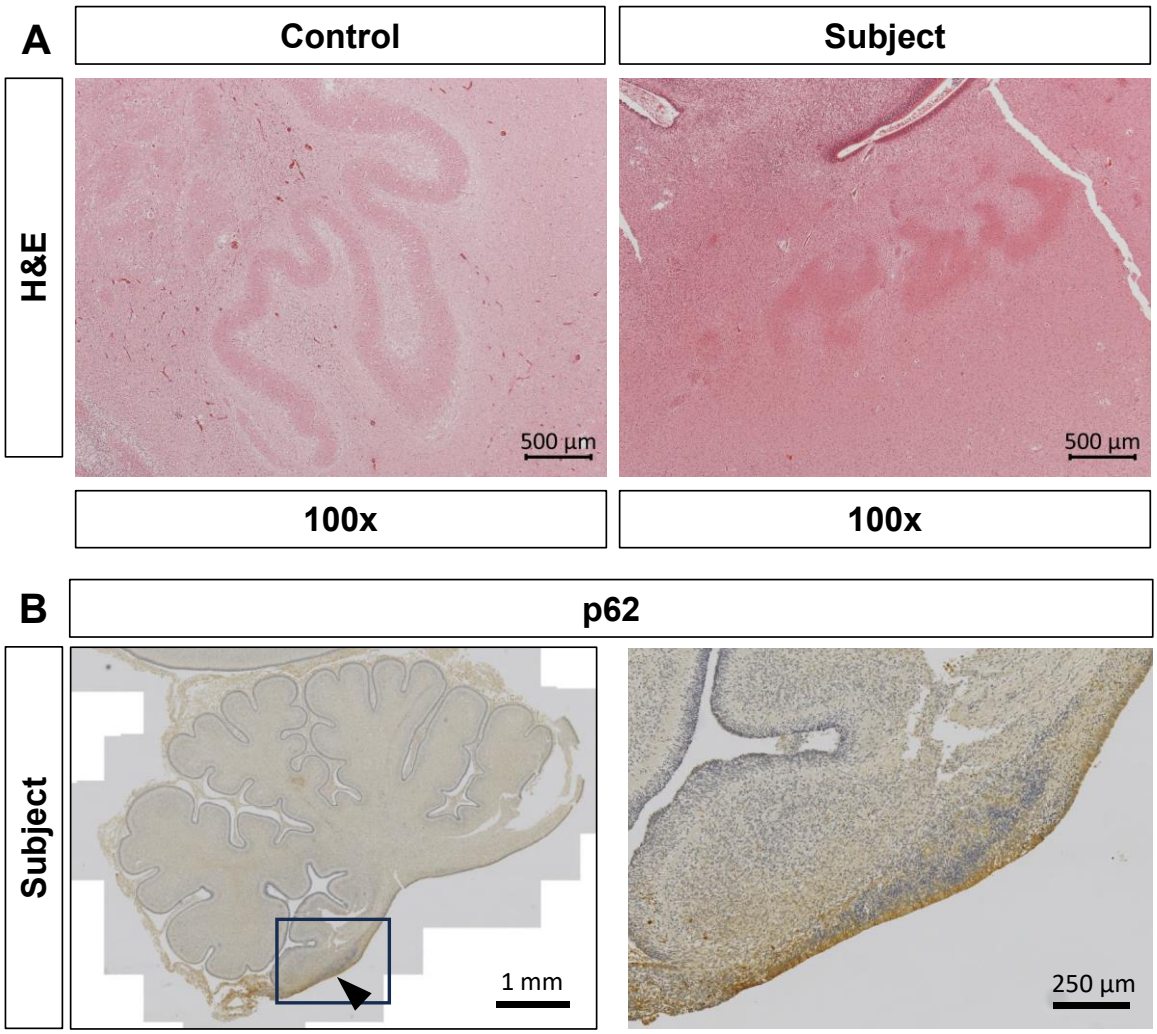


**Figure 5.5 Malformation of cerebellar nuclei and p62 accumulation in proliferative zone of the ATG7 subject. A.** H&E staining of control and subject cerebellum, with the control showing a well-defined dentate nucleus, while the subject has a segmented dentate nucleus. **B.** Immunohistochemical staining of subject cerebellum. Left shows whole cerebellum, with rhombic lip denotes by arrow. Right, enlarged view of rhombic lip denoted in left by box. Staining shows p62 accumulation in the ventricular and subventricular zones of the rhombic lip.

### 5.3.4 ATG7 subject corpus callosum shows p62 accumulation in migrating neurons.

In addition to cerebellar hypoplasia and ataxia, atrophy of the corpus callosum is also commonly seen in all described *ATG7* patients (Collier et al., 2021). In light of this, the corpus callosum of the *ATG7* subject, along with the controls, was examined for abnormalities with H&E staining. This showed spongiform changes localised to one half of the corpus callosum of the subject, but not the controls (**Figure 5.6A**). IHC

staining with p62 antibodies of serial sections showed distinct p62 positive puncta, which were also localised to one half of the corpus callosum, in the subject, but not in the controls (**Figure 5.6A**). To identify the p62 positive cells in the subject corpus callosum, immunofluorescence was performed using an oligodendrocyte marker, OLIG2. The p62 puncta in the corpus callosum of the subject did not co-localise with OLIG2, suggesting they were not oligodendrocytes. However, a small number of p62

positive OLIG2 positive oligodendrocytes were identified in the cortex of the subject (**Figure 5.6B**).

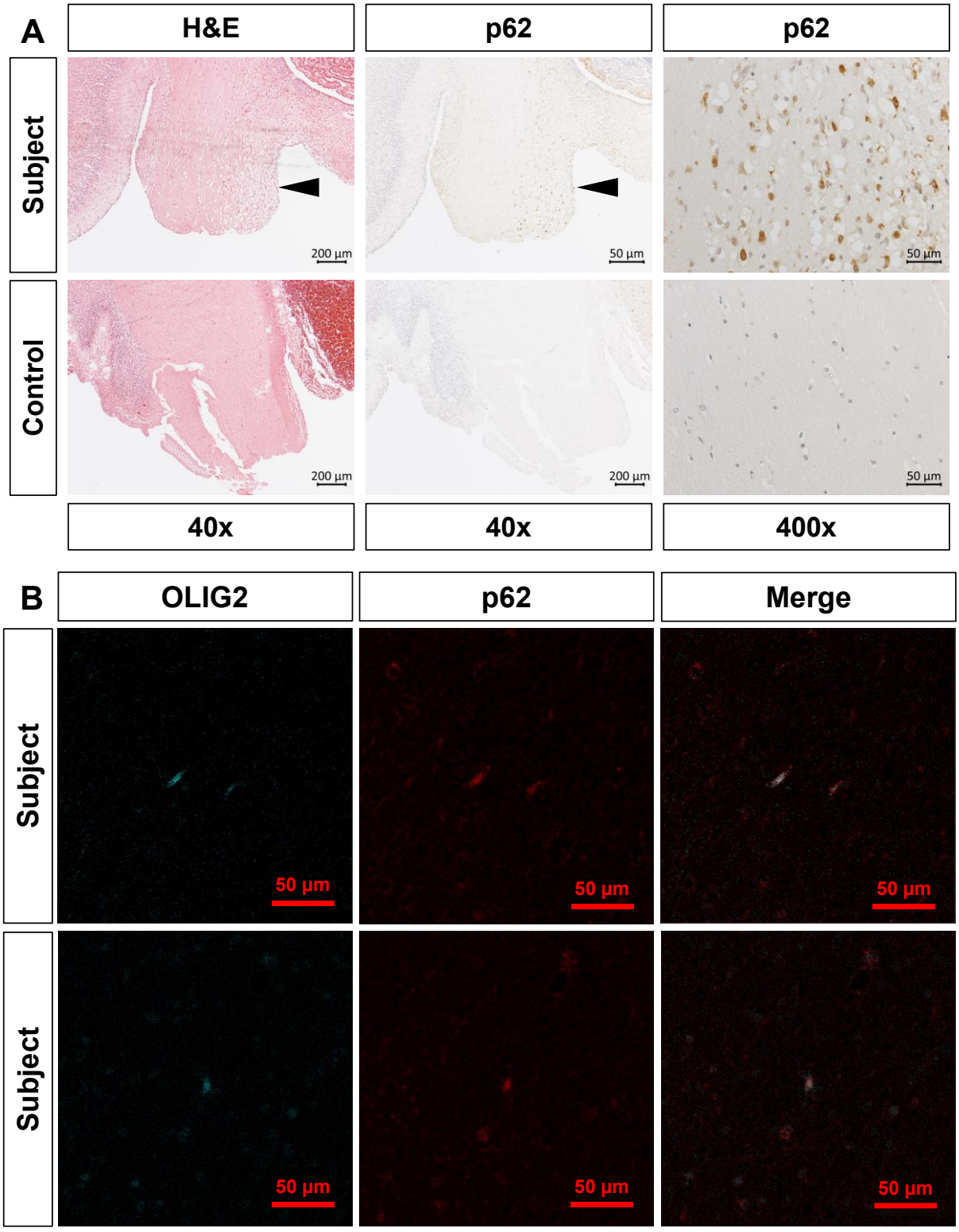


**Figure 5.6 Distinct p62 puncta and spongiform changes in subject corpus callosum and p62 positive oligodendrocytes in the cortex. A. S**ubject and control corpus callosum stained with H&E (left), showing spongiform changes localized to one side of the corpus callosum, indicated by

arrowhead. IHC of p62 stained corpus callosum (centre and right) showing distinct p62 puncta, again localised to one side of the corpus callosum in the subject, indicated by arrowhead. **B.** In the subject cortex there is a small number of OLIG2 positive oligodendrocytes positive for p62, which were not found in the control.

Additional immunofluorescence was undertaken with p62 and the mature neuronal marker, NeuN. The majority of neuron in the developing brain will be expressing NeuN by 24 gestational weeks (Sarnat et al., 1998). Only a small number of the p62 positive puncta colocalised with NeuN staining (**Figure 5.7A**). Additionally, there was a clear decrease in the number of NeuN positive cells in the corpus callosum. Given the gestational age of the tissue, and that some of the p62 positive cells were mature neurons, an immature neuronal marker was used, doublecortin (DCX) to reveal if the remaining p62 positive cells were neurons yet to mature. This revealed that most of the remaining p62 positive cells were immature neurons (**Figure 5.7B**). Together this suggests that in the corpus callosum, maturing neurons migrating towards the cerebral cortex are the cells which are most susceptible to loss of ATG7.

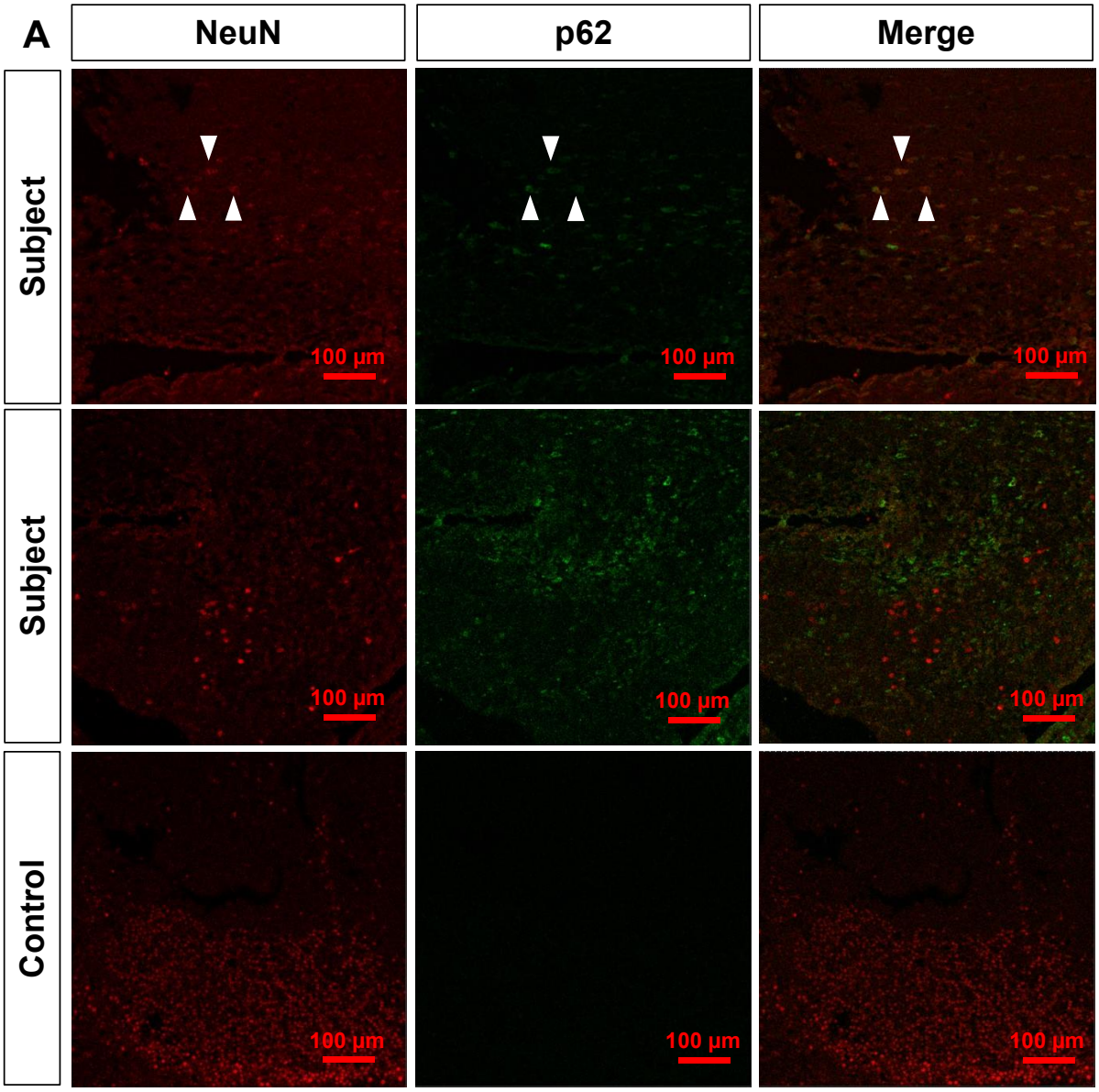
A
NeuN
p62
Merge
Subject
Subject
Control
100 μm
100 μm
100 μm
100 μm
100 μm
100 μm
100 μm
100 μm
100 μm

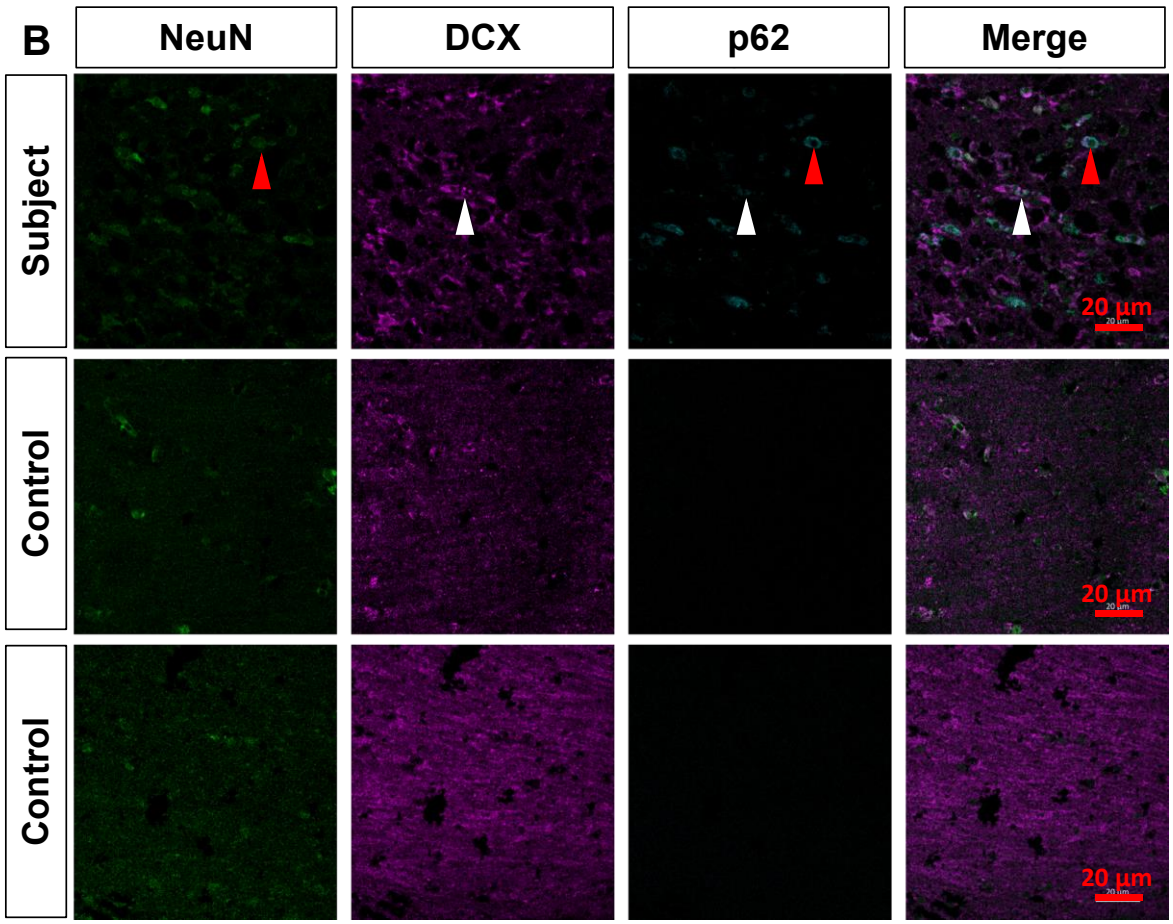


**Figure 5.7 Identification of p62 positive neurons in the corpus callosum. A.** Immunofluorescence images of subject corpus callosum showing that a number of p62 positive puncta colocalise with NeuN positive neurons (top). However, the majority of NeuN staining does not colocalise with p62. **B.** Immunofluorescence images of subject corpus callosum demonstrating that p62 positive cells are mature NeuN positive neurons (red arrowhead), or immature DCX positive neurons (white arrowhead).

In addition, a single ballooned neuron was also observed in the corpus callosum of the subject, indicating neuronal damage. There were no ballooned neurons observed in any of the age matched controls (**Figure 5.8**).

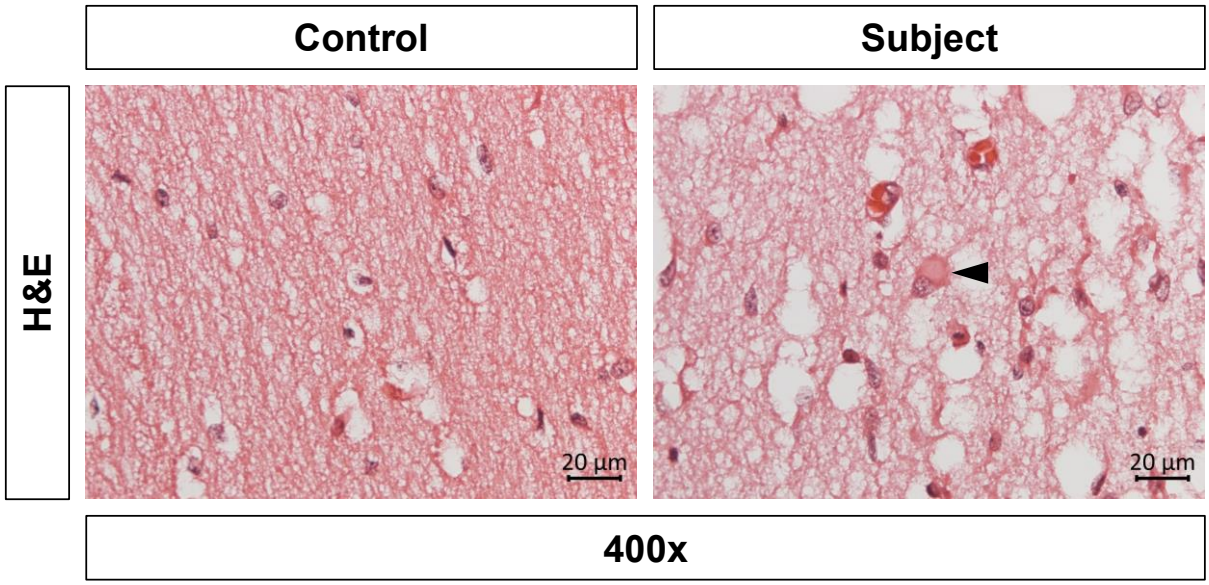


**Figure 5.8 H&E staining of ballooned neurons in ATG7 subject corpus callosum.**A single ballooned neuron was identified in the corpus callosum of the subject, denoted by black arrow.

### 5.3.5 Non-migrated neurons surround olivary nucleus in the ATG7 subject medulla.

As the dentate nucleus in the *ATG7* subject cerebellum was found to be malformed, the olivary nucleus was also subjected to H&E staining to determine whether formation of other nuclei was affected by the loss of ATG7. Initially the olivary nucleus looked to be correctly formed, with its classical oval appearance, comparable to the structures observed in the control (**Figure 5.9A**). However, additional sections from a different level of the medulla showed that the olivary nucleus was surrounded by non-migrated cells, presumed to be neurons (**Figure 5.9A**). This was not consistent with the control olivary nucleus, which appeared to be formed correctly.

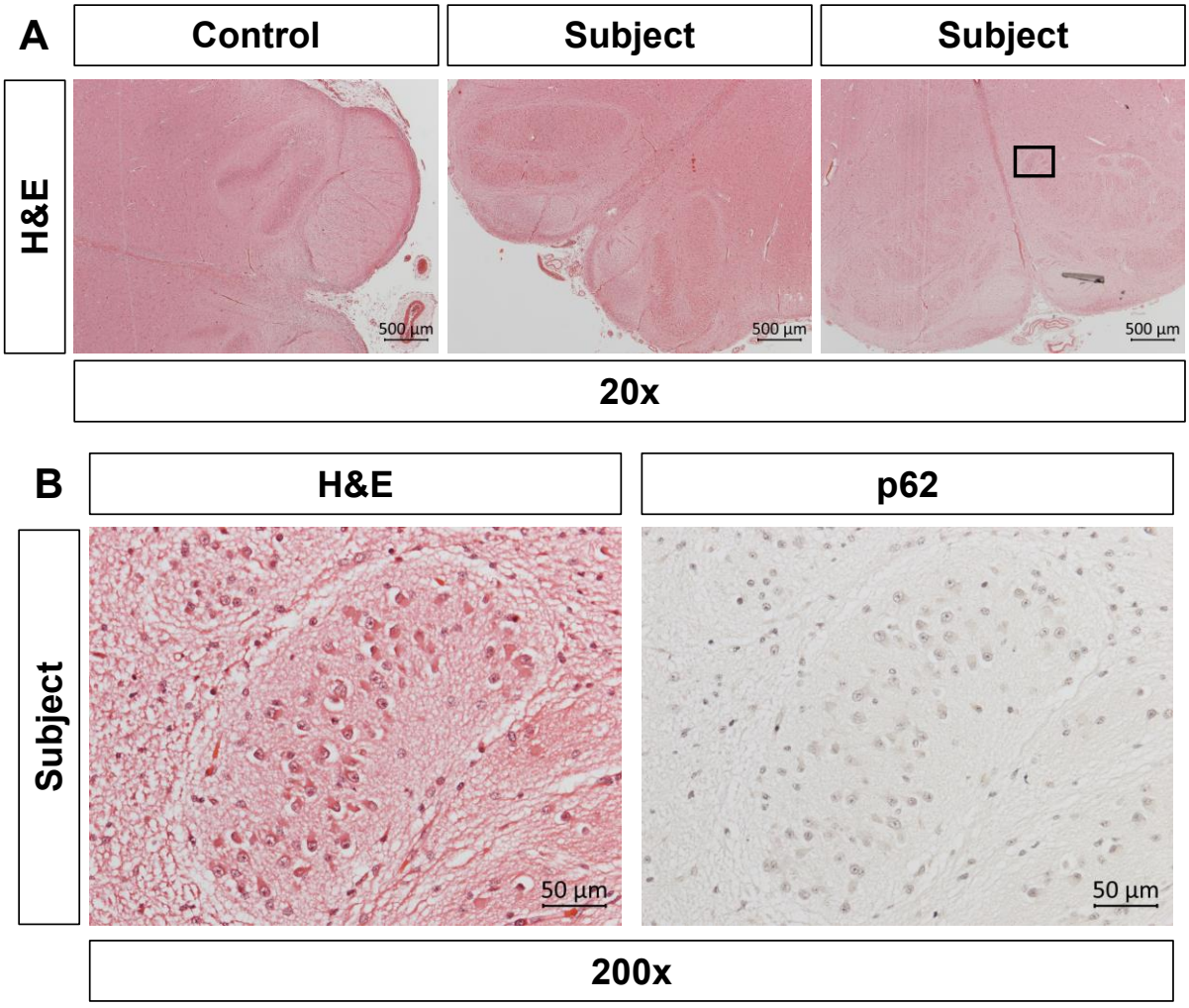


**Figure 5.9 Non-migrated cells surrounding ATG7 subject's olivary nucleus. A.** H&E-stained sections of control and subject inferior olivary nucleus, showing that in one section the subject appears no different to the control. **B.** In another section of subject tissue, H&E staining shows the inferior olivary nucleus appears to be surrounded with non-migrated cells (left and centre). Staining for p62 shows that these structures are not p62 positive (right).

Following the identification of non-migrated neurons surrounding the olivary nucleus in the subject, serial sections from the subject and the control were stained for p62 to ascertain if the non-migrated cells were accumulating p62. Staining with p62, showed that the non-migrated cells surrounding the olivary nucleus were not p62 positive, suggesting the failure of the cells to migrate was not due to the cell's loss of degradation (**Figure 5.9B**).

### 5.3.6 Astrocytes accumulate in regions of the ATG7 subject's brain

As abnormalities had been found throughout the brain regions of the *ATG7* subject, further investigations were undertaken to identify if these were associated with cell death. Cleaved caspase-3 is central to apoptosis, with caspase 3 being activated by either one or both of caspase 8 and caspase 9, producing cleaved caspase-3, which is indicative of cell death via apoptosis (Taatjes et al., 2008). Immunofluorescence analysis using MAP2 as a neuronal marker and GFAP as an astrocytic marker, was used alongside cleaved caspase 3 to identify any apoptotic cells.

Analyses of the corpus callosum and cerebral cortex revealed minimal staining for cleaved caspase-3 (**Figure 5.10A and B**). Interestingly, an increase in astrocytes in both the subject's corpus callosum and cerebral cortex was observed, however a formal quantification was not possible due to lack of tissue. There was minimal staining for cleaved caspase-3 in the olivary nucleus, including the non-migrated neurons (**Figure 5.10C**). In addition, increased GFAP positive astrocytes in the cerebellum of the subject were observed, but lack of control tissue prevented direct comparison (**Figure 5.10D**). However, the cause of astrocyte accumulation is hard to determine given the lack of cell death usually associated with astrocyte accumulation.

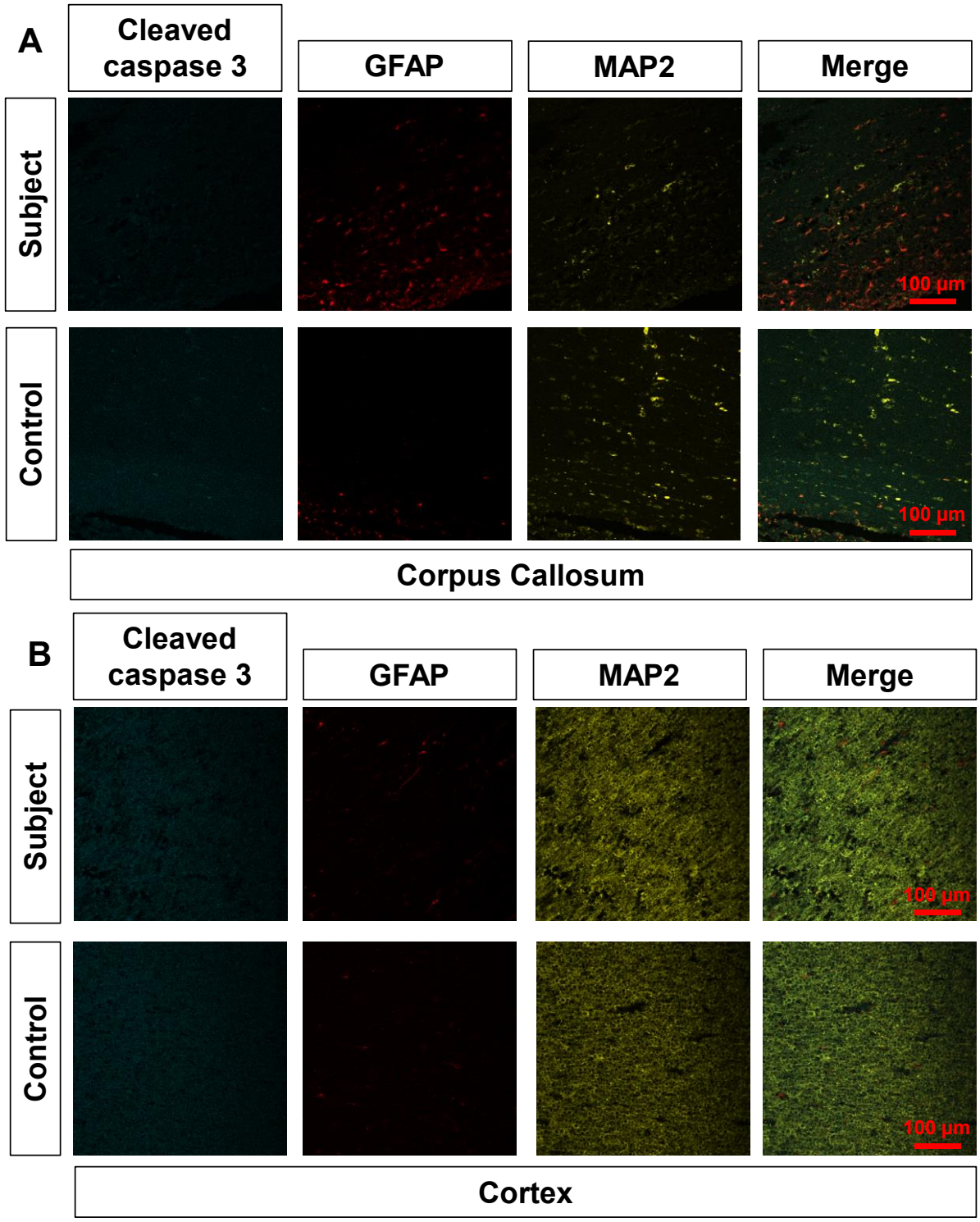
A
Cleaved caspase 3
GFAP
MAP2
Merge
Subject
Control
100 µm
100 µm
Corpus Callosum
B
Cleaved caspase 3
GFAP
MAP2
Merge
Subject
Control
100 µm
100 µm
Cortex

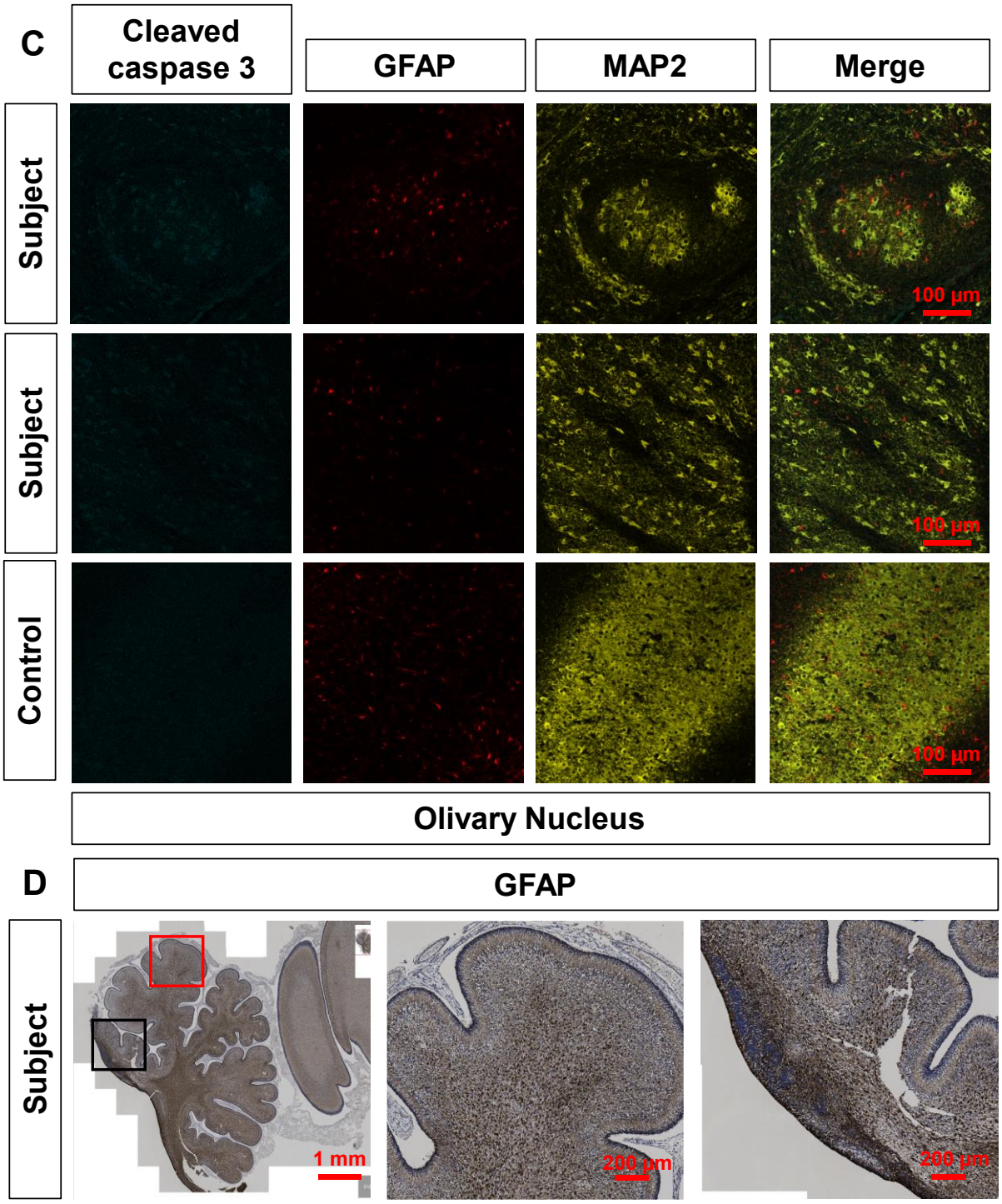


**Figure 5.10 Immunofluorescence and immunohistochemical analysis of apoptosis and cell specific changes in the subject. A.** MAP2 and GFAP staining identified neurons and astrocytes, respectively. Subject corpus callosum appears to have accumulation of astrocytes, but neither subject nor control show distinct cleaved caspase 3-staining. **B.** MAP2 and GFAP staining identified neurons and astrocytes, respectively. Subject cerebral cortex has small increase in astrocytes, but neither subject nor control show distinct cleaved caspase 3-staining. **C.** MAP2 and GFAP staining identified neurons and astrocytes, respectively. Neither subject or control shows distinct cleaved caspase-3 staining. **D.** Immunohistochemical analysis of subject cerebellum using

astrocyte marker GFAP. Subject shows abundant GFAP positive astrocytes in cerebellar folia (red square and middle) and rhombic lip (black square and left). Images captured using 10x objective.

## 5.4 Discussion

This chapter describes the characterisation of a foetal subject harbouring recessively-inherited loss of function *ATG7* variants; p.Ser593Ilefs*17 and p.Gln571* . The subject had polymalformative syndrome, along with corpus callosum abnormalities, features consistent with other *ATG7* patients (Collier et al., 2021). Frozen foetal liver tissue demonstrated the subject had undetectable levels of ATG7, accompanied by an increase in p62. IHC staining of FFPE brain tissue demonstrated distinct p62 puncta in the folia of the subject cerebellum, in addition to neutral lipid accumulation in certain cells of the cerebellum. While the p62 positive cells were not Purkinje cells, unmigrated clusters of Purkinje cells were observed, which were also not p62 positive. There also appeared to be fewer Purkinje cells in the Purkinje layer of the cerebellar cortex. Finally, malformation of the dentate nucleus was observed in the ATG7 subject. As observed in the cerebellum, there were p62 positive cells in the corpus callosum, which were a mix of mature and immature neurons. A ballooned neuron was also observed, indicating poor neuronal health, which was not observed in the control brains. Additionally, there also appeared to be far fewer NeuN positive mature neurons in the subject. In the medulla, there were clusters of unmigrated neurons surrounding the olivary nucleus, however, these were not p62 positive. Cleaved caspase-3 staining demonstrated very few apoptotic cells, despite astrocyte accumulation in the subject corpus callosum and cerebral cortex.

Together, these data demonstrate a catabolic deficit in the subject's liver and brain. The increased levels of p62 in frozen liver tissue demonstrates the accumulation of cytosolic cargo marked for degradation, indicating an autophagy deficit. The p62 puncta in the corpus callosum and cerebellum show that this is observable in brain tissue also, which is unsurprising given the neurological presentation of subjects with *ATG7* variants. The specificity of the p62 staining is curious, however. In the cerebellum p62 staining is observed within specific cells of the folia, and in the corpus callosum it is again observed only in certain cells. This would suggest that certain cell types are more susceptible than others. In the corpus callosum, it looks as though the majority of the p62 positive cells are neuronal, meaning the p62 positive cells in the cerebellar folia are likely to be neuronal also. This is supported by other cell types

positive for p62 in the cortex and cerebellum being minimal. In the cerebellum these neurons are likely to be neurons destined for the external granular layer, which sits in the outermost section of the cortex (Ábrahám et al., 2001).

One of the most interesting findings in cerebellum, and medulla, are the observed un-migrated cell clusters in the *ATG7* subject. The lack of p62 staining in these clusters suggests this finding is not a direct consequence of autophagy impairment. This leaves two possibilities, firstly that migration itself is being hindered because of dysfunctional autophagy. Cell migration relies on formation and degradation of focal adhesions and this degradation of focal adhesions is dependent on autophagy (Sharifi et al., 2016). Focal adhesions are protein scaffolds which connect the cell's cytoskeleton, the turnover of these protein scaffolds at the leading edge of a migrating cell facilitate movement through the extracellular matrix (Geiger & Yamada, 2011). Even though more general autophagy may not be impaired, as indicated by the lack of p62 accumulation, focal adhesion degradation has been demonstrated to be Neighbour of BRCA1 (NBR1) specific, therefore staining for NBR1 accumulation may help to elucidate this (Kenific et al., 2016).

Secondly, an explanation for observing cell clusters mid migration is an effect extrinsic to the neurons themselves. It could be possible that RGCs, along with basal progenitors, are negatively affected by the loss of autophagy. As well as their role in generating neurons, RGCs play an important role in directing neuronal migration (Rakic, 1972). The poorly formed dentate nucleus, and lack of migrating cells surrounding it, suggests that migration is not responsible for the malformation. However, radial glia are thought to only carry neurons to the marginal zone, in the cortical plate (Nadarajah et al., 2001). The final stages of migration rely on separate molecular mechanisms, not relying on RGCs, so it may be this final stage of migration which is impaired, however this would be a neuronal issue separate from RGCs (Noctor et al., 2004; Franco et al., 2011). However, some external granule neurons, and Purkinje cells are able to migrate to their correct position, suggesting migration is functioning along both radial glial dependant and non-radial glial dependant pathways. As a result of this, the most likely reason for the un-migrated cells is due to hindered focal adhesion turnover, slowing migration. The reduction in Purkinje cells in the subject is still curious however, as the number of un-migrated Purkinje cells does not appear sufficient to fill the incomplete Purkinje layer in the subject.

The most localised p62 staining is observed in the $RL^{VZ}$. As discussed, (**Chapter 5.1.4),** the rhombic lip is one of the two proliferative zones in the developing cerebellum and is the major proliferative zone after 10 post conception weeks (Haldipur et al., 2019). While the RL expands and forms its subventricular zone after 10 post conception weeks, the majority of cerebellar growth occurs after 25 weeks, so the 24-week timepoint of the subject is just preceding this (Ábrahám et al., 2001). The accumulation of p62 in the $RL^{VZ}$ just prior to large scale proliferation is likely damaging. Also, loss of *ATG7* has been shown to interfere with the cell cycle of neural stem cells (Shen et al., 2024). This could offer an explanation for the increased number of astrocytes observed, with cell cycle regulating the production of neurons over glia (Shen et al., 2024). However, RGCs, which reside in the RL, will stain positive for GFAP (Parnavelas & Nadarajah, 2001), so without comparison to control the source of astrocyte accumulation cannot be identified. Another explanation for increased astrocyte numbers could be in response to damage as glia, including astrocytes, have been shown to respond to local damage resulting in accumulations of glia known as glial scars (Nespoli et al., 2024). However, the lack of cell death across the investigated brain regions does not support this.

While previous cases have been described with cerebellar hypoplasia, when compared to controls and existing literature on cerebellar development, the subject appears to have a well-formed cerebellum. The 24-week timepoint may explain the relatively well-formed cerebellum. The negative impacts associated with p62 accumulation, including potential cell death, would heavily impact the proliferative potential of the rhombic lip, resulting in impaired cerebellar growth. Additionally, if the ventricular zone, which generates the Purkinje cells prior to week 10, had the same p62 accumulation it could explain the diminished number of Purkinje cells in the Purkinje layer of the subject. The p62 accumulation and subsequent cell death of progenitors will reduce the proliferative capacity, thus reducing the number of cells in the Purkinje layer when compared to age matched controls.

Finally, the accumulation of neutral lipids in the cerebellum of the subject, and not the control was an unexpected finding, as it has not been reported in previous central nervous system conditional *ATG* knockout mouse models (Komatsu et al., 2006; Hara et al., 2006a). However, autophagy plays an important role in lipid degradation, as discussed (**Chapter 1.3.4**). In the cell lipids are stored as lipid droplets, where neutral

lipids are surrounded in a protein containing phospholipid membrane (Martin & Parton, 2005). These neutral lipids can be used for metabolism, membrane production or steroid hormone production (Martin & Parton, 2006). Loss of *ATG7* and *ATG5* have both been shown to increase lipid droplet and triglyceride and cholesterol accumulation in mouse hepatocytes and embryonic fibroblasts (Singh et al., 2009). Autophagy mediated cholesterol trafficking has also been implicated in hormone production (Texada et al., 2019). Loss of autophagy in *Drosophila* models results in decreased cholesterol trafficking and increase in cholesterol dense lipid droplets, which produces a systemic growth impairment (Texada et al., 2019). Given its appearance in the cerebral cortex, it would be interesting to investigate other tissues which have a larger role in hormone production, to determine if this neutral lipid accumulation is also evident there. If neutral lipid accumulation, likely due to aberrant lipophagy, was confirmed in hormone producing tissues, it would likely explain the developmental delay seen amongst the original *ATG7* cohort (Collier et al., 2021).

# 6 A *de novo* heterozygous *ATG7* variant associated with cerebellar ataxia and developmental delay

## 6.1 Introduction

### 6.1.1 Congenital disorders of *ATG7*

A cohort of twelve subjects from five unrelated families harbouring distinct deleterious bi-allelic *ATG7* variants has recently been identified and characterised (Collier et al., 2021). While these subjects presented with variable neurological phenotypes, there were shared characteristics; all individuals presented with intellectual disability, delayed development and ataxia, with brain MRI showing cerebellar hypoplasia and atrophy of the posterior corpus callosum. All subjects harboured deleterious biallelic *ATG7* variants resulting in either a complete loss or decrease in steady-state ATG7 protein levels, with other autophagy related proteins affected to varying degrees. In *ATG7*-subject derived fibroblasts, functional autophagy flux assays showed that autophagy was occurring but at reduced rates, which was supported by a significant reduction in autophagic sequestration. However, transmission electron microscopy studies showed that some *ATG7* subject fibroblasts with a complete absence of ATG7 were still able to form autophagosomes, implying the presence of a compensatory mechanism.

Across the five families, there were nine distinct *ATG7* variants identified, with four families harbouring compound heterozygous variants, and one family harbouring a homozygous *ATG7* variant (Collier et al., 2021). The c.1975C>T, c.2080-2A>G, c.1727G>A and c.1870C>T variants are all documented in gnomAD with 373, 162, 15 and 9 heterozygous individuals identified respectively, with no reports of pathogenicity (Chen et al., 2023). The gnomAD data, alongside the unaffected parents of the original *ATG7* cohort, provides a large pool of unaffected individuals harbouring recessive *ATG7* variants (Chen et al., 2023; Collier et al., 2021). This would robustly suggest that the mechanism underlying *ATG7* related neurological disease relies on recessive inheritance of two *ATG7* variants.

### 6.1.2 *ATG7* mouse models

The hypothesis of recessive inheritance is supported by mouse models of *Atg7*. Universal knockout of *Atg7* from mouse models resulted in a neonatal lethal phenotype, as discussed (**Chapter 1.6.4**), however, the heterozygous offspring from the same origin were born healthy with no obvious pathology (Komatsu et al., 2005). The *Atg7*$^{+/-}$ were also able to generate Atg5-Atg12 conjugate, along with producing LC3-II. In addition, when *Atg7*$^{+/-}$ mice were crossed with GFP-LC3 transgenic mice, they were still able to generate autophagosomes. In contrast, the *Atg7*$^{-/-}$ mice that were unable to form the Atg5-Atg12 conjugates or LC3-II, and when crossed with the GFP-LC3 mice they were unable to form autophagosomes. Together, this suggests that a single functional Atg7 allele is sufficient for correct autophagy function in mice.

Alongside the universal *Atg7* mouse knockout model, a central nervous system conditional knockout model has been generated, as discussed (**Chapter 1.6.5)** (Komatsu et al., 2006). These models relied on using *Atg7*$^{flox/flox}$ *and Atg7*$^{+/flox}$ mice, crossed with mice harbouring the Cre recombinase under the Nestin promoter, thus generating a central nervous system specific knockout of *Atg7.* The focus of the study was the homozygous knockout *Atg7*$^{flox/flox}$*;nestin-Cre* mouse model. This full CNS *Atg7* knockout model resulted in neurodegeneration and behavioural abnormalities, along with neuronal loss in cerebral cortex and cerebellum and an increased number of ubiquitin positive inclusions. The homozygous *ATG7* CNS knockout mice also died prematurely, 28 weeks after birth.The control used in all these investigations was a heterozygous knockout *Atg7*$^{+/flox}$;nestin-Cre mouse. In this control mouse model none of the notable pathological findings of the *Atg7*$^{flox/flox}$*;nestin-Cre* mouse were observed. They also found comparable levels of ATG5-ATG12 conjugate and basal LC3-II in the *Atg7*$^{flox/flox}$*;nestin-Cre* mouse, hence it being used as a control. This again lends weight to the argument for the requirement of biallelic *ATG7* variants for pathogenicity.

### 6.1.3 *ATG7* patient cohort – Family 4

Interestingly, the c.782A>G (p.Gln261Arg) variant found in Family 4 is predicted to be benign according to *in silico* tools (Collier et al., 2021). MutationTaster predicts the variant to be a polymorphism, with PolyPhen-2 giving a score of 0.0, benign (Schwarz et al., 2014; Adzhubei et al., 2010). This contrasts with all other variants described, where MutationTaster predictions are disease causing, and PolyPhen-2 scores of

>0.997, probably damaging. This *in silico* assessment of the variant being benign suggests the two subjects (P6, P7) from Family 4, which have some of the least severe phenotypes described, could have a presentation similar to that of a heterozygous *ATG7* subject. However, it is also possible, the compound missense variants in Family 4 are both having a small effect on autophagy, which are additive to one another, resulting in the clear attenuation of autophagy flux in Family 4 fibroblasts.

In this chapter I present my studies supporting the extensive genetic testing of a family who revealed what is believed to be the first *de novo* heterozygous missense *ATG7* variant, affecting a highly conserved amino acid. Clinically, the subject presents similarly to the previously described *ATG7* cohort with biallelic variants, whilst functional analyses using subject-derived primary fibroblasts revealed a minimal functional autophagy deficit.

## 6.2 Methods

### 6.2.1 Genetic analyses

Clinical exome sequencing was undertaken by Professor Michel Koenig at CHU Montpellier, France. Clinical exome sequencing was performed as trio analysis (index subject and unaffected parents) as previously reported, using the TruSight One Expanded kit that targets approximately 6700 genes, most of them involved in human inherited diseases (Benkirane et al., 2021). Sequencing was performed using Illumina NextSeq technology with 150-bp paired-end reads (Montpellier CHRU NGS platform). Sequence alignment and variant calling were performed following the Broad Institute's Genome Analysis Toolkit (GATK) best practices, using an in-house pipeline "Nenufaar" (https://github.com/beboche/nenufaar). Sequence reads were aligned against the reference human genome (UCSC hg19). Variants were annotated with Annovar (Wang et al., 2010). The mean depth of coverage per sample was over 100x, and on average more than 95% of the targeted regions were covered at a minimum level of 30x. *In silico* filtering was performed using a panel of 490 genes, corresponding to the majority of known ataxia and related disorder genes, applying the American College of Medical Genetics and Genomics (ACMG) guidelines for clinical sequence interpretation (Richards et al., 2015). Variants with a global population frequency of > 1% were

excluded (GnomAD, 1000genomes (Auton et al., 2015)). Variants with a frequency > 0.1 % in genes for dominant or X-linked conditions were classified as benign. Pathogenicity arguments were provided by Clinvar or Clinsig pathogenic match (Landrum et al., 2018), deleterious prediction by SIFT (Ng, 2003) and/or PolyPhen-2 (Adzhubei et al., 2010) for missense variants, prediction of splice site alteration or cryptic site activation by NNsplice (Phillips et al., 2006) and MaxENT (Reese et al., 1997) softwares, prediction of truncation (nonsense and frameshift mutations) or prediction of deleterious in-frame mutations (conservation with BLAST searches). In the event that no pathogenic or likely pathogenic variants were identified in the *in silico* 490 gene panel, the entire clinical exome was analysed applying the same guidelines. Familial segregation of the probable pathogenic variant was confirmed by Sanger sequencing of the family trio (index subject and unaffected parents).

### 6.2.2 Assessment of autophagy in subject cells

Primary control and subject fibroblasts were cultured as described (**Chapter 2.6.2**). Autophagy was induced chemically and then inhibited at a late stage as described (**Chapter 2.7.5**). Cells were harvested and the protein concentration was estimated as described (**Chapter 2.7.2**). Proteins were separated by SDS-PAGE and immunoblotted as described (**Chapter 2.7**).

### 6.2.3 Protein modelling

Structural predictions of ATG7 (UniProtKB identifier: O953521-1) and p.Arg481Pro ATG7 were rendered using Phyre2 servers using standard settings (Kelley et al., 2015). Analysis of potential interactions with LC3 performed using the crystal structure of Atg7$^{(CTD)}$-Atg8 (Protein Data Bank: 3VH4) as previously described (Noda et al., 2011).

## 6.3 Results

### 6.3.1 Subject presents with cerebellar ataxia and developmental delay

The proband was a female child, born to non-consanguineous parents. Pregnancy and delivery were uneventful; family history was uneventful. The individual was referred at 3 months of age for recent paroxysmal episodes of loss of consciousness

with generalized clonic jerks, lasting 2 minutes; parents also reported isolated erratic limb jerks. Neurological examination at referral disclosed poor eye contact, irritability and no head control. Electroencephalographic (EEG) recording showed left-sided centro-parietal low-voltage spikes and spike-waves; burst of spikes lasting less than 20 seconds were associated to erratic non focalized asynchrones myoclonic jerks of the limbs. Phenobarbital treatment rapidly controlled the epileptic seizures, and EEG recording follow-up was normal; treatment was discontinued one year later, without epileptic recurrence.

Investigations were performed between 3 and 6 months of age: plasma electrolyte dosage, blood cell count, plasma acylcarnitine profile, blood and urinary amino acid screening, urinary organic acid screening, plasma folate and B12 dosage, cerebrospinal fluid analysis (cells, glucose, lactate, neurotransmitters profile) were normal; skeletal radiogram, abdominal ultrasound scan, ophthamological examination, brainstem auditory and evoked potential recording were normal. Cerebral Magnetic Resonance Imaging (MRI) performed at 4 months reported as normal; control MRI at 4.5 years of age showed moderate superior vermian hypoplasia, small anterior pituitary lobe and soft thinning of corpus callosum isthmus (**Figure 6.1A and B**).

Early psychomotor achievements were normal; the individual was able to sit unaided at 8 months of age, she walked with support and repeated syllabes at 12 months. She was able to walk alone at 18 months, with unsteady gait; dysmetria was noticed at 2 years of age. Mild cerebellar signs progressively improved but persisted throughout the follow-up until 17 years of age, especially clumsiness, poor fine motor skills and unbalanced gait. Learning disabilities were noticed from the age of 5. Cognitive functioning (Wechsler Intelligence Scale for Children IV) was assessed at 7 years of age; and disclosed heterogeneous mild cognitive deficiency (Verbal Comprehension Index: 86, Perceptual Reasoning: 69; Working Memory 52; Processing Speed: 69), associated to attention deficiency. Psychomotor rehabilitation and speech therapy were provided; methylphenidate treatment was initiated at 7 years of age and improved attention deficit disorders. The individual underwent a special education program with human assistance. At last assessment at 17 years of age, the individual just ended her professional training as sale assistant; she was independent in daily living activities; cranial perimeter, height and weight growth and sexual characteristics'

development were normal, no dysmorphic features were noted. Clinical examination disclosed action tremor with dysmetria and adiadochokinesia, coordination difficulties, lower limb brisk reflexes, walking on a line was unbalanced and standing on one limb was unsteady.

### 6.3.2 Identification of a *de novo* heterozygous c.1442G>C *ATG7* variant

Clinical exome sequencing of the family trio performed by Prof. Michel Koenig identified a *de novo* missense *ATG7* c.1442G>C variant (RefSeq: NM_006395.1), resulting in a p.Arg481Pro amino acid substitution. No other pathogenic or likely pathogenic variants were identified. The p.Arg481Pro variant lies in the Walker B motif of the ATG7 protein, a region involved in $Mg^{2+}$ chelation and ATP hydrolysis, which is found in the C-terminal domain (CTD) of the protein. The affected amino acid (p.Arg481) is highly conserved across a number of species, hinting at its functional significance (**Figure 6.1C**).

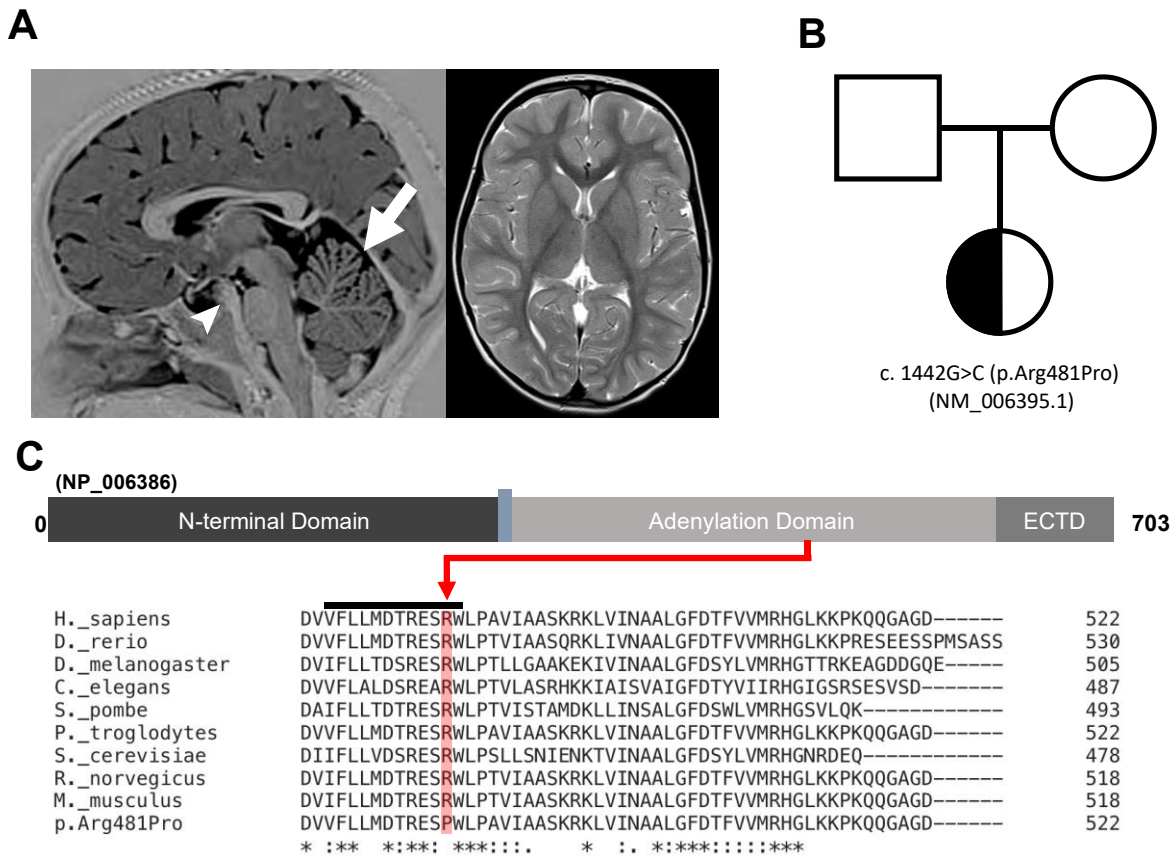


**Figure 6.1. Neuroimaging and summary of de novo *ATG7* variant in Subject. A. Brain MRI performed at four years of age. A.** Right; Sagittal T1-weighted image reveals subtle

abnormalities with moderate superior vermian hypoplasia, small anterior pituitary lobe and soft thinning of corpus callosum isthmus. Left**;** Axial T2-weighted image shows no ventriculomegaly, normal basal ganglia and no white matter changes. **B.** Pedigree demonstrating the de novo c.1442G>C; p.Arg481Pro (RefSeq accession number: NM_006395.1) variant present in the proband. **C.** Position of the de novo p.Arg481Pro variant (NP_006386) in ATG7 (ECTD = extreme C-terminal domain). Sequences of ATG7 orthologues from different species aligned using Clustal Omega, shows the conserved Walker B motif (solid black line) and the position of the variant in this conserved region (highlighted in red). (* shows fully conserved residue; : shows conservation of groups with strongly similar properties; . Shows conservation of groups with weakly conserved properties).

### 6.3.3 The *ATG7* p.Arg481Pro variant may effect LC3B adenylation

In order to visualise any structural differences between the wild type ATG7 protein and the p.Arg481Pro ATG7 variant, *in silico* models of the two proteins were rendered using the Phyre2 software. The models showed minimal overall structural differences. Wild type ATG7 is predicted to form 5 hydrogen bonds from the p.Arg481 residue, with three of these joining its functional group to the adjacent β sheet (**Figure 6.2A**). Meanwhile, the p.Arg481Pro ATG7 variant was predicted to form a single hydrogen bond, losing its interactions with the adjacent β sheet (**Figure 6.2B**). However, the position of these adjacent residues is not predicted to change, suggesting the loss of binding potential does not affect the protein's tertiary structure.

While the p.Arg481Pro variant may not have significant structural effects on ATG7, previous *S. cerevisiae* structures of Atg7 complexed with Atg8 (a yeast LC3 homologue) show that p.Arg481 (*S. cerevisiae*: Arg443) directly interacts with the relatively unstructured C-terminal tail of Atg8 at Thr114 (**Figure 6.2C**) (Noda et al., 2011). This interaction is in the form of a hydrogen bond derived from an $NH_2$ group of Arg481's functional group, suggesting that the interaction would not be possible in the subject given proline's lack of $NH_2$ in its functional group. This is supported by the loss of hydrogen bonding seen in the modelling of the p.Arg481Pro ATG7 variant. Disruption of the hydrogen bond may lead to a disorientation of the ATG8 C-terminal tail, reducing the efficacy of thioester linkage to ATG7's catalytic Cys507. Loss of this linkage would negatively affect eventual shuttling to the N-terminal domain of ATG7 for PE conjugation. In addition, while there are five interactions between Atg7 and the C-terminal tail of Atg8, in the $Atg7^{CTD}$-Atg8 model (PDB: 3VH4), p.Arg481 is the only residue involved in these interactions, suggesting functional importance.

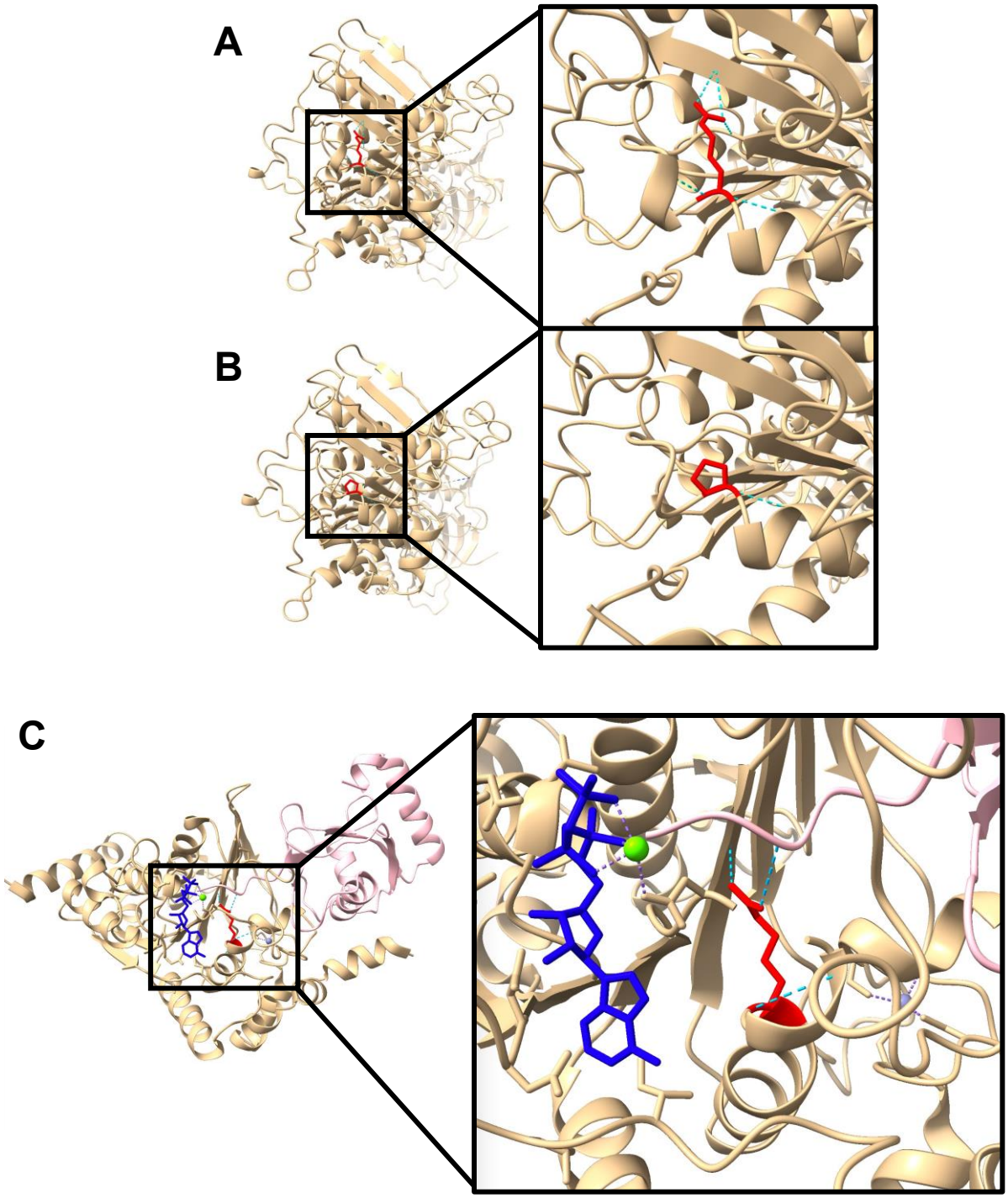


**Figure 6.2. Comparisons of Phyre rendered models of ATG7 (tan), with residue 481 highlighted (red), showing the predicted interactions of residue 481 (cyan). A.** Phyre rendered model of wild type ATG7 (UniProtKB identifier: O95352-1). Arg481 is predicted to produce 5 hydrogen bonds, with three of those coming from its functional group. **B.** Phyre rendered model of ATG7 variant (p.Arg481Pro), with proline predicted to produce a single hydrogen bond. However, despite the loss of interactions, the distances between the Cα of residue 481 and the Cα of the residues with which it no longer interacts, are not predicted to change, suggesting the loss of these interactions do not affect the protein's overall tertiary structure. **C.** S. cerevisiae crystal

structure of the Atg7 C-terminal domain ($Atg7^{CTD}$) complexed with Atg8 (shown in pink) and MgATP (shown in green and blue), Ser477 (S. cerevisiae: Ser439) is hidden in the enlarged image. The structure shows Arg481 (S. cerevisiae: Arg446) interacting with the C-terminal domain of Atg8, a relatively unstructured domain, which interacts with Arg481 via a hydrogen bond from one of its two $NH_2$ groups to Atg8's Thr114. The lack of hydrogen bonds from proline's functional group seen in B, suggests this would not be possible in an Arg481Pro variant. This is supported by the hydrogen bond stemming from an $NH_2$ group in the arginine residue, which would be lacking in a proline variant. This may lead to a disorientation of the ATG8 C-terminal tail, reducing the efficacy of thioester linkage to ATG7's catalytic Cys507, negatively effecting eventual shuttling to ATG7's N-terminal domain for PE conjugation. In addition to this, while there 5 interactions between Atg7 and Atg8's C-terminal tail, Arg481 is the only residue involved which is conserved throughout other E1 enzymes, hinting at its functional importance.

### 6.3.4 *De novo* p.Arg481Pro *ATG7* variant causes mild autophagy impairment

Primary control and subject-derived *ATG7* fibroblasts, obtained during the first year of life, were cultured under basal conditions, lysed and separated using SDS polyacrylamide gel electrophoresis before immunoblotting to investigate the steady-state levels of autophagy related proteins. Immunoblotting showed that ATG7 levels were decreased in the subject, along with a robust steady-state increase in autophagy adapter protein p62, when compared to age-matched controls (**Figure 6.3A**). The protein levels of conjugated ATG5-ATG12 and ATG3 appeared to be unchanged between the *ATG7* subject and controls. As ATG7 is an E1-like enzyme which functions as a homodimer, non-reducing gel electrophoresis was performed to determine whether the p.Arg481Pro ATG7 variant had a negative effect on ATG7 dimerisation. Immunoblot analysis showed that the subject had a clear decrease in the levels of ATG7 homodimer, with ATG7 monomers appearing to be comparable to the controls (**Figure 6.3B**). This may be accounted for by the overall reduction in ATG7 protein levels observed under reducing conditions.

To infer the rate at which autophagy is occurring in cells, autophagy flux assays of one, two and four hours were performed to determine the relative levels of LC3-II when autophagy is stimulated, but autophagosome-lysosome fusion is inhibited. AZD8055 stimulates autophagosome formation, and therefore LC3-II production, by inhibiting mTORC1 (Zhao et al., 2014). Chloroquine blocks lysosomal fusion to the

autophagosome, preventing the recycling of LC3-II back into LC3-I by ATG4. Combined, this allows the visualisation of LC3-II production, allowing us to infer the rate of autophagy in subject samples when compared to relevant controls. Autophagy flux assays showed a mild, but consistent, decrease in dynamic flux (**Figure 6.3C**) with our collective data showing that the *de novo ATG7* variant is pathogenic.

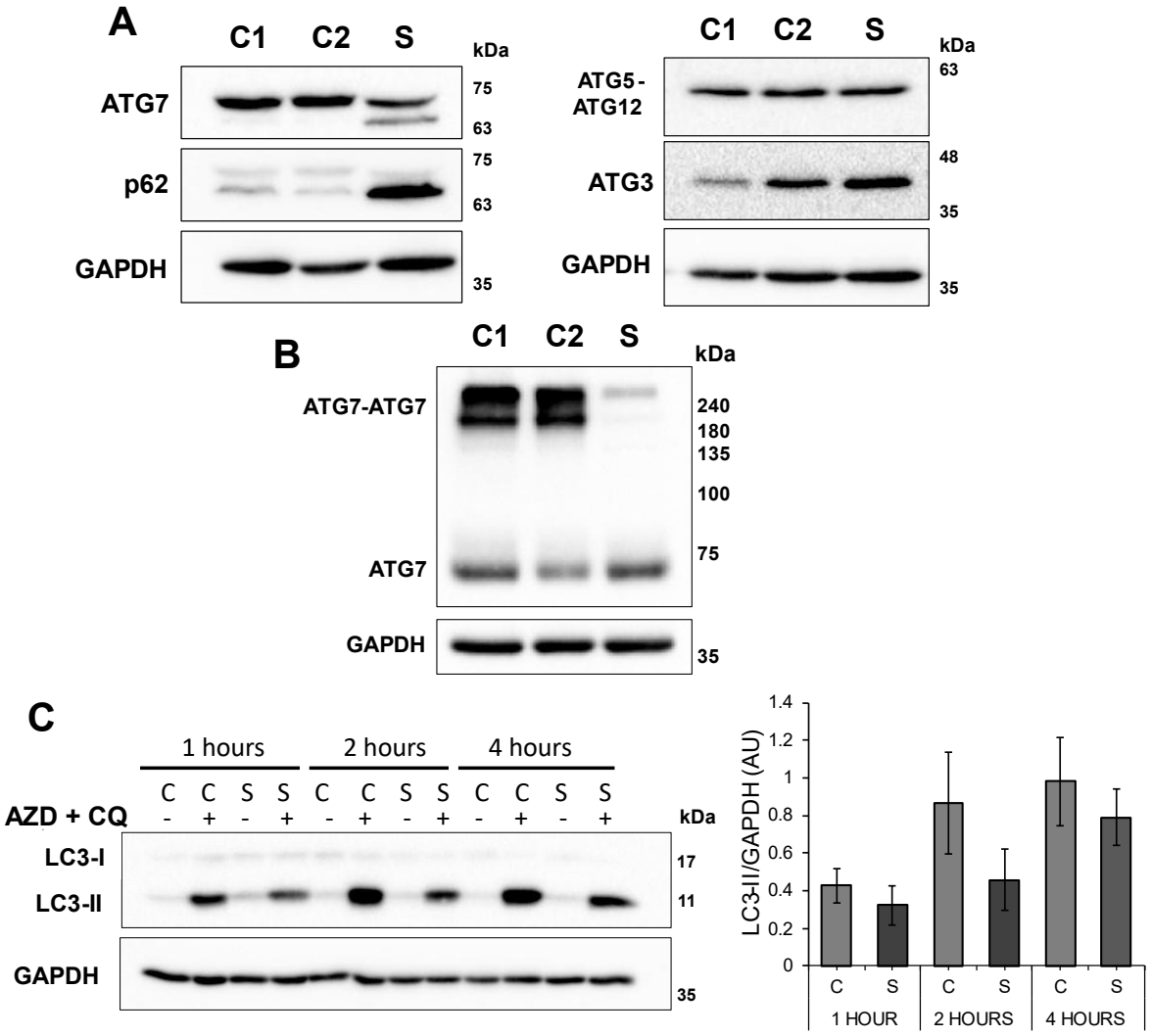


**Figure 6.3. Western blot analysis of autophagy related proteins in two paediatric controls (C1, C2) and subject primary fibroblasts (S). A**. Immunoblotting demonstrated a decrease in ATG7 in the subject, relative to the control lines, with an increase in p62 in the subject (n=3). Additionally, there is no visible change in ATG5-ATg12 conjugate or ATG3 in the subject relative to the control lines. (n=2). **B.** Analysis of ATG7 homodimerization under non-reducing conditions, as described (**Chapter 2.7.3**) indicates a reduction in the level of ATG7 homodimer (n=3). **C**. Representative autophagy flux blot for cells incubated for the indicated time or without 100 μM chloroquine (CQ) and 1 μM AZD8055 (AZD). Immunoblot analysis for LC3 showed a decrease in

the production of LC3-II in the subject when compared to Control 1 (left). (n=3) (no significance, two factor ANOVA, p>0.05).

## 6.4 Discussion

We identified a female subject through clinical exome sequencing of a family trio, with a novel *de novo* heterozygous missense *ATG7* variant, which is evidenced as the cause of her neurological phenotype. The resulting p.Arg481Pro change lies within the highly conserved Walker B motif of the ATG7 protein, which is known to play a critical role in the adenylation of LC3-I. Structural modelling of the mutant protein indicated that there were no major conformational changes in the ATG7 protein. However, this residue has previously been shown to interact with Atg8 during adenylation in yeast, suggesting the amino acid change may directly affect the function of ATG7. Functional assessment of subject-derived fibroblasts including immunoblotting demonstrated that there was a decrease in steady-state ATG7 levels compared to that found in controls, which was reflected by a decrease in ATG7 homodimers observed under non-reducing conditions. This decrease in ATG7 levels is accompanied by accumulation of p62, suggesting that the decrease in ATG7 results in attenuated degradation of cellular components marked for autophagy. An assessment of dynamic autophagic flux in subject-derived cells revealed a mild, but statistically non-significant impairment in the conversion of LC3-I to LC3-II, a key process in the stimulation of autophagy that is driven by ATG7.

The data raises some interesting points for consideration. First, the *in silico* structural modelling data suggest that the p.Arg481Pro variant could potentially effect the ATG7 interaction with LC3. The crystal structures previously generated using *S. cerevisiae* Atg7's C-terminal domain and Atg8 imply that the Arg481 residue (Arg433 in *S. cerevisiae)* directly interacts with Atg8 (Noda et al., 2011). However, the decreased ATG7 levels noted on immunoblots indicate that variant ATG7 is unstable, and therefore degraded. Non-reducing immunoblots show that while there is a noticeable decrease in ATG7 dimers, subject cells are still able to form a limited amount of homodimers and maintain a pool of ATG7 monomers consistent with those observed in control cells. While the remaining ATG7 homodimers are sufficient to support LC3-II production, there does appear to be an autophagy impairment, illustrated by the accumulation of p62, thereby suggesting a haploinsufficiency. While the

haploinsufficiency in the subject primary fibroblasts is capable of supporting autophagy flux, in the affected neural tissues this may not be the case given their post-mitotic nature, thus driving the neuro-centric clinical phenotype.

A cohort of subjects harbouring damaging bi-allelic *ATG7* variants has previously been described (Collier et al., 2021). Parental samples were studied to confirm that all affected individuals inherited recessive *ATG7* variants from their clinically unaffected parents. The subject reported here represents what is believed to be the first *de novo* heterozygous case involving *ATG7*, highlighting some key differences between this case and the original cohort. In the previously described cohort with bi-allelic variants, those with the most severe autophagy deficits presented with a milder neurological phenotype, while those with less severe autophagy deficits showed severe phenotypes. The subject presented here has a mild autophagy deficit coupled with a mild phenotype. The subject is now 18 years of age and able to maintain a relatively good quality of life, being able to walk alone, live independently and work. In contrast some previously described subjects with some remaining ATG7 function were unable to achieve walking. This suggests the possibility of an alternate disease mechanism underlying the disease in this case. This is supported by the inheritance of the loss of function variants seen in the original cohort. All *ATG7* variants reported to date were inherited recessively, indicating the parents were harbouring a single recessive variant with no pathogenic consequences. Here however, a heterozygous *ATG7* variant is sufficient to produce a disease phenotype. This may be due to the position of the variant, lying in the highly conserved Walker B motif, which is not the case for any of the previously reported variants, suggesting the disease mechanism could be variant dependent.

The potential haploinsufficiency is interesting in this case given the number of heterozygous, non-affected individuals. Efforts are currently underway to obtain primary fibroblast samples from one the unaffected parents of Family 1 of the original subject cohort. This would allow direct immunoblot comparison of ATG7 and p62 levels between the subject presented in this chapter and a heterozygous carrier of a different variant. This is with the aim of delineating the relationship between the minor decrease in autophagy flux and the specific pathogenic variant observed in the subject, compared to the other previously described *ATG7* carriers. In addition to this, subject samples are being sent to Professor Emma Baple (Royal Devon and Exeter NHS

Foundation Trust and Exeter University) for whole genome sequencing to exclude any genetic cause.

An interesting finding is the accumulation of p62 in subject cells. The p62 accumulation would indicate that the small effect observed on dynamic autophagic flux does have a sizeable effect on cellular homeostasis, as cellular components marked for degradation are accumulating. However, this increase in p62 does not appear to be proportionate with the minimal autophagy defect observed when compared to the previously characterized *ATG7* subjects (Collier et al., 2021). While p62 is best characterised as an autophagy adapter protein, facilitating the targeting of ubiquitinated proteins to LC3-II on expanding autophagosomes, it also plays a role in NFκB (nuclear factor Kappa B subunit 1) and Nrf2 (nuclear factor erythroid 2-related factor 2) signalling (Chen et al., 2020). In this case, it is tempting to speculate that an increase in reactive oxygen species - which is normally associated with autophagy disruption – could lead to p62 competitively binding to Keap1 via its Keap1-interacting region (KIR), freeing Nrf2 from Keap1, to which it is normally bound (Komatsu et al., 2005; Wu et al., 2009; Lau et al., 2010). This allows Nrf2 to translocate to the nucleus where it acts as a transcription factor for antioxidant elements and detoxifying enzymes as a response to oxidative stress. However, as part of this oxidative stress response, Nrf2 also induces the transcription of *SQSTM1* as part of a feed-forward mechanism, leading to a further increase in p62 (Saito et al., 2016). This further increase may be the underlying mechanism behind the disproportionate p62 increase compared to the minimal autophagy flux decrease. This would also be supported if there was a not as overwhelming increase in other adapter proteins like NBR1 (Neighbour of BRCA 1), or OPTN (optineurin), as these adapters lack the KIR domain of p62.

In summary, the collective data suggest an alternative disease mechanism is possible in *ATG7*-related neurological disease and that *de novo* heterozygous *ATG7* variants can cause a neurological presentation without the necessity of an additional pathogenic variant on the second allele. The identification of further families with heterozygous *ATG7* variants is necessary to fully elucidate the extent of different genetic mechanisms underlying *ATG7*-related neurological disease.

# 7 Developmental and molecular consequences of *ATG12* variants in neurological disease

## 7.1 Introduction

### 7.1.1 ATG12 in autophagy

As discussed (**Chapter 1.1.3**), in humans autophagy relies on two core conjugation pathways, the LC3 conjugation pathway, and the ATG5-ATG12 conjugation pathway, upon which the former relies (**Figure 1.1**) (Glick et al., 2010b). ATG12 is a ubiquitin-like protein which binds to ATG5 via a covalent bond which forms between C-terminus of ATG12 at Gly186 and the side chain of ATG5 at Lys149 residue. This ATG5-ATG12 bond requires the interaction of ATG7 and ATG10 in order to form the ATG5-ATG12 heterodimer (Mizushima et al., 1998). Once formed, the ATG5-ATG12 heterodimer associates with ATG16L1 to form a stable complex (Mizushima et al., 1999). Alongside this, inactive LC3 is cleaved at the C-terminus by a cysteine protease ATG4B, resulting in LC3 shortening to 120 residues long (Agrotis et al., 2019b). The cleavage exposes a glycine at the C-terminal end of LC3, resulting in LC3 becoming active, where it is known as LC3-I. LC3-I is then adenylated at its exposed glycine by ATG7. ATG3, which associates with the ATG5-ATG12-ATG16L1 complex, binds to LC3-I, and the ATG5-ATG12 complex induces the transfer of LC3-I from ATG3 to PE, forming LC3-II (Kirkin et al., 2009b; Hanada et al., 2007). Insertion of LC3-II into the expanding phagophore results in a slight disruption of the membrane, allowing addition of further phospholipids into the membrane, while asymmetric recruitment of LC3-II by the ATG5-ATG12-ATG16L1 complex promotes the curvature of the phagophore (Maruyama et al., 2021b; Glick et al., 2010b).

The crystal structure of the human ATG5-ATG12-ATG16N (the N terminal region of ATG16L1) complex has previously been published with a resolution of 2.7 Å (PDB ID 2DYM), and in complex with ATG3 to a resolution of 2.2 Å (PDB ID 4NAW) (Otomo et al., 2013; Metlagel et al., 2013). Structures show that the ATG5-ATG12 conjugate relies on the covalent bond between ATG12's Gly186 and Atg5's Lys149 to stabilise a hydrophobic interface between the two molecules (Otomo et al., 2013). While it has been demonstrated that the covalent linkage between ATG5 and ATG12 is not required for the proper localisation of ATG5 to forming phagophores, it is required for

the lipidation of LC3-I, and insertion into the expanding structures (Mizushima et al., 2001). Additionally, disruption of the hydrophobic interface between the two molecules can also lead to- destabilisation of the ATG5-ATG12 complex. This destabilisation reduces the E3 activity of the ATG5-ATG12 heterodimer, having a negative effect on its role in LC3-I conjugation to PE (Otomo et al., 2013). In ATG12, the point mutations V62R, G63D, A138R, W139F or W139Y are all able to effectively prevent LC3 lipidation. All these residues are found in a continuous functional patch spanning both ATG5 and ATG12, with similar point mutations in the ATG5 component of the patch also impairs the E3 activity of the complex (Otomo et al., 2013).

Alongside disrupting ATG12's conjugation to ATG5, the point mutations in K54D and K72D and W73A in ATG12 can disrupt its interaction with ATG3. ATG3 is formed of a E2-like ubiquitin domain and a flexible linker region. Numerous residues in the ATG3 flexible region are responsible for various electrostatic interactions with ATG12, however no interactions have been observed between ATG3 and ATG5 (Metlagel et al., 2013; Otomo et al., 2013). Point mutations in the ATG3 flexible region, such as D156A, M157A, Y160A, and E161A reduce the binding affinity of ATG3 to ATG12 in the ATG5-ATG12-ATG16N complex. Further, experiments have shown that this reduction in interaction between ATG3 and ATG12 has a negative impact on the production of LC3-II (Metlagel et al., 2013). It is important to note that while *in-vitro* studies have shown that the ATG5-ATG12 conjugate alone is enough for the function of the E3-like ubiquitin activity of the complex, *in-vivo* studies have demonstrated that ATG16N must also be bound, as ATG12 nor ATG5-ATG16N are capable of functioning as an E3-like enzyme (Hanada et al., 2007; Fujioka et al., 2008; Fujita et al., 2008).

### 7.1.2 *ATG12* models

Given the complicated nature of autophagy in mammalian systems, *Saccharomyces cerevisiae* was initially utilised to investigate the role of Atg12 in autophagy, then known as Apg12. The homozygous knockout of *atg12* in this model system resulted in a loss of autophagosome accumulation upon starvation of carbon, nitrogen or single amino acids (Tsukada & Ohsumi, 1993). The atg12 null yeast had a reduced viability in nitrogen starvation conditions, along with defective sporulation, a finding also seen in the fission yeast *Schizosaccharomyces pombe* (Tsukada & Ohsumi, 1993; Mukaiyama et al., 2009). Complete and conditional *Atg12* knockout mice have been

previously generated. Similar to Atg5 and Atg7 null mice, ATG12 null mice die within the first 24 hours after birth (Malhotra et al., 2015; Kuma et al., 2017). Mouse embryonic fibroblasts (MEFs) generated from the *Atg12* null mouse embryos showed complete loss of LC3-II production, under both basal and starvation culture conditions. Additionally, *Atg12* null MEFs presented with increased levels of the autophagy adapter proteins p62 and NBR1, indicating the accumulation of intracellular components tagged for degradation (Malhotra et al., 2015). These finding suggest that loss of ATG12 is incompatible with life in mice, due to impaired LC3-II production and intracellular degradation.

A human embryonic stem cell (hESC) model of *ATG12* has also been developed to investigate the role of ATG12 in mitochondrial network remodelling during neural differentiation, a key process for proper neural differentiation, as discussed (**Chapter 1.3.2**) (Ordureau et al., 2021). Initially, *ATG12* null hESCs had a proteome similar to those of the differentiating hESCs, including induction of upstream mitophagy signalling, previously discussed (**Chapter 1.3.1**) and cell cycle exit through days 1 and 2 of the 12-day differentiation protocol. However, as differentiation progressed the increase in mitophagy observed on immunoblots from day 4 of differentiation in wild type cells was not observed in the *ATG12* null line. Despite a loss of canonical autophagy pathway, and therefore mitophagy, residual level of mitophagy was still observed during differentiation, which was comparable to that preceding differentiation, indicating the presence of a non-canonical mitophagy pathway (Ordureau et al., 2021). Proteomic analysis at 0, 4 and 12 days of differentiation comparing the wild type lines and the ATG12 null lines also demonstrated differences that throughout the differentiation protocol, there was a decrease in the subunits of the core autophagy machinery, including ATG5 and ATG16L1, and an increase in autophagy adapter proteins, including GABARAPL2, showing that removal of ATG12 has a subtle wider effect on basal autophagy. Despite the subtle nature of the decrease in general autophagy, there was a significantly higher mitochondrial load in the *ATG12* null neurons compared to wild type after 12 days of differentiation (Ordureau et al., 2021). This indicated that the residual non canonical mitophagy is insufficient for correct mitochondrial remodelling in neurons lacking *ATG12*. In addition to this the Golgi and endoplasmic reticulum (but not ribosomes) were also increased in *ATG12* null neurons at the end of the 12-day differentiation. Together, these data suggest that

while the wider autophagy deficit resulting from deletion of *ATG12* may not be as severe as deletion of other autophagy genes, the resulting effect on other organelles, like mitochondria, Golgi and ER are significant, as cells exit the cell cycle during neural differentiation (Ordureau et al., 2021). However, it is important to note there were no prolonged differentiation experiments performed to investigate the effects of these changes on cellular function or fitness.

### 7.1.3 Alternative roles of ATG12

ATG12 has been described to play a role in mitochondria-mediated apoptosis. For this function, ATG12 forms a heterodimer with ATG3, and this conjugation is distinct from ATG12's conjugation to ATG5 and does not require ATG10 (Radoshevich et al., 2010). Instead, the ATG3-ATG12 conjugate relies on the E2-like catalytic activity of ATG3 to form a covalent bond between ATG12 and the Lys243 of ATG3 (Radoshevich et al., 2010). This conjugate does not have a role in basal autophagy, instead it functions independently to regulate mitochondrial mass and morphology. Loss of this ATG3-ATG12 conjugate results in an increase in mitochondrial load, despite functioning autophagy, and to a level over that seen in autophagy deficient cells, as well an increase in mitochondrial fragmentation due to reduced fusion events (Radoshevich et al., 2010). Alongside regulating mitochondrial homeostasis, the ATG3-ATG12 complex also plays a role in Bcl-2 mediated cell death. Loss of the ATG3-ATG12 conjugate results in an increase in Bcl-$x_{L,}$ an anti-apoptotic member of the Bcl-2 family leading to decreased cell death in challenged cells, despite their poor mitochondrial health (Radoshevich et al., 2010). However, another report has questioned the need for ATG12's conjugation to ATG3 to fulfil its role in cell death (Rubinstein et al., 2011). While they maintain that ATG12 plays a key role in Bcl-2 mediated cell death, they describe that ATG12 is capable of interacting with and activating Bcl-2 members other than Bcl-$x_{L,}$ to induce cell death, and is indispensable in this process (Rubinstein et al., 2011). Regardless of the conjecture surrounding the exact Bcl-2 proteins involved, ATG12 has been shown to play a key role in mitochondrial homeostasis and cell death, with significant cellular implications when its function is impaired.

## 7.2 Methods

### 7.2.1 Whole Exome Sequencing

For Family 1 (S1 and S2), trio genomic sequencing was undertaken via the NHS testing pathway (R14 test, gene agnostic trio investigations for acutely unwell children with a likely monogenic disorder). Subsequently, S2 was consented and recruited to a NIHR funded Trio WES project (‘Diagnosis of Mitochondrial Disease without Muscle”; IRAS 655610; REC: 20/NE/0272). Repeat WES sequencing was performed for S1 to allow data analysis to be performed as a quad. Research WES was undertaken using 2 µg EDTA blood DNA for S1, S2 and their parents; the Twist exome reagent (Twist Biosciences) used for library capture and sequenced on an Illumina NovaSeq 6000 sequencer using 2×150 paired-end sequencing. All WES samples were aligned to the GRCh38 human genome build using the Burrows Wheeler Aligner (BWA) (Li & Durbin, 2009); variant calling was performed using the GATK HaplotypeCaller (version 3.4). All variants were annotated using Ensembl Variant Effect Predictor (VEP), and a minor allele frequency of MAF<0.01 (gnomAD v3.1) was used to define the rare variant dataset for each member of the quad for Family 1 (McLaren et al., 2016). Each variant in S1 and S2 was first denoted as maternal or paternal, then genes with biallelic variants segregating between the two siblings were determined. SpliceAI was used to predict the likely impact of putative splicing variants.

For Family 2 (S3), WES of the subject was performed by Professor Eirik Frengen at University Hospital Oslo. Fastq files were aligned against the GRCh38 human reference genome using the Burrows-Wheeler Aligner (BWA) v.0.7.8. with duplicate reads removed using Picard v.1.119 (http://broadinstitute.github.io/picard/), indel realignment, base quality recalibration and variant calling was performed using the Genome Analysis Toolkit (GATK) v.3.4 (Li & Durbin, 2009; McKenna et al., 2010; DePristo et al., 2011). Variant annotation was performed using the Ensembl Variant Effect Predictor (VEP) (McLaren et al., 2016). The variant calling file (VCF) analysed using the FILTUS program (Vigeland et al., 2016). Variants with allelic frequency >0.01 in gnomAD v4.1.0 (gnomad.broadinstitute.org) or with a Combined Annotation Dependent Depletion (CADD) phred score <15 *in silico* tool were discarded (Kircher et al., 2014; Karczewski et al., 2020). Finally, prioritization of variants focused on missense, nonsense, frameshift, and small insertion/deletion variants, with an

anticipated autosomal recessive (homozygous and compound heterozygous) and autosomal dominant (*de novo*) mode of inheritance. For Family 2 the study was approved by the Regional Committee for Medical Research Ethics – South-East Norway, REK 2010/1152a.

The subjects in Family 1 and Family 2 were connected through the GeneMatcher platform (Sobreira et al., 2015).

### 7.2.2 Sanger sequencing confirmation of *ATG12* variants

Blood derived genomic DNA was subject to PCR amplification and Sanger sequencing to confirm the presence of the identified *ATG12* variants using the described primers (**Table 7.1**). PCR products were purified using ExoI and Shrimp Alkaline Phosphatase (Promega) and Sanger sequenced using the ABI BigDye terminator cycle-sequencing kits v3.1 (Life Technologies, Carlsbad, CA) before capillary electrophoresis using a 3730xl DNA analyzer running the proprietary DNA Sequencing Analysis Software v. 5.1 (Applied Biosystems, Foster City, CA). Sequences were visualised using FinchTV (Family 1) and SeqScape Software v.2.7 (Family 2) (Thermo Fisher Scientific).

**Table 7.1 Primers used for genomic DNA confirmation of *ATG12* subject variants.**

| Target | Primer sequence |
|---|---|
| ATG12_ex3_FWD (Family 1) | GAAAGTCATCTTTTCTACCCCAGA |
| ATG12_ex3_REV (Family 1) | TTGTGGGTAAGTGGGGACAT |
| ATG12_Family2_FWD (Family 2) | ACAAGTAGGAGCAATGGGTGT |
| ATG12_Family2_REV (Family 2) | AGCTCATTCATGCCTAAGATGCT |

### 7.2.3 RNA studies

Complimentary DNA (cDNA) was derived from total RNA extracted from subject (Family 1) and age-matched control fibroblasts cultured as described (**Chapter 2.6.2).** Reverse transcription of 2 µg RNA was performed using MMLV reverse transcription

system and random hexamer primers (Promega, Hampshire, UK). Primers designed to amplify cDNA spanning from exon 1 of *ATG12* through to its 3'-UTR were used for PCR amplification (**Table 7.2**) and DNA electrophoresis using a 2% agarose gel facilitated identification of normal and abnormal length cDNA fragments. Amplicons were subject to DNA sequencing to determine the effect of the subject variant (c.363+3A>T) present in Family 1 on mRNA splicing.

**Table 7.2. Primers used for cDNA investigations of ATG12 splice variant in Family 1.**

| Target | Primer sequence |
|---|---|
| ATG12_cDNA_FWD (Family 1) | GGATGTCTCCCCAGAAACAA |
| ATG12_cDNA_REV (Family 1) | AACAAGTAGGAGCAATGGGTGT |

### 7.2.4 Protein Modelling

The previously described crystal structure for the ATG5-ATG12-ATG3-ATG16N complex was obtained from RCSB PDB (4NAW) (Metlagel et al., 2013). To generate a model of the full length ATG5-ATG12-ATG3-ATG16N complex, the canonical full-length sequences were obtained from UniProtKB with the accession numbers: Q9H1Y0-1, O94817-1, Q9NT62-1 and Q676U5-1 respectively (Bateman et al., 2021). Multimer structures were modelled using AlphaFold-MULTIMER under standard settings (Evans et al., 2022).

### 7.2.5 Immunoblotting analysis of subject fibroblasts

Primary control and subject fibroblasts were cultured as described (**Chapter 2.6.2**). Samples were harvested and protein concentrations were estimated as described (**Chapter 2.7.2**). Proteins were separated and immunoblotted as described (**Chapter 2.7**).

### 7.2.6 Bulk autophagic sequestration activity assay (LDH sequestration assay)

Autophagic sequestration assays were performed by measuring the activity of autophagosomal lactate dehydrogenase (LDH) as previously described (Luhr et al.,

2018,‘Engedal et al., 2019). Subject cells were cultured using standard tissue culture conditions, in DMEM with high glucose (Gibco/Life Technologies), supplemented with 1X GlutaMAX, 10% FBS and 100 U/ml Penicillin-Streptomycin. To induce autophagy, cultures were acutely deprived of serum and amino acids using Earle’s balanced salt solution (EBSS) with 100 nM Bafilomycin A1 (BafA1) for 3 hours at 37°C at 5% $CO_2$. Cells were harvested using 0.25% trypsin-EDTA and collected in PBS containing 5% BSA. After centrifugation at 500 x *g* for 5 minutes at 4°C, cells were resuspended in sucrose solution (10% w/v, ice cold). Subsequently, plasma membrane disruption was accomplished using electroporation (BioRad, 2kV, 25 µF, and 400 Ω with a pulse of ~8 ms duration). Cells were resuspended in 400 µl phosphate-buffered sucrose (100 mM sodium monophosphate, 2 mM EDTA, 2 mM DTT and 1.75% sucrose, pH 7.5). Following this, 550 µl of the disrupted cell suspension was resuspended in 900 µl ice-cold resuspension buffer (50 mM sodium monophosphate, 1 mM EDTA, 1 mM DTT) for the sedimented measurement ($LDH_{‘Sediment’}$). Autophagic vacuoles were then sedimented by centrifugation at 18,000 x *g* for 45 minutes at 4°C. The resulting supernatant was aspirated and flash frozen using liquid nitrogen and stored at -80°C.

For total LDH measurement, 100 µl from the disrupted cell suspension solution was collected, flash frozen with liquid nitrogen and stored at -80°C ($LDH_{‘Total’}$). $LDH_{”Sediment”}$ was diluted in resuspension buffer with 1% Triton X-405 and $LDH_{‘Total’}$ with 1.5% Triton X-405 in a cold room for 30 minutes with agitation. Subsequently, samples were centrifuged at 18,000 x *g* for 5 minutes at 4 °C, after which LDH activity was measured as described previously in a working solution containing 0.6 mM pyruvate and 0.36 mM NADH (Luhr et al., 2018,‘Engedal et al., 2019).

### 7.2.7 Transmission electron microscopy

Following a 3-hour autophagy induction under starvation conditions ±BafA1, as described above, cultures were fixed for 30 minutes with 2% glutaraldehyde in 0.1 M Sodium Cacodylate (NaCac) buffer (pH 7.4) at room temperature. After fixation, cells were washed twice (3 minutes per wash) with NaCac buffer. Samples were osmified with 1% reduced osmium before dehydration and flat embedding into epoxy resin (TAAB). Resin was polymerized at 60°C overnight, and cross-sectioned. The 60 to 70 nm sections were collected on Pioloform-coated, single slot grids, and poststained

with uranyl acetate and lead citrate. Samples were imaged on a JEM 1400 microscope (JEOL) equipped with an Orius SC 1000B CCD camera (Gatan, Inc).

### 7.2.8 Yeast strains and growth media

*Saccharomyces cerevisiae* strains used in this study are listed below (**Table 7.3**). OC588 (BY4742, *atg8*::GFP-ATG8-URA3, *ura3Δ0, his3Δ1, leu2Δ0, lys2Δ0*) was obtained by integration of plasmid *pP$_{1K}$GFP-ATG8(406) at BY4742 chromosomal ATG8 locus* (Xie et al., 2008). *GFP-Atg8 Atg12*Δ (OC744) and pho8Δ60 *Atg12*Δ (OC747) strains were created by genomic integration of a deletion cassette PCR fragment amplified from OC751 strain in *GFP-Atg8 (OC588)* and pho8Δ60 (OC613) strains respectively.

**Table 7.3. Genotype and source of *S. cerevisiae* used.**

| Strain | Genotype | Source |
|---|---|---|
| OC751 | BY4742, *atg12::KanMX4, ura3Δ0, his3Δ1, leu2Δ0, lys2Δ0* | Yeast KnockOut Collection (Giaever & Nislow, 2014) |
| OC588 | BY4742, *atg8::GFP-ATG8-URA3, ura3Δ0, his3Δ1, leu2Δ0, lys2Δ0* | This study |
| OC613 | BY4742, *pho8::pho8Δ60-URA3KL, ura3Δ0, his3Δ1, leu2Δ0, lys2Δ0* | (Leboutet et al., 2023) |
| OC744 | BY4742, *atg8::GFP-ATG8-URA3, atg12::KanMX4, ura3Δ0, his3Δ1, leu2Δ0, lys2Δ0* | This study |
| OC747 | BY4742, *pho8::pho8Δ60-URA3KL, atg12::KanMX4, ura3Δ0, his3Δ1, leu2Δ0, lys2Δ0* | This study |

Yeast cells were grown to log phase in complete synthetic medium (CSM: 0.17% yeast nitrogen base, 0.5% ammonium sulfate, 2% glucose and amino acids without uracil or leucine). YNB-N (0.17% yeast nitrogen base without ammonium sulfate and amino acids and 2% glucose) was used as nitrogen starvation medium.

### 7.2.9 Plasmids

The *atg12* gene with 500bp upstream and downstream regions was amplified by PCR, cloned in TA pCR™4-TOPO® vector (ThermoFisher Scientific) and sequence was verified. Atg12-W166S or Atg12-A184V were generated by introducing a point mutation using the Phusion™ Site-Directed Mutagenesis kit (Thermoscientific) in pCR4-ATG12. *Atg12* and mutant sequences were cloned into pRS315 vector at XbaI and PstI sites. The oligonucleotide sequences used for these constructions are listed below (**Table 7.4**).

**Table 7.4. Primers used for the generation of wild type and atg12 variant plasmids.**

| ***Target*** | ***Sequence*** |
|---|---|
| Atg12 cloning Fwd | 5’ AGTCTAGAACCTAGTCTTCCATTTACATCG 3’ |
| Atg12 cloning Rev | 5’ AACTGCAGGGGTCTTTGGTGAAAAAGGG 3’ |
| Atg12 W166S mutagenesis Fwd | 5’ TTGGTGAACTTTCGATGCAATTCAAGAC 3’ |
| Atg12 W166S mutagenesis Rev | 5’ TATTTTGCTGCGGACTTGGC 3’ |
| Atg12 A184V mutagenesis Fwd | 5’ TTGTGCATCCGTAGTGTTTGGTTAAATAC 3’ |
| Atg12 A184V mutagenesis Rev | 5’ TAACTTACAATAAGCTCATCATTAGTC 3’ |

### 7.2.10 GFP-Atg8 processing assay

The GFP-atg8 processing assay is adapted from the protocol published by Guimaraes and colleagues (Guimaraes et al., 2015). Cells were grown to log phase in CSM without uracil, ± leucine according to the strains, then were transferred to nitrogen starvation medium for 6 hours. At different time points, 3 mL of cells were collected, washed with water then resuspended in 200 µL of ice-cold 10% trichloroacetic acid (TCA). Cells were broken using glass beads for 10 minutes at 4°C and centrifuged. Pellets were resuspended in 1x Laemmli sample buffer and boiled. A volume corresponding to 1.5 x $10^7$ cells was loaded on 12% SDS-polyacrylamide gel, transferred onto nitrocellulose membrane, and probed with anti-GFP antibodies (Roche) or anti-Pgk1 antibodies (Invitrogen), followed by peroxidase-conjugated anti-mouse antibody. Detection was performed with Amersham ECL Western Blotting

System, and signals were captured with camera of Chemidoc Imaging Systems (Bio Rad) and quantified using ImageJ.

The autophagic flux was quantified by the ratio between the intensity of the free GFP and the intensity of the total GFP (percentage of free GFP). The ratio between intensities of the GFP-Atg8 and Pgk1 was used to compare the amount of undegraded protein.

### 7.2.11 Fluorescence microscopy

*S. cerevisiae* cells were grown to log phase in CSM without uracil and leucine then were transferred to nitrogen starvation medium for 4h. At different time points, cells were collected and observed in three-dimensional deconvolution microscope DMIRE2 (Leica Microsystems) equipped with an HCxPL APO 100 × oil CS objective, NA = 1.40 (Leica Microsystems) and an incubation chamber. Images were captured by a 20-MHz Cool SNAPHQ2 charge-coupled device camera (Roper Technologies), with a z-optical spacing of 0.2 µm. Metamorph sofware (Molecular Devices) was used to acquire z-series and to deconvolve the images.

## 7.3 Results

### 7.3.1 *ATG12* subjects present with cerebellar and callosal hypoplasia and developmental delay

S1 (Family 1, **Figure 7.1A**), a female infant, was the first child born to non-consanguineous British parents following IVF and an unremarkable pregnancy. Born at term, by normal vaginal delivery, she weighed 3.225 kg ($25^{th}$-$50^{th}$ centile) and unremarkable postnatal condition. Newborn examination was normal with the exception of overlapping $4^{th}$ and $5^{th}$ toes bilaterally. On day 3 of life, she exhibited feeding difficulties, excessive weight loss and jaundice. On examination, she was hypotonic and required supplementary oxygen for apnoea associated with feeding. A swallowing assessment revealed poor coordination and nasogastric tube feeding was commenced.

Neurological review at 5 weeks of age identified central hypotonia and a good, but not sustained, sucking reflex. Initially, tone and anti-gravity movements of the limbs were normal, but on further review at 2 months, movements were generally reduced, and

she was unable to fix and follow. By 7 months a clinical diagnosis of infantile spasms was supported by an abnormal electroencephalogram (EEG) demonstrating evolving hypsarrhythmia and anti-epileptic medications were commenced. A contemporaneous cranial MRI revealed diffuse parenchymal volume loss involving both grey and white matter, cerebellar vermis hypoplasia and posterior callosal hypoplasia (**Figure 7.1A**). S1 died aged 12 months.

Further clinical review by paediatric neurology led to a range of neurological, metabolic, genetic and radiological investigations that were diagnostically uninformative. Blood and fibroblasts were taken for cytogenetic and molecular analysis.

S2, a male infant and younger sibling of S1, was born at 38+5 weeks gestation by normal vaginal delivery and weighed 3.615kg ($50^{th}$–$75^{th}$ centile). No resuscitation was required at birth, but he was noted to be hypotonic, less active than expected and had bilateral positional talipes with overlapping toes on both feet. He was admitted to the neonatal intensive care unit due to low oxygen saturations and tachypnoea, where he was initially treated for transient tachypnoea of the newborn. A persistent oxygen requirement and feeding difficulties prompted further medical investigations.

At 2 weeks of age, recurrent seizures were treated with levetiracetam. Neurological examination revealed nystagmus, reduced anti-gravity movements and hypotonia. A cranial MRI at 11 days of age demonstrated a structural malformation with deep sulcation of the right occipital lobe and cerebellar and posterior callosal hypoplasia.

Ongoing feeding difficulties prompted insertion of a gastrostomy at 4 months old. Around this time increased seizure activity was noted and while initial EEGs had been unremarkable, by 4 months the EEG was consistent with epileptic encephalopathy. Blood and fibroblasts were taken for cytogenetic and molecular analysis.

S3 (Family 2, **Figure 7.1A**), a male, is the fourth child of healthy consanguineous, first cousin, parents from Syria. His two oldest siblings are healthy. One older sister had difficulty with walking and speaking, impaired vision with nystagmus and died at the age of 7 years from end stage kidney disease (ESKD). Many of these features were similar to S3, suggesting she may have had the same disease as S3; however, no genetic analyses were available. S3 parents also report three previous pregnancy losses.

Pregnancy and neonatal period of S3 were reported normal, with psychomotor delay only becoming evident during the first year of life. At 3 years of age, he experienced seizures.

At 4 years of age, he was diagnosed with kidney disease, anemia and thrombocytopenia. A clearly defined renal diagnosis has never been applied, but he subsequently developed ESKD. He received peritoneal dialysis from 8 to 13 years of age, the latter age at which a renal transplant was performed. Renal ultrasound and renal MRI before the transplant showed bilateral atrophic kidneys with small cysts.

At 9 years of age, he was diagnosed with pancreatitis and cholecystitis, cholecystectomy was performed and he also had surgical repair of large bilateral inguinal hernias. He is severely growth retarded with Z-score for length at -6 SD before the renal transplant. Growth remains impaired and has not improved 2 years after transplantation. He has been diagnosed with hypothyroidism and receives thyroxine replacement therapy.

He has limited verbal language skills, moderate intellectual disability and wears hearing aids to assist with bilateral sensorineural hearing impairment. He walks only with the aid of a walker due to ataxia. He has had dry and scaly skin since early childhood. Brain MRI obtained at 12 years of age showed atrophy of both cerebellar hemispheres and the vermis, posterior callosal hypoplasia, and widespread bilateral polymicrogyria (**Figure 7.1B**). An ophthalmological examination revealed bilateral optic atrophy and typical Bull's eye maculopathy.

His clinical appearance in adolescence is one of short stature, with a slender build. He has microcephaly, down slanting almond-shaped eyes and blepharophimosis. He has a broad nasal bridge, anteverted nostrils, long philtrum and cupid's bow upper lip. His ears are low set with an irregular helix, and he has sparse head hair (**Figure 7.1C**). He also has bilateral fifth finger clinodactyly of both hands.

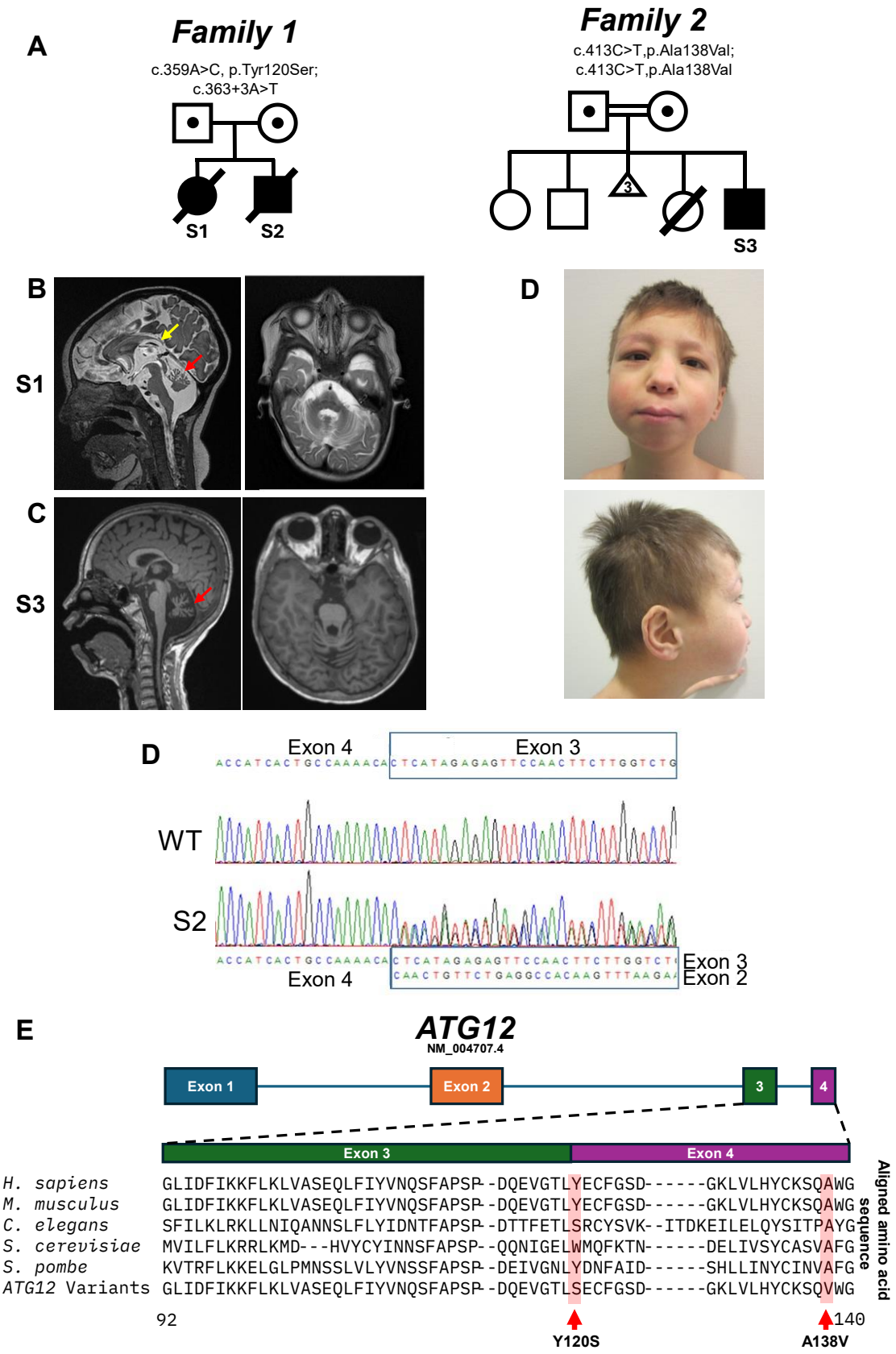


**Figure 7.1 Family pedigrees and identification of ATG12 variants A.** Pedigrees of Families 1 and 2 and their ATG12 genotypes. **B.** Brain MRI of S1 at 7 months of age (left). T2 weighted image

showing posterior atrophy of the corpus callosum and cerebellar vermian hypoplasia, denoted by yellow and red arrows, respectively. Brain MRI of S3 at 12 years of age. Midline sagittal T1-weighted image showing posterior atrophy of the corpus callosum and cerebellar vermian hypoplasia, denoted by yellow and red arrows respectively (right). **C.** Clinical photography of S3 at the 12 years of age showing craniofacial abnormalities. **D.** Sanger sequencing of S2 cDNA showing splicing defects due to the c.363+3A>T variant. The double peaks detected are in line with the sequences of ATG12 exon 2 and 3 as indicated **E.** Schematic of ATG12 (RefSeq accession number NM_004707.4), with multiple sequence alignment of orthologues from various species, aligned using Clustal Omega, demonstrating the conservation of the amino acid residues involved.

### 7.3.2 Genomic analyses revealed bi-allelic *ATG12* variants

Microarray analysis (array CGH) undertaken for siblings S1 and S2 revealed an 11 kb copy number loss at 9p24.3 (including exons 40-44 of *DOCK8*) for S1 only with no phenotypic correlation. Rapid gene agnostic trio WES analysis for S1 identified bi-allelic variants of unknown significance in *SEMA6B* and *PRMT7*, however these were not found to segregate with S2. Repeat (research based) trio WES sequencing was undertaken for S1 and S2 given their shared but undiagnosed presentation (performed by NHS Highly Specialised Service for Rare Mitochondrial Disorders). Initial investigation of variants that segregated between the siblings and were inherited biparentally failed to identify any suitable targets, but by investigating variants segregating between the two affected siblings (irrespective of the parent of origin), two heterozygous variants were identified in the *ATG12* gene. Firstly *ATG12* (NM_004707): Chr5(GRCh38):115832606T>G, c.359A>C; p.Tyr120Ser missense variant with a CADD PHRED score of 24.4 was identified. The variant has been reported on gnomAD V4.1.0 with the reference rs370194003 with an allele frequency of $2.578x10^{-5}$. Additionally, an *ATG12* (NM_004707): Chr5(GRCh38):115832599T>A, c.363+3A>T, putative splice variant was identified (**Figure 7.1A**, left). The splice site variant has been reported on gnomAD V4.1.0 with the reference rs753409628 and an allele frequency of $2.373x10^{-5}$ and one homozygote. The variant has a CADD PHRED score of 24.2 and SpliceAI score of 0.830. Visualisation of the BAM files using the IGV allowed visual confirmation that the maternal putative splice variant was present, and the complexity of the adjacent polynucleotide tract proffers an explanation for the variant no call. Variants were interpreted according to the American College of Medical

Genetics (ACMG) guidelines (Richards et al., 2015). All *ATG12* variants and their segregation in the family were confirmed using Sanger sequencing. Analysis of fibroblast-derived RNA from S2 demonstrates skipping of exon 3 (**Figure 7.1D**), this is predicted to cause the in-frame deletion of 20 residues.

We performed WES of S3 and data analysis according to a recessive mode of inheritance and identified the following homozygous missense variant *ATG12* (NM_004707): CHR5(GRCH38:115831814G>A; C.413C>T; p.Ala138Val, with a CADD phred score of 31. The variant single nucleotide polymorphism is known as rs377580028 and reported with allele frequency of $1.12x10^{-5}$ in gnomAD v4.1.0, only in heterozygosity. Sanger sequencing of the family trio confirmed the variant to be in homozygosity in S3 and in heterozygosity in his healthy parents (**Figure 7.1A**). No sample was available for genetic testing from the sister.

### 7.3.3 ATG12 variants disrupt ATG5-ATG12-ATG3-ATG16N interaction

*In silico* analysis using the AlphaFold structure of ATG12 shows that both the p.Tyr120Ser variant of Family 1 and p.Ala138Val variant of Family 2 map the ubiquitin like fold of ATG12 (**Figure 7.2A**). The crystal structure of ATG5-ATG12 in complex with the minimal interacting regions of ATG16L1 and ATG3 has been previously determined to 2.2 Å resolution (**Figure 7.2B**) (Metlagel et al., 2013). Using AlphaFold-MULTIMER, the current ATG16L1-ATG5-ATG12-ATG3 structure was expanded to include full-length ATG3 protein in the modelling (Graham et al., 2023; Evans et al., 2022). The expanded model recapitulates the reported interaction surface between ATG12 and ATG5 but reveals beyond the crystal structure how full-length ATG3 wraps around ATG12 extensively (**Figure 7.2C**).

The two missense variants identified (p.Tyr120Ser and p.Ala138Val) map to different segments of ATG12, both appear to be near the external face of ATG12. Importantly, both residues also directly interact with ATG3 (**Figure 7.2C**). Among over 2000 ATG12 orthologues, Tyr120 is conserved among 44% of sequences, while Ala138 is nearly invariant at 89% of sequences (Graham et al., 2023). The Tyr120Ser and Ala138Val substitutions likely impact on ATG12 interaction with both ATG5 and ATG3. Relevant to this, a similar substitution at Ala138 (i.e. Ala138Arg) showed reduced binding of ATG16L1-ATG5-ATG12 to ATG3, and abolished LC3 lipidation *in vitro* (Otomo et al., 2013).

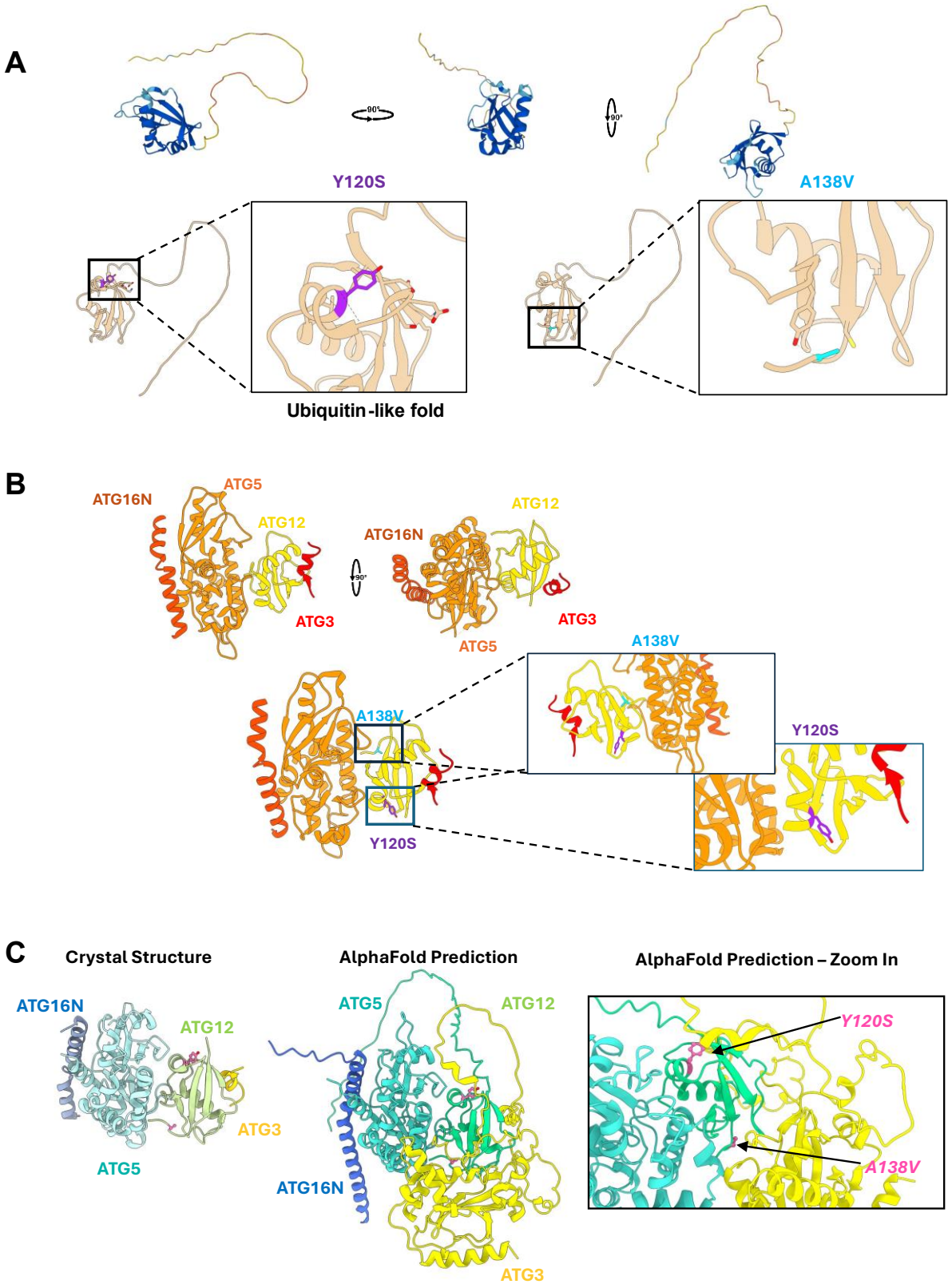


**Figure 7.2. In silico structural analysis of ATG12 variants illustrating the effect on complex formation. A.** Alphafold prediction of ATG12 structure (Accession number: O98417). Position of Y120S variant in the ubiquitin fold of ATG12 is shown in purple. Position of A138V variant is shown in blue. Broken lines denote hydrogen bonds formed by residue of interest. **B.** Existing crystal

structure of the ATG16L1-ATG5-ATG12-ATG3 complex (RCSB PDB accession: 4NAW) showing their proximity to ATG12's interface with ATG5. **C.** Comparison of the existing crystal structure of the ATG16L1-ATG5-ATG12-ATG3 complex and our expanded structure using full length sequences with the subject variants annotated in pink. The expanded AlphaFold prediction shows the full length ATG3 sequence wrapped around ATG12, placing the variants in close proximity to the interfaces with both ATG5 and ATG3.

### 7.3.4 *ATG12* variants impair autophagy flux and intracellular degradation

Next, the impact of *ATG12* variants on the ATG5-ATG12 complex and other autophagy related proteins was assessed by immunoblotting in control and *ATG12* subject-derived fibroblasts. Under basal conditions, both S2 (c.363+3A>T; p.Tyr120Ser) and S3 (p.Ala138Val; p.Ala138Val) had stable levels of the core autophagy effectors ATG7 and ATG3, along with stable levels of p62, an autophagy adapter protein (**Figure 7.3A**). S2 showed a clear loss of the ATG5-ATG12 dimer, along with diminished ATG12 monomer, suggesting that the reduction in ATG5-ATG12 dimer is due to a loss of ATG12. In contrast, cells from S3 revealed stable levels of ATG5-ATG12 dimer and ATG12 monomer. Further probing with antibodies against ATG5, identified the presence of stable ATG5 monomer in S2 only (**Figure 7.3A**).

Subsequently, autophagy flux was comparatively assessed between control and S2 and S3 fibroblasts. Non-selective autophagy was induced in primary fibroblasts using the mTORC1 inhibitor AZD8055 in the presence or absence of chloroquine (CQ), which attenuates autophagosome lysosome fusion, thus blocking autophagy flux (Mauthe et al., 2018; Zhao et al., 2014). As expected, mTORC inhibition led to robust accumulation of LC3-II, the human homologue of yeast Atg8, which was further increased upon CQ treatment in control cells. In contrast, both S2 and S3 cells demonstrated modest reductions in LC3-II stabilisation when compared to controls (**Figure 7.3B**). To complement these findings, non-selective autophagy flux was also measured using the classical LDH sequestration assay (performed in collaboration with Dr. Tom McWilliams lab, Helsinki). Interestingly, bulk autophagic sequestration of endogenous cargo was decreased in cells from S3, whilst the sequestration activity in cells from S2 were normal (**Figure 7.3C**).

To further characterise the nature of the autophagy defect observed in subject-derived fibroblasts, transmission electron microscopy (TEM) analyses was undertaken in the presence or absence of Bafilomycin A1, a lysosome vATPase inhibitor which block autophagic flux (performed in collaboration with Dr. Tom McWilliams lab, Helsinki) (Mauvezin & Neufeld, 2015). TEM analysis identified that the early steps of phagophore formation and sequestration appeared normal, indicated by the presence of double membrane vesicles in both subject cell lines. However, the presence of abundant amphisomes, an autophagy intermediate formed by fusion of an autophagosome with an endosome, suggests autophagosome maturation and autolysosome formation is affected by *ATG12* variants (**Figure 7.3D**). Together, these data provide robust evidence that *ATG12* variants can be pathogenic by altering autophagic flux.

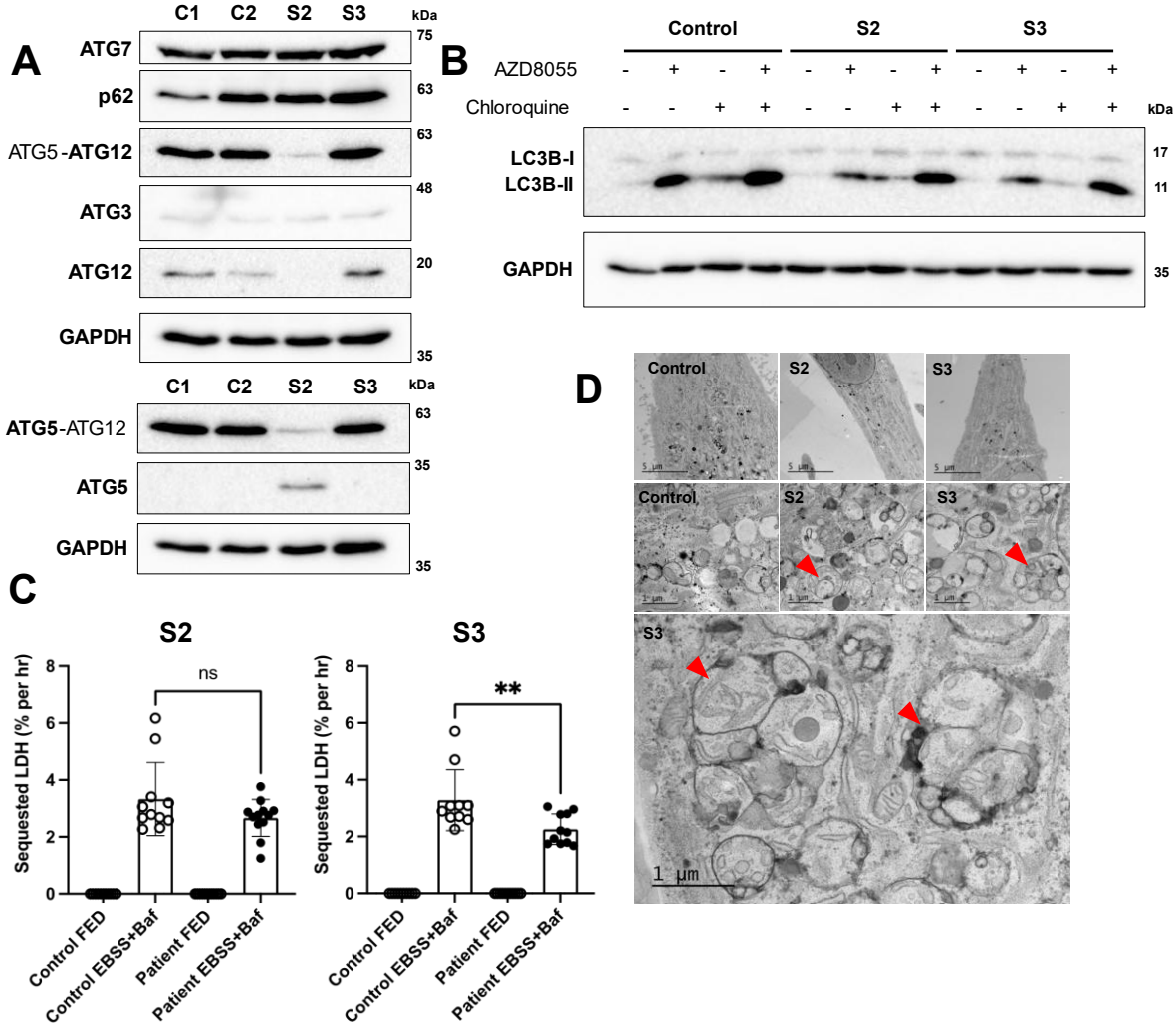


**Figure 7.3. Immunoblot analysis of subject-derived fibroblasts show decreased ATG12 levels. A.** Immunoblot of steady state levels of autophagy related proteins in controls (C1 and C2)

and subject derived fibroblasts (S2 and S3). Immunoblots show decreased ATG5-ATG12 heterodimer and loss of detectable ATG12 monomer in cells from S2, but not S3. Additional blots show stabilisation of free ATG5 in S2, but not in S3. Labels in bold denote the antibody used for detection of heterodimer. (n=3) **B**. Immunoblot of autophagy flux assay. Subject-derived cells were treated with 1 μM AZD8055 to initiate autophagy and 100 μM chloroquine to block autophagosome-lysosome fusion for 2 hours before harvesting to probe the rate of LC3-II production. Both cell lines showed mild attenuation of LC3-II production when compared to the control fibroblasts. (n=3) **C**. Quantification of LDH sequestration per hour under basal (FED) or starvation conditions (EBSS+BAF) with lysosome acidification inhibited by 100 nm Bafilomycin A1 for 3 hours. Only S3 cells showed a significant decrease in bulk autophagic sequestration. (n=3) (**p < 0.01 Ordinary one way analysis of variance and Sidak's multiple comparison test)) **D**. Transmission electron micrographs of starved Control and Subject-derived fibroblasts with starvation and Bafilomycin A1 treatment for 3 hours prior to fixation. All samples show amphisomes (arrowheads), with subject-derived cells appearing to have an accumulation of amphisomes.

### 7.3.5 *In vivo* complementation of *atg12* null *Saccharomyces cerevisiae* fails to recover autophagy flux

The analysis of autophagic flux in subject-derived primary cells revealed subtle biochemical deficits and altered ultrastructural features in autophagic flux. As *ATG12* and the autophagy process are evolutionarily conserved, complementation studies in in *S. cerevisiae* expressing homologous *atg12* variants were used to assess their effects on autophagy *in vivo* (in collaboration with Dr. Renaud Legouis, Paris-Saclay University, France). Sequence alignments demonstrated $ATG12^{Y120}$ and $ATG12^{A138}$ of the human ATG12 correspond to $Atg12^{W166}$ and $Atg12^{A184}$ of yeast Atg12, respectively (**Figure 7.4A**). *Atg12* null mutant (*Atg12Δ)* complemented with either wild type ATG12*,* $Atg12^{W166S}$, $Atg12^{A184V}$, or the empty pRS315 vector. First, a GFP-Atg8 processing assay was used to assess autophagic flux (Guimaraes et al., 2015). While Atg8 (yeast homologue of LC3) is readily degraded in the vacuole (the yeast's degradative compartment), the GFP linked to it exhibits a degree of resistance to vacuolar hydrolysis, resulting in free GFP as its linked atg8 is degraded. The detection of unbound GFP allows for quantification of autophagic activity in various contexts.

Wild type *GFP-Atg8* and *Atg12Δ::Atg12* strains exhibited the expected response, accumulation of free GFP over time, indicative of functioning autophagy. *Atg12Δ::*pRS315 however showed no detectable free GFP (**Figure 7.4B**). *Atg12Δ*

complemented with the Atg12$^{W166S}$ and Atg12$^{A184V}$ mutants failed to recover the levels of free GFP, however, low levels of free GFP were detected in both cases, suggesting autophagy is not completely abolished (**Figure 7.4B**). This decrease in delivery of autophagic material to the vacuole was also confirmed with microscopy. Punctate GFP signals indicative of autophagosomal structures were still able to form in strains harboring Atg12$^{W166S}$ and Atg12$^{A184V}$ variants, however their number was greatly decreased (**Figure 7.4C**). Additional quantification of GFP presence in the vacuole also confirmed a reduction in the delivery of GFP to the degradative compartment (**Figure 7.4C**).

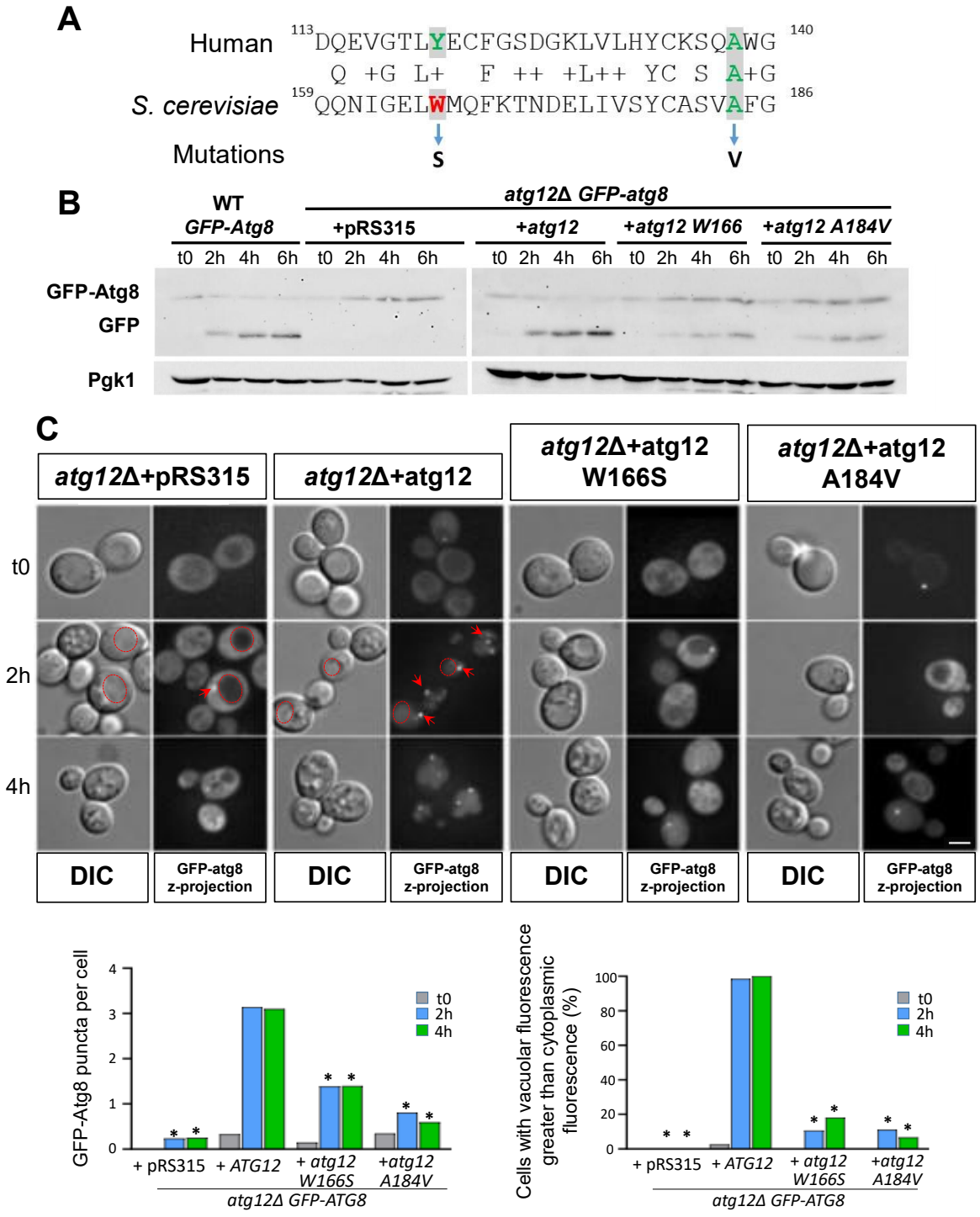


**Figure 7.4 The yeast atg12 W166S and A184V mutants display decreased autophagy. A.** Alignment of the human (UniProtKB: O98417) and yeast ATG12 (UniProtKB: P38316) sequences covering the mutated amino acids W166S and A184V. **B.** GFP-Atg8 processing assay was performed on WT strain and atg12Δ strains transformed by plasmid expressing ATG12, mutated ATG12 (W166S and A184V) or the empty vector (pRS315). Cells were harvested before (t0) and at 2, 4 and 6 hours after nitrogen starvation. **C.** GFP-Atg8 live imaging in *atg12*Δ strain transformed with plasmid expressing Atg12 or mutated Atg12. Cells were collected before (t0), and at 2 and 4

hours after nitrogen starvation. Red arrows indicate autophagosomes or isolation membranes and red circles indicate the yeast vacuole (scale bar = 3 μm). Graphs show average dots per cell and the percentage of cells with increased vacuolar GFP signal. Significant average dots per cell differences against the *atg12Δ* strain expressing ATG12 plasmid (**p* < 0.001 Kruskall-Wallis test) (n=3). Significant vacuolar fluorescence against the *atg12Δ* strain expressing ATG12 plasmid (**p* < 0.001 Kruskall-Wallis test) (n=3).

## 7.4 Discussion

This chapter describes three subjects from two unrelated families harboring previously unreported pathogenic variants in the core autophagy gene *ATG12.* The *ATG12* subjects share a neurodevelopmental phenotype of ataxia, intellectual disability and delayed development with neuroradiology showing cerebellar and posterior corpus callosum hypoplasia (**Figure 7.1B**). One subject also presented with optic atrophy, sensorineural hearing loss and dysmorphia, alongside an end stage kidney disease.

*In silico* analyses using published X-ray crystal structures, combined with AlphaFold structural modelling, suggest that the p.Tyr120Ser and p.Ala138Val ATG12 variants map to a ubiquitin-like fold in ATG12, potentially affecting its propensity to form stable interactions with ATG3. While loss of the stable ATG5-ATG12 complex in S2 cells was observed, this was not the case in S3 cells, although both cell lines appeared to exhibit altered autophagic flux. Electron microscopy analyses of ATG12-deficient subject cells revealed that autophagosomes can form despite *ATG12* variants. Subject-derived cells demonstrated abundant amphisomes, a hybrid degradative compartment generated by the fusion of autophagosomes with late endosomes/multivesicular bodies (Ganesan & Cai, 2021). This suggests that autophagosomes within ATG12 variant cells retain some ability to fuse with other compartments, however, their abnormal accumulation in subject-derived cells suggest these are unable to mature into autolysosomes, which are observed in control cells. Additionally, *Atg12* null *S. cerevisiae* cells are unable to recover autophagy when complemented with *ATG12* subject equivalent missense *Atg12* variants, suggesting the identified *ATG12* variants have a negative effect *in vivo.* Regardless, while the *Atg12* variants retain partial function, the wide variety of autophagy assays undertaken demonstrate that the *ATG12* variants described are detrimental, and result in an autophagy impairment. This, combined with the neurological phenotypes observed in both families, suggest

that the autophagy impairment stemming from *ATG12* variants is incompatible with sustaining neural integrity in humans.

The range of phenotype severity in the *ATG12* subject cohort is interesting. S1 and S2 were found to have smaller reduction in LC3-I to LC3-II lipidation, despite their loss of the ATG5-ATG12 complex. Furthermore, they were unable to survive past early childhood, with S1 dying of intractable infantile spasms and epileptic encephalopathy at 12 months, and S2 also being diagnosed with epileptic encephalopathy and dying in early childhood. In contrast, the S3 was found to maintain their ATG5-ATG12 complex but has a more severe reduction in LC3-I lipidation. Despite this, S3 appears to have a less severe neurological phenotype, but with the complication of kidney disease. The kidney disease phenotype is also observed in their uncharacterized sibling, suggesting they too may have been affected with the same genetic variants. As the parents of Family 2 are first cousins, resulting in large regions of homozygosity, another genetic cause of the kidney disease cannot be ruled out. However, no other likely pathogenic variants were identified in the WES analysis. It is worth noting that the early lethality observed in Family 1 may have prevented a kidney disease phenotype from developing. Kidney disease has not been reported in the *ATG7* or *ATG5* cohorts (Collier et al., 2021; Kim et al., 2016). This line of thinking also provides an explanation for the limited number early lethality outcomes associated with *ATG* variants. Here S1 and S2 were reported to harbor *ATG12* variants associated with early lethality, with only one other *ATG* subject reported to have the same severe phenotype, present in the *ATG7* cohort as described (**Chapter 1.5.3**). While this may be due to the phenotype being rare among *ATG* disorders, it seems more likely that these early lethal phenotypes are not being reported due to a lack of genetic diagnosis, as seen here in the sibling of S3, and will increase as next generation sequencing continues to become more widespread in the diagnostic process.

Considering the similarities observed between congenital autophagy disorders, the accumulation of amphisomes in *ATG12*-deficient subject-derived fibroblasts is a novel finding. The abnormal accumulation of amphisomes is a hallmark of autophagic stress in neurodegenerative disease (Ganesan & Cai, 2021). In fibroblasts, amphisomes are relatively short lived due to their impending fusion with endolysosomes. However, in neurons the fusion of late endosomes provides autophagosomes with the retrograde movement required to be transported to the cell body where the majority of

degradation occurs (Cai et al., 2010). This extended half-life of amphisomes in neurons may result in their accumulation above that seen in the subject fibroblasts. The exaggerated accumulation of amphisomes could explain the increased susceptibility of neural tissue. Further work into the stage at which amphisome maturation is impaired, and their distribution between peripheral processes and cell bodies at the time of impairment would shed greater light on the nature of the autophagy impairment observed.

Next generation sequencing efforts have been instrumental in revealing novel congenital autophagy associated defects that were once thought to be incompatible with life. Although still exceedingly rare, these findings extend the repertoire of genetic variants linked to autophagy dysfunction, and further emphasize the clinical significance of autophagy for human nervous system health and disease. It is anticipated that the discovery and profiling of additional *ATG* variants will pave the way for therapeutic interventions, aimed at ameliorating both rare and idiopathic disorders associated with autophagy dysfunction.

# 8 General Discussion

Autophagy is a key catabolic process in mammalian cells, playing a central role in cellular homeostasis. Extrinsic autophagy disruption plays a role in a number of neurodegenerative diseases such as Alzheimer's and Parkinson's disease, however, variants in a number of autophagy genes have also been described as pathogenic. Impairment of autophagy at almost all stages of the pathway can result in a variety of neurological disorders, however, to date very few core autophagy genes have been described as pathogenic. Previous reports of core autophagy proteins include *ATG4D, ATG5, ATG7* and *ATG9B*, all resulting in a neurological phenotype, however with varying levels of autophagy impairment. To better understand this emerging group of disorders, further work was required. This thesis aimed to generate a clinically relevant disease model of *ATG7* related neurological disease. Production of *ATG7* knockout iPSCs and the differentiation of these into neuron-astrocyte co-cultures would allow for the characterisation of neural specific biochemical defects, alongside the characterisation of neural differentiation and development. The aim was to also functionally characterise the ATG7 neuronal models to determine any impairment conveyed by loss of ATG7 on their activity. Additionally, this thesis aimed to expand the understanding of disease mechanisms of *ATG7* related neurological disorders by characterising additional *ATG7* subjects. This thesis also aimed to expand the core autophagy disorders by reporting a novel disease gene, *ATG12*.

Development of a tissue-specific disease model demonstrated that *ATG7* KO iPSCs can undergo neural induction and differentiate to neurons and astrocytes. *ATG7*$^{-/-}$ neuron-astrocyte co-culture had an attenuation of both core autophagy conjugation systems, with undetectable LC3-II (**Chapter 4.3.1**). Cultures also demonstrated developmental changes in relation to neurite outgrowth and cell proliferation over time (**Chapter 4.3.2**). There were also cell type-specific differences between cultures, with *ATG7*$^{+/-}$ cultures having increased numbers of astrocytes, and *ATG7*$^{-/-}$ cultures having fewer astrocytes than wild type co-cultures. Additionally, both *ATG7*$^{+/-}$ and *ATG7*$^{-/-}$ had increased astrocytic cell death, with minimal caspase-3 mediated neuronal death (**Chapter 4.3.3**). Finally, *ATG7* modulation also resulted in perturbations in calcium handling in response to glutamate stimulus (**Chapter 4.3.4**)

The research described in this thesis also expands upon the existing literature regarding congenital disorders of *ATG* genes. The identification of the first *de novo* heterozygous patient harbouring a missense *ATG7* variant demonstrates a novel disease mechanism for *ATG* gene disorders (**Chapter 6.3.1**). Additionally, the identification of a foetal case harbouring recessively inherited loss of function variants in *ATG7* is the first case in which *ATG7* were found to be incompatible with life (**Chapter 5.3**). This patient presented similarly to previously described *ATG7* patients, with developmental delay, cerebellar hypoplasia and posterior atrophy of the corpus callosum (**Chapter 5.3.1**). The availability of FFPE brain tissue from this individual resulted in the identification of surprisingly little caspase mediated cell death, and p62 accumulation in the cerebellum's proliferative zone (**Chapter 5.3.3**). This is the first indication that neurological phenotypes linked with *ATG7* disorders are associated with defective cell proliferation in earlier developmental stages, as opposed to cell death later in development. Characterisation of a novel disease gene, *ATG12*, expanded the collection of human *ATG* disorders. ATG12 joins ATG5 and ATG7 in demonstrating the importance of the ATG5-ATG12 conjugation system in human development. Individuals shared the developmental delay and cerebellar hypoplasia phenotype seen in other *ATG* disorders, with a moderate decrease in LC3-II conjugation (**Chapter 7.3**).

## 8.1 *In-vitro* iPSC derived *ATG7*$^{-/-}$ neurons do not accumulate p62

One of the most interesting findings is the disparity between neuronal and astrocytic p62 accumulation observed in the *ATG7* co-culture models. Neurons in *ATG7*$^{-/-}$ cultures do not appear to have accumulation of p62 under immunofluorescence analysis, yet western blot analysis of cultures show a clear accumulation of p62 (**Chapter 4.3.1**). Given the co-culture nature of the model, and the lack of co-localisation of MAP2 with the p62 staining, this would suggest astrocytes are accumulating p62 as opposed to neurons. The reason for the specificity is unclear. One explanation would be negative selection against neurons accumulating p62 during the cell death observed in weeks four to eight of differentiation observed in the timepoint point analysis of culture differentiation. This would mean that the remaining neurons are able to overcome their loss of canonical autophagy and clear their p62

and associated ubiquitinated proteins through different mechanisms, which are yet to be determined. While there have been alternative autophagy routes described, as discussed (**Chapter 1.2**), further investigations would be required to identify the mechanism underlying this phenomenon.

This does pose the question as to why the same process has occurred in the astrocytic populations of the co-culture. It is likely the astrocytic population are more resistant to the accumulation of p62, so the negative selection has not occurred by the end of differentiation. This hypothesis would also account for the increased number of astrocytes positive for cleaved caspase-3 compared to neurons after differentiation. At the end of differentiation, the more susceptible neurons have already undergone cell death, but the more resilient astrocytes are still undergoing the selection process. However, the lack of astrocytic marker included in the immunofluorescence panel makes drawing these conclusions difficult.

To this end, work is underway to differentiate *ATG7*$^{+/+}$, *ATG7*$^{+/-}$ and *ATG7*$^{-/-}$ co-cultures and perform an immunofluorescence based timepoint analysis of neuron-astrocyte populations to determine generation of each cell type, alongside p62 and cleaved caspase 3 staining. This will determine the progression of p62 accumulation in neurons and astrocytes, and how that p62 accumulation relates to cell death in neurons and then astrocytes through differentiation. Concurrently, RNA sequencing of separate neuron and astrocyte populations will be undertaken to determine the pathways associated with p62 clearance in the surviving neuron and astrocyte populations. This is technically challenging. As discussed (**Chapter 4.1.2**), the use of a co-culture model holds benefits such as faster development and synapse formation, but it also poses downstream challenges. To obtain separate transcriptomes for the neurons and astrocytes, they require cell sorting. Optimisation experiments have shown poor viability and sample quality post sorting. To address this problem, single cell RNA sequencing could be used. This would circumvent the need for splitting the neuron and astrocyte populations and would also provide greater detail as to the subpopulations of neurons and astrocytes generated during differentiation of the *ATG7* neural models (Sant et al., 2023). Alternatively, a fluorescence activated nuclei sort can be used prior to a bulk RNA sequencing on the nuclear transcriptome in both the neuron and astrocyte populations across the *ATG7* neural models (Chongtham et al., 2021; Slane et al., 2020; Khan et al., 2024). The aim of this RNA sequencing,

regardless of method, is to elucidate if non-canonical autophagy is responsible for the lack of p62 accumulation in *ATG7*$^{-/-}$ neurons, or an alternative pathway.

## 8.2 *ATG7* related cell cycle disruption impedes normal neural differentiation

The trend in astrocyte number across the two neural *ATG7* culture models was unexpected when compared to wild type. The increased number of astrocytes in the *ATG7*$^{+/-}$ compared to *ATG7*$^{+/+}$ cultures may be due to non-autophagic functions of *ATG7*, this is suggested by the lack of p62 accumulation observed in *ATG7*$^{+/-}$ cultures (**Chapter 4.3.1**). *ATG7* plays a role in the cell cycle separate from its role in autophagy, as discussed (**Chapter 1.6.3**). Dysregulation of the cell cycle has been demonstrated to have detrimental effects on aymmertric division and neuronal differentiation (Lim & Kaldis, 2012; Calegari & Huttner, 2003).

Recent work using *in-vivo* and *in-vitro Atg7* KO mouse models has demonstrated the role of *Atg7* in cell cycle maintenance in neural stem cell and the effect of its modulation (Shen et al., 2024). Loss of *Atg7* was shown to result in dysregulation of symmetrical and asymmetrical division in mice peripheral nervous system and neurospheres. The dysregulation of cell division was a result of cell cycle disruption via p53 and its mediators which led to a shortening of the G1 phase of the cell cycle, which in turn resulted in an increase in glia being produced, and a decrease in neurons. Autophagy modulation was unable to fully recover this phenotype (Shen et al., 2024). *ATG7* mediated cell cycle disruption would account for the increased number of astrocytes in *ATG7*$^{+/-}$ cultures compared to *ATG7*$^{+/+}$ cultures. The significant decrease in astrocytes in the *ATG7*$^{-/-}$ model could be contradictory to this. However, the increased astrocytic cell death at the eight-week time point may offer an explanation (**Chapter 4.3.3**). While an increased number of astrocytes may be produced during differentiation of *ATG7*$^{-/-}$ cultures, their reduced autophagy capacity means they are more susceptible to cell death than *ATG7*$^{+/-}$ cultures, reducing astrocyte numbers at the end of differentiation.

Timepoint analysis of the differentiation and development of *ATG7* neural cultures demonstrated an increased expansion of *ATG7*$^{+/-}$ and *ATG7*$^{-/-}$ cell clusters, suggesting an increase in cell division under *ATG7* modulation. Cell cycle dysregulation may also account for these changes. ATG7 impairment drives a shortening of G1 due to loss of

p53 induced expression of p21, a key factor in inhibiting transition from G1 to S phase (Lee et al., 2012). This produces increased cell division, accounting for the increased expansion of *ATG7*$^{+/-}$ and *ATG7*$^{-/-}$ cell clusters (**Chapter 4.3.2**).

This cell cycle disruption may also account for some of the interesting findings in the foetal subject harbouring p.Ser593Ilefs*fs/p.Gln571* *ATG7* variant. A key finding in the subject was the non-migrated Purkinje cells observed in the cerebellum and non-migrated cells surrounding the olivary nucleus. The lack of p62 accumulation and cleaved caspase-3 staining in these cells suggest minimal catabolic impairment or proteotoxic accumulation, posing the question as to why they have not reached the cortex if not due to autophagy impairment. An explanation could lie in the cerebellum's proliferative zone.

The two proliferative zones of the cerebellum, the ventricular zone and the rhombic lip, are temporally regulated. The VZ producing Purkinje cells during weeks 8-10 post conception, and the RL producing glutamatergic neurons after 10 weeks post conception predominantly (Haldipur et al., 2019). Cell cycle regulation has been reported to be involved in the temporal regulation of neuron production. Lengthening of the G1 stage of the cell cycle is associated with a premature switch from symmetrical to asymmetrical divisions, resulting in premature production of neurons in mice embryos (Calegari & Huttner, 2003). *ATG7* related modulation of the cell cycle results in the opposite of this, shortening of G1, so could be proposed to have the opposing affect. Shortening of G1 may result in a delay in neuron production from the brain's proliferative zones. This would result in production of neurons at timepoints later than in controls, resulting in cells migrating where their wild type counterparts have taken up their place in the cortex. This would also provide some explanation for the apparent reduction in number of NeuN positive neurons surrounding the corpus callosum if this were conserved in the cerebral VZ (**Chapter 5.3.4**). While autophagy is a key process involved in neuronal migration, the lack of p62 accumulation in these non-migrated neurons suggests focal autophagy may not be to blame (Sharifi et al., 2016; Geiger & Yamada, 2011).

While the p62 accumulation in the foetal p.Ser593Ilefs*fs/p.Gln571* subject's RL may be suggestive of a more autophagy centric mechanism, *ATG7* mediated cell cycle dysregulation was also associated with p62 accumulation in NSCs (Shen et al., 2024).

However, due to tissue restrictions and limited access to specific structures due to the nature of FFPE tissue, possibilities for further investigations are limited. The neural model however could provide more insight. An immunofluorescence timepoint analysis of neuron and astrocyte differentiation would give insight into the timeline of co-culture differentiation and possibly provide a better understanding of the non-migrated neurons in the foetal p.Ser593Ilefs*fs/p.Gln571* subject.

The lack of cell death in the foetal p.Ser593Ilefs*fs/p.Gln571* subject may be due to the more supportive conditions found *in-vivo* when compared to *in-vitro.* The increase in astrocytes could also be associated with tissue damage in the foetal subject, as part of a gliosis response (Wang et al., 2018). However, the ubiquitous nature of the astrocytes found in the foetal p.Ser593Ilefs*fs/p.Gln571* subject suggest this may not be the case, further work would be required to identify the nature of the astrocytes. While tissue availability limits the possibility of further tissue work, a more detailed analysis of astrocyte production in the *ATG7*$^{-/-}$ co-culture model compared to that that of the *ATG7*$^{+/+}$ co-culture model would provide greater insight into the generation of astrocytes from proliferative zones in response to ATG7 loss.

## 8.3 Alternative cause of cell death in *ATG7* related neurological disease

The *ATG7*$^{+/-}$ and *ATG7*$^{-/-}$ co-cultures show a clear caspase-3 mediated cell death at the end of their differentiation, as well as cell cluster growth analysis suggesting cell death from week four of differentiation. The most obvious reason for this cell death would be proteotoxicity resulting from loss of autophagy, especially due to the lack of p62 positive neurons at the end of differentiation, as discussed (**Chapter 4.3.3**). However, an alternative candidate mechanism could be excitotoxicity. Both *ATG7*$^{+/-}$ and *ATG7*$^{-/-}$ cultures demonstrated impaired calcium recovery following glutamate stimulus. Cytotoxicity involves an initial stimulus, like glutamate, and subsequent spike in intracellular calcium and then recovery, which is followed by a second increase in intracellular calcium after a latency period. This second calcium influx is associated with cell death via proapoptotic pathways and neuronal swelling from osmotic potential of increased ion content (Randall & Thayer, 1992; Tymianski et al., 1993; Beck et al., 2003). Both *ATG7*$^{+/-}$ and *ATG7*$^{+/-}$ neural cultures demonstrated impaired calcium

handling, and cell death after four-weeks differentiation, which continued throughout as discussed (**Chapter** Error! Reference source not found.**4.3**)

*In-vitro* action potentials have been described from 7 days after neuronal induction, with others describing action potentials from 3 weeks using similar neuronal induction protocols, demonstrating the variable nature of neuronal maturation in culture (Bullmann et al., 2024; Lam et al., 2017). As for the *ATG7* neural models described in this thesis, functional imaging was only carried out after eight-weeks of differentiation. However, action potentials commencing from week four would provide a mechanism of cell death in the neural model. As transient action potentials start to be generated in the cultures, *ATG7*$^{+/-}$ and *ATG7*$^{-/-}$ neurons undergo excitotoxicity due to inability to remove intracellular calcium, a problem not shared by the wild type model. As these would be transient currents, cell death is restricted to the most frequently firing neurons. This would also explain the lack of neuronal death observed after eight-weeks differentiation. The neurons most susceptible have already undergone apoptosis due to excitotoxicity.

Excitotoxicity would also provide some explanation as to the lack of neuronal cell death in the foetal subject. At 24 weeks post conception, there are active synapses, however in specific regions with synaptic connectivity increasing through development (Sarnat, 2023). For example, cerebellar development continues after birth, with synapses continuing to form postnatally. If excitotoxicity is the central cause of neuronal death, the ability to investigate this would be dependent on the stage of development of the available tissue. The single timepoint and limited tissue available would make this difficult to investigate in the foetal subject. However further work utilising the neuronal model involving calcium imaging at various timepoints through differentiation may aid this work.

## 8.4 Novel disease mechanism for *ATG* related neurological disorders

The p.Arg481Pro subject represents the first reported subject harbouring a single heterozygous variant in *ATG7*. While this may just seem the newest discovery in an expanding cohort of *ATG* patients described in literature, it does not conform with previous findings on genetic manipulation of autophagy.

Decades of work across various model systems have elaborated the intricate molecular regulation and function of autophagy. As part of this work, numerous knockout mouse models of various *ATG* genes have been produced and characterised, including models of *Atg12*, *Atg5* and *Atg7* (Malhotra et al., 2015; Kuma et al., 2004; Komatsu et al., 2005). All three of these global knockout models result in perinatal lethality, with the conclusion that variants in these genes are incompatible with human life. However, recent publications and this thesis describes cases of subjects harbouring bi-allelic variants in *ATG12, ATG5, ATG7, ATG4D and ATG9B* surviving past birth, with some subjects reaching ages towards the population life expectancy (Collier et al., 2021; Kim et al., 2016; Morimoto et al., 2023; Kılıç et al., 2024). This demonstrates a clear disparity between the global knockout mouse approach to modelling autophagy and ATG subjects, suggesting a supplemental or compensatory autophagy pathways in humans which are not present in mice. To observe a phenotype similar to that seen in the subjects, conditional models with CNS specific knockouts are required, which have been generated and studied in the case of Atg5 and Atg7 (Komatsu et al., 2006; Hara et al., 2006b).

In both models, heterozygous *Atg5* and *Atg7* KO mice were used as controls, described in literature as *Atg5*$^{+/flox}$;nestin-*Cre* and *Atg7*$^{+/flox}$;nestin-*Cre* mice, (Hara et al., 2006b; Komatsu et al., 2006). These heterozygous mice are reported as having no disease phenotype, with heterozygous *Atg7* knockout mice having Atg5-Atg12 and LC3-II levels comparable to wild type mice on immunoblots, suggesting loss of a single allele is not damaging to autophagy function. However, in contrast to this, the p.Arg481Pro subject has a clear phenotype, despite being biochemically similar, as described (**Chapter 6.3.1**). The p.Arg481 Pro subject also had ATG5-ATG12 levels comparable to controls, and production of LC3-II in the absence of chemical modulation, even if flux was moderately impaired in the presence of AZD8055 and chloroquine. It is important to note the tissues being investigated in each case, however. The tissue specificity of autophagy must be considered when comparing subject primary fibroblast data and brain homogenates from murine models. It is possible the autophagy impairment is more severe in the more metabolically demanding neural tissues of the p.Arg481Pro subject. However, comparison with the iPSC derived neural model may aid in this comparison.

The iPSC derived *ATG7*$^{+/-}$ knockout neural model also showed normal levels of ATG5-ATG12 conjugate when compared to wild type cultures and LC3-II production in the absence of chemical autophagy modulation, with moderately impaired autophagy flux, similar to p.Arg481Pro primary fibroblasts. The key difference is a lack of p62 accumulation in the *ATG7*$^{+/-}$ neural model, which is observed in the primary fibroblasts of the p.Arg481Pro subject. This may suggest that the p.Arg481Pro variant is having a dominant negative effect not observed in the *ATG7*$^{+/-}$ neural model. This could indicate a novel disease mechanism for core *ATG* related congenital disorders of autophagy. While there is potential for this to be due to a second pathogenic variant not identified in the clinical exome performed for the subject, the attenuated flux and p62 accumulation do point towards the autophagy impairment being central to the p.Arg481Pro subject's pathology.

## 8.5 A novel congenital disorder of autophagy: *ATG12*

Finally, this identification of a novel disease gene reinforces the expanding nature of core autophagy disorders. While a novel disease gene, the neuroradiological findings are remarkably consistent with those reported in *ATG7* and *ATG5* cases (Kim et al., 2016; Collier et al., 2021). A unifying aspect of the various *ATG* cases in existing literature, and this thesis, is cerebellar vermis hypoplasia. In addition to this, the hypoplasia of the corpus callosum observed in S3 of the *ATG12* cohort is also consistent with the *ATG7* and *ATG5* cohorts. It is unclear as to why these areas appear to be most susceptible to damage, but the consistency across the cohort would suggest these areas are more reliant on autophagy during differentiation and development. Included in the common presentations of *ATG* cases is ataxia, a common observation in cases of cerebellar hypoplasia (Millen & Gleeson, 2008; Collier et al., 2021; Kim et al., 2016).

The similarity of patient presentation and the closely related nature of the genes involved would suggest they all share a similar underlying disease mechanism. However, the work in this thesis suggests in the *ATG7* cohort, autophagy impairment may not be the only driving factor of disease pathology. However, *ATG12* does not have similar effects on the cell cycle. It does however play a role in apoptosis, as discussed (**Chapter 7.1.3**). ATG12 plays a role in Bcl-2 mediated cell death, with *ATG12* knockdown resulting in increased cell survival in stressed cells (Radoshevich

et al., 2010; Rubinstein et al., 2011). This increased survival may result in survival of cells under proteotoxic stress which would normally undergo cell death, exaggerating the damage associated cells in a state of proteotoxic stress. While this mechanism would still require the loss of autophagy associated with *ATG12* variants, it would be exaggerated by the non-autophagic role of ATG12. While there is no existing direct link between *ATG12*'s role in apoptosis pathway and disease pathology, the ATG7 data presented in this thesis suggests non-autophagic roles also need to be considered when assessing pathological mechanisms underlying disorders of *ATG* genes.

Further work into the mechanisms underlying *ATG* related neurological disorders will also help in diagnosing and developing treatments for these rare genetic disorders. The similarities between the various *ATG* cohorts, might suggest a generalised autophagy modulation therapy would be effective for the described disorders. However, the involvement of autophagy independent mechanisms might result in these requiring a more specific interventions, such as gene therapy approaches. However, given the clear developmental component in these childhood-onset disorders, further insights are needed to identify intervention points that could offer maximum benefit.

## 8.6 Concluding remarks

This thesis describes a clinically relevant *ATG7* disease model generated by CRISPR/Cas9 genome editing in iPSCs and subsequent neuron-astrocyte differentiation into co-culture. The *ATG7* neural model recapitulated the biochemical phenotype of previously described *ATG7* patients. It also demonstrated altered neural development and differentiation as well impaired calcium handling in functional assays. Complementing this work is the first study on *ATG7* subject's brain tissue which supported the iPSC model work with p62 accumulation in the cerebellar proliferative zone and astrocyte accumulation in the corpus callosum and cortex. Neuron accumulation in the corpus callosum, cerebellum and medulla of the *ATG7* subject tissue also supported the cell model's altered neural differentiation. Additionally, characterisation of the first heterozygous patient harbouring a *de novo* *ATG7* variant demonstrated how different mechanisms of *ATG7* related neurological disease are possible. The novel mechanism associated with the p.Arg481Pro variant is supported by the lack of p62 accumulation in the *ATG7*$^{+/-}$ neural model, which

contrasts to the p.Arg481Pro subject. Finally, this thesis added to the growing number of core autophagy genes, once thought essential to autophagy, that are associated with human disease. This cohort presented with similar neurological phenotypes as other *ATG* disorders, including cerebellar hypoplasia. Biochemical analysis indicated moderately impaired autophagic flux, with variants unable to fully recovery autophagy in yeast complementation models. This cohort demonstrates that there will likely be a growing number of congenital autophagy disorders as research continues and whole exome and whole genome sequencing become more common. The growing number of congenital autophagy disorders highlights the importance of research focussed on tissue specific models of disease. In line with this, the potential non-autophagic role *ATG7* implicated by the iPSC derived model and the foetal p.Ser593Ilefs*fs/p.Gln571* subject described in this thesis show consideration for the non-autophagic function of these proteins is also important.

# 9 References


Abdollahpour, H., Alawi, M., Kortüm, F., Beckstette, M., Seemanova, E., Komárek, V., Rosenberger, G. & Kutsche, K. (2015) 'An AP4B1 frameshift mutation in siblings with intellectual disability and spastic tetraplegia further delineates the AP-4 deficiency syndrome.', *European journal of human genetics : EJHG*, 23(2), pp. 256–9.

Abdollahzadeh, I., Schwarten, M., Gensch, T., Willbold, D. & Weiergräber, O.H. (2017) 'The Atg8 Family of Proteins—Modulating Shape and Functionality of Autophagic Membranes', *Frontiers in Genetics*, 8.

Ábrahám, H., Tornóczky, T., Kosztolányi, G. & Seress, L. (2001) 'Cell formation in the cortical layers of the developing human cerebellum', *International Journal of Developmental Neuroscience*, 19(1), pp. 53–62.

Adzhubei, Ivan A., Schmidt, S., Peshkin, L., Ramensky, V.E., Gerasimova, A., Bork, P., Kondrashov, A.S. & Sunyaev, S.R. (2010) 'A method and server for predicting damaging missense mutations', *Nature Methods 2010 7:4*, 7(4), pp. 248–249.

Adzhubei, Ivan A, Schmidt, S., Peshkin, L., Ramensky, V.E., Gerasimova, A., Bork, P., Kondrashov, A.S. & Sunyaev, S.R. (2010) 'A method and server for predicting damaging missense mutations', *Nature Methods*, 7(4), pp. 248–249.

Agarraberes, F.A., Terlecky, S.R. & Dice, J.F. (1997) 'An Intralysosomal hsp70 Is Required for a Selective Pathway of Lysosomal Protein Degradation', *The Journal of Cell Biology*, 137(4), pp. 825–834.

Agrotis, A., von Chamier, L., Oliver, H., Kiso, K., Singh, T. & Ketteler, R. (2019a) 'Human ATG4 autophagy proteases counteract attachment of ubiquitin-like LC3/GABARAP proteins to other cellular proteins', *Journal of Biological Chemistry*, 294(34), pp. 12610–12621.

Agrotis, A., von Chamier, L., Oliver, H., Kiso, K., Singh, T. & Ketteler, R. (2019b) 'Human ATG4 autophagy proteases counteract attachment of ubiquitin-like LC3/GABARAP proteins to other cellular proteins', *Journal of Biological Chemistry*, 294(34), pp. 12610–12621.

Airaksinen, M.S. & Saarma, M. (2002) 'The GDNF family: Signalling, biological functions and therapeutic value', *Nature Reviews Neuroscience 2002 3:5*, 3(5), pp. 383–394.

Alegre-Abarrategui, J., Christian, H., Lufino, M.M.P., Mutihac, R., Venda, L.L., Ansorge, O. & Wade-Martins, R. (2009) 'LRRK2 regulates autophagic activity and localizes to specific membrane microdomains in a novel human genomic reporter cellular model.', *Human molecular genetics*, 18(21), pp. 4022–34.

Allen, G.F.G., Toth, R., James, J. & Ganley, I.G. (2013) 'Loss of iron triggers PINK1/Parkin-independent mitophagy', *EMBO reports*, 14(12), pp. 1127–1135.

Almeida, S., Gascon, E., Tran, H., Chou, H.J., Gendron, T.F., DeGroot, S., Tapper, A.R., Sellier, C., Charlet-Berguerand, N., Karydas, A., Seeley, W.W., Boxer, A.L., Petrucelli, L., Miller, B.L. & Gao, F.-B. (2013) 'Modeling key pathological features of frontotemporal dementia with C9ORF72 repeat expansion in iPSC-derived human neurons', *Acta Neuropathologica*, 126(3), pp. 385–399.

Altamimi, T.R., Chowdhury, B., Singh, K.K., Zhang, L., Mahmood, M.U., Pan, Y., Quan, A., Teoh, H., Verma, S. & Lopaschuk, G.D. (2019) 'A novel role of endothelial autophagy as a regulator of myocardial fatty acid oxidation', *The Journal of Thoracic and Cardiovascular Surgery*, 157(1), pp. 185–193.

Alzheimer's Association (2019) '2019 Alzheimer's disease facts and figures', *Alzheimer's & Dementia*, 15(3), pp. 321–387.

Amick, J., Tharkeshwar, A.K., Talaia, G. & Ferguson, S.M. (2020) 'PQLC2 recruits the C9orf72 complex to lysosomes in response to cationic amino acid starvation', *Journal of Cell Biology*, 219(1), .

Amps, K., Andrews, P.W., Anyfantis, G., Armstrong, L., Avery, S., Baharvand, H., Baker, J., Baker, D., Munoz, M.B., Beil, S., Benvenisty, N., Ben-Yosef, D., Biancotti, J.C., Bosman, A., Brena, R.M., Brison, D., Caisander, G., Camarasa, M. V., Chen, J., et al. (2011) 'Screening ethnically diverse human embryonic stem cells identifies a chromosome 20 minimal amplicon conferring growth advantage', *Nature Biotechnology 2011 29:12*, 29(12), pp. 1132–1144.

Arias, E., Koga, H., Diaz, A., Mocholi, E., Patel, B. & Cuervo, A.M. (2015) 'Lysosomal mTORC2/PHLPP1/Akt Regulate Chaperone-Mediated Autophagy', *Molecular Cell*, 59(2), pp. 270–284.

Ashford, T.P. & Porter, K.R. (1962) 'CYTOPLASMIC COMPONENTS IN HEPATIC CELL LYSOSOMES', *Journal of Cell Biology*, 12(1), pp. 198–202.

Ashkenazi, A., Bento, C.F., Ricketts, T., Vicinanza, M., Siddiqi, F., Pavel, M., Squitieri, F., Hardenberg, M.C., Imarisio, S., Menzies, F.M. & Rubinsztein, D.C. (2017) 'Polyglutamine tracts regulate beclin 1-dependent autophagy', *Nature*, 545(7652), pp. 108–111.

Auton, A., Abecasis, G.R., Altshuler, D.M., Durbin, R.M., Abecasis, G.R., Bentley, D.R., Chakravarti, A., Clark, A.G., Donnelly, P., Eichler, E.E., Flicek, P., Gabriel, S.B., Gibbs, R.A., Green, E.D., Hurles, M.E., Knoppers, B.M., Korbel, J.O.,

Lander, E.S., Lee, C., et al. (2015) ‘A global reference for human genetic variation’, *Nature*, 526(7571), pp. 68–74.

Avery, S., Hirst, A.J., Baker, D., Lim, C.Y., Alagaratnam, S., Skotheim, R.I., Lothe, R.A., Pera, M.F., Colman, A., Robson, P., Andrews, P.W. & Knowles, B.B. (2013) ‘BCL-XL mediates the strong selective advantage of a 20q11.21 amplification commonly found in human embryonic stem cell cultures’, *Stem cell reports*, 1(5), pp. 379–386.

Axe, E.L., Walker, S.A., Manifava, M., Chandra, P., Roderick, H.L., Habermann, A., Griffiths, G. & Ktistakis, N.T. (2008) ‘Autophagosome formation from membrane compartments enriched in phosphatidylinositol 3-phosphate and dynamically connected to the endoplasmic reticulum’, *The Journal of Cell Biology*, 182(4), pp. 685–701.

Ban, B.-K., Jun, M.-H., Ryu, H.-H., Jang, D.-J., Ahmad, S.T. & Lee, J.-A. (2013) ‘Autophagy Negatively Regulates Early Axon Growth in Cortical Neurons’, *Molecular and Cellular Biology*, 33(19), pp. 3907–3919.

Bandyopadhyay, U., Kaushik, S., Varticovski, L. & Cuervo, A.M. (2008) ‘The Chaperone-Mediated Autophagy Receptor Organizes in Dynamic Protein Complexes at the Lysosomal Membrane’, *Molecular and Cellular Biology*, 28(18), pp. 5747–5763.

Barth, S., Glick, D. & Macleod, K.F. (2010) ‘Autophagy: assays and artifacts’, *The Journal of Pathology*, 221(2), pp. 117–124.

Bateman, A., Martin, M.-J., Orchard, S., Magrane, M., Agivetova, R., Ahmad, S., Alpi, E., Bowler-Barnett, E.H., Britto, R., Bursteinas, B., Bye-A-Jee, H., Coetzee, R., Cukura, A., Da Silva, A., Denny, P., Dogan, T., Ebenezer, T., Fan, J., Castro, L.G., et al. (2021) ‘UniProt: the universal protein knowledgebase in 2021’, *Nucleic Acids Research*, 49(D1), pp. D480–D489.

Beck, J., Lenart, B., Kintner, D.B. & Sun, D. (2003) ‘Na-K-Cl Cotransporter Contributes to Glutamate-Mediated Excitotoxicity’, *The Journal of Neuroscience*, 23(12), pp. 5061–5068.

Benkirane, M., Marelli, C., Guissart, C., Roubertie, A., Ollagnon, E., Choumert, A., Fluchère, F., Magne, F.O., Halleb, Y., Renaud, M., Larrieu, L., Baux, D., Patat, O., Bousquet, I., Ravel, J.-M., Cuntz-Shadfar, D., Sarret, C., Ayrignac, X., Rolland, A., et al. (2021) ‘High rate of hypomorphic variants as the cause of inherited ataxia and related diseases: study of a cohort of 366 families’, *Genetics in Medicine*, 23(11), pp. 2160–2170.

Bezzi, P., Carmignoto, G., Pasti, L., Vesce, S., Rossi, D., Rizzini, B.L., Pozzan, T. & Volterra, A. (1998) ‘Prostaglandins stimulate calcium-dependent glutamate release in astrocytes’, *Nature*, 391(6664), pp. 281–285.

Bezzi, P., Gundersen, V., Galbete, J.L., Seifert, G., Steinhäuser, C., Pilati, E. & Volterra, A. (2004) ‘Astrocytes contain a vesicular compartment that is competent for regulated exocytosis of glutamate’, *Nature Neuroscience*, 7(6), pp. 613–620.

Bhaskara, R.M., Grumati, P., Garcia-Pardo, J., Kalayil, S., Covarrubias-Pinto, A., Chen, W., Kudryashev, M., Dikic, I. & Hummer, G. (2019) ‘Curvature induction and membrane remodeling by FAM134B reticulon homology domain assist selective ER-phagy.’, *Nature communications*, 10(1), p. 2370.

Bhoj, E.J., Li, D., Harr, M., Edvardson, S., Elpeleg, O., Chisholm, E., Juusola, J., Douglas, G., Guillen Sacoto, M.J., Siquier-Pernet, K., Saadi, A., Bole-Feysot, C., Nitschke, P., Narravula, A., Walke, M., Horner, M.B., Day-Salvatore, D.-L., Jayakar, P., Vergano, S.A.S., et al. (2016) ‘Mutations in TBCK, Encoding TBC1-Domain-Containing Kinase, Lead to a Recognizable Syndrome of Intellectual Disability and Hypotonia.’, *American journal of human genetics*, 98(4), pp. 782–8.

Bjørkøy, G., Lamark, T., Brech, A., Outzen, H., Perander, M., Øvervatn, A., Stenmark, H. & Johansen, T. (2005) ‘p62/SQSTM1 forms protein aggregates degraded by autophagy and has a protective effect on huntingtin-induced cell death’, *The Journal of Cell Biology*, 171(4), pp. 603–614.

Bolshakov, V.Y. & Siegelbaum, S.A. (1994) ‘Postsynaptic Induction and Presynaptic Expression of Hippocampal Long-Term Depression’, *Science*, 264(5162), pp. 1148–1152.

Boukhris, A., Stevanin, G., Feki, I., Denora, P., Elleuch, N., Miladi, M.I., Goizet, C., Truchetto, J., Belal, S., Brice, A. & Mhiri, C. (2009) ‘Tunisian hereditary spastic paraplegias: clinical variability supported by genetic heterogeneity.’, *Clinical genetics*, 75(6), pp. 527–36.

Boya, P., Codogno, P. & Rodriguez-Muela, N. (2018) ‘Autophagy in stem cells: Repair, remodelling and metabolic reprogramming’, *Development (Cambridge)*, 145(4), .

Braak, H., Sandmann-Keil, D., Gai, W. & Braak, E. (1999) ‘Extensive axonal Lewy neurites in Parkinson’s disease: a novel pathological feature revealed by α-synuclein immunocytochemistry’, *Neuroscience Letters*, 265(1), pp. 67–69.

Brenner, D., Sieverding, K., Srinidhi, J., Zellner, S., Secker, C., Yilmaz, R., Dyckow, J., Amr, S., Ponomarenko, A., Tunaboylu, E., Douahem, Y., Schlag, J.S., Rodríguez Martínez, L., Kislinger, G., Niemann, C., Nalbach, K., Ruf, W.P., Uhl, J., Hollenbeck, J., et al. (2024) ‘A TBK1 variant causes autophagolysosomal and motoneuron pathology without neuroinflammation in mice’, *Journal of Experimental Medicine*, 221(5), .

Brini, M., Calì, T., Ottolini, D. & Carafoli, E. (2014) ‘Neuronal calcium signaling: function and dysfunction’, *Cellular and Molecular Life Sciences*, 71(15), pp. 2787–2814.

Budanov, A. V. & Karin, M. (2008) ‘p53 Target Genes Sestrin1 and Sestrin2 Connect Genotoxic Stress and mTOR Signaling’, *Cell*, 134(3), pp. 451–460.

Budisantoso, T., Harada, H., Kamasawa, N., Fukazawa, Y., Shigemoto, R. & Matsui, K. (2013) ‘Evaluation of glutamate concentration transient in the synaptic cleft of the rat calyx of Held’, *The Journal of Physiology*, 591(1), pp. 219–239.

Bullmann, T., Kaas, T., Ritzau-Jost, A., Whner, A., Kirmann, T., Rizalar, F.S., Holzer, M., Nerlich, J., Puchkov, D., Geis, C., Eilers, J., Kittel, R.J., Arendt, T., Haucke, V. & Hallermann, S. (2024) ‘Human iPSC-Derived Neurons with Reliable Synapses and Large Presynaptic Action Potentials’, *The Journal of Neuroscience*, 44(24), p. e0971232024.

Bunker, E.N., Le Guerroué, F., Wang, C., Strub, M., Werner, A., Tjandra, N. & Youle, R.J. (2023) ‘Nix interacts with WIPI2 to induce mitophagy.’, *The EMBO journal*, 42(22), p. e113491.

Bystron, I., Blakemore, C. & Rakic, P. (2008) ‘Development of the human cerebral cortex: Boulder Committee revisited’, *Nature Reviews Neuroscience*, 9(2), pp. 110–122.

Cadwell, K., Patel, K.K., Komatsu, M., Virgin, H.W. & Stappenbeck, T.S. (2009) ‘A common role for Atg16L1, Atg5 and Atg7 in small intestinal Paneth cells and Crohn disease.’, *Autophagy*, 5(2), pp. 250–2.

Cai, Q., Lu, L., Tian, J.-H., Zhu, Y.-B., Qiao, H. & Sheng, Z.-H. (2010) ‘Snapin-Regulated Late Endosomal Transport Is Critical for Efficient Autophagy-Lysosomal Function in Neurons’, *Neuron*, 68(1), pp. 73–86.

Calegari, F. & Huttner, W.B. (2003) ‘An inhibition of cyclin-dependent kinases that lengthens, but does not arrest, neuroepithelial cell cycle induces premature neurogenesis’, *Journal of Cell Science*, 116(24), pp. 4947–4955.

Cao, Y., Cai, J., Li, X., Yuan, N. & Zhang, S. (2016) ‘Autophagy governs erythroid differentiation both in vitro and in vivo’, *Hematology*, 21(4), pp. 225–233.

Cao, Yu, Zheng, J., Wan, H., Sun, Y., Fu, S., Liu, S., He, B., Cai, G., Cao, Yang, Huang, H., Li, Q., Ma, Y., Chen, S., Wang, F. & Jiang, H. (2023) ‘A mitochondrial SCF-FBXL4 ubiquitin E3 ligase complex degrades BNIP3 and NIX to restrain mitophagy and prevent mitochondrial disease.’, *The EMBO journal*, 42(13), p. e113033.

Carroll, B., Otten, E.G., Manni, D., Stefanatos, R., Menzies, F.M., Smith, G.R., Jurk, D., Kenneth, N., Wilkinson, S., Passos, J.F., Attems, J., Veal, E.A., Teyssou, E., Seilhean, D., Millecamps, S., Eskelinen, E.-L., Bronowska, A.K., Rubinsztein,

D.C., Sanz, A., et al. (2018) ‘Oxidation of SQSTM1/p62 mediates the link between redox state and protein homeostasis’, *Nature Communications*, 9(1), p. 256.

Casali, C., Valente, E.M., Bertini, E., Montagna, G., Criscuolo, C., De Michele, G., Villanova, M., Damiano, M., Pierallini, A., Brancati, F., Scarano, V., Tessa, A., Cricchi, F., Grieco, G.S., Muglia, M., Carella, M., Martini, B., Rossi, A., Amabile, G.A., et al. (2004) ‘Clinical and genetic studies in hereditary spastic paraplegia with thin corpus callosum.’, *Neurology*, 62(2), pp. 262–8.

Chambers, S.M., Fasano, C.A., Papapetrou, E.P., Tomishima, M., Sadelain, M. & Studer, L. (2009) ‘Highly efficient neural conversion of human ES and iPS cells by dual inhibition of SMAD signaling’, *Nature Biotechnology 2009 27:3*, 27(3), pp. 275–280.

Chavis, P., Fagni, L., Lansman, J.B. & Bockaert, J. (1996) ‘Functional coupling between ryanodine receptors and L-type calcium channels in neurons’, *Nature*, 382(6593), pp. 719–722.

Chen, G., Hou, Z., Gulbranson, D.R. & Thomson, J.A. (2010) ‘Actin-Myosin Contractility Is Responsible for the Reduced Viability of Dissociated Human Embryonic Stem Cells’, *Cell Stem Cell*, 7(2), pp. 240–248.

Chen, S., Francioli, L.C., Goodrich, J.K., Collins, R.L., Kanai, M., Wang, Q., Alföldi, J., Watts, N.A., Vittal, C., Gauthier, L.D., Poterba, T., Wilson, M.W., Tarasova, Y., Phu, W., Grant, R., Yohannes, M.T., Koenig, Z., Farjoun, Y., Banks, E., et al. (2023) ‘A genomic mutational constraint map using variation in 76,156 human genomes’, *Nature 2023 625:7993*, 625(7993), pp. 92–100.

Chen, T., Shen, L., Yu, J., Wan, H., Guo, A., Chen, J., Long, Y., Zhao, J. & Pei, G. (2011) ‘Rapamycin and other longevity-promoting compounds enhance the generation of mouse induced pluripotent stem cells’, *Aging Cell*, 10(5), pp. 908–911.

Chen, Ying, Li, Qi, Li, Qihang, Xing, S., Liu, Yang, Liu, Yijun, Chen, Yao, Liu, W., Feng, F. & Sun, H. (2020) ‘p62/SQSTM1, a Central but Unexploited Target: Advances in Its Physiological/Pathogenic Functions and Small Molecular Modulators’, *Journal of Medicinal Chemistry*, 63(18), pp. 10135–10157.

Chiang, H.-L., Terlecky, S.R., Plant, C.P. & Dice, J.F. (1989) ‘A Role for a 70-Kilodalton Heat Shock Protein in Lysosomal Degradation of Intracellular Proteins’, *Science*, 246(4928), pp. 382–385.

Chiduza, G.N., Garza-Garcia, A., Almacellas, E., De Tito, S., Pye, V.E., van Vliet, A.R., Cherepanov, P. & Tooze, S.A. (2024) ‘ATG9B is a tissue-specific homotrimeric lipid scramblase that can compensate for ATG9A’, *Autophagy*, 20(3), pp. 557–576.

Chong, J.X., Caputo, V., Phelps, I.G., Stella, L., Worgan, L., Dempsey, J.C., Nguyen, A., Leuzzi, V., Webster, R., Pizzuti, A., Marvin, C.T., Ishak, G.E., Ardern-Holmes, S., Richmond, Z., University of Washington Center for Mendelian Genomics, Bamshad, M.J., Ortiz-Gonzalez, X.R., Tartaglia, M., Chopra, M., et al. (2016) 'Recessive Inactivating Mutations in TBCK, Encoding a Rab GTPase-Activating Protein, Cause Severe Infantile Syndromic Encephalopathy.', *American journal of human genetics*, 98(4), pp. 772–81.

Chongtham, M.C., Butto, T., Mungikar, K., Gerber, S. & Winter, J. (2021) 'INTACT vs. FANS for Cell-Type-Specific Nuclei Sorting: A Comprehensive Qualitative and Quantitative Comparison.', *International journal of molecular sciences*, 22(10), .

Choubey, V., Safiulina, D., Vaarmann, A., Cagalinec, M., Wareski, P., Kuum, M., Zharkovsky, A. & Kaasik, A. (2011) 'Mutant A53T α-Synuclein Induces Neuronal Death by Increasing Mitochondrial Autophagy', *Journal of Biological Chemistry*, 286(12), pp. 10814–10824.

Choudhary, V., Ojha, N., Golden, A. & Prinz, W.A. (2015) 'A conserved family of proteins facilitates nascent lipid droplet budding from the ER', *Journal of Cell Biology*, 211(2), pp. 261–271.

Chung, W.-S., Allen, N.J. & Eroglu, C. (2015) 'Astrocytes Control Synapse Formation, Function, and Elimination', *Cold Spring Harbor Perspectives in Biology*, 7(9), p. a020370.

Cinque, L., Forrester, A., Bartolomeo, R., Svelto, M., Venditti, R., Montefusco, S., Polishchuk, E., Nusco, E., Rossi, A., Medina, D.L., Polishchuk, R., De Matteis, M.A. & Settembre, C. (2015) 'FGF signalling regulates bone growth through autophagy', *Nature*, 528(7581), pp. 272–275.

Cinque, L., De Leonibus, C., Iavazzo, M., Krahmer, N., Intartaglia, D., Salierno, F.G., De Cegli, R., Di Malta, C., Svelto, M., Lanzara, C., Maddaluno, M., Wanderlingh, L.G., Huebner, A.K., Cesana, M., Bonn, F., Polishchuk, E., Hübner, C.A., Conte, I., Dikic, I., et al. (2020) 'MiT/TFE factors control ER-phagy via transcriptional regulation of FAM134B.', *The EMBO journal*, 39(17), p. e105696.

Clarke, L.E. & Barres, B.A. (2013a) 'Emerging roles of astrocytes in neural circuit development', *Nat Rev Neurosci*, 14(5), pp. 311–321.

Clarke, L.E. & Barres, B.A. (2013b) 'Emerging roles of astrocytes in neural circuit development', *Nature Reviews Neuroscience*, 14(5), pp. 311–321.

Clements, J.D., Lester, R.A.J., Tong, G., Jahr, C.E. & Westbrook, G.L. (1992) 'The Time Course of Glutamate in the Synaptic Cleft', *Science*, 258(5087), pp. 1498–1501.

Collier, J.J., Guissart, C., Oláhová, M., Sasorith, S., Piron-Prunier, F., Suomi, F., Zhang, D., Martinez-Lopez, N., Leboucq, N., Bahr, A., Azzarello-Burri, S., Reich,

S., Schöls, L., Polvikoski, T.M., Meyer, P., Larrieu, L., Schaefer, A.M., Alsaif, H.S., Alyamani, S., et al. (2021) ‘Developmental Consequences of Defective ATG7-Mediated Autophagy in Humans’, *New England Journal of Medicine*, 384(25), pp. 2406–2417.

Coupé, B., Ishii, Y., Dietrich, M.O., Komatsu, M., Horvath, T.L. & Bouret, S.G. (2012) ‘Loss of Autophagy in Pro-opiomelanocortin Neurons Perturbs Axon Growth and Causes Metabolic Dysregulation’, *Cell Metabolism*, 15(2), pp. 247–255.

Courchet, J., Lewis, T.L., Lee, S., Courchet, V., Liou, D.-Y., Aizawa, S. & Polleux, F. (2013) ‘Terminal Axon Branching Is Regulated by the LKB1-NUAK1 Kinase Pathway via Presynaptic Mitochondrial Capture’, *Cell*, 153(7), pp. 1510–1525.

Covone, A.E., Fiorillo, C., Acquaviva, M., Trucco, F., Morana, G., Ravazzolo, R. & Minetti, C. (2016) ‘WES in a family trio suggests involvement of TECPR2 in a complex form of progressive motor neuron disease.’, *Clinical genetics*, 90(2), pp. 182–5.

Cuervo, A.M. & Dice, J.F. (1996) ‘A Receptor for the Selective Uptake and Degradation of Proteins by Lysosomes’, *Science*, 273(5274), pp. 501–503.

Cullup, T., Kho, A.L., Dionisi-Vici, C., Brandmeier, B., Smith, F., Urry, Z., Simpson, M.A., Yau, S., Bertini, E., McClelland, V., Al-Owain, M., Koelker, S., Koerner, C., Hoffmann, G.F., Wijburg, F.A., ten Hoedt, A.E., Rogers, R.C., Manchester, D., Miyata, R., et al. (2013) ‘Recessive mutations in EPG5 cause Vici syndrome, a multisystem disorder with defective autophagy.’, *Nature genetics*, 45(1), pp. 83–7.

Cunha, L.D., Yang, M., Carter, R., Guy, C., Harris, L., Crawford, J.C., Quarato, G., Boada-Romero, E., Kalkavan, H., Johnson, M.D.L., Natarajan, S., Turnis, M.E., Finkelstein, D., Opferman, J.T., Gawad, C. & Green, D.R. (2018) ‘LC3-Associated Phagocytosis in Myeloid Cells Promotes Tumor Immune Tolerance’, *Cell*, 175(2), pp. 429-441.e16.

Deas, E., Plun-Favreau, H., Gandhi, S., Desmond, H., Kjaer, S., Loh, S.H.Y., Renton, A.E.M., Harvey, R.J., Whitworth, A.J., Martins, L.M., Abramov, A.Y. & Wood, N.W. (2011) ‘PINK1 cleavage at position A103 by the mitochondrial protease PARL’, *Human Molecular Genetics*, 20(5), pp. 867–879.

DeLuca, H.F. & Engstrom, G.W. (1961) ‘CALCIUM UPTAKE BY RAT KIDNEY MITOCHONDRIA’, *Proceedings of the National Academy of Sciences*, 47(11), pp. 1744–1750.

DePristo, M.A., Banks, E., Poplin, R., Garimella, K. V, Maguire, J.R., Hartl, C., Philippakis, A.A., del Angel, G., Rivas, M.A., Hanna, M., McKenna, A., Fennell, T.J., Kernytsky, A.M., Sivachenko, A.Y., Cibulskis, K., Gabriel, S.B., Altshuler, D. & Daly, M.J. (2011) ‘A framework for variation discovery and genotyping using next-generation DNA sequencing data’, *Nature Genetics*, 43(5), pp. 491–498.

Derynck, R. & Zhang, Y.E. (2003) ‘Smad-dependent and Smad-independent pathways in TGF-β family signalling’, *Nature 2003 425:6958*, 425(6958), pp. 577–584.

DeYoung, M.P., Horak, P., Sofer, A., Sgroi, D. & Ellisen, L.W. (2008) ‘Hypoxia regulates TSC1/2-mTOR signaling and tumor suppression through REDD1-mediated 14-3-3 shuttling.’, *Genes & development*, 22(2), pp. 239–51.

Diao, J., Liu, R., Rong, Y., Zhao, M., Zhang, J., Lai, Y., Zhou, Q., Wilz, L.M., Li, J., Vivona, S., Pfuetzner, R.A., Brunger, A.T. & Zhong, Q. (2015) ‘ATG14 promotes membrane tethering and fusion of autophagosomes to endolysosomes’, *Nature*, 520(7548), pp. 563–566.

DiFiglia, M., Sapp, E., Chase, K.O., Davies, S.W., Bates, G.P., Vonsattel, J.P. & Aronin, N. (1997) ‘Aggregation of Huntingtin in Neuronal Intranuclear Inclusions and Dystrophic Neurites in Brain’, *Science*, 277(5334), pp. 1990–1993.

Diniz, L.P., Almeida, J.C., Tortelli, V., Vargas Lopes, C., Setti-Perdigão, P., Stipursky, J., Kahn, S.A., Romão, L.F., de Miranda, J., Alves-Leon, S.V., de Souza, J.M., Castro, N.G., Panizzutti, R. & Gomes, F.C.A. (2012) ‘Astrocyte-induced Synaptogenesis Is Mediated by Transforming Growth Factor β Signaling through Modulation of d-Serine Levels in Cerebral Cortex Neurons’, *Journal of Biological Chemistry*, 287(49), pp. 41432–41445.

Dionisi Vici, C., Sabetta, G., Gambarara, M., Vigevano, F., Bertini, E., Boldrini, R., Parisi, S.G., Quinti, I., Aiuti, F. & Fiorilli, M. (1988) ‘Agenesis of the corpus callosum, combined immunodeficiency, bilateral cataract, and hypopigmentation in two brothers.’, *American journal of medical genetics*, 29(1), pp. 1–8.

Dooley, H.C., Razi, M., Polson, H.E.J., Girardin, S.E., Wilson, M.I. & Tooze, S.A. (2014a) ‘WIPI2 Links LC3 Conjugation with PI3P, Autophagosome Formation, and Pathogen Clearance by Recruiting Atg12–5-16L1’, *Molecular Cell*, 55(2), pp. 238–252.

Dubois, J., Benders, M., Borradori-Tolsa, C., Cachia, A., Lazeyras, F., Ha-Vinh Leuchter, R., Sizonenko, S. V., Warfield, S.K., Mangin, J.F. & Hüppi, P.S. (2008) ‘Primary cortical folding in the human newborn: an early marker of later functional development’, *Brain*, 131(8), pp. 2028–2041.

Dubois, J, Benders, M., Cachia, A., Lazeyras, F., Ha-Vinh Leuchter, R., Sizonenko, S. V., Borradori-Tolsa, C., Mangin, J.F. & Huppi, P.S. (2008) ‘Mapping the Early Cortical Folding Process in the Preterm Newborn Brain’, *Cerebral Cortex*, 18(6), pp. 1444–1454.

Dunlop, E.A., Hunt, D.K., Acosta-Jaquez, H.A., Fingar, D.C. & Tee, A.R. (2011) ‘ULK1 inhibits mTORC1 signaling, promotes multisite Raptor phosphorylation and hinders substrate binding’, *Autophagy*, 7(7), pp. 737–747.

Durgan, J., Lystad, A.H., Sloan, K., Carlsson, S.R., Wilson, M.I., Marcassa, E., Ulferts, R., Webster, J., Lopez-Clavijo, A.F., Wakelam, M.J., Beale, R., Simonsen, A., Oxley, D. & Florey, O. (2021) 'Non-canonical autophagy drives alternative ATG8 conjugation to phosphatidylserine', *Molecular Cell*, 81(9), pp. 2031-2040.e8.

Duyao, M., Ambrose, C., Myers, R., Novelletto, A., Persichetti, F., Frontali, M., Folstein, S., Ross, C., Franz, M., Abbott, M., Gray, J., Conneally, P., Young, A., Penney, J., Hollingsworth, Z., Shoulson, I., Lazzarini, A., Falek, A., Koroshetz, W., et al. (1993) 'Trinucleotide repeat length instability and age of onset in Huntington's disease', *Nature Genetics*, 4(4), pp. 387–392.

Duyckaerts, C., Delatour, B. & Potier, M.-C. (2009) 'Classification and basic pathology of Alzheimer disease', *Acta Neuropathologica*, 118(1), pp. 5–36.

Ebato, C., Uchida, T., Arakawa, M., Komatsu, M., Ueno, T., Komiya, K., Azuma, K., Hirose, T., Tanaka, K., Kominami, E., Kawamori, R., Fujitani, Y. & Watada, H. (2008) 'Autophagy Is Important in Islet Homeostasis and Compensatory Increase of Beta Cell Mass in Response to High-Fat Diet', *Cell Metabolism*, 8(4), pp. 325–332.

Edlich, F., Banerjee, S., Suzuki, M., Cleland, M.M., Arnoult, D., Wang, C., Neutzner, A., Tjandra, N. & Youle, R.J. (2011) 'Bcl-xL retrotranslocates Bax from the mitochondria into the cytosol', *Cell*, 145(1), p. 104.

Eguchi, T., Sakurai, M., Wang, Y., Saito, C., Yoshii, G., Wileman, T., Mizushima, N., Kuwahara, T. & Iwatsubo, T. (2024) 'The V-ATPase–ATG16L1 axis recruits LRRK2 to facilitate the lysosomal stress response', *Journal of Cell Biology*, 223(3), .

Elcocks, H., Brazel, A.J., McCarron, K.R., Kaulich, M., Husnjak, K., Mortiboys, H., Clague, M.J. & Urbé, S. (2023) 'FBXL4 ubiquitin ligase deficiency promotes mitophagy by elevating NIX levels.', *The EMBO journal*, 42(13), p. e112799.

Elleuch, N., Bouslam, N., Hanein, S., Lossos, A., Hamri, A., Klebe, S., Meiner, V., Birouk, N., Lerer, I., Grid, D., Bacq, D., Tazir, M., Zelenika, D., Argov, Z., Durr, A., Yahyaoui, M., Benomar, A., Brice, A. & Stevanin, G. (2007) 'Refinement of the SPG15 candidate interval and phenotypic heterogeneity in three large Arab families.', *Neurogenetics*, 8(4), pp. 307–15.

Engedal, N., Luhr, M., Szalai, P. & Seglen, P.O. (2019) 'Measurement of bulk autophagy by a cargo sequestration assay', in *Methods in Molecular Biology*. [Online]. Humana Press Inc. pp. 307–313.

Evans, M.J. & Kaufman, M.H. (1981) 'Establishment in culture of pluripotential cells from mouse embryos', *Nature 1981 292:5819*, 292(5819), pp. 154–156.

Evans, R., O'Neill, M., Pritzel, A., Antropova, N., Senior, A., Green, T., Žídek, A., Bates, R., Blackwell, S., Yim, J., Ronneberger, O., Bodenstein, S., Zielinski, M., Bridgland, A., Potapenko, A., Cowie, A., Tunyasuvunakool, K., Jain, R., Clancy, E., et al. (2022) 'Protein complex prediction with AlphaFold-Multimer', *bioRxiv*,

Fader, C.M., Sánchez, D.G., Mestre, M.B. & Colombo, M.I. (2009) 'TI-VAMP/VAMP7 and VAMP3/cellubrevin: two v-SNARE proteins involved in specific steps of the autophagy/multivesicular body pathways', *Biochimica et Biophysica Acta (BBA) - Molecular Cell Research*, 1793(12), pp. 1901–1916.

Fadok, V.A., Bratton, D.L., Konowal, A., Freed, P.W., Westcott, J.Y. & Henson, P.M. (1998) 'Macrophages that have ingested apoptotic cells in vitro inhibit proinflammatory cytokine production through autocrine/paracrine mechanisms involving TGF-beta, PGE2, and PAF.', *Journal of Clinical Investigation*, 101(4), pp. 890–898.

Fan, W., Nassiri, A. & Zhong, Q. (2011) 'Autophagosome targeting and membrane curvature sensing by Barkor/Atg14(L)', *Proceedings of the National Academy of Sciences*, 108(19), pp. 7769–7774.

Filimonenko, M., Isakson, P., Finley, K.D., Anderson, M., Jeong, H., Melia, T.J., Bartlett, B.J., Myers, K.M., Birkeland, H.C.G., Lamark, T., Krainc, D., Brech, A., Stenmark, H., Simonsen, A. & Yamamoto, A. (2010) 'The selective macroautophagic degradation of aggregated proteins requires the PI3P-binding protein Alfy.', *Molecular cell*, 38(2), pp. 265–79.

Fischer, T.D., Wang, C., Padman, B.S., Lazarou, M. & Youle, R.J. (2020) 'STING induces LC3B lipidation onto single-membrane vesicles via the V-ATPase and ATG16L1-WD40 domain', *Journal of Cell Biology*, 219(12), .

Fleming, A., Bourdenx, M., Fujimaki, M., Karabiyik, C., Krause, G.J., Lopez, A., Martín-Segura, A., Puri, C., Scrivo, A., Skidmore, J., Son, S.M., Stamatakou, E., Wrobel, L., Zhu, Y., Cuervo, A.M. & Rubinsztein, D.C. (2022) 'The different autophagy degradation pathways and neurodegeneration', *Neuron*, 110(6), pp. 935–966.

Florey, O., Gammoh, N., Kim, S.E., Jiang, X. & Overholtzer, M. (2015) 'V-ATPase and osmotic imbalances activate endolysosomal LC3 lipidation', *Autophagy*, 11(1), pp. 88–99.

Forrester, A., De Leonibus, C., Grumati, P., Fasana, E., Piemontese, M., Staiano, L., Fregno, I., Raimondi, A., Marazza, A., Bruno, G., Iavazzo, M., Intartaglia, D., Seczynska, M., van Anken, E., Conte, I., De Matteis, M.A., Dikic, I., Molinari, M. & Settembre, C. (2019) 'A selective ER-phagy exerts procollagen quality control via a Calnexin-FAM134B complex.', *The EMBO journal*, 38(2), .

Franco, S.J., Martinez-Garay, I., Gil-Sanz, C., Harkins-Perry, S.R. & Müller, U. (2011) ‘Reelin Regulates Cadherin Function via Dab1/Rap1 to Control Neuronal Migration and Lamination in the Neocortex’, *Neuron*, 69(3), pp. 482–497.

Frank, M., Duvezin-Caubet, S., Koob, S., Occhipinti, A., Jagasia, R., Petcherski, A., Ruonala, M.O., Priault, M., Salin, B. & Reichert, A.S. (2012) ‘Mitophagy is triggered by mild oxidative stress in a mitochondrial fission dependent manner’, *Biochimica et Biophysica Acta (BBA) - Molecular Cell Research*, 1823(12), pp. 2297–2310.

Fu, S., Yang, L., Li, P., Hofmann, O., Dicker, L., Hide, W., Lin, X., Watkins, S.M., Ivanov, A.R. & Hotamisligil, G.S. (2011) ‘Aberrant lipid metabolism disrupts calcium homeostasis causing liver endoplasmic reticulum stress in obesity’, *Nature*, 473(7348), pp. 528–531.

Fujikake, N., Shin, M. & Shimizu, S. (2018) ‘Association Between Autophagy and Neurodegenerative Diseases’, *Frontiers in Neuroscience*, 12.

Fujioka, Y., Noda, N.N., Fujii, K., Yoshimoto, K., Ohsumi, Y. & Inagaki, F. (2008) ‘In vitro reconstitution of plant Atg8 and Atg12 conjugation systems essential for autophagy’, *Journal of Biological Chemistry*, 283(4), pp. 1921–1928.

Fujishima, Y., Nishiumi, S., Masuda, A., Inoue, J., Nguyen, N.M.T., Irino, Y., Komatsu, M., Tanaka, K., Kutsumi, H., Azuma, T. & Yoshida, M. (2011) ‘Autophagy in the intestinal epithelium reduces endotoxin-induced inflammatory responses by inhibiting NF-κB activation’, *Archives of Biochemistry and Biophysics*, 506(2), pp. 223–235.

Fujita, N., Itoh, T., Omori, H., Fukuda, M., Noda, T. & Yoshimori, T. (2008) ‘The Atg16L complex specifies the site of LC3 lipidation for membrane biogenesis in autophagy’, *Molecular Biology of the Cell*, 19(5), pp. 2092–2100.

Fujita, N., Saitoh, T., Kageyama, S., Akira, S., Noda, T. & Yoshimori, T. (2009) ‘Differential Involvement of Atg16L1 in Crohn Disease and Canonical Autophagy’, *Journal of Biological Chemistry*, 284(47), pp. 32602–32609.

Galluzzi, L., Baehrecke, E.H., Ballabio, A., Boya, P., Bravo-San Pedro, J.M., Cecconi, F., Choi, A.M., Chu, C.T., Codogno, P., Colombo, M.I., Cuervo, A.M., Debnath, J., Deretic, V., Dikic, I., Eskelinen, E., Fimia, G.M., Fulda, S., Gewirtz, D.A., Green, D.R., et al. (2017) ‘Molecular definitions of autophagy and related processes’, *The EMBO Journal*, 36(13), pp. 1811–1836.

Ganesan, D. & Cai, Q. (2021) ‘Understanding amphisomes’, *Biochemical Journal*, 478(10), pp. 1959–1976.

Gao, C., Cao, W., Bao, L., Zuo, W., Xie, G., Cai, T., Fu, W., Zhang, J., Wu, W., Zhang, X. & Chen, Y.-G. (2010) ‘Autophagy negatively regulates Wnt signalling by promoting Dishevelled degradation’, *Nature Cell Biology*, 12(8), pp. 781–790.

Geiger, B. & Yamada, K.M. (2011) ‘Molecular Architecture and Function of Matrix Adhesions’, *Cold Spring Harbor Perspectives in Biology*, 3(5), pp. a005033–a005033.

Giaever, G. & Nislow, C. (2014) ‘The Yeast Deletion Collection: A Decade of Functional Genomics’, *Genetics*, 197(2), p. 451.

Gladkova, C., Maslen, S.L., Skehel, J.M. & Komander, D. (2018) ‘Mechanism of parkin activation by PINK1’, *Nature*, 559(7714), pp. 410–414.

Gleichmann, M. & Mattson, M.P. (2011) ‘Neuronal Calcium Homeostasis and Dysregulation’, *Antioxidants & Redox Signaling*, 14(7), pp. 1261–1273.

Glick, D., Barth, S. & Macleod, K.F. (2010a) ‘Autophagy: cellular and molecular mechanisms’, *The Journal of Pathology*, 221(1), pp. 3–12.

Glick, D., Barth, S. & Macleod, K.F. (2010b) ‘Autophagy: cellular and molecular mechanisms’, *The Journal of Pathology*, 221(1), pp. 3–12.

Goizet, C., Boukhris, A., Maltete, D., Guyant-Maréchal, L., Truchetto, J., Mundwiller, E., Hanein, S., Jonveaux, P., Roelens, F., Loureiro, J., Godet, E., Forlani, S., Melki, J., Auer-Grumbach, M., Fernandez, J.C., Martin-Hardy, P., Sibon, I., Sole, G., Orignac, I., et al. (2009) ‘SPG15 is the second most common cause of hereditary spastic paraplegia with thin corpus callosum.’, *Neurology*, 73(14), pp. 1111–9.

Gómez-Casati, M.E., Murtie, J.C., Rio, C., Stankovic, K., Liberman, M.C. & Corfas, G. (2010) ‘Nonneuronal cells regulate synapse formation in the vestibular sensory epithelium via erbB-dependent BDNF expression’, *Proceedings of the National Academy of Sciences*, 107(39), pp. 17005–17010.

Graham, C., Stansfield, P. & Chris, R. (2023) *Conservation-Colab: Conservation to 3D structure Colab v1.0.2*. [Online]

Grover, L.M. & Teyler, T.J. (1990) ‘Two components of long-term potentiation induced by different patterns of afferent activation’, *Nature*, 347(6292), pp. 477–479.

Guardia, C.M., Tan, X.-F., Lian, T., Rana, M.S., Zhou, W., Christenson, E.T., Lowry, A.J., Faraldo-Gómez, J.D., Bonifacino, J.S., Jiang, J. & Banerjee, A. (2020) ‘Structure of Human ATG9A, the Only Transmembrane Protein of the Core Autophagy Machinery’, *Cell Reports*, 31(13), p. 107837.

Gui, X., Yang, H., Li, T., Tan, X., Shi, P., Li, M., Du, F. & Chen, Z.J. (2019) ‘Autophagy induction via STING trafficking is a primordial function of the cGAS pathway’, *Nature*, 567(7747), pp. 262–266.

Guimaraes, R.S., Delorme-Axford, E., Klionsky, D.J. & Reggiori, F. (2015) ‘Assays for the biochemical and ultrastructural measurement of selective and nonselective

types of autophagy in the yeast Saccharomyces cerevisiae', *Methods*, 75pp. 141–150.

Gunhanlar, N., Shpak, G., van der Kroeg, M., Gouty-Colomer, L.A., Munshi, S.T., Lendemeijer, B., Ghazvini, M., Dupont, C., Hoogendijk, W.J.G., Gribnau, J., de Vrij, F.M.S. & Kushner, S.A. (2018) 'A simplified protocol for differentiation of electrophysiologically mature neuronal networks from human induced pluripotent stem cells', *Molecular Psychiatry*, 23(5), pp. 1336–1344.

Gwinn, D.M., Shackelford, D.B., Egan, D.F., Mihaylova, M.M., Mery, A., Vasquez, D.S., Turk, B.E. & Shaw, R.J. (2008a) 'AMPK Phosphorylation of Raptor Mediates a Metabolic Checkpoint', *Molecular Cell*, 30(2), pp. 214–226.

Gwinn, D.M., Shackelford, D.B., Egan, D.F., Mihaylova, M.M., Mery, A., Vasquez, D.S., Turk, B.E. & Shaw, R.J. (2008b) 'AMPK Phosphorylation of Raptor Mediates a Metabolic Checkpoint', *Molecular Cell*, 30(2), pp. 214–226.

Haack, T.B., Ignatius, E., Calvo-Garrido, J., Iuso, A., Isohanni, P., Maffezzini, C., Lönnqvist, T., Suomalainen, A., Gorza, M., Kremer, L.S., Graf, E., Hartig, M., Berutti, R., Paucar, M., Svenningsson, P., Stranneheim, H., Brandberg, G., Wedell, A., Kurian, M.A., et al. (2016) 'Absence of the Autophagy Adaptor SQSTM1/p62 Causes Childhood-Onset Neurodegeneration with Ataxia, Dystonia, and Gaze Palsy.', *American journal of human genetics*, 99(3), pp. 735–743.

Haldipur, P., Aldinger, K.A., Bernardo, S., Deng, M., Timms, A.E., Overman, L.M., Winter, C., Lisgo, S.N., Razavi, Silvestri, E., Manganaro, L., Adle-Biassette, H., Guimiot, F., Russo, R., Kidron, D., Hof, P.R., Gerrelli, D., Lindsay, S.J., Dobyns, W.B., et al. (2019) 'Spatiotemporal expansion of primary progenitor zones in the developing human cerebellum', *Science*, 366(6464), pp. 454–460.

Haldipur, P., Bharti, U., Alberti, C., Sarkar, C., Gulati, G., Iyengar, S., Gressens, P. & Mani, S. (2011) 'Preterm Delivery Disrupts the Developmental Program of the Cerebellum' Olivier Baud (ed.), *PLoS ONE*, 6(8), p. e23449.

Halliwell, J.A., Baker, D., Judge, K., Quail, M.A., Oliver, K., Betteridge, E., Skelton, J., Andrews, P.W. & Barbaric, I. (2021) 'Nanopore Sequencing Indicates That Tandem Amplification of Chromosome 20q11.21 in Human Pluripotent Stem Cells Is Driven by Break-Induced Replication', *Stem Cells and Development*, 30(11), pp. 578–586.

Hampe, J., Franke, A., Rosenstiel, P., Till, A., Teuber, M., Huse, K., Albrecht, M., Mayr, G., De La Vega, F.M., Briggs, J., Günther, S., Prescott, N.J., Onnie, C.M., Häsler, R., Sipos, B., Fölsch, U.R., Lengauer, T., Platzer, M., Mathew, C.G., et al. (2007) 'A genome-wide association scan of nonsynonymous SNPs identifies a susceptibility variant for Crohn disease in ATG16L1', *Nature Genetics*, 39(2), pp. 207–211.

Hanada, T., Noda, N.N., Satomi, Y., Ichimura, Y., Fujioka, Y., Takao, T., Inagaki, F. & Ohsumi, Y. (2007) 'The Atg12-Atg5 conjugate has a novel E3-like activity for protein lipidation in autophagy', *Journal of Biological Chemistry*, 282(52), pp. 37298–37302.

Hanna, R.A., Quinsay, M.N., Orogo, A.M., Giang, K., Rikka, S. & Gustafsson, Å.B. (2012) 'Microtubule-associated Protein 1 Light Chain 3 (LC3) Interacts with Bnip3 Protein to Selectively Remove Endoplasmic Reticulum and Mitochondria via Autophagy', *Journal of Biological Chemistry*, 287(23), pp. 19094–19104.

Hara, K., Maruki, Y., Long, X., Yoshino, K., Oshiro, N., Hidayat, S., Tokunaga, C., Avruch, J. & Yonezawa, K. (2002) 'Raptor, a Binding Partner of Target of Rapamycin (TOR), Mediates TOR Action', *Cell*, 110(2), pp. 177–189.

Hara, T., Nakamura, K., Matsui, M., Yamamoto, A., Nakahara, Y., Suzuki-Migishima, R., Yokoyama, M., Mishima, K., Saito, I., Okano, H. & Mizushima, N. (2006a) 'Suppression of basal autophagy in neural cells causes neurodegenerative disease in mice', *Nature*, 441(7095), pp. 885–889.

Hara, T., Nakamura, K., Matsui, M., Yamamoto, A., Nakahara, Y., Suzuki-Migishima, R., Yokoyama, M., Mishima, K., Saito, I., Okano, H. & Mizushima, N. (2006b) 'Suppression of basal autophagy in neural cells causes neurodegenerative disease in mice', *Nature*, 441(7095), pp. 885–889.

Hardies, K., May, P., Djémié, T., Tarta-Arsene, O., Deconinck, T., Craiu, D., AR working group of the EuroEPINOMICS RES Consortium, Helbig, I., Suls, A., Balling, R., Weckhuysen, S., De Jonghe, P. & Hirst, J. (2015) 'Recessive loss-of-function mutations in AP4S1 cause mild fever-sensitive seizures, developmental delay and spastic paraplegia through loss of AP-4 complex assembly.', *Human molecular genetics*, 24(8), pp. 2218–27.

Hardiman, O., Al-Chalabi, A., Chio, A., Corr, E.M., Logroscino, G., Robberecht, W., Shaw, P.J., Simmons, Z. & van den Berg, L.H. (2017) 'Amyotrophic lateral sclerosis', *Nature Reviews Disease Primers*, 3(1), p. 17071.

Harnett, M.M., Pineda, M.A., Latré de Laté, P., Eason, R.J., Besteiro, S., Harnett, W. & Langsley, G. (2017) 'From Christian de Duve to Yoshinori Ohsumi: More to autophagy than just dining at home', *Biomedical Journal*, 40(1), pp. 9–22.

Harris, J.J., Jolivet, R. & Attwell, D. (2012) 'Synaptic Energy Use and Supply', *Neuron*, 75(5), pp. 762–777.

Hata, A. & Chen, Y.G. (2016) 'TGF-β Signaling from Receptors to Smads', *Cold Spring Harbor Perspectives in Biology*, 8(9), .

He, J., Kang, L., Wu, T., Zhang, J., Wang, H., Gao, H., Zhang, Y., Huang, B., Liu, W., Kou, Z., Zhang, H. & Gao, S. (2012) 'An Elaborate Regulation of Mammalian Target of Rapamycin Activity Is Required for Somatic Cell Reprogramming

Induced by Defined Transcription Factors', *https://home.liebertpub.com/scd*, 21(14), pp. 2630–2641.

Heimer, G., Oz-Levi, D., Eyal, E., Edvardson, S., Nissenkorn, A., Ruzzo, E.K., Szeinberg, A., Maayan, C., Mai-Zahav, M., Efrati, O., Pras, E., Reznik-Wolf, H., Lancet, D., Goldstein, D.B., Anikster, Y., Shalev, S.A., Elpeleg, O. & Ben Zeev, B. (2016) 'TECPR2 mutations cause a new subtype of familial dysautonomia like hereditary sensory autonomic neuropathy with intellectual disability.', *European journal of paediatric neurology : EJPN : official journal of the European Paediatric Neurology Society*, 20(1), pp. 69–79.

Heo, J.-M., Ordureau, A., Paulo, J.A., Rinehart, J. & Harper, J.W. (2015) 'The PINK1-PARKIN Mitochondrial Ubiquitylation Pathway Drives a Program of OPTN/NDP52 Recruitment and TBK1 Activation to Promote Mitophagy', *Molecular Cell*, 60(1), pp. 7–20.

Heo, J.-M., Ordureau, A., Swarup, S., Paulo, J.A., Shen, K., Sabatini, D.M. & Harper, J.W. (2018) 'RAB7A phosphorylation by TBK1 promotes mitophagy via the PINK-PARKIN pathway', *Science Advances*, 4(11), .

Herbst, S., Campbell, P., Harvey, J., Bernard, E.M., Papayannopoulos, V., Wood, N.W., Morris, H.R. & Gutierrez, M.G. (2020) 'LRRK2 activation controls the repair of damaged endomembranes in macrophages.', *The EMBO journal*, 39(18), p. e104494.

Hernandez, D., Torres, C.A., Setlik, W., Cebrián, C., Mosharov, E. V, Tang, G., Cheng, H.-C., Kholodilov, N., Yarygina, O., Burke, R.E., Gershon, M. & Sulzer, D. (2012) 'Regulation of presynaptic neurotransmission by macroautophagy.', *Neuron*, 74(2), pp. 277–84.

Himuro, M., Miyatsuka, T., Suzuki, L., Miura, M., Katahira, T., Goto, H., Nishida, Y., Sasaki, S., Koike, M., Shiota, C., Gittes, G.K., Fujitani, Y. & Watada, H. (2019) 'Cellular autophagy in α cells plays a role in the maintenance of islet architecture', *Journal of the Endocrine Society*,

Ho, W.Y., Tai, Y.K., Chang, J.-C., Liang, J., Tyan, S.-H., Chen, S., Guan, J.-L., Zhou, H., Shen, H.-M., Koo, E. & Ling, S.-C. (2019) 'The ALS-FTD-linked gene product, C9orf72, regulates neuronal morphogenesis via autophagy', *Autophagy*, 15(5), pp. 827–842.

Homem, C.C.F., Repic, M. & Knoblich, J.A. (2015) 'Proliferation control in neural stem and progenitor cells', *Nature Reviews Neuroscience*, 16(11), pp. 647–659.

Hughes, E.G., Elmariah, S.B. & Balice-Gordon, R.J. (2010) 'Astrocyte secreted proteins selectively increase hippocampal GABAergic axon length, branching, and synaptogenesis', *Molecular and Cellular Neuroscience*, 43(1), pp. 136–145.

Ichimura, Y., Kirisako, T., Takao, T., Satomi, Y., Shimonishi, Y., Ishihara, N., Mizushima, N., Tanida, I., Kominami, E., Ohsumi, M., Noda, T. & Ohsumi, Y. (2000) 'A ubiquitin-like system mediates protein lipidation', *Nature*, 408(6811), pp. 488–492.

Ichimura, Y., Kumanomidou, T., Sou, Y.S., Mizushima, T., Ezaki, J., Ueno, T., Kominami, E., Yamane, T., Tanaka, K. & Komatsu, M. (2008) 'Structural Basis for Sorting Mechanism of p62 in Selective Autophagy', *Journal of Biological Chemistry*, 283(33), pp. 22847–22857.

Inman, G.J., Nicolás, F.J. & Hill, C.S. (2002) 'Nucleocytoplasmic Shuttling of Smads 2, 3, and 4 Permits Sensing of TGF-β Receptor Activity', *Molecular Cell*, 10(2), pp. 283–294.

Inoki, K., Li, Y., Xu, T. & Guan, K.-L. (2003) 'Rheb GTPase is a direct target of TSC2 GAP activity and regulates mTOR signaling', *Genes & Development*, 17(15), pp. 1829–1834.

Inoue, J., Nishiumi, S., Fujishima, Y., Masuda, A., Shiomi, H., Yamamoto, K., Nishida, M., Azuma, T. & Yoshida, M. (2012) 'Autophagy in the intestinal epithelium regulates Citrobacter rodentium infection', *Archives of Biochemistry and Biophysics*, 521(1–2), pp. 95–101.

Inoue, K., Rispoli, J., Kaphzan, H., Klann, E., Chen, E.I., Kim, J., Komatsu, M. & Abeliovich, A. (2012) 'Macroautophagy deficiency mediates age-dependent neurodegeneration through a phospho-tau pathway', *Molecular Neurodegeneration*, 7(1), p. 48.

Itakura, E., Kishi, C., Inoue, K. & Mizushima, N. (2008) 'Beclin 1 Forms Two Distinct Phosphatidylinositol 3-Kinase Complexes with Mammalian Atg14 and UVRAG' Suresh Subramani (ed.), *Molecular Biology of the Cell*, 19(12), pp. 5360–5372.

Itakura, E., Kishi-Itakura, C., Koyama-Honda, I. & Mizushima, N. (2012) 'Structures containing Atg9A and the ULK1 complex independently target depolarized mitochondria at initial stages of Parkin-mediated mitophagy', *Journal of Cell Science*,

Itakura, E., Kishi-Itakura, C. & Mizushima, N. (2012) 'The Hairpin-type Tail-Anchored SNARE Syntaxin 17 Targets to Autophagosomes for Fusion with Endosomes/Lysosomes', *Cell*, 151(6), pp. 1256–1269.

Jia, W., Pua, H.H., Li, Q.-J. & He, Y.-W. (2011) 'Autophagy regulates endoplasmic reticulum homeostasis and calcium mobilization in T lymphocytes.', *Journal of immunology (Baltimore, Md. : 1950)*, 186(3), pp. 1564–74.

Jiang, P., Nishimura, T., Sakamaki, Y., Itakura, E., Hatta, T., Natsume, T. & Mizushima, N. (2014) 'The HOPS complex mediates autophagosome–lysosome

fusion through interaction with syntaxin 17' Tamotsu Yoshimori (ed.), *Molecular Biology of the Cell*, 25(8), pp. 1327–1337.

Jiang, X., Wang, X., Ding, X., Du, M., Li, B., Weng, X., Zhang, J., Li, L., Tian, R., Zhu, Q., Chen, S., Wang, L., Liu, W., Fang, L., Neculai, D. & Sun, Q. (2020) 'FAM134B oligomerization drives endoplasmic reticulum membrane scission for ER-phagy.', *The EMBO journal*, 39(5), p. e102608.

Jin, S.M., Lazarou, M., Wang, C., Kane, L.A., Narendra, D.P. & Youle, R.J. (2010) 'Mitochondrial membrane potential regulates PINK1 import and proteolytic destabilization by PARL', *Journal of Cell Biology*, 191(5), pp. 933–942.

Jinek, M., Chylinski, K., Fonfara, I., Hauer, M., Doudna, J.A. & Charpentier, E. (2012) 'A programmable dual-RNA-guided DNA endonuclease in adaptive bacterial immunity', *Science*, 337(6096), pp. 816–821.

Jinek, M., East, A., Cheng, A., Lin, S., Ma, E. & Doudna, J. (2013) 'RNA-programmed genome editing in human cells', *eLife*, 2013(2), .

Johnson, M.A., Weick, J.P., Pearce, R.A. & Zhang, S.-C. (2007) 'Functional Neural Development from Human Embryonic Stem Cells: Accelerated Synaptic Activity via Astrocyte Coculture', *The Journal of Neuroscience*, 27(12), pp. 3069–3077.

Jourdain, P., Bergersen, L.H., Bhaukaurally, K., Bezzi, P., Santello, M., Domercq, M., Matute, C., Tonello, F., Gundersen, V. & Volterra, A. (2007) 'Glutamate exocytosis from astrocytes controls synaptic strength', *Nature Neuroscience*, 10(3), pp. 331–339.

Jovanov-Milošević, N., Petanjek, Z., Petrović, D., Judaš, M. & Kostović, I. (2010) 'Morphology, molecular phenotypes and distribution of neurons in developing human corpus callosum', *European Journal of Neuroscience*, 32(9), pp. 1423–1432.

Juhász, G., Érdi, B., Sass, M. & Neufeld, T.P. (2007) 'Atg7-dependent autophagy promotes neuronal health, stress tolerance, and longevity but is dispensable for metamorphosis in Drosophila', *Genes & Development*, 21(23), pp. 3061–3066.

Jumper, J., Evans, R., Pritzel, A., Green, T., Figurnov, M., Ronneberger, O., Tunyasuvunakool, K., Bates, R., Žídek, A., Potapenko, A., Bridgland, A., Meyer, C., Kohl, S.A.A., Ballard, A.J., Cowie, A., Romera-Paredes, B., Nikolov, S., Jain, R., Adler, J., et al. (2021) 'Highly accurate protein structure prediction with AlphaFold', *Nature*, 596(7873), pp. 583–589.

Jung, C.H., Jun, C.B., Ro, S.-H., Kim, Y.-M., Otto, N.M., Cao, J., Kundu, M. & Kim, D.-H. (2009) 'ULK-Atg13-FIP200 Complexes Mediate mTOR Signaling to the Autophagy Machinery' Sandra L. Schmid (ed.), *Molecular Biology of the Cell*, 20(7), pp. 1992–2003.

Jung, H.S., Chung, K.W., Won Kim, J., Kim, J., Komatsu, M., Tanaka, K., Nguyen, Y.H., Kang, T.M., Yoon, K.-H., Kim, J.-W., Jeong, Y.T., Han, M.S., Lee, M.-K., Kim, K.-W., Shin, J. & Lee, M.-S. (2008) 'Loss of Autophagy Diminishes Pancreatic β Cell Mass and Function with Resultant Hyperglycemia', *Cell Metabolism*, 8(4), pp. 318–324.

Jung, S., Choe, S., Woo, H., Jeong, H., An, H.-K., Moon, H., Ryu, H.Y., Yeo, B.K., Lee, Y.W., Choi, H., Mun, J.Y., Sun, W., Choe, H.K., Kim, E.-K. & Yu, S.-W. (2020) 'Autophagic death of neural stem cells mediates chronic stress-induced decline of adult hippocampal neurogenesis and cognitive deficits', *Autophagy*, 16(3), pp. 512–530.

Kadir, R., Harel, T., Markus, B., Perez, Y., Bakhrat, A., Cohen, I., Volodarsky, M., Feintsein-Linial, M., Chervinski, E., Zlotogora, J., Sivan, S., Birnbaum, R.Y., Abdu, U., Shalev, S. & Birk, O.S. (2016) 'ALFY-Controlled DVL3 Autophagy Regulates Wnt Signaling, Determining Human Brain Size' Stefan Mundlos (ed.), *PLOS Genetics*, 12(3), p. e1005919.

Karczewski, K.J., Francioli, L.C., Tiao, G., Cummings, B.B., Alföldi, J., Wang, Q., Collins, R.L., Laricchia, K.M., Ganna, A., Birnbaum, D.P., Gauthier, L.D., Brand, H., Solomonson, M., Watts, N.A., Rhodes, D., Singer-Berk, M., England, E.M., Seaby, E.G., Kosmicki, J.A., et al. (2020) 'The mutational constraint spectrum quantified from variation in 141,456 humans', *Nature*, 581(7809), pp. 434–443.

Karsli-Uzunbas, G., Guo, J.Y., Price, S., Teng, X., Laddha, S. V, Khor, S., Kalaany, N.Y., Jacks, T., Chan, C.S., Rabinowitz, J.D. & White, E. (2014) 'Autophagy Is Required for Glucose Homeostasis and Lung Tumor Maintenance', *Cancer Discovery*, 4(8), pp. 914–927.

Katayama, H., Kogure, T., Mizushima, N., Yoshimori, T. & Miyawaki, A. (2011) 'A Sensitive and Quantitative Technique for Detecting Autophagic Events Based on Lysosomal Delivery', *Chemistry & Biology*, 18(8), pp. 1042–1052.

Kato, S., Sumi-Akamaru, H., Fujimura, H., Sakoda, S., Kato, M., Hirano, A., Takikawa, M. & Ohama, E. (2001) 'Copper chaperone for superoxide dismutase co-aggregates with superoxide dismutase 1 (SOD1) in neuronal Lewy body-like hyaline inclusions: an immunohistochemical study on familial amyotrophic lateral sclerosis with SOD1 gene mutation', *Acta Neuropathologica*, 102(3), pp. 233–238.

Kauffman, K.J., Yu, S., Jin, J., Mugo, B., Nguyen, N., O'Brien, A., Nag, S., Lystad, A.H. & Melia, T.J. (2018) 'Delipidation of mammalian Atg8-family proteins by each of the four ATG4 proteases', *Autophagy*, pp. 1–19.

Kaushik, S. & Cuervo, A.M. (2016) 'AMPK-dependent phosphorylation of lipid droplet protein PLIN2 triggers its degradation by CMA', *Autophagy*, 12(2), pp. 432–438.

Kaushik, S. & Cuervo, A.M. (2015) ‘Degradation of lipid droplet-associated proteins by chaperone-mediated autophagy facilitates lipolysis’, *Nature Cell Biology*, 17(6), pp. 759–770.

Kawamoto, E.M., Vivar, C. & Camandola, S. (2012) ‘Physiology and Pathology of Calcium Signaling in the Brain’, *Frontiers in Pharmacology*, 3.

Kelley, L.A., Mezulis, S., Yates, C.M., Wass, M.N. & Sternberg, M.J.E. (2015) ‘The Phyre2 web portal for protein modeling, prediction and analysis’, *Nature Protocols*, 10(6), pp. 845–858.

Kenific, C.M., Stehbens, S.J., Goldsmith, J., Leidal, A.M., Faure, N., Ye, J., Wittmann, T. & Debnath, J. (2016) ‘NBR1 enables autophagy-dependent focal adhesion turnover’, *Journal of Cell Biology*, 212(5), pp. 577–590.

Khan, T., Whyte, J.J., Schulz, L.C. & Roberts, R.M. (2024) ‘Fluorescence-activated nuclear sorting (FANS) of nuclei from in vitro-generated syncytiotrophoblast’, *Placenta*,

Kihara, A., Noda, T., Ishihara, N. & Ohsumi, Y. (2001) ‘Two distinct Vps34 phosphatidylinositol 3-kinase complexes function in autophagy and carboxypeptidase Y sorting in Saccharomyces cerevisiae.’, *The Journal of cell biology*, 152(3), pp. 519–30.

Kim, D.-H., Sarbassov, D.D., Ali, S.M., Latek, R.R., Guntur, K.V.P., Erdjument-Bromage, H., Tempst, P. & Sabatini, D.M. (2003) ‘GβL, a Positive Regulator of the Rapamycin-Sensitive Pathway Required for the Nutrient-Sensitive Interaction between Raptor and mTOR’, *Molecular Cell*, 11(4), pp. 895–904.

Kim, H., Zahir, T., Tator, C.H. & Shoichet, M.S. (2011) ‘Effects of dibutyryl cyclic-AMP on survival and neuronal differentiation of neural stem/progenitor cells transplanted into spinal cord injured rats’, *PloS one*, 6(6), .

Kim, H.-J., Cho, M.-H., Shim, W.H., Kim, J.K., Jeon, E.-Y., Kim, D.-H. & Yoon, S.-Y. (2017) ‘Deficient autophagy in microglia impairs synaptic pruning and causes social behavioral defects.’, *Molecular psychiatry*, 22(11), pp. 1576–1584.

Kim, J., Kundu, M., Viollet, B. & Guan, K.-L. (2011) ‘AMPK and mTOR regulate autophagy through direct phosphorylation of Ulk1’, *Nature Cell Biology*, 13(2), pp. 132–141.

Kim, J.-Y., Zhao, H., Martinez, J., Doggett, T.A., Kolesnikov, A. V., Tang, P.H., Ablonczy, Z., Chan, C.-C., Zhou, Z., Green, D.R. & Ferguson, T.A. (2013) ‘Noncanonical Autophagy Promotes the Visual Cycle’, *Cell*, 154(2), pp. 365–376.

Kim, M., Sandford, E., Gatica, D., Qiu, Y., Liu, X., Zheng, Y., Schulman, B.A., Xu, J., Semple, I., Ro, S.-H., Kim, B., Mavioglu, R.N., Tolun, A., Jipa, A., Takats, S.,

Karpati, M., Li, J.Z., Yapici, Z., Juhasz, G., et al. (2016) ‘Mutation in ATG5 reduces autophagy and leads to ataxia with developmental delay’, *eLife*, 5.

Kircher, M., Witten, D.M., Jain, P., O’Roak, B.J., Cooper, G.M. & Shendure, J. (2014) ‘A general framework for estimating the relative pathogenicity of human genetic variants’, *Nature Genetics*, 46(3), pp. 310–315.

Kirkin, V., McEwan, D.G., Novak, I. & Dikic, I. (2009a) ‘A Role for Ubiquitin in Selective Autophagy’, *Molecular Cell*, 34(3), pp. 259–269.

Kirkin, V., McEwan, D.G., Novak, I. & Dikic, I. (2009b) ‘A Role for Ubiquitin in Selective Autophagy’, *Molecular Cell*, 34(3), pp. 259–269.

Kitada, T., Asakawa, S., Hattori, N., Matsumine, H., Yamamura, Y., Minoshima, S., Yokochi, M., Mizuno, Y. & Shimizu, N. (1998) ‘Mutations in the parkin gene cause autosomal recessive juvenile parkinsonism’, *Nature*, 392(6676), pp. 605–608.

Kılıç, S., Esmen, K., Oto, A.M., Kose, T.B., Sever-Bahçekapılı, M., Eren-Koçak, E., Demir, Ş., Hız, A.S., Karakülah, G., Bağrıyanık, H.A., Öztürk, M. & Diril, M.K. (2024) *Characterization of a novel neurodevelopmental rare disease caused by a mutation within the autophagy gene ATG9B*.

Klionsky, D.J. (2008) ‘Autophagy revisited: A conversation with Christian de Duve’, *Autophagy*, 4(6), pp. 740–743.

Komatsu, M., Tanida, I., Ueno, T., Ohsumi, M., Ohsumi, Y. & Kominami, E. (2001) ‘The C-terminal Region of an Apg7p/Cvt2p Is Required for Homodimerization and Is Essential for Its E1 Activity and E1-E2 Complex Formation’, *Journal of Biological Chemistry*, 276(13), pp. 9846–9854.

Komatsu, M., Waguri, S., Chiba, T., Murata, S., Iwata, J., Tanida, I., Ueno, T., Koike, M., Uchiyama, Y., Kominami, E. & Tanaka, K. (2006) ‘Loss of autophagy in the central nervous system causes neurodegeneration in mice’, *Nature*, 441(7095), pp. 880–884.

Komatsu, M., Waguri, S., Koike, M., Sou, Y., Ueno, T., Hara, T., Mizushima, N., Iwata, J., Ezaki, J., Murata, S., Hamazaki, J., Nishito, Y., Iemura, S., Natsume, T., Yanagawa, T., Uwayama, J., Warabi, E., Yoshida, H., Ishii, T., et al. (2007) ‘Homeostatic Levels of p62 Control Cytoplasmic Inclusion Body Formation in Autophagy-Deficient Mice’, *Cell*, 131(6), pp. 1149–1163.

Komatsu, M., Waguri, S., Ueno, T., Iwata, J., Murata, S., Tanida, I., Ezaki, J., Mizushima, N., Ohsumi, Y., Uchiyama, Y., Kominami, E., Tanaka, K. & Chiba, T. (2005) ‘Impairment of starvation-induced and constitutive autophagy in Atg7-deficient mice’, *Journal of Cell Biology*, 169(3), pp. 425–434.

Komatsu, M., Wang, Q.J., Holstein, G.R., Friedrich, V.L., Iwata, J., Kominami, E., Chait, B.T., Tanaka, K. & Yue, Z. (2007) ‘Essential role for autophagy protein

Atg7 in the maintenance of axonal homeostasis and the prevention of axonal degeneration.', *Proceedings of the National Academy of Sciences of the United States of America*, 104(36), pp. 14489–94.

Kondapalli, C., Kazlauskaite, A., Zhang, N., Woodroof, H.I., Campbell, D.G., Gourlay, R., Burchell, L., Walden, H., Macartney, T.J., Deak, M., Knebel, A., Alessi, D.R. & Muqit, M.M.K. (2012) 'PINK1 is activated by mitochondrial membrane potential depolarization and stimulates Parkin E3 ligase activity by phosphorylating Serine 65', *Open Biology*, 2(5), p. 120080.

Kopan, R. & Ilagan, Ma.X.G. (2009) 'The Canonical Notch Signaling Pathway: Unfolding the Activation Mechanism', *Cell*, 137(2), pp. 216–233.

Korolchuk, V.I., Saiki, S., Lichtenberg, M., Siddiqi, F.H., Roberts, E.A., Imarisio, S., Jahreiss, L., Sarkar, S., Futter, M., Menzies, F.M., O'Kane, C.J., Deretic, V. & Rubinsztein, D.C. (2011) 'Lysosomal positioning coordinates cellular nutrient responses', *Nature Cell Biology*, 13(4), pp. 453–460.

Kostovic, I. & Goldman-Rakic, P.S. (1983) 'Transient cholinesterase staining in the mediodorsal nucleus of the thalamus and its connections in the developing human and monkey brain', *Journal of Comparative Neurology*, 219(4), pp. 431–447.

Kostović, I. & Judaš, M. (2002) 'Correlation between the sequential ingrowth of afferents and transient patterns of cortical lamination in preterm infants', *The Anatomical Record*, 267(1), pp. 1–6.

Kostović, I., Radoš, M., Kostović-Srzentić, M. & Krsnik, Ž. (2021) 'Fundamentals of the Development of Connectivity in the Human Fetal Brain in Late Gestation: From 24 Weeks Gestational Age to Term', *Journal of Neuropathology & Experimental Neurology*, 80(5), pp. 393–414.

Koyano, F., Okatsu, K., Kosako, H., Tamura, Y., Go, E., Kimura, M., Kimura, Y., Tsuchiya, H., Yoshihara, H., Hirokawa, T., Endo, T., Fon, E.A., Trempe, J.-F., Saeki, Y., Tanaka, K. & Matsuda, N. (2014) 'Ubiquitin is phosphorylated by PINK1 to activate parkin', *Nature*, 510(7503), pp. 162–166.

Krivec, N., Ghosh, M.S. & Spits, C. (2024) 'Gains of 20q11.21 in human pluripotent stem cells: Insights from cancer research', *Stem Cell Reports*, 19(1), pp. 11–27.

Kugler, P. & Schmitt, A. (1999) 'Glutamate transporter EAAC1 is expressed in neurons and glial cells in the rat nervous system.', *Glia*, 27(2), pp. 129–42.

Kuma, A., Hatano, M., Matsui, M., Yamamoto, A., Nakaya, H., Yoshimori, T., Ohsumi, Y., Tokuhisa, T. & Mizushima, N. (2004) 'The role of autophagy during the early neonatal starvation period', *Nature*, 432(7020), pp. 1032–1036.

Kuma, A., Komatsu, M. & Mizushima, N. (2017) 'Autophagy-monitoring and autophagy-deficient mice', *Autophagy*, 13(10), p. 1619.

Labelle, C. & Leclerc, N. (2000) ‘Exogenous BDNF, NT-3 and NT-4 differentially regulate neurite outgrowth in cultured hippocampal neurons’, *Developmental Brain Research*, 123(1), pp. 1–11.

LaFerla, F.M., Green, K.N. & Oddo, S. (2007) ‘Intracellular amyloid-β in Alzheimer’s disease’, *Nature Reviews Neuroscience*, 8(7), pp. 499–509.

Lam, R.S., Töpfer, F.M., Wood, P.G., Busskamp, V. & Bamberg, E. (2017) ‘Functional Maturation of Human Stem Cell-Derived Neurons in Long-Term Cultures.’, *PloS one*, 12(1), p. e0169506.

LaMantia, A. & Rakic, P. (1990) ‘Axon overproduction and elimination in the corpus callosum of the developing rhesus monkey’, *The Journal of Neuroscience*, 10(7), pp. 2156–2175.

Landrum, M.J., Lee, J.M., Benson, M., Brown, G.R., Chao, C., Chitipiralla, S., Gu, B., Hart, J., Hoffman, D., Jang, W., Karapetyan, K., Katz, K., Liu, C., Maddipatla, Z., Malheiro, A., McDaniel, K., Ovetsky, M., Riley, G., Zhou, G., et al. (2018) ‘ClinVar: improving access to variant interpretations and supporting evidence’, *Nucleic Acids Research*, 46(D1), pp. D1062–D1067.

Lattante, S., de Calbiac, H., Le Ber, I., Brice, A., Ciura, S. & Kabashi, E. (2015) ‘Sqstm1 knock-down causes a locomotor phenotype ameliorated by rapamycin in a zebrafish model of ALS/FTLD’, *Human Molecular Genetics*, 24(6), pp. 1682–1690.

Lau, A., Wang, X.-J., Zhao, F., Villeneuve, N.F., Wu, T., Jiang, T., Sun, Z., White, E. & Zhang, D.D. (2010) ‘A Noncanonical Mechanism of Nrf2 Activation by Autophagy Deficiency: Direct Interaction between Keap1 and p62’, *Molecular and Cellular Biology*, 30(13), pp. 3275–3285.

Lazarou, M., Sliter, D.A., Kane, L.A., Sarraf, S.A., Wang, C., Burman, J.L., Sideris, D.P., Fogel, A.I. & Youle, R.J. (2015) ‘The ubiquitin kinase PINK1 recruits autophagy receptors to induce mitophagy’, *Nature*, 524(7565), pp. 309–314.

Leboutet, R., Largeau, C., Müller, L., Prigent, M., Quinet, G., Rodriguez, M.S., Cuif, M.-H., Hoppe, T., Culetto, E., Lefebvre, C. & Legouis, R. (2023) ‘LGG-1/GABARAP lipidation is not required for autophagy and development in Caenorhabditis elegans’, *eLife*, 12.

Lee, E., Koo, Y., Ng, A., Wei, Y., Luby-Phelps, K., Juraszek, A., Xavier, R.J., Cleaver, O., Levine, B. & Amatruda, J.F. (2014) ‘Autophagy is essential for cardiac morphogenesis during vertebrate development’, *Autophagy*, 10(4), pp. 572–587.

Lee, I.H., Kawai, Y., Fergusson, M.M., Rovira, I.I., Bishop, A.J.R., Motoyama, N., Cao, L. & Finkel, T. (2012) ‘Atg7 Modulates p53 Activity to Regulate Cell Cycle and Survival During Metabolic Stress’, *Science*, 336(6078), pp. 225–228.

Lee, J.-H., Yang, D.-S., Goulbourne, C.N., Im, E., Stavrides, P., Pensalfini, A., Chan, H., Bouchet-Marquis, C., Bleiwas, C., Berg, M.J., Huo, C., Peddy, J., Pawlik, M., Levy, E., Rao, M., Staufenbiel, M. & Nixon, R.A. (2022) 'Faulty autolysosome acidification in Alzheimer's disease mouse models induces autophagic build-up of Aβ in neurons, yielding senile plaques', *Nature Neuroscience*, 25(6), pp. 688–701.

Lee, J.-Y., Nagano, Y., Taylor, J.P., Lim, K.L. & Yao, T.-P. (2010) 'Disease-causing mutations in Parkin impair mitochondrial ubiquitination, aggregation, and HDAC6-dependent mitophagy', *Journal of Cell Biology*, 189(4), pp. 671–679.

Lee, Y.-K. & Lee, J.-A. (2016) 'Role of the mammalian ATG8/LC3 family in autophagy: differential and compensatory roles in the spatiotemporal regulation of autophagy', *BMB Reports*, 49(8), pp. 424–430.

Lennie, P. (2003) 'The Cost of Cortical Computation', *Current Biology*, 13(6), pp. 493–497.

De León Reyes, N.S., Bragg-Gonzalo, L. & Nieto, M. (2020) 'Development and plasticity of the corpus callosum', *Development*, 147(18), .

Leto, K., Arancillo, M., Becker, E.B.E., Buffo, A., Chiang, C., Ding, B., Dobyns, W.B., Dusart, I., Haldipur, P., Hatten, M.E., Hoshino, M., Joyner, A.L., Kano, M., Kilpatrick, D.L., Koibuchi, N., Marino, S., Martinez, S., Millen, K.J., Millner, T.O., et al. (2016) 'Consensus Paper: Cerebellar Development', *The Cerebellum*, 15(6), pp. 789–828.

Leung, A.W., Leung, A.W., Murdoch, B., Salem, A.F., Prasad, M.S., Gomez, G.A. & García-Castro, M.I. (2016) 'WNT/β-catenin signaling mediates human neural crest induction via a pre-neural border intermediate', *Development*, 143(3), pp. 398–410.

Levitt, P. & Rakic, P. (1980) 'Immunoperoxidase localization of glial fibrillary acidic protein in radial glial cells and astrocytes of the developing rhesus monkey brain', *Journal of Comparative Neurology*, 193(3), pp. 815–840.

Li, H. & Durbin, R. (2009) 'Fast and accurate short read alignment with Burrows–Wheeler transform', *Bioinformatics*, 25(14), pp. 1754–1760.

Li, H., Li, D., Ma, Z., Qian, Z., Kang, X., Jin, X., Li, F., Wang, X., Chen, Q., Sun, H. & Wu, S. (2018) 'Defective autophagy in osteoblasts induces endoplasmic reticulum stress and causes remarkable bone loss.', *Autophagy*, 14(10), pp. 1726–1741.

Li, J., Tang, X. & Chen, X. (2011) 'Comparative effects of TGF-β2/Smad2 and TGF-β2/Smad3 signaling pathways on proliferation, migration, and extracellular matrix production in a human lens cell line', *Experimental eye research*, 92(3), pp. 173–179.

Li, J.-Q., Tan, L. & Yu, J.-T. (2014) ‘The role of the LRRK2 gene in Parkinsonism’, *Molecular Neurodegeneration*, 9(1), p. 47.

Li, M., Hou, Y., Wang, J., Chen, X., Shao, Z.-M. & Yin, X.-M. (2011) ‘Kinetics Comparisons of Mammalian Atg4 Homologues Indicate Selective Preferences toward Diverse Atg8 Substrates’, *Journal of Biological Chemistry*, 286(9), pp. 7327–7338.

Li, M., Lu, G., Hu, J., Shen, X., Ju, J., Gao, Y., Qu, L., Xia, Y., Chen, Y. & Bai, Y. (2016) ‘EVA1A/TMEM166 Regulates Embryonic Neurogenesis by Autophagy’, *Stem Cell Reports*, 6(3), pp. 396–410.

Li, W., Li, J. & Bao, J. (2012) ‘Microautophagy: lesser-known self-eating’, *Cellular and Molecular Life Sciences*, 69(7), pp. 1125–1136.

Li, X., Wu, X.-Q., Deng, R., Li, D.-D., Tang, J., Chen, W.-D., Chen, J.-H., Ji, J., Jiao, L., Jiang, S., Yang, F., Feng, G.-K., Senthilkumar, R., Yue, F., Zhang, H.-L., Wu, R.-Y., Yu, Y., Xu, X.-L., Mai, J., et al. (2017) ‘CaMKII-mediated Beclin 1 phosphorylation regulates autophagy that promotes degradation of Id and neuroblastoma cell differentiation’, *Nature Communications*, 8(1), p. 1159.

Liénard, C., Pintart, A. & Bomont, P. (2024) ‘Neuronal Autophagy: Regulations and Implications in Health and Disease’, *Cells*, 13(1), p. 103.

Lim, S. & Kaldis, P. (2012) ‘Loss of Cdk2 and Cdk4 Induces a Switch from Proliferation to Differentiation in Neural Stem Cells’, *Stem Cells*, 30(7), pp. 1509–1520.

Limperopoulos, C., Soul, J.S., Gauvreau, K., Huppi, P.S., Warfield, S.K., Bassan, H., Robertson, R.L., Volpe, J.J. & du Plessis, A.J. (2005) ‘Late Gestation Cerebellar Growth Is Rapid and Impeded by Premature Birth’, *Pediatrics*, 115(3), pp. 688–695.

Liu, X., Li, Y., Wang, X., Xing, R., Liu, K., Gan, Q., Tang, C., Gao, Z., Jian, Y., Luo, S., Guo, W. & Yang, C. (2017) ‘The BEACH-containing protein WDR81 coordinates p62 and LC3C to promote aggrephagy’, *Journal of Cell Biology*, 216(5), pp. 1301–1320.

Lizaso, A., Tan, K.-T. & Lee, Y.-H. (2013) ‘β-adrenergic receptor-stimulated lipolysis requires the RAB7-mediated autolysosomal lipid degradation’, *Autophagy*, 9(8), pp. 1228–1243.

Lohmann, C. & Wong, R.O.L. (2005) ‘Regulation of dendritic growth and plasticity by local and global calcium dynamics’, *Cell Calcium*, 37(5), pp. 403–409.

Luhr, M., Szalai, P. & Engedal, N. (2018) ‘The lactate dehydrogenase sequestration assay — A simple and reliable method to determine bulk autophagic sequestration activity in mammalian cells’, *Journal of Visualized Experiments*, 2018(137), p. e57971.

Lv, X., Jiang, H., Li, B., Liang, Q., Wang, S., Zhao, Q. & Jiao, J. (2014) 'The Crucial Role of Atg5 in Cortical Neurogenesis During Early Brain Development', *Scientific Reports*, 4(1), p. 6010.

MacDonald, M. (1993) 'A novel gene containing a trinucleotide repeat that is expanded and unstable on Huntington's disease chromosomes', *Cell*, 72(6), pp. 971–983.

Mackenzie, I.R.A., Bigio, E.H., Ince, P.G., Geser, F., Neumann, M., Cairns, N.J., Kwong, L.K., Forman, M.S., Ravits, J., Stewart, H., Eisen, A., McClusky, L., Kretzschmar, H.A., Monoranu, C.M., Highley, J.R., Kirby, J., Siddique, T., Shaw, P.J., Lee, V.M., et al. (2007) 'Pathological TDP-43 distinguishes sporadic amyotrophic lateral sclerosis from amyotrophic lateral sclerosis with SOD1 mutations', *Annals of Neurology*, 61(5), pp. 427–434.

Magi, S., Piccirillo, S., Amoroso, S. & Lariccia, V. (2019) 'Excitatory Amino Acid Transporters (EAATs): Glutamate Transport and Beyond.', *International journal of molecular sciences*, 20(22), .

Maillard, C., Cavallin, M., Piquand, K., Philbert, M., Bault, J.P., Millischer, A.E., Moshous, D., Rio, M., Gitiaux, C., Boddaert, N., Masson, C., Thomas, S. & Bahi-Buisson, N. (2017) 'Prenatal and postnatal presentations of corpus callosum agenesis with polymicrogyria caused by EGP5 mutation.', *American journal of medical genetics. Part A*, 173(3), pp. 706–711.

Majeski, A.E. & Fred Dice, J. (2004) 'Mechanisms of chaperone-mediated autophagy', *The International Journal of Biochemistry & Cell Biology*, 36(12), pp. 2435–2444.

Malhotra, R., Warne, J.P., Salas, E., Xu, A.W. & Debnath, J. (2015) 'Loss of Atg12, but not Atg5, in pro-opiomelanocortin neurons exacerbates diet-induced obesity.', *Autophagy*, 11(1), pp. 145–54.

Martin, S. & Parton, R.G. (2005) 'Caveolin, cholesterol, and lipid bodies', *Seminars in Cell & Developmental Biology*, 16(2), pp. 163–174.

Martin, S. & Parton, R.G. (2006) 'Lipid droplets: a unified view of a dynamic organelle', *Nature Reviews Molecular Cell Biology*, 7(5), pp. 373–378.

Martinez-Lopez, N., Garcia-Macia, M., Sahu, S., Athonvarangkul, D., Liebling, E., Merlo, P., Cecconi, F., Schwartz, G.J. & Singh, R. (2016) 'Autophagy in the CNS and Periphery Coordinate Lipophagy and Lipolysis in the Brown Adipose Tissue and Liver', *Cell Metabolism*, 23(1), pp. 113–127.

Martinez-Vicente, M., Talloczy, Z., Wong, E., Tang, G., Koga, H., Kaushik, S., de Vries, R., Arias, E., Harris, S., Sulzer, D. & Cuervo, A.M. (2010) 'Cargo recognition failure is responsible for inefficient autophagy in Huntington's disease', *Nature Neuroscience*, 13(5), pp. 567–576.

Maruyama, T., Alam, J.Md., Fukuda, T., Kageyama, S., Kirisako, H., Ishii, Y., Shimada, I., Ohsumi, Y., Komatsu, M., Kanki, T., Nakatogawa, H. & Noda, N.N. (2021a) 'Membrane perturbation by lipidated Atg8 underlies autophagosome biogenesis', *Nature Structural & Molecular Biology*, 28(7), pp. 583–593.

Maruyama, T., Alam, J.Md., Fukuda, T., Kageyama, S., Kirisako, H., Ishii, Y., Shimada, I., Ohsumi, Y., Komatsu, M., Kanki, T., Nakatogawa, H. & Noda, N.N. (2021b) 'Membrane perturbation by lipidated Atg8 underlies autophagosome biogenesis', *Nature Structural & Molecular Biology*, 28(7), pp. 583–593.

Masiero, E., Agatea, L., Mammucari, C., Blaauw, B., Loro, E., Komatsu, M., Metzger, D., Reggiani, C., Schiaffino, S. & Sandri, M. (2009) 'Autophagy Is Required to Maintain Muscle Mass', *Cell Metabolism*, 10(6), pp. 507–515.

Matoba, K., Kotani, T., Tsutsumi, A., Tsuji, T., Mori, T., Noshiro, D., Sugita, Y., Nomura, N., Iwata, S., Ohsumi, Y., Fujimoto, T., Nakatogawa, H., Kikkawa, M. & Noda, N.N. (2020) 'Atg9 is a lipid scramblase that mediates autophagosomal membrane expansion', *Nature Structural & Molecular Biology*, 27(12), pp. 1185–1193.

Matsunaga, K., Morita, E., Saitoh, T., Akira, S., Ktistakis, N.T., Izumi, T., Noda, T. & Yoshimori, T. (2010) 'Autophagy requires endoplasmic reticulum targeting of the PI3-kinase complex via Atg14L', *Journal of Cell Biology*, 190(4), pp. 511–521.

Matsuura, A., Tsukada, M., Wada, Y. & Ohsumi, Y. (1997) 'Apg1p, a novel protein kinase required for the autophagic process in Saccharomyces cerevisiae', *Gene*, 192(2), pp. 245–250.

Mauch, D.H., Nägler, K., Schumacher, S., Göritz, C., Müller, E.-C., Otto, A. & Pfrieger, F.W. (2001) 'CNS Synaptogenesis Promoted by Glia-Derived Cholesterol', *Science*, 294(5545), pp. 1354–1357.

Mauthe, M., Orhon, I., Rocchi, C., Zhou, X., Luhr, M., Hijlkema, K.-J., Coppes, R.P., Engedal, N., Mari, M. & Reggiori, F. (2018) 'Chloroquine inhibits autophagic flux by decreasing autophagosome-lysosome fusion', *Autophagy*, 14(8), pp. 1435–1455.

Mauvezin, C. & Neufeld, T.P. (2015) 'Bafilomycin A1 disrupts autophagic flux by inhibiting both V-ATPase-dependent acidification and Ca-P60A/SERCA-dependent autophagosome-lysosome fusion', *Autophagy*, 11(8), pp. 1437–1438.

McEwan, D.G., Popovic, D., Gubas, A., Terawaki, S., Suzuki, H., Stadel, D., Coxon, F.P., Miranda de Stegmann, D., Bhogaraju, S., Maddi, K., Kirchof, A., Gatti, E., Helfrich, M.H., Wakatsuki, S., Behrends, C., Pierre, P. & Dikic, I. (2015) 'PLEKHM1 Regulates Autophagosome-Lysosome Fusion through HOPS Complex and LC3/GABARAP Proteins', *Molecular Cell*, 57(1), pp. 39–54.

McKenna, A., Hanna, M., Banks, E., Sivachenko, A., Cibulskis, K., Kernytsky, A., Garimella, K., Altshuler, D., Gabriel, S., Daly, M. & DePristo, M.A. (2010) 'The Genome Analysis Toolkit: A MapReduce framework for analyzing next-generation DNA sequencing data', *Genome Research*, 20(9), pp. 1297–1303.

McLaren, W., Gil, L., Hunt, S.E., Riat, H.S., Ritchie, G.R.S., Thormann, A., Flicek, P. & Cunningham, F. (2016) 'The Ensembl Variant Effect Predictor', *Genome Biology*, 17(1), p. 122.

McWilliams, T.G., Prescott, A.R., Allen, G.F.G., Tamjar, J., Munson, M.J., Thomson, C., Muqit, M.M.K. & Ganley, I.G. (2016) 'mito -QC illuminates mitophagy and mitochondrial architecture in vivo', *Journal of Cell Biology*, 214(3), pp. 333–345.

McWilliams, T.G., Prescott, A.R., Montava-Garriga, L., Ball, G., Singh, F., Barini, E., Muqit, M.M.K., Brooks, S.P. & Ganley, I.G. (2018) 'Basal Mitophagy Occurs Independently of PINK1 in Mouse Tissues of High Metabolic Demand', *Cell Metabolism*, 27(2), pp. 439-449.e5.

McWilliams, T.G., Prescott, A.R., Villarejo-Zori, B., Ball, G., Boya, P. & Ganley, I.G. (2019) 'A comparative map of macroautophagy and mitophagy in the vertebrate eye', *Autophagy*, 15(7), pp. 1296–1308.

Mead, R.J., Shan, N., Reiser, H.J., Marshall, F. & Shaw, P.J. (2023) 'Amyotrophic lateral sclerosis: a neurodegenerative disorder poised for successful therapeutic translation', *Nature Reviews Drug Discovery*, 22(3), pp. 185–212.

Melguizo-Sanchis, D., Xu, Y., Taheem, D., Yu, M., Tilgner, K., Barta, T., Gassner, K., Anyfantis, G., Wan, T., Elango, R., Alharthi, S., El-Harouni, A.A., Przyborski, S., Adam, S., Saretzki, G., Samarasinghe, S., Armstrong, L. & Lako, M. (2018) 'iPSC modeling of severe aplastic anemia reveals impaired differentiation and telomere shortening in blood progenitors.', *Cell death & disease*, 9(2), p. 128.

Mennerick, S., Dhond, R.P., Benz, A., Xu, W., Rothstein, J.D., Danbolt, N.C., Isenberg, K.E. & Zorumski, C.F. (1998) 'Neuronal Expression of the Glutamate Transporter GLT-1 in Hippocampal Microcultures', *The Journal of Neuroscience*, 18(12), pp. 4490–4499.

Mercer, T.J., Gubas, A. & Tooze, S.A. (2018) 'A molecular perspective of mammalian autophagosome biogenesis.', *The Journal of biological chemistry*, 293(15), pp. 5386–5395.

Merkle, F.T., Ghosh, S., Genovese, G., Handsaker, R.E., Kashin, S., Meyer, D., Karczewski, K.J., O'Dushlaine, C., Pato, C., Pato, M., MacArthur, D.G., McCarroll, S.A. & Eggan, K. (2022) 'Whole-genome analysis of human embryonic stem cells enables rational line selection based on genetic variation', *Cell Stem Cell*, 29(3), pp. 472-486.e7.

Metlagel, Z., Otomo, C., Takaesu, G. & Otomo, T. (2013) ‘Structural basis of ATG3 recognition by the autophagic ubiquitin-like protein ATG12’, *Proceedings of the National Academy of Sciences*, 110(47), pp. 18844–18849.

Metzger, S., Saukko, M., Van Che, H., Tong, L., Puder, Y., Riess, O. & Nguyen, H.P. (2010) ‘Age at onset in Huntington’s disease is modified by the autophagy pathway: implication of the V471A polymorphism in Atg7’, *Human Genetics*, 128(4), pp. 453–459.

Metzger, S., Walter, C., Riess, O., Roos, R.A.C., Nielsen, J.E., Craufurd, D. & Nguyen, H.P. (2013) ‘The V471A Polymorphism in Autophagy-Related Gene ATG7 Modifies Age at Onset Specifically in Italian Huntington Disease Patients’ Xiao-Jiang Li (ed.), *PLoS ONE*, 8(7), p. e68951.

Michiels, C.F., Fransen, P., De Munck, D.G., De Meyer, G.R.Y. & Martinet, W. (2015) ‘Defective autophagy in vascular smooth muscle cells alters contractility and Ca 2+ homeostasis in mice’, *American Journal of Physiology-Heart and Circulatory Physiology*, 308(6), pp. H557–H567.

Millen, K.J. & Gleeson, J.G. (2008) ‘Cerebellar Development and Disease’, *Current opinion in neurobiology*, 18(1), p. 12.

Min, S.-W., Chen, X., Tracy, T.E., Li, Y., Zhou, Y., Wang, C., Shirakawa, K., Minami, S.S., Defensor, E., Mok, S.A., Sohn, P.D., Schilling, B., Cong, X., Ellerby, L., Gibson, B.W., Johnson, J., Krogan, N., Shamloo, M., Gestwicki, J., et al. (2015) ‘Critical role of acetylation in tau-mediated neurodegeneration and cognitive deficits’, *Nature Medicine*, 21(10), pp. 1154–1162.

Mizushima, N., Noda, T. & Ohsumi, Y. (1999) ‘Apg16p is required for the function of the Apg12p-Apg5p conjugate in the yeast autophagy pathway’, *EMBO Journal*, 18(14), pp. 3888–3896.

Mizushima, N., Noda, T., Yoshimori, T., Tanaka, Y., Ishii, T., George, M.D., Klionsky, D.J., Ohsumi, M. & Ohsumi, Y. (1998) ‘A protein conjugation system essential for autophagy’, *Nature*, 395(6700), pp. 395–398.

Mizushima, N., Yamamoto, A., Hatano, M., Kobayashi, Y., Kabey, Y., Suzuki, K., Tokuhis, T., Ohsumi, Y. & Yoshimori, T. (2001) ‘Dissection of autophagosome formation using Apg5-deficient mouse embryonic stem cells’, *Journal of Cell Biology*, 152(4), pp. 657–667.

Molliver, M.E., Kostovic´, I. & Van Der Loos, H. (1973) ‘The development of synapses in cerebral cortex of the human fetus’, *Brain Research*, 50(2), pp. 403–407.

Molnár, Z., Clowry, G.J., Šestan, N., Alzu’bi, A., Bakken, T., Hevner, R.F., Hüppi, P.S., Kostović, I., Rakic, P., Anton, E.S., Edwards, D., Garcez, P., Hoerder-

Suabedissen, A. & Kriegstein, A. (2019) ‘New insights into the development of the human cerebral cortex’, *Journal of Anatomy*, 235(3), pp. 432–451.

Moore, A.S. & Holzbaur, E.L.F. (2016) ‘Dynamic recruitment and activation of ALS-associated TBK1 with its target optineurin are required for efficient mitophagy’, *Proceedings of the National Academy of Sciences*, 113(24), .

Moreno-De-Luca, A., Helmers, S.L., Mao, H., Burns, T.G., Melton, A.M.A., Schmidt, K.R., Fernhoff, P.M., Ledbetter, D.H. & Martin, C.L. (2011) ‘Adaptor protein complex-4 (AP-4) deficiency causes a novel autosomal recessive cerebral palsy syndrome with microcephaly and intellectual disability.’, *Journal of medical genetics*, 48(2), pp. 141–4.

Morimoto, M., Bhambhani, V., Gazzaz, N., Davids, M., Sathiyaseelan, P., Macnamara, E.F., Lange, J., Lehman, A., Zerfas, P.M., Murphy, J.L., Acosta, M.T., Wang, C., Alderman, E., Adam, M., Alvarez, R.L., Alvey, J., Amendola, L., Andrews, A., Ashley, E.A., et al. (2023) ‘Bi-allelic ATG4D variants are associated with a neurodevelopmental disorder characterized by speech and motor impairment’, *npj Genomic Medicine*, 8(1), p. 4.

Mortensen, M., Ferguson, D.J.P., Edelmann, M., Kessler, B., Morten, K.J., Komatsu, M. & Simon, A.K. (2010) ‘Loss of autophagy in erythroid cells leads to defective removal of mitochondria and severe anemia in vivo.’, *Proceedings of the National Academy of Sciences of the United States of America*, 107(2), pp. 832–7.

Mortensen, M., Soilleux, E.J., Djordjevic, G., Tripp, R., Lutteropp, M., Sadighi-Akha, E., Stranks, A.J., Glanville, J., Knight, S., Jacobsen, S.-E.W., Kranc, K.R. & Simon, A.K. (2011) ‘The autophagy protein Atg7 is essential for hematopoietic stem cell maintenance.’, *The Journal of experimental medicine*, 208(3), pp. 455–67.

Mukaiyama, H., Kajiwara, S., Hosomi, A., Giga-Hama, Y., Tanaka, N., Nakamura, T. & Takegawa, K. (2009) ‘Autophagy-deficient Schizosaccharomyces pombe mutants undergo partial sporulation during nitrogen starvation’, *Microbiology*, 155(12), pp. 3816–3826.

Muto, V., Flex, E., Kupchinsky, Z., Primiano, G., Galehdari, H., Dehghani, M., Cecchetti, S., Carpentieri, G., Rizza, T., Mazaheri, N., Sedaghat, A., Vahidi Mehrjardi, M.Y., Traversa, A., Di Nottia, M., Kousi, M.M., Jamshidi, Y., Ciolfi, A., Caputo, V., Malamiri, R.A., et al. (2018) ‘Biallelic SQSTM1 mutations in early-onset, variably progressive neurodegeneration.’, *Neurology*, 91(4), pp. e319–e330.

Nadarajah, B., Brunstrom, J.E., Grutzendler, J., Wong, R.O.L. & Pearlman, A.L. (2001) ‘Two modes of radial migration in early development of the cerebral cortex’, *Nature Neuroscience*, 4(2), pp. 143–150.

Nakamura, A., Izumi, K., Umehara, F., Kuriyama, M., Hokezu, Y., Nakagawa, M., Shimmyozu, K., Izumo, S. & Osame, M. (1995) 'Familial spastic paraplegia with mental impairment and thin corpus callosum.', *Journal of the neurological sciences*, 131(1), pp. 35–42.

Nespoli, E., Hakani, M., Hein, T.M., May, S.N., Danzer, K., Wirth, T., Baumann, B. & Dimou, L. (2024) 'Glial cells react to closed head injury in a distinct and spatiotemporally orchestrated manner', *Scientific Reports*, 14(1), p. 2441.

Ng, P.C. (2003) 'SIFT: predicting amino acid changes that affect protein function', *Nucleic Acids Research*, 31(13), pp. 3812–3814.

Nguyen, H.T., Geens, M., Mertzanidou, A., Jacobs, K., Heirman, C., Breckpot, K. & Spits, C. (2014) 'Gain of 20q11.21 in human embryonic stem cells improves cell survival by increased expression of Bcl-xL', *Molecular Human Reproduction*, 20(2), pp. 168–177.

Nguyen, T.B., Louie, S.M., Daniele, J.R., Tran, Q., Dillin, A., Zoncu, R., Nomura, D.K. & Olzmann, J.A. (2017) 'DGAT1-Dependent Lipid Droplet Biogenesis Protects Mitochondrial Function during Starvation-Induced Autophagy', *Developmental Cell*, 42(1), pp. 9-21.e5.

Nguyen, T.N., Padman, B.S., Usher, J., Oorschot, V., Ramm, G. & Lazarou, M. (2016) 'Atg8 family LC3/GABARAP proteins are crucial for autophagosome-lysosome fusion but not autophagosome formation during PINK1/Parkin mitophagy and starvation.', *The Journal of cell biology*, 215(6), pp. 857–874.

Nguyen-Dien, G.T., Kozul, K.-L., Cui, Y., Townsend, B., Kulkarni, P.G., Ooi, S.S., Marzio, A., Carrodus, N., Zuryn, S., Pagano, M., Parton, R.G., Lazarou, M., Millard, S.S., Taylor, R.W., Collins, B.M., Jones, M.J. & Pagan, J.K. (2023) 'FBXL4 suppresses mitophagy by restricting the accumulation of NIX and BNIP3 mitophagy receptors.', *The EMBO journal*, 42(13), p. e112767.

Nilsson, P., Loganathan, K., Sekiguchi, M., Matsuba, Y., Hui, K., Tsubuki, S., Tanaka, M., Iwata, N., Saito, T. & Saido, T.C. (2013) 'Aβ Secretion and Plaque Formation Depend on Autophagy', *Cell Reports*, 5(1), pp. 61–69.

Nishida, Y., Arakawa, S., Fujitani, K., Yamaguchi, H., Mizuta, T., Kanaseki, T., Komatsu, M., Otsu, K., Tsujimoto, Y. & Shimizu, S. (2009) 'Discovery of Atg5/Atg7-independent alternative macroautophagy', *Nature*, 461(7264), pp. 654–658.

Nixon, R.A., Wegiel, J., Kumar, A., Yu, W.H., Peterhoff, C., Cataldo, A. & Cuervo, A.M. (2005) 'Extensive Involvement of Autophagy in Alzheimer Disease: An Immuno-Electron Microscopy Study', *Journal of Neuropathology & Experimental Neurology*, 64(2), pp. 113–122.

Noctor, S.C., Martínez-Cerdeño, V., Ivic, L. & Kriegstein, A.R. (2004) 'Cortical neurons arise in symmetric and asymmetric division zones and migrate through specific phases', *Nature Neuroscience*, 7(2), pp. 136–144.

Noctor, S.C., Martínez-Cerdeño, V. & Kriegstein, A.R. (2008) 'Distinct behaviors of neural stem and progenitor cells underlie cortical neurogenesis', *Journal of Comparative Neurology*, 508(1), pp. 28–44.

Noda, N.N., Kumeta, H., Nakatogawa, H., Satoo, K., Adachi, W., Ishii, J., Fujioka, Y., Ohsumi, Y. & Inagaki, F. (2008) 'Structural basis of target recognition by Atg8/LC3 during selective autophagy', *Genes to Cells*, 13(12), pp. 1211–1218.

Noda, N.N., Ohsumi, Y. & Inagaki, F. (2010) 'Atg8-family interacting motif crucial for selective autophagy', *FEBS Letters*, 584(7), pp. 1379–1385.

Noda, N.N., Satoo, K., Fujioka, Y., Kumeta, H., Ogura, K., Nakatogawa, H., Ohsumi, Y. & Inagaki, F. (2011) 'Structural Basis of Atg8 Activation by a Homodimeric E1, Atg7', *Molecular Cell*, 44(3), pp. 462–475.

Noda, T. & Klionsky, D.J. (2008) *Chapter 3 The Quantitative Pho8Δ60 Assay of Nonspecific Autophagy*, in [Online]. pp. 33–42.

Nosarti, C., Giouroukou, E., Healy, E., Rifkin, L., Walshe, M., Reichenberg, A., Chitnis, X., Williams, S.C.R. & Murray, R.M. (2008) 'Grey and white matter distribution in very preterm adolescents mediates neurodevelopmental outcome', *Brain*, 131(1), pp. 205–217.

Novak, I., Kirkin, V., McEwan, D.G., Zhang, J., Wild, P., Rozenknop, A., Rogov, V., Löhr, F., Popovic, D., Occhipinti, A., Reichert, A.S., Terzic, J., Dötsch, V., Ney, P.A. & Dikic, I. (2010) 'Nix is a selective autophagy receptor for mitochondrial clearance', *EMBO reports*, 11(1), pp. 45–51.

Nowakowski, T.J., Pollen, A.A., Sandoval-Espinosa, C. & Kriegstein, A.R. (2016) 'Transformation of the Radial Glia Scaffold Demarcates Two Stages of Human Cerebral Cortex Development', *Neuron*, 91(6), pp. 1219–1227.

Ogmundsdottir, M.H., Fock, V., Sooman, L., Pogenberg, V., Dilshat, R., Bindesbøll, C., Ogmundsdottir, H.M., Simonsen, A., Wilmanns, M. & Steingrimsson, E. (2018) 'A short isoform of ATG7 fails to lipidate LC3/GABARAP', *Scientific Reports*, 8(1), p. 14391.

Ordureau, A., Kraus, F., Zhang, J., An, H., Park, S., Ahfeldt, T., Paulo, J.A. & Harper, J.W. (2021) 'Temporal proteomics during neurogenesis reveals large-scale proteome and organelle remodeling via selective autophagy', *Molecular Cell*, 81(24), pp. 5082-5098.e11.

Ordureau, A., Sarraf, S.A., Duda, D.M., Heo, J.-M., Jedrychowski, M.P., Sviderskiy, V.O., Olszewski, J.L., Koerber, J.T., Xie, T., Beausoleil, S.A., Wells, J.A., Gygi, S.P., Schulman, B.A. & Harper, J.W. (2014) 'Quantitative Proteomics Reveal a

Feedforward Mechanism for Mitochondrial PARKIN Translocation and Ubiquitin Chain Synthesis', *Molecular Cell*, 56(3), pp. 360–375.

Otomo, C., Metlagel, Z., Takaesu, G. & Otomo, T. (2013) 'Structure of the human ATG12~ATG5 conjugate required for LC3 lipidation in autophagy', *Nature Structural & Molecular Biology*, 20(1), pp. 59–66.

Paar, M., Jüngst, C., Steiner, N.A., Magnes, C., Sinner, F., Kolb, D., Lass, A., Zimmermann, R., Zumbusch, A., Kohlwein, S.D. & Wolinski, H. (2012) 'Remodeling of Lipid Droplets during Lipolysis and Growth in Adipocytes', *Journal of Biological Chemistry*, 287(14), pp. 11164–11173.

Pacelli, C., Giguère, N., Bourque, M.-J., Lévesque, M., Slack, R.S. & Trudeau, L.-É. (2015) 'Elevated Mitochondrial Bioenergetics and Axonal Arborization Size Are Key Contributors to the Vulnerability of Dopamine Neurons', *Current Biology*, 25(18), pp. 2349–2360.

Palmer, J.E., Wilson, N., Son, S.M., Obrocki, P., Wrobel, L., Rob, M., Takla, M., Korolchuk, V.I. & Rubinsztein, D.C. (2024) 'Autophagy, aging, and age-related neurodegeneration', *Neuron*,

Pansri, P., Phanthong, P., Suthprasertporn, N., Kitiyanant, Y., Tubsuwan, A., Dinnyes, A., Kobolak, J. & Kitiyanant, N. (2021) 'Brain-derived neurotrophic factor increases cell number of neural progenitor cells derived from human induced pluripotent stem cells', *PeerJ*, 9.

Paridaen, J.T.M.L. & Huttner, W.B. (2014) 'Neurogenesis during development of the vertebrate central nervous system.', *EMBO reports*, 15(4), pp. 351–64.

Park, J.-M., Jung, C.H., Seo, M., Otto, N.M., Grunwald, D., Kim, K.H., Moriarity, B., Kim, Y.-M., Starker, C., Nho, R.S., Voytas, D. & Kim, D.-H. (2016) 'The ULK1 complex mediates MTORC1 signaling to the autophagy initiation machinery via binding and phosphorylating ATG14', *Autophagy*, 12(3), pp. 547–564.

Parlati, F., McNew, J.A., Fukuda, R., Miller, R., Söllner, T.H. & Rothman, J.E. (2000) 'Topological restriction of SNARE-dependent membrane fusion', *Nature*, 407(6801), pp. 194–198.

Parnavelas, J.G. & Nadarajah, B. (2001) 'Radial Glial Cells', *Neuron*, 31(6), pp. 881–884.

Paul, L.K., Van Lancker-Sidtis, D., Schieffer, B., Dietrich, R. & Brown, W.S. (2003) 'Communicative deficits in agenesis of the corpus callosum: Nonliteral language and affective prosody', *Brain and Language*, 85(2), pp. 313–324.

Peña-Martinez, C., Rickman, A.D. & Heckmann, B.L. (2022) 'Beyond autophagy: LC3-associated phagocytosis and endocytosis', *Science Advances*, 8(43), .

Peterson, T.R., Laplante, M., Thoreen, C.C., Sancak, Y., Kang, S.A., Kuehl, W.M., Gray, N.S. & Sabatini, D.M. (2009) 'DEPTOR Is an mTOR Inhibitor Frequently Overexpressed in Multiple Myeloma Cells and Required for Their Survival', *Cell*, 137(5), pp. 873–886.

Pfanner, N. (2021) *Editor's evaluation: Towards a molecular mechanism underlying mitochondrial protein import through the TOM and TIM23 complexes*.

Pfeffer, S.R. (2023) 'LRRK2 phosphorylation of Rab GTPases in Parkinson's disease.', *FEBS letters*, 597(6), pp. 811–818.

Pfrieger, F.W. & Barres, B.A. (1997) 'Synaptic Efficacy Enhanced by Glial Cells in Vitro', *Science*, 277(5332), pp. 1684–1687.

Phillips, S.J., Anderson, R.P. & Schapire, R.E. (2006) 'Maximum entropy modeling of species geographic distributions', *Ecological Modelling*, 190(3–4), pp. 231–259.

Pirooznia, S.K., Yuan, C., Khan, M.R., Karuppagounder, S.S., Wang, L., Xiong, Y., Kang, S.U., Lee, Y., Dawson, V.L. & Dawson, T.M. (2020) 'PARIS induced defects in mitochondrial biogenesis drive dopamine neuron loss under conditions of parkin or PINK1 deficiency', *Molecular Neurodegeneration*, 15(1), p. 17.

Pivovarova, N.B. & Andrews, S.B. (2010) 'Calcium-dependent mitochondrial function and dysfunction in neurons', *The FEBS Journal*, 277(18), pp. 3622–3636.

Polymeropoulos, M.H., Lavedan, C., Leroy, E., Ide, S.E., Dehejia, A., Dutra, A., Pike, B., Root, H., Rubenstein, J., Boyer, R., Stenroos, E.S., Chandrasekharappa, S., Athanassiadou, A., Papapetropoulos, T., Johnson, W.G., Lazzarini, A.M., Duvoisin, R.C., Di Iorio, G., Golbe, L.I., et al. (1997) 'Mutation in the α-Synuclein Gene Identified in Families with Parkinson's Disease', *Science*, 276(5321), pp. 2045–2047.

Porter, J.T. & McCarthy, K.D. (1996) 'Hippocampal Astrocytes In Situ Respond to Glutamate Released from Synaptic Terminals', *The Journal of Neuroscience*, 16(16), pp. 5073–5081.

Price, P.J. & Brewer, G.J. (2001) 'Serum-Free Media for Neural Cell Cultures: Adult and Embryonic', in *Protocols for Neural Cell Culture*. [Online]. New Jersey: Humana Press. pp. 255–264.

Puente, C., Hendrickson, R.C. & Jiang, X. (2016) 'Nutrient-regulated Phosphorylation of ATG13 Inhibits Starvation-induced Autophagy.', *The Journal of biological chemistry*, 291(11), pp. 6026–6035.

Radoshevich, L., Murrow, L., Chen, N., Fernandez, E., Roy, S., Fung, C. & Debnath, J. (2010) 'ATG12 Conjugation to ATG3 Regulates Mitochondrial Homeostasis and Cell Death', *Cell*, 142(4), p. 590.

Radulovic, M., Schink, K.O., Wenzel, E.M., Nähse, V., Bongiovanni, A., Lafont, F. & Stenmark, H. (2018) ‘ESCRT-mediated lysosome repair precedes lysophagy and promotes cell survival.’, *The EMBO journal*, 37(21), .

Rakic, P. (1972) ‘Mode of cell migration to the superficial layers of fetal monkey neocortex’, *Journal of Comparative Neurology*, 145(1), pp. 61–83.

Rakic, P. & Sidman, R.L. (1970) ‘Histogenesis of cortical layers in human cerebellum, particularly the lamina dissecans’, *Journal of Comparative Neurology*, 139(4), pp. 473–500.

Rakic, P. & Yakovlev, P.I. (1968) ‘Development of the corpus callosum and cavum septi in man’, *Journal of Comparative Neurology*, 132(1), pp. 45–72.

Ramos-Campoy, O., Ávila-Polo, R., Grau-Rivera, O., Antonell, A., Clarimón, J., Rojas-García, R., Charif, S., Santiago-Valera, V., Hernandez, I., Aguilar, M., Almenar, C., Lopez-Villegas, D., Bajo, L., Pastor, P., Van der Zee, J., Lladó, A., Sanchez-Valle, R. & Gelpi, E. (2018) ‘Systematic Screening of Ubiquitin/p62 Aggregates in Cerebellar Cortex Expands the Neuropathological Phenotype of the C9orf72 Expansion Mutation’, *Journal of Neuropathology & Experimental Neurology*, 77(8), pp. 703–709.

Ran, F.A., Hsu, P.D., Wright, J., Agarwala, V., Scott, D.A. & Zhang, F. (2013) ‘Genome engineering using the CRISPR-Cas9 system’, *Nature Protocols*, 8(11), pp. 2281–2308.

Randall, R. & Thayer, S. (1992) ‘Glutamate-induced calcium transient triggers delayed calcium overload and neurotoxicity in rat hippocampal neurons’, *The Journal of Neuroscience*, 12(5), pp. 1882–1895.

Rangaraju, V., Calloway, N. & Ryan, T.A. (2014) ‘Activity-Driven Local ATP Synthesis Is Required for Synaptic Function’, *Cell*, 156(4), pp. 825–835.

Rappe, A., Vihinen, H.A., Suomi, F., Hassinen, A.J., Ehsan, H., Jokitalo, E.S. & McWilliams, T.G. (2024) ‘Longitudinal autophagy profiling of the mammalian brain reveals sustained mitophagy throughout healthy aging’, *The EMBO Journal*, 43(23), pp. 6199–6231.

Ravikumar, B. (2002) ‘Aggregate-prone proteins with polyglutamine and polyalanine expansions are degraded by autophagy’, *Human Molecular Genetics*, 11(9), pp. 1107–1117.

Reese, M.G., Eeckman, F.H., Kulp, D. & Haussler, D. (1997) ‘Improved Splice Site Detection in Genie’, *Journal of Computational Biology*, 4(3), pp. 311–323.

Rharass, T., Lantow, M., Gbankoto, A., Weiss, D.G., Panáková, D. & Lucas, S. (2017) ‘Ascorbic acid alters cell fate commitment of human neural progenitors in a WNT/β-catenin/ROS signaling dependent manner’, *Journal of Biomedical Science*, 24(1), .

Richards, S., Aziz, N., Bale, S., Bick, D., Das, S., Gastier-Foster, J., Grody, W.W., Hegde, M., Lyon, E., Spector, E., Voelkerding, K. & Rehm, H.L. (2015) 'Standards and guidelines for the interpretation of sequence variants: a joint consensus recommendation of the American College of Medical Genetics and Genomics and the Association for Molecular Pathology', *Genetics in Medicine*, 17(5), pp. 405–424.

Rioux, J.D., Xavier, R.J., Taylor, K.D., Silverberg, M.S., Goyette, P., Huett, A., Green, T., Kuballa, P., Barmada, M.M., Datta, L.W., Shugart, Y.Y., Griffiths, A.M., Targan, S.R., Ippoliti, A.F., Bernard, E.-J., Mei, L., Nicolae, D.L., Regueiro, M., Schumm, L.P., et al. (2007) 'Genome-wide association study identifies new susceptibility loci for Crohn disease and implicates autophagy in disease pathogenesis', *Nature Genetics*, 39(5), pp. 596–604.

Rubinstein, A.D., Eisenstein, M., Ber, Y., Bialik, S. & Kimchi, A. (2011) 'The autophagy protein atg12 associates with antiapoptotic Bcl-2 family members to promote mitochondrial apoptosis', *Molecular Cell*, 44(5), pp. 698–709.

Saint-Jeannet, J. P. (2013). Patterning the vertebrate neural plate by Wnt signaling. In *Madame Curie Bioscience Database*. Landes Bioscience.

Saito, T., Ichimura, Y., Taguchi, K., Suzuki, T., Mizushima, T., Takagi, K., Hirose, Y., Nagahashi, M., Iso, T., Fukutomi, T., Ohishi, M., Endo, K., Uemura, T., Nishito, Y., Okuda, S., Obata, M., Kouno, T., Imamura, R., Tada, Y., et al. (2016) 'p62/Sqstm1 promotes malignancy of HCV-positive hepatocellular carcinoma through Nrf2-dependent metabolic reprogramming', *Nature Communications*, 7(1), p. 12030.

Saitoh, T., Fujita, N., Jang, M.H., Uematsu, S., Yang, B.-G., Satoh, T., Omori, H., Noda, T., Yamamoto, N., Komatsu, M., Tanaka, K., Kawai, T., Tsujimura, T., Takeuchi, O., Yoshimori, T. & Akira, S. (2008) 'Loss of the autophagy protein Atg16L1 enhances endotoxin-induced IL-1β production', *Nature*, 456(7219), pp. 264–268.

Saitsu, H., Nishimura, T., Muramatsu, K., Kodera, H., Kumada, S., Sugai, K., Kasai-Yoshida, E., Sawaura, N., Nishida, H., Hoshino, A., Ryujin, F., Yoshioka, S., Nishiyama, K., Kondo, Y., Tsurusaki, Y., Nakashima, M., Miyake, N., Arakawa, H., Kato, M., et al. (2013) 'De novo mutations in the autophagy gene WDR45 cause static encephalopathy of childhood with neurodegeneration in adulthood.', *Nature genetics*, 45(4), pp. 445–9, 449e1.

Salvador, N., Aguado, C., Horst, M. & Knecht, E. (2000) 'Import of a Cytosolic Protein into Lysosomes by Chaperone-mediated Autophagy Depends on Its Folding State', *Journal of Biological Chemistry*, 275(35), pp. 27447–27456.

Sancak, Y., Bar-Peled, L., Zoncu, R., Markhard, A.L., Nada, S. & Sabatini, D.M. (2010) 'Ragulator-Rag Complex Targets mTORC1 to the Lysosomal Surface and Is Necessary for Its Activation by Amino Acids', *Cell*, 141(2), pp. 290–303.

Sancak, Y., Peterson, T.R., Shaul, Y.D., Lindquist, R.A., Thoreen, C.C., Bar-Peled, L. & Sabatini, D.M. (2008) 'The Rag GTPases Bind Raptor and Mediate Amino Acid Signaling to mTORC1', *Science*, 320(5882), pp. 1496–1501.

Sancak, Y., Thoreen, C.C., Peterson, T.R., Lindquist, R.A., Kang, S.A., Spooner, E., Carr, S.A. & Sabatini, D.M. (2007) 'PRAS40 Is an Insulin-Regulated Inhibitor of the mTORC1 Protein Kinase', *Molecular Cell*, 25(6), pp. 903–915.

Sanjuan, M.A., Dillon, C.P., Tait, S.W.G., Moshiach, S., Dorsey, F., Connell, S., Komatsu, M., Tanaka, K., Cleveland, J.L., Withoff, S. & Green, D.R. (2007) 'Toll-like receptor signalling in macrophages links the autophagy pathway to phagocytosis', *Nature*, 450(7173), pp. 1253–1257.

Sant, P., Rippe, K. & Mallm, J.-P. (2023) 'Approaches for single-cell RNA sequencing across tissues and cell types', *Transcription*, 14(3–5), pp. 127–145.

Sarkar, A., Tindle, C., Pranadinata, R.F., Reed, S., Eckmann, L., Stappenbeck, T.S., Ernst, P.B. & Das, S. (2017) 'ELMO1 Regulates Autophagy Induction and Bacterial Clearance During Enteric Infection', *The Journal of Infectious Diseases*, 216(12), pp. 1655–1666.

Sarnat, H.B. (2023) 'Sequences of synaptogenesis in the human fetal and neonatal brain by synaptophysin immunocytochemistry', *Frontiers in Cellular Neuroscience*, 17p. 1105183.

Sarnat, H.B., Nochlin, D. & Born, D.E. (1998) 'Neuronal nuclear antigen (NeuN): A marker of neuronal maturation in the early human fetal nervous system', *Brain and Development*, 20(2), pp. 88–94.

Sasaki, S. (2011) 'Autophagy in Spinal Cord Motor Neurons in Sporadic Amyotrophic Lateral Sclerosis', *Journal of Neuropathology & Experimental Neurology*, 70(5), pp. 349–359.

Sauvé, V., Sung, G., Soya, N., Kozlov, G., Blaimschein, N., Miotto, L.S., Trempe, J.-F., Lukacs, G.L. & Gehring, K. (2018) 'Publisher Correction: Mechanism of parkinSauvé, V., Sung, G., Soya, N., Kozlov, G., Blaimschein, N., Miotto, L. S., Trempe, J.-F., Lukacs, G. L., & Gehring, K. (2018). Publisher Correction: Mechanism of parkin activation by phosphorylation. Nature Structu', *Nature Structural & Molecular Biology*, 25(8), pp. 744–744.

Scherzinger, E., Lurz, R., Turmaine, M., Mangiarini, L., Hollenbach, B., Hasenbank, R., Bates, G.P., Davies, S.W., Lehrach, H. & Wanker, E.E. (1997) 'Huntingtin-Encoded Polyglutamine Expansions Form Amyloid-like Protein Aggregates In Vitro and In Vivo', *Cell*, 90(3), pp. 549–558.

Schott, M.B., Weller, S.G., Schulze, R.J., Krueger, E.W., Drizyte-Miller, K., Casey, C.A. & McNiven, M.A. (2019) 'Lipid droplet size directs lipolysis and lipophagy catabolism in hepatocytes', *Journal of Cell Biology*, 218(10), pp. 3320–3335.

Schroeder, B., Schulze, R.J., Weller, S.G., Sletten, A.C., Casey, C.A. & McNiven, M.A. (2015) 'The small GTPase Rab7 as a central regulator of hepatocellular lipophagy', *Hepatology*, 61(6), pp. 1896–1907.

Schwarz, J.M., Cooper, D.N., Schuelke, M. & Seelow, D. (2014) 'MutationTaster2: mutation prediction for the deep-sequencing age', *Nature Methods 2014 11:4*, 11(4), pp. 361–362.

Scotter, E.L., Vance, C., Nishimura, A.L., Lee, Y.-B., Chen, H.-J., Urwin, H., Sardone, V., Mitchell, J.C., Rogelj, B., Rubinsztein, D.C. & Shaw, C.E. (2014) 'Differential roles of the ubiquitin proteasome system and autophagy in the clearance of soluble and aggregated TDP-43 species.', *Journal of cell science*, 127(Pt 6), pp. 1263–78.

Senft, A.D., Costello, I., King, H.W., Mould, A.W., Bikoff, E.K. & Robertson, E.J. (2018) 'Combinatorial Smad2/3 Activities Downstream of Nodal Signaling Maintain Embryonic/Extra-Embryonic Cell Identities during Lineage Priming', *Cell reports*, 24(8), pp. 1977-1985.e7.

Settembre, C., Di Malta, C., Polito, V.A., Arencibia, M.G., Vetrini, F., Erdin, S., Erdin, S.U., Huynh, T., Medina, D., Colella, P., Sardiello, M., Rubinsztein, D.C. & Ballabio, A. (2011) 'TFEB Links Autophagy to Lysosomal Biogenesis', *Science*, 332(6036), pp. 1429–1433.

Settembre, C., Zoncu, R., Medina, D.L., Vetrini, F., Erdin, Serkan, Erdin, SerpilUckac, Huynh, T., Ferron, M., Karsenty, G., Vellard, M.C., Facchinetti, V., Sabatini, D.M. & Ballabio, A. (2012) 'A lysosome-to-nucleus signalling mechanism senses and regulates the lysosome via mTOR and TFEB', *The EMBO Journal*, 31(5), pp. 1095–1108.

Sharifi, M.N., Mowers, E.E., Drake, L.E., Collier, C., Chen, H., Zamora, M., Mui, S. & Macleod, K.F. (2016) 'Autophagy Promotes Focal Adhesion Disassembly and Cell Motility of Metastatic Tumor Cells through the Direct Interaction of Paxillin with LC3', *Cell Reports*, 15(8), pp. 1660–1672.

Shen, Y., Li, T., Sun, C., Cheng, X., Chen, Z., Wang, G. & Yang, X. (2024) 'Atg7 autophagy-independent role on governing neural stem cell fate could be potentially applied for regenerative medicine', *Cell Death & Differentiation*, 31(10), pp. 1375–1388.

Shi, Y., Kirwan, P. & Livesey, F.J. (2012) 'Directed differentiation of human pluripotent stem cells to cerebral cortex neurons and neural networks', *Nat Protoc*, 7(10), pp. 1836–1846.

Shin, J.-H., Ko, H.S., Kang, H., Lee, Y., Lee, Y.-I., Pletinkova, O., Troconso, J.C., Dawson, V.L. & Dawson, T.M. (2011) 'PARIS (ZNF746) Repression of PGC-1α Contributes to Neurodegeneration in Parkinson's Disease', *Cell*, 144(5), pp. 689–702.

Shintani, T. (1999) 'Apg10p, a novel protein-conjugating enzyme essential for autophagy in yeast', *The EMBO Journal*, 18(19), pp. 5234–5241.

Shoshani, T., Faerman, A., Mett, I., Zelin, E., Tenne, T., Gorodin, S., Moshel, Y., Elbaz, S., Budanov, A., Chajut, A., Kalinski, H., Kamer, I., Rozen, A., Mor, O., Keshet, E., Leshkowitz, D., Einat, P., Skaliter, R. & Feinstein, E. (2002) 'Identification of a Novel Hypoxia-Inducible Factor 1-Responsive Gene, RTP801 , Involved in Apoptosis', *Molecular and Cellular Biology*, 22(7), pp. 2283–2293.

Silvestri, L., Caputo, V., Bellacchio, E., Atorino, L., Dallapiccola, B., Valente, E.M. & Casari, G. (2005) 'Mitochondrial import and enzymatic activity of PINK1 mutants associated to recessive parkinsonism', *Human Molecular Genetics*, 14(22), pp. 3477–3492.

Singh, K.K., Lovren, F., Pan, Y., Quan, A., Ramadan, A., Matkar, P.N., Ehsan, M., Sandhu, P., Mantella, L.E., Gupta, N., Teoh, H., Parotto, M., Tabuchi, A., Kuebler, W.M., Al-Omran, M., Finkel, T. & Verma, S. (2015) 'The Essential Autophagy Gene ATG7 Modulates Organ Fibrosis via Regulation of Endothelial-to-Mesenchymal Transition', *Journal of Biological Chemistry*, 290(5), pp. 2547–2559.

Singh, R., Kaushik, S., Wang, Y., Xiang, Y., Novak, I., Komatsu, M., Tanaka, K., Cuervo, A.M. & Czaja, M.J. (2009) 'Autophagy regulates lipid metabolism', *Nature*, 458(7242), pp. 1131–1135.

Singleton, A.B., Farrer, M., Johnson, J., Singleton, A., Hague, S., Kachergus, J., Hulihan, M., Peuralinna, T., Dutra, A., Nussbaum, R., Lincoln, S., Crawley, A., Hanson, M., Maraganore, D., Adler, C., Cookson, M.R., Muenter, M., Baptista, M., Miller, D., et al. (2003) 'α-Synuclein Locus Triplication Causes Parkinson's Disease', *Science*, 302(5646), pp. 841–841.

Slane, D., Berendzen, K.W., Witthöft, J. & Jürgens, G. (2020) *Transcriptomic Profiling of the Arabidopsis Embryonic Epidermis Using FANS in Combination with RNAseq*, in [Online]. pp. 151–164.

Sobreira, N., Schiettecatte, F., Valle, D. & Hamosh, A. (2015) 'GeneMatcher: A Matching Tool for Connecting Investigators with an Interest in the Same Gene', *Human Mutation*, 36(10), pp. 928–930.

Son, S.M., Park, S.J., Stamatakou, E., Vicinanza, M., Menzies, F.M. & Rubinsztein, D.C. (2020) 'Leucine regulates autophagy via acetylation of the mTORC1 component raptor', *Nature Communications*, 11(1), p. 3148.

Sou, Y., Waguri, S., Iwata, J., Ueno, T., Fujimura, T., Hara, T., Sawada, N., Yamada, A., Mizushima, N., Uchiyama, Y., Kominami, E., Tanaka, K. & Komatsu, M. (2008) 'The Atg8 conjugation system is indispensable for proper development of autophagic isolation membranes in mice.', *Molecular biology of the cell*, 19(11), pp. 4762–75.

Sousa, S.B., Ramos, F., Garcia, P., Pais, R.P., Paiva, C., Beales, P.L., Moore, G.E., Saraiva, J.M. & Hennekam, R.C.M. (2014) 'Intellectual disability, coarse face, relative macrocephaly, and cerebellar hypotrophy in two sisters.', *American journal of medical genetics. Part A*, 164A(1), pp. 10–4.

Spillane, M., Ketschek, A., Merianda, T.T., Twiss, J.L. & Gallo, G. (2013) 'Mitochondria Coordinate Sites of Axon Branching through Localized Intra-axonal Protein Synthesis', *Cell Reports*, 5(6), pp. 1564–1575.

Spillantini, M.G., Schmidt, M.L., Lee, V.M.-Y., Trojanowski, J.Q., Jakes, R. & Goedert, M. (1997) 'α-Synuclein in Lewy bodies', *Nature*, 388(6645), pp. 839–840.

Staerk, J., Dawlaty, M.M., Gao, Q., Maetzel, D., Hanna, J., Sommer, C.A., Mostoslavsky, G. & Jaenisch, R. (2010) 'Reprogramming of Human Peripheral Blood Cells to Induced Pluripotent Stem Cells', *Cell Stem Cell*, 7(1), pp. 20–24.

Stavoe, A.K.H. & Holzbaur, E.L.F. (2019) 'Autophagy in Neurons', *Annual Review of Cell and Developmental Biology*, 35(1), pp. 477–500.

Subramanian, L., Bershteyn, M., Paredes, M.F. & Kriegstein, A.R. (2017) 'Dynamic behaviour of human neuroepithelial cells in the developing forebrain', *Nature Communications*, 8(1), p. 14167.

Sultan, S., Li, L., Moss, J., Petrelli, F., Cassé, F., Gebara, E., Lopatar, J., Pfrieger, F.W., Bezzi, P., Bischofberger, J. & Toni, N. (2015) 'Synaptic Integration of Adult-Born Hippocampal Neurons Is Locally Controlled by Astrocytes', *Neuron*, 88(5), pp. 957–972.

Sun, C., Seranova, E., Cohen, M.A., Chipara, M., Roberts, J., Astuti, D., Palhegyi, A.M., Acharjee, A., Sedlackova, L., Kataura, T., Otten, E.G., Panda, P.K., Lara-Reyna, S., Korsgen, M.E., Kauffman, K.J., Huerta-Uribe, A., Zatyka, M., Silva, L.F.S.E., Torresi, J., et al. (2023) 'NAD depletion mediates cytotoxicity in human neurons with autophagy deficiency', *Cell Reports*, 42(5), p. 112372.

Sun, D., Wu, R., Zheng, J., Li, P. & Yu, L. (2018) 'Polyubiquitin chain-induced p62 phase separation drives autophagic cargo segregation', *Cell Research*, 28(4), pp. 405–415.

Sun, L., Wu, J., Du, F., Chen, X. & Chen, Z.J. (2013) 'Cyclic GMP-AMP Synthase Is a Cytosolic DNA Sensor That Activates the Type I Interferon Pathway', *Science*, 339(6121), pp. 786–791.

Sun, N., Yun, J., Liu, J., Malide, D., Liu, C., Rovira, I.I., Holmström, K.M., Fergusson, M.M., Yoo, Y.H., Combs, C.A. & Finkel, T. (2015) 'Measuring In Vivo Mitophagy', *Molecular Cell*, 60(4), pp. 685–696.

Sundaramoorthy, V., Walker, A.K., Tan, V., Fifita, J.A., Mccann, E.P., Williams, K.L., Blair, I.P., Guillemin, G.J., Farg, M.A. & Atkin, J.D. (2015) 'Defects in optineurin- and myosin VI-mediated cellular trafficking in amyotrophic lateral sclerosis', *Human Molecular Genetics*, 24(13), pp. 3830–3846.

Sundaramoorthy, V., Walker, A.K., Tan, V., Fifita, J.A., Mccann, E.P., Williams, K.L., Blair, I.P., Guillemin, G.J., Farg, M.A. & Atkin, J.D. (2017) 'Defects in optineurin- and myosin VI-mediated cellular trafficking in amyotrophic lateral sclerosis', *Human Molecular Genetics*, 26(17), pp. 3452–3452.

Suraweera, A., Münch, C., Hanssum, A. & Bertolotti, A. (2012) 'Failure of Amino Acid Homeostasis Causes Cell Death following Proteasome Inhibition', *Molecular Cell*, 48(2), pp. 242–253.

Sutton, G., Kelsh, R.N. & Scholpp, S. (2021) 'Review: The Role of Wnt/β-Catenin Signalling in Neural Crest Development in Zebrafish', *Frontiers in Cell and Developmental Biology*, 9p. 782445.

Suzuki, S., Akamatsu, W., Kisa, F., Sone, T., Ishikawa, K., Kuzumaki, N., Katayama, H., Miyawaki, A., Hattori, N. & Okano, H. (2017) 'Efficient induction of dopaminergic neuron differentiation from induced pluripotent stem cells reveals impaired mitophagy in PARK2 neurons', *Biochemical and Biophysical Research Communications*, 483(1), pp. 88–93.

Taatjes, D.J., Sobel, B.E. & Budd, R.C. (2008) 'Morphological and cytochemical determination of cell death by apoptosis', *Histochemistry and Cell Biology*, 129(1), pp. 33–43.

Takahashi, K., Tanabe, K., Ohnuki, M., Narita, M., Ichisaka, T., Tomoda, K. & Yamanaka, S. (2007) 'Induction of Pluripotent Stem Cells from Adult Human Fibroblasts by Defined Factors', *Cell*, 131(5), pp. 861–872.

Takahashi, K. & Yamanaka, S. (2006) 'Induction of Pluripotent Stem Cells from Mouse Embryonic and Adult Fibroblast Cultures by Defined Factors', *Cell*, 126(4), pp. 663–676.

Tanaka, A., Cleland, M.M., Xu, S., Narendra, D.P., Suen, D.-F., Karbowski, M. & Youle, R.J. (2010) 'Proteasome and p97 mediate mitophagy and degradation of mitofusins induced by Parkin', *Journal of Cell Biology*, 191(7), pp. 1367–1380.

Tang, Q., Gao, P., Arzberger, T., Höllerhage, M., Herms, J., Höglinger, G. & Koeglsperger, T. (2021) 'Alpha-Synuclein defects autophagy by impairing SNAP29-mediated autophagosome-lysosome fusion', *Cell Death & Disease*, 12(10), p. 854.

Tanida, I., Mizushima, N., Kiyooka, M., Ohsumi, M., Ueno, T., Ohsumi, Y. & Kominami, E. (1999) 'Apg7p/Cvt2p: A Novel Protein-activating Enzyme Essential for Autophagy' Randy W. Schekman (ed.), *Molecular Biology of the Cell*, 10(5), pp. 1367–1379.

Tanji, K., Mori, F., Mimura, J., Itoh, K., Kakita, A., Takahashi, H. & Wakabayashi, K. (2010) 'Proteinase K-resistant α-synuclein is deposited in presynapses in human Lewy body disease and A53T α-synuclein transgenic mice', *Acta Neuropathologica*, 120(2), pp. 145–154.

Tao, Y. & Zhang, S.C. (2016) 'Neural Subtype Specification from Human Pluripotent Stem Cells', *Cell Stem Cell*, 19(5), pp. 573–586.

Tauchi-Sato, K., Ozeki, S., Houjou, T., Taguchi, R. & Fujimoto, T. (2002) 'The Surface of Lipid Droplets Is a Phospholipid Monolayer with a Unique Fatty Acid Composition', *Journal of Biological Chemistry*, 277(46), pp. 44507–44512.

Teinert, J., Behne, R., Wimmer, M. & Ebrahimi-Fakhari, D. (2020) 'Novel insights into the clinical and molecular spectrum of congenital disorders of autophagy', *Journal of Inherited Metabolic Disease*, 43(1), pp. 51–62.

Terashima, M., Ishikawa, A., Männer, J., Yamada, S. & Takakuwa, T. (2021) 'Early development of the cortical layers in the human brain', *Journal of Anatomy*, 239(5), pp. 1039–1049.

Texada, M.J., Malita, A., Christensen, C.F., Dall, K.B., Faergeman, N.J., Nagy, S., Halberg, K.A. & Rewitz, K. (2019) 'Autophagy-Mediated Cholesterol Trafficking Controls Steroid Production', *Developmental Cell*, 48(5), pp. 659-671.e4.

Teyssou, E., Takeda, T., Lebon, V., Boillée, S., Doukouré, B., Bataillon, G., Sazdovitch, V., Cazeneuve, C., Meininger, V., LeGuern, E., Salachas, F., Seilhean, D. & Millecamps, S. (2013) 'Mutations in SQSTM1 encoding p62 in amyotrophic lateral sclerosis: genetics and neuropathology', *Acta Neuropathologica*, 125(4), pp. 511–522.

Thomas, A.C., Williams, H., Setó-Salvia, N., Bacchelli, C., Jenkins, D., O'Sullivan, M., Mengrelis, K., Ishida, M., Ocaka, L., Chanudet, E., James, C., Lescai, F., Anderson, G., Morrogh, D., Ryten, M., Duncan, A.J., Pai, Y.J., Saraiva, J.M., Ramos, F., et al. (2014) 'Mutations in SNX14 cause a distinctive autosomal-recessive cerebellar ataxia and intellectual disability syndrome.', *American journal of human genetics*, 95(5), pp. 611–21.

Tong, M., Saito, T., Zhai, P., Oka, S., Mizushima, W., Nakamura, M., Ikeda, S., Shirakabe, A. & Sadoshima, J. (2019) 'Mitophagy Is Essential for Maintaining Cardiac Function During High Fat Diet-Induced Diabetic Cardiomyopathy', *Circulation Research*, 124(9), pp. 1360–1371.

Torisu, T., Torisu, K., Lee, I.H., Liu, J., Malide, D., Combs, C.A., Wu, X.S., Rovira, I.I., Fergusson, M.M., Weigert, R., Connelly, P.S., Daniels, M.P., Komatsu, M., Cao, L. & Finkel, T. (2013) 'Autophagy regulates endothelial cell processing, maturation and secretion of von Willebrand factor', *Nature Medicine*, 19(10), pp. 1281–1287.

Tra, T., Gong, L., Kao, L.-P., Li, X.-L., Grandela, C., Devenish, R.J., Wolvetang, E. & Prescott, M. (2011) 'Autophagy in Human Embryonic Stem Cells' Martin Pera (ed.), *PLoS ONE*, 6(11), p. e27485.

Traynelis, S.F., Wollmuth, L.P., McBain, C.J., Menniti, F.S., Vance, K.M., Ogden, K.K., Hansen, K.B., Yuan, H., Myers, S.J. & Dingledine, R. (2010) 'Glutamate Receptor Ion Channels: Structure, Regulation, and Function' David Sibley (ed.), *Pharmacological Reviews*, 62(3), pp. 405–496.

Trentesaux, C., Fraudeau, M., Pitasi, C.L., Lemarchand, J., Jacques, S., Duche, A., Letourneur, F., Naser, E., Bailly, K., Schmitt, A., Perret, C. & Romagnolo, B. (2020) 'Essential role for autophagy protein ATG7 in the maintenance of intestinal stem cell integrity.', *Proceedings of the National Academy of Sciences of the United States of America*, 117(20), pp. 11136–11146.

Tsuboyama, K., Koyama-Honda, I., Sakamaki, Y., Koike, M., Morishita, H. & Mizushima, N. (2016) 'The ATG conjugation systems are important for degradation of the inner autophagosomal membrane', *Science*, 354(6315), pp. 1036–1041.

Tsujimoto, K., Takamatsu, H. & Kumanogoh, A. (2023) 'The Ragulator complex: delving its multifunctional impact on metabolism and beyond', *Inflammation and Regeneration 2023 43:1*, 43(1), pp. 1–10.

Tsukada, M. & Ohsumi, Y. (1993) 'Isolation and characterization of autophagy-defective mutants of Saccharomyces cerevisiae', *FEBS Letters*, 333(1–2), pp. 169–174.

Tu, J.C., Xiao, B., Yuan, J.P., Lanahan, A.A., Leoffert, K., Li, M., Linden, D.J. & Worley, P.F. (1998) 'Homer Binds a Novel Proline-Rich Motif and Links Group 1 Metabotropic Glutamate Receptors with IP3 Receptors', *Neuron*, 21(4), pp. 717–726.

Turco, E., Witt, M., Abert, C., Bock-Bierbaum, T., Su, M.-Y., Trapannone, R., Sztacho, M., Danieli, A., Shi, X., Zaffagnini, G., Gamper, A., Schuschnig, M., Fracchiolla, D., Bernklau, D., Romanov, J., Hartl, M., Hurley, J.H., Daumke, O. & Martens, S. (2019) 'FIP200 Claw Domain Binding to p62 Promotes Autophagosome Formation at Ubiquitin Condensates', *Molecular Cell*, 74(2), pp. 330-346.e11.

Tymianski, M., Charlton, M., Carlen, P. & Tator, C. (1993) 'Source specificity of early calcium neurotoxicity in cultured embryonic spinal neurons', *The Journal of Neuroscience*, 13(5), pp. 2085–2104.

Ueda, M., Katayama, Y., Kamiya, T., Mishina, M., Igarashi, H., Okubo, S., Senda, M., Iwabuchi, K. & Terashi, A. (1998) 'Hereditary spastic paraplegia with a thin corpus callosum and thalamic involvement in Japan.', *Neurology*, 51(6), pp. 1751–4.

Ullian, E.M., Sapperstein, S.K., Christopherson, K.S. & Barres, B.A. (2001) 'Control of Synapse Number by Glia', *Science*, 291(5504), pp. 657–661.

Valente, E.M., Abou-Sleiman, P.M., Caputo, V., Muqit, M.M.K., Harvey, K., Gispert, S., Ali, Z., Del Turco, D., Bentivoglio, A.R., Healy, D.G., Albanese, A., Nussbaum, R., González-Maldonado, R., Deller, T., Salvi, S., Cortelli, P., Gilks, W.P., Latchman, D.S., Harvey, R.J., et al. (2004) 'Hereditary Early-Onset Parkinson's Disease Caused by Mutations in PINK1', *Science*, 304(5674), pp. 1158–1160.

Vance, C., Rogelj, B., Hortobágyi, T., De Vos, K.J., Nishimura, A.L., Sreedharan, J., Hu, X., Smith, B., Ruddy, D., Wright, P., Ganesalingam, J., Williams, K.L., Tripathi, V., Al-Saraj, S., Al-Chalabi, A., Leigh, P.N., Blair, I.P., Nicholson, G., de Belleroche, J., et al. (2009) 'Mutations in FUS, an RNA Processing Protein, Cause Familial Amyotrophic Lateral Sclerosis Type 6', *Science*, 323(5918), pp. 1208–1211.

Vargas, J.N.S., Hamasaki, M., Kawabata, T., Youle, R.J. & Yoshimori, T. (2022) 'The mechanisms and roles of selective autophagy in mammals', *Nature Reviews Molecular Cell Biology 2022 24:3*, 24(3), pp. 167–185.

Vázquez, P., Arroba, A.I., Cecconi, F., de la Rosa, E.J., Boya, P. & De Pablo, F. (2012) 'Atg5 and Ambra1 differentially modulate neurogenesis in neural stem cells', *Autophagy*, 8(2), pp. 187–199.

Velázquez, A.P., Tatsuta, T., Ghillebert, R., Drescher, I. & Graef, M. (2016) 'Lipid droplet–mediated ER homeostasis regulates autophagy and cell survival during starvation', *Journal of Cell Biology*, 212(6), pp. 621–631.

Verkerk, A.J.M.H., Schot, R., Dumee, B., Schellekens, K., Swagemakers, S., Bertoli-Avella, A.M., Lequin, M.H., Dudink, J., Govaert, P., van Zwol, A.L., Hirst, J., Wessels, M.W., Catsman-Berrevoets, C., Verheijen, F.W., de Graaff, E., de Coo, I.F.M., Kros, J.M., Willemsen, R., Willems, P.J., et al. (2009) 'Mutation in the AP4M1 gene provides a model for neuroaxonal injury in cerebral palsy.', *American journal of human genetics*, 85(1), pp. 40–52.

Lo Verso, F., Carnio, S., Vainshtein, A. & Sandri, M. (2014) 'Autophagy is not required to sustain exercise and PRKAA1/AMPK activity but is important to prevent mitochondrial damage during physical activity', *Autophagy*, 10(11), pp. 1883–1894.

Vigeland, M.D., Gjøtterud, K.S. & Selmer, K.K. (2016) 'FILTUS: a desktop GUI for fast and efficient detection of disease-causing variants, including a novel autozygosity detector', *Bioinformatics*, 32(10), pp. 1592–1594.

Volpe, J.J. (2009) 'Cerebellum of the Premature Infant: Rapidly Developing, Vulnerable, Clinically Important', *Journal of Child Neurology*, 24(9), pp. 1085–1104.

Walker, F.O. (2007) 'Huntington's disease', *The Lancet*, 369(9557), pp. 218–228.

Wang, H., Song, G., Chuang, H., Chiu, C., Abdelmaksoud, A., Ye, Y. & Zhao, L. (2018) 'Portrait of glial scar in neurological diseases.', *International journal of immunopathology and pharmacology*, 31p. 2058738418801406.

Wang, J., Chen, S., Pan, C., Li, G. & Tang, Z. (2022) 'Application of Small Molecules in the Central Nervous System Direct Neuronal Reprogramming', *Frontiers in bioengineering and biotechnology*, 10.

Wang, K., Li, M. & Hakonarson, H. (2010) 'ANNOVAR: functional annotation of genetic variants from high-throughput sequencing data', *Nucleic Acids Research*, 38(16), pp. e164–e164.

Wang, L., Yu, C., Lu, Y., He, P., Guo, J., Zhang, C., Song, Q., Ma, D., Shi, T. & Chen, Y. (2007) 'TMEM166, a novel transmembrane protein, regulates cell autophagy and apoptosis', *Apoptosis*, 12(8), pp. 1489–1502.

Wang, L., Zhou, J., Yan, S., Lei, G., Lee, C.-H. & Yin, X.-M. (2017) 'Ethanol-triggered Lipophagy Requires SQSTM1 in AML12 Hepatic Cells', *Scientific Reports*, 7(1), p. 12307.

Wang, S., Xia, P., Ye, B., Huang, G., Liu, J. & Fan, Z. (2013) 'Transient activation of autophagy via Sox2-mediated suppression of mTOR is an important early step in reprogramming to pluripotency', *Cell stem cell*, 13(5), pp. 617–625.

Wang, Zheng, Miao, G., Xue, X., Guo, X., Yuan, C., Wang, Zhaoyu, Zhang, G., Chen, Y., Feng, D., Hu, J. & Zhang, H. (2016) 'The Vici Syndrome Protein EPG5 Is a Rab7 Effector that Determines the Fusion Specificity of Autophagosomes with Late Endosomes/Lysosomes', *Molecular Cell*, 63(5), pp. 781–795.

Watanabe, K., Ueno, M., Kamiya, D., Nishiyama, A., Matsumura, M., Wataya, T., Takahashi, J.B., Nishikawa, S., Nishikawa, S.I., Muguruma, K. & Sasai, Y. (2007) 'A ROCK inhibitor permits survival of dissociated human embryonic stem cells', *Nature Biotechnology 2007 25:6*, 25(6), pp. 681–686.

Webster, C.P., Smith, E.F., Bauer, C.S., Moller, A., Hautbergue, G.M., Ferraiuolo, L., Myszczynska, M.A., Higginbottom, A., Walsh, M.J., Whitworth, A.J., Kaspar, B.K., Meyer, K., Shaw, P.J., Grierson, A.J. & De Vos, K.J. (2016) 'The C9orf72 protein interacts with Rab1a and the ULK1 complex to regulate initiation of autophagy.', *The EMBO journal*, 35(15), pp. 1656–76.

De Wert, G. & Mummery, C. (2003) ‘Human embryonic stem cells: research, ethics and policy’, *Human Reproduction*, 18(4), pp. 672–682.

Wilkinson, S. (2019) ‘ER-phagy: shaping up and destressing the endoplasmic reticulum’, *The FEBS Journal*, 286(14), pp. 2645–2663.

Willard, S.S. & Koochekpour, S. (2013) ‘Glutamate, glutamate receptors, and downstream signaling pathways.’, *International journal of biological sciences*, 9(9), pp. 948–59.

Winslow, A.R., Chen, C.-W., Corrochano, S., Acevedo-Arozena, A., Gordon, D.E., Peden, A.A., Lichtenberg, M., Menzies, F.M., Ravikumar, B., Imarisio, S., Brown, S., O’Kane, C.J. & Rubinsztein, D.C. (2010) ‘α-Synuclein impairs macroautophagy: implications for Parkinson’s disease.’, *The Journal of cell biology*, 190(6), pp. 1023–37.

Wirth, M., Zhang, W., Razi, M., Nyoni, L., Joshi, D., O’Reilly, N., Johansen, T., Tooze, S.A. & Mouilleron, S. (2019) ‘Molecular determinants regulating selective binding of autophagy adapters and receptors to ATG8 proteins’, *Nature Communications*, 10(1), p. 2055.

Wold, M.S., Lim, J., Lachance, V., Deng, Z. & Yue, Z. (2016) ‘ULK1-mediated phosphorylation of ATG14 promotes autophagy and is impaired in Huntington’s disease models’, *Molecular Neurodegeneration*, 11(1), p. 76.

Wong, Y.C. & Holzbaur, E.L.F. (2014a) ‘Optineurin is an autophagy receptor for damaged mitochondria in parkin-mediated mitophagy that is disrupted by an ALS-linked mutation’, *Proceedings of the National Academy of Sciences*, 111(42), .

Wong, Y.C. & Holzbaur, E.L.F. (2014b) ‘The Regulation of Autophagosome Dynamics by Huntingtin and HAP1 Is Disrupted by Expression of Mutant Huntingtin, Leading to Defective Cargo Degradation’, *The Journal of Neuroscience*, 34(4), pp. 1293–1305.

Wu, C.C., Lien, C.C., Hou, W.H., Chiang, P.M. & Tsai, K.J. (2016) ‘Gain of BDNF Function in Engrafted Neural Stem Cells Promotes the Therapeutic Potential for Alzheimer’s Disease’, *Scientific Reports*, 6.

Wu, J.J., Quijano, C., Chen, E., Liu, H., Cao, L., Fergusson, M.M., Rovira, I.I., Gutkind, S., Daniels, M.P., Komatsu, M. & Finkel, T. (2009) ‘Mitochondrial dysfunction and oxidative stress mediate the physiological impairment induced by the disruption of autophagy’, *Aging*, 1(4), pp. 425–437.

Wu, X., Fleming, A., Ricketts, T., Pavel, M., Virgin, H., Menzies, F.M. & Rubinsztein, D.C. (2016) ‘Autophagy regulates Notch degradation and modulates stem cell development and neurogenesis’, *Nature Communications*, 7(1), p. 10533.

Wurzer, B., Zaffagnini, G., Fracchiolla, D., Turco, E., Abert, C., Romanov, J. & Martens, S. (2015) ‘Oligomerization of p62 allows for selection of ubiquitinated cargo and isolation membrane during selective autophagy.’, *eLife*, 4p. e08941.

Xia, Q., Wang, H., Hao, Z., Fu, C., Hu, Q., Gao, F., Ren, H., Chen, D., Han, J., Ying, Z. & Wang, G. (2016) ‘TDP-43 loss of function increases TFEB activity and blocks autophagosome-lysosome fusion.’, *The EMBO journal*, 35(2), pp. 121–42.

Xie, Z., Nair, U. & Klionsky, D.J. (2008) ‘Atg8 controls phagophore expansion during autophagosome formation.’, *Molecular biology of the cell*, 19(8), pp. 3290–8.

Xu, L., Kang, Y., Çöl, S. & Massagué, J. (2002) ‘Smad2 Nucleocytoplasmic Shuttling by Nucleoporins CAN/Nup214 and Nup153 Feeds TGFβ Signaling Complexes in the Cytoplasm and Nucleus’, *Molecular Cell*, 10(2), pp. 271–282.

Yamaguchi, J., Suzuki, C., Nanao, T., Kakuta, S., Ozawa, K., Tanida, I., Saitoh, T., Sunabori, T., Komatsu, M., Tanaka, K., Aoki, S., Sakimura, K. & Uchiyama, Y. (2018) ‘Atg9a deficiency causes axon-specific lesions including neuronal circuit dysgenesis’, *Autophagy*, 14(5), pp. 764–777.

Yamaguchi, M., Satoo, K., Suzuki, H., Fujioka, Y., Ohsumi, Y., Inagaki, F. & Noda, N.N. (2018) ‘Atg7 Activates an Autophagy-Essential Ubiquitin-like Protein Atg8 through Multi-Step Recognition’, *Journal of Molecular Biology*, 430(3), pp. 249–257.

Yamano, K., Wang, C., Sarraf, S.A., Münch, C., Kikuchi, R., Noda, N.N., Hizukuri, Y., Kanemaki, M.T., Harper, W., Tanaka, K., Matsuda, N. & Youle, R.J. (2018) ‘Endosomal Rab cycles regulate Parkin-mediated mitophagy’, *eLife*, 7.

Yamano, K. & Youle, R.J. (2013) ‘PINK1 is degraded through the N-end rule pathway’, *Autophagy*, 9(11), pp. 1758–1769.

Yang, K., Yu, B., Cheng, C., Cheng, T., Yuan, B., Li, K., Xiao, J., Qiu, Z. & Zhou, Y. (2017) ‘Mir505–3p regulates axonal development via inhibiting the autophagy pathway by targeting Atg12’, *Autophagy*, 13(10), pp. 1679–1696.

Yapici, Z. & Eraksoy, M. (2005) ‘Non-progressive congenital ataxia with cerebellar hypoplasia in three families’, *Acta Paediatrica*, 94(2), pp. 248–253.

Yim, W.W.-Y. & Mizushima, N. (2020) ‘Lysosome biology in autophagy’, *Cell Discovery*, 6(1), p. 6.

Yuan, Y., Zheng, Y., Zhang, X., Chen, Y., Wu, X., Wu, J., Shen, Z., Jiang, L., Wang, L., Yang, W., Luo, J., Qin, Z., Hu, W. & Chen, Z. (2017) ‘BNIP3L/NIX-mediated mitophagy protects against ischemic brain injury independent of PARK2’, *Autophagy*, 13(10), pp. 1754–1766.

Zaffagnini, G., Savova, A., Danieli, A., Romanov, J., Tremel, S., Ebner, M., Peterbauer, T., Sztacho, M., Trapannone, R., Tarafder, A.K., Sachse, C. & Martens, S. (2018) ‘p62 filaments capture and present ubiquitinated cargos for autophagy’, *The EMBO Journal*, 37(5), .

Zaidi, A., Barŕon, L., Sharov, V.S., Schöneich, C., Michaelis, E.K. & Michaelis, M.L. (2003) ‘Oxidative Inactivation of Purified Plasma Membrane Ca 2+ -ATPase by Hydrogen Peroxide and Protection by Calmodulin’, *Biochemistry*, 42(41), pp. 12001–12010.

Zanotti, S., Smerdel-Ramoya, A., Stadmeyer, L. & Canalis, E. (2008) ‘Activation of the ERK pathway in osteoblastic cells, role of gremlin and BMP-2’, *Journal of Cellular Biochemistry*, 104(4), pp. 1421–1426.

Zhang, J., Loyd, M.R., Randall, M.S., Waddell, M.B., Kriwacki, R.W. & Ney, P.A. (2012) ‘A short linear motif in BNIP3L (NIX) mediates mitochondrial clearance in reticulocytes’, *Autophagy*, 8(9), pp. 1325–1332.

Zhang, J., Randall, M.S., Loyd, M.R., Dorsey, F.C., Kundu, M., Cleveland, J.L. & Ney, P.A. (2009) ‘Mitochondrial clearance is regulated by Atg7-dependent and -independent mechanisms during reticulocyte maturation’, *Blood*, 114(1), pp. 157–164.

Zhang, Q., Pangršič, T., Kreft, M., Kržan, M., Li, N., Sul, J.-Y., Halassa, M., Van Bockstaele, E., Zorec, R. & Haydon, P.G. (2004) ‘Fusion-related Release of Glutamate from Astrocytes’, *Journal of Biological Chemistry*, 279(13), pp. 12724–12733.

Zhang, S., Tong, M., Zheng, D., Huang, H., Li, L., Ungermann, C., Pan, Y., Luo, H., Lei, M., Tang, Z., Fu, W., Chen, S., Liu, X. & Zhong, Q. (2023) ‘C9orf72-catalyzed GTP loading of Rab39A enables HOPS-mediated membrane tethering and fusion in mammalian autophagy’, *Nature Communications*, 14(1), p. 6360.

Zhang, Y., Cross, S.D., Stanton, J.B., Marmorstein, A.D., Le, Y.Z. & Marmorstein, L.Y. (2017) ‘Early AMD-like defects in the RPE and retinal degeneration in aged mice with RPE-specific deletion of Atg5 or Atg7.’, *Molecular vision*, 23pp. 228–241.

Zhao, D.Y., Bäuerlein, F.J.B., Saha, I., Hartl, F.U., Baumeister, W. & Wilfling, F. (2024) ‘Autophagy preferentially degrades non-fibrillar polyQ aggregates’, *Molecular Cell*, 84(10), pp. 1980-1994.e8.

Zhao, L., Teng, B., Wen, L., Feng, Q., Wang, H., Li, N., Wang, Y. & Liang, Z. (2014) ‘mTOR inhibitor AZD8055 inhibits proliferation and induces apoptosis in laryngeal carcinoma.’, *International journal of clinical and experimental medicine*, 7(2), pp. 337–47.

Zhou, H., Qian, X., Xu, N., Zhang, S., Zhu, G., Zhang, Y., Liu, D., Cheng, C., Zhu, X., Liu, Y., Lu, L., Tang, J., Chai, R. & Gao, X. (2020) ‘Disruption of Atg7-dependent

autophagy causes electromotility disturbances, outer hair cell loss, and deafness in mice', *Cell Death & Disease*, 11(10), p. 913.

Zhou, X., Xie, L., Xia, L., Bergmann, F., Büchler, M.W., Kroemer, G., Hackert, T. & Fortunato, F. (2017) 'RIP3 attenuates the pancreatic damage induced by deletion of ATG7', *Cell Death & Disease*, 8(7), pp. e2918–e2918.

Zimprich, A., Biskup, S., Leitner, P., Lichtner, P., Farrer, M., Lincoln, S., Kachergus, J., Hulihan, M., Uitti, R.J., Calne, D.B., Stoessl, A.J., Pfeiffer, R.F., Patenge, N., Carbajal, I.C., Vieregge, P., Asmus, F., Müller-Myhsok, B., Dickson, D.W., Meitinger, T., et al. (2004) 'Mutations in LRRK2 Cause Autosomal-Dominant Parkinsonism with Pleomorphic Pathology', *Neuron*, 44(4), pp. 601–607.

Ziv, N.E. (2018) 'Maintaining the active zone: Demand, supply and disposal of core active zone proteins', *Neuroscience Research*, 127pp. 70–77.